Copper *N*-Heterocyclic Carbenes: Novel Electrochemical Synthesis, Stabilisation of Variable Oxidation States and Unusual Carbene Reactivity

Benjamin Richard Morris Lake

Submitted in accordance with the requirements for the degree of
Doctor of Philosophy

The University of Leeds
School of Chemistry

June, 2014

The candidate confirms that the work submitted is his/her own, except where work which has formed part of jointly-authored publications has been included. The contribution of the candidate and the other authors to this work has been explicitly indicated below. The candidate confirms that appropriate credit has been given within the thesis where reference has been made to the work of others.

Jointly Authored Publications

Simple and versatile selective synthesis of neutral and cationic copper(I) N-heterocyclic carbene complexes using an electrochemical procedure

Benjamin R. M. Lake, Emma K. Bullough, Thomas J. Williams, Adrian C. Whitwood, Marc A. Little and Charlotte E. Willans. *Chemical Communications*, **2012**, 48, 4887-4889.

CANDIDATE'S CONTRIBUTION

The work described within this publication is presented in Chapter 2 of this thesis. The candidate synthesised and characterised all of the compounds reported in the manuscript, apart from 3 of the compounds, which were synthesised and characterised by Dr Emma K Bullough and Dr Thomas J Williams. The X-ray crystallographic data was all collected by the candidate, apart from for one of the compounds, which was collected by Dr Adrian C Whitwood. Dr Marc A Little helped the candidate manipulate some of the crystallographic data and prepare the data for publication. The manuscript was prepared by Dr Charlotte E Willans.

Structural Diversity of Copper(I)–N-Heterocyclic Carbene Complexes; Ligand Tuning Facilitates Isolation of the First Structurally Characterised Copper(I)–NHC Containing a Copper(I)–Alkene Interaction

Benjamin R. M. Lake and Charlotte E. Willans. *Chemistry - A European Journal*, **2013**, 19, 16780-16790.

CANDIDATE'S CONTRIBUTION

The work described within this publication is presented in Chapter 3 and Chapter 4 of this thesis. The candidate synthesised and characterised all of the compounds reported in the manuscript and collected and manipulated all of the X-ray crystallographic data. The manuscript was prepared by Dr Charlotte E Willans and the candidate.

Remarkable Stability of Copper(II)–N-Heterocyclic Carbene Complexes Void of an Anionic Tether

Benjamin R. M. Lake and Charlotte E. Willans. *Organometallics*, **2014**, 33 (8), 2027–2038.

CANDIDATE'S CONTRIBUTION

The work described within this publication is presented in Chapter 4 and Chapter 5 of this thesis. The candidate synthesised and characterised all of the compounds reported in the manuscript and collected and manipulated all of the X-ray crystallographic data. The manuscript was prepared by Dr Charlotte E Willans and the candidate.

Acknowledgements

This research has been carried out by a team which has included Dr Alireza Ariafard (University of Tasmania). My own contributions, fully and explicitly indicated in the thesis, have been in the synthesis and characterisation of all compounds. The other members of the group and their contributions have been as follows: performance of the DFT calculations.

First and foremost, I would like to thank Dr Charlotte Willans for giving me the opportunity to undertake this PhD project and for all of her excellent supervision during the time I have been here. I have found the project extremely rewarding, and have learnt an unbelievable amount in such a short period of time.

I would also like to thank the technical staff; including Mrs Tanya Marinko-Covell and Mr Ian Blakeley for running my elemental analyses, Mr Simon Barrett for being forever disgruntled and for running the occasional long-run NMR spectrum (when a compound had the same solubility as brick dust) and Dr Stuart Warriner for obtaining the odd mass spectrum in cases where the ligand and metal centre didn't fancy flying together.

Special thanks must go to Emma for showing me the ropes early in my PhD and for being unwaveringly cheerful, and to Chris, Steph, Rianne and Tom for enjoying a drink (or twenty). I would also like to thank past 1.32 members, in particular, Tia for ruling the lab with an iron fist, Marc 'Dr Crystallography' Little for teaching me so much about X-ray crystallography and for his penchant for spending a month's salary on adult entertainment and even to Jake Fielden for being the absolute pinnacle of 'cowboy'. More thanks must go to current 1.32 members including Flora for her love of coins and orchids, Vikki for being unable to maintain her balance after a few pints, Mike (and Janice) for generally being large and in charge, Jordan for being able to empty an entire argon cylinder in about 20 minutes and Heba for her love of camels and pyramids, and latterly her taste for the booze.

I've got to give a massive thanks to the Lads-on-Tour, Jonny and James, for generally having the prettiest faces/most Chinese hair I have ever seen, and for your skill in a certain body part-related observation game. The presence of you two throughout my PhD has, quite frankly, been an inspiration.

I must thank all of my family members, and in particular my parents for giving me the best possible start to life (and education). This achievement would not have been possible without you. And finally, I would like to thank my wonderful girlfriend, Rosie, for her constant love and support over the past two and a half years. This achievement is dedicated to you.

Abstract

This thesis concerns the synthesis, structural characterisation and reactivity of a range of novel organometallic complexes. The research primarily focuses on *N*-heterocyclic carbenes as ligands, and their coordination to copper cations.

A novel electrochemical synthetic procedure for the synthesis of Cu^{I}-NHC complexes is described. It was found that this procedure was suitable for the synthesis of a wide range of Cu^{I}-NHC complexes, containing either bulky, non-bulky or base sensitive functional groups. Furthermore, the synthetic procedure was found to be highly selective, producing [Cu(NHC)X]-type complexes when X is a coordinating anion, and $[Cu(NHC)_2]X$-type complexes when X is a non-coordinating anion.

The structural chemistry of Cu^{I}-NHC complexes containing pendant *N*-allyl groups was explored, with the resultant complexes displaying an array of coordination geometries about the Cu^{I} centres. By careful modification of these ligands, the first example of a Cu^{I}-NHC complex containing a Cu^{I}-alkene interaction was observed.

The coordination chemistry of NHC ligands containing pyridyl substituents, which act as ancillary donors, was investigated. Cu^{I}-NHC complexes containing these ligands were found to be catalytically competent in an Ullmann-type etherification reaction. Additionally, exposure of solutions of some of these Cu^{I}-NHC complexes to atmospheric conditions allowed the crystallographic characterisation of rare examples of Cu^{II}-NHC complexes.

Finally, the rational synthesis of a range of unusual Cu^{II}-NHC complexes was performed, with the resulting complexes being structurally characterised. It was found that, under certain circumstances, oxidative decomposition of the NHC ligand within the coordination sphere of a copper centre can occur. The formation of 2-haloimidazolium and C-C coupled *bis*-imidazolium salts, *via* oxidative degradation, was investigated using a combined experimental and computational study.

Table of Contents

List of Figures

Chapter 1

Chapter 2

Chapter 3

Chapter 4

List of Schemes

Chapter 1

Chapter 5

List of Tables

Chapter 2

Chapter 3

Chapter 4

Chapter 5

List of Abbreviations

Å	Angstrom, 1 x 10^{-10} m
ArH	Protons attached to an aromatic ring
ax	Axial
br	Broad
$^{13}C\{^{1}H\}$	Proton-decoupled carbon (NMR)
COD	Cyclooctadiene
COSY	Correlation spectroscopy
dba	Dibenzylideneacetone
DCM	Dichloromethane
DEA	Diethanolamine
Deg	Degrees
ΔG	Change in Gibbs free energy
d	Doublet resonance
dept	Distortionless enhancement by polarisation transfer
DFT	Density functional theory
DMF	Dimethylformamide
DMS	Dimethylsulfide
DMSO	Dimethylsulfoxide
DROR	Disproportionation - reductive elimination - oxidative addition - reductive elimination
e.g.	*exempli gratia* (for the sake of example)
eq	Equatorial
ESI	Electrospray ionisation
et al.	*et alia* (and others)
etc.	*et cetera*
G	Gibbs free energy

HOMO	Highest occupied molecular orbital
HRMS	High resolution mass spectrometry
i.e.	*id est* (that is)
IMH	Intermolecular multicentre hetero-acceptor hydrogen bond
imH	Protons attached to the C4 and C5 carbon atoms of the imidazole ring
Hz	Hertz
J	NMR coupling constant
K	Kelvin
kcal	Kilocalorie
LMCT	Ligand-to-metal charge transfer
LUMO	Lowest unoccupied molecular orbital
NBS	*N*-Bromosuccinimide
NHC	*N*-Heterocyclic carbene
NMR	Nuclear magnetic resonance
m	Multiplet resonance
mA	Milliamps
MECP	Minimum energy crossing point
mesH	Protons attached to a mesityl aromatic ring
MHz	Megahertz
MLCT	Metal-to-ligand charge transfer
MS	Mass spectrometry
m/z	Mass to charge ratio
pK_a	Logarithmic value of the acid dissociation constant
ppm	Parts per million
pyH	Protons attached to pyridine ring
rt	Room temperature
s	Singlet resonance
Selectfluor	1-Chloromethyl-4-fluoro-1,4-diazoniabicyclo[2.2.2]octane *bis*(tetrafluoroborate)

sept	Septet resonance
SOF	Site occupation factor
s.u.s	Standard uncertainties
Q	Total charge, C or A s
t	Triplet resonance
THF	Tetrahydrofuran
tht	Tetrahydrothiophene
TM	Transition metal

Chapter 1

Introduction

1.1 Overview

The work presented within this thesis details the synthesis, structural chemistry and catalytic application of a range of *N*-heterocyclic carbene (NHC) complexes. As such, this introductory chapter aims to provide a basic introduction to the field of carbene chemistry, and specifically, to the chemistry of NHCs. The relevant state of the art research in the field will also be presented, in a succinct manner, which should help the reader place in to context the work reported in this thesis.

1.2 Organometallic Chemistry

Organometallic chemistry is generally considered to be concerned with the synthesis of compounds containing carbon-metal(loid) bonds, and is an area of chemistry with a long and rich history. Indeed, many consider that the field was born as far back as 1760, with the report of the synthesis of what we now know as tetramethyldiarsine, 'cacodyl', by Louis-Claude de Gassicourt (Figure 1.1).[1]

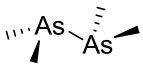

Figure 1.1 Tetramethyldiarsine, 'cacodyl'

Further significant progress was made in the field in 1831 when William Zeise reported the synthesis of his eponymous organometallic compound, potassium trichloro(ethene)platinate(II), *i.e.* Zeise's salt (Figure 1.2).[2]

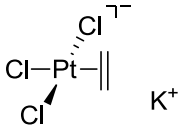

Figure 1.2 Zeise's salt

Since these seminal early reports, the field of organometallic chemistry has grown rapidly, with its importance to chemistry in general being highlighted by the award of several Nobel Prizes in Chemistry to researchers working in organometallic chemistry. These include the award of the 1912 Nobel Prize to Victor Grignard "for the discovery of the so-called Grignard reagent, which in recent years has greatly advanced the progress of organic chemistry",[3] the 1963 Nobel Prize

to Karl Ziegler and Guilio Natta "for their discoveries in the field of the chemistry and technology of high polymers",[4] and the 1973 Nobel Prize to Ernst Otto Fischer and Geoffrey Wilkinson "for their pioneering work, performed independently, on the chemistry of the organometallic, so called sandwich compounds".[5] More recently, the 2005 Nobel Prize in Chemistry was awarded jointly to Yves Chauvin, Robert Grubbs and Richard Schrock for their ground-breaking work on the development of transition metal-catalysed metathesis chemistry, for use in organic synthesis.[6] Indeed, this Nobel Prize-winning work helps to strongly illustrate the profound ability of carbenes to influence the behaviour and reactivity of transition metal ions.

1.3 Carbenes

A carbene is an uncharged, divalent carbon centre, possessing six valence electrons.[7] Depending on the hybridisation of the carbon centre, sp or sp^2, the carbene adopts a linear or bent geometry. An sp-hybridised carbon centre contains two degenerate, orthogonal, non-bonding p-orbitals (designated p_x and p_y) and thus typically takes on an approximately linear geometry (Figure 1.3). Both p-orbitals contain one unpaired electron, which are spin-aligned, giving linear carbenes triplet multiplicity.[7a] As a result, triplet carbenes are often thought of as diradicals.[7b] The parallel alignment of electrons follows Hund's rule; that the maximum multiplicity has the lowest energy when filling degenerate orbitals.

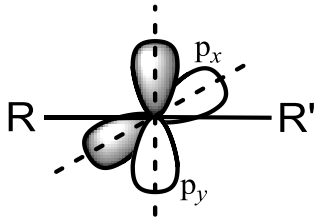

Figure 1.3 Orbital diagram of an sp-hybridised linear carbene[7a, 7b]

Carbenes with sp^2-hybridisation at the carbon centre generally adopt a bent geometry.[7a] As a result of the sp^2-hybridisation, orbital degeneracy is broken and thus the p_x-orbital gains some s-orbital character (σ-orbital), while the p_y-orbital remains essentially unchanged (p_π-orbital) (Figure 1.4).[7b]

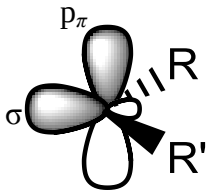

Figure 1.4 Orbital diagram of an sp^2-hybridised bent carbene[7a, 7b]

As a result of the loss of degeneracy due to the change in orbital hybridisation, and concomitant lowering in energy of the σ-orbital with respect to the p_π-orbital (due to it gaining s-orbital character), four different electronic configurations are possible for an sp^2-hybridised bent carbene (Figure 1.5). Three of the four configurations have singlet multiplicity (**1**, **2** and **3** – Figure 1.5), while the fourth has triplet multiplicity (**4**).[7b]

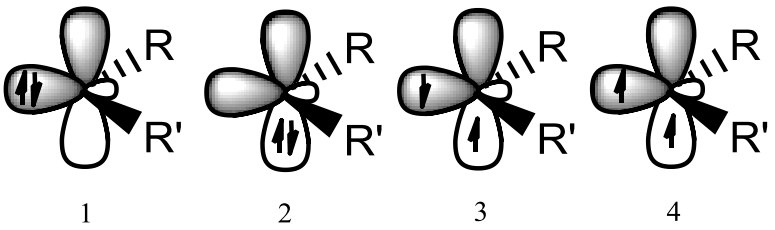

Figure 1.5 Possible electron configurations of an sp^2-hybridised bent carbene[7a, 7b]

In Figure 1.5, **1** and **2** both contain one full and one empty orbital. The σ-orbital is fully occupied in **1** while the p_π-orbital is fully occupied in **2**. As described previously, the lower energy configuration of these is **1** due to the stabilisation provided by the p_x-orbital gaining s-orbital character. **3** can be described as an excited singlet, formed by promotion of a σ-electron to the higher energy p_π-orbital without a change of spin. **4** is a bent, sp^2-hybridised, triplet carbene with one electron in each orbital.[7b]

The multiplicity of the carbene and thus geometry adopted is related to the energy difference between the σ and p_π-orbitals. Large energy separations favour singlet multiplicities, with occupancy only of the σ-orbital. Conversely, much smaller energy separations would favour triplet multiplicities with one electron in each orbital (σ and p_π). The α-substituents, located adjacent to the carbene centre, can have a significant effect on orbital energy separation and thus on the multiplicity and geometry of the carbene. In fact, the electronic influence of these α-substituents perhaps has the biggest effect on the multiplicity of carbenes.[7b]

The electronic effect of the α-substituents can be split into two components; an inductive effect (I effect) and a mesomeric effect (M effect).[7b] An inductive effect is defined as the polarisation of a bond between two atoms of differing electronegativities.[8] Electronegative atoms such as oxygen and nitrogen, for example, tend to withdraw electron density towards themselves and away from the more electropositive element to which they are bound. This is a negative inductive effect. With respect to a carbenic centre, an α-substituent which exerts a negative inductive (-I) effect would act to withdraw electron density away from the σ-orbital, thus lowering it in energy relative to the p_π-orbital. Hence, the energy separation between the σ and p_π-orbitals is increased, favouring singlet multiplicity and a bent geometry.[7b]

The mesomeric effect is frequently referred to as the resonance effect and is propagated by movement of π-electron density through a conjugated system. Generally, functional groups

containing π-bonds such as carbonyl, nitro and cyano groups act to withdraw π-electron density and are said to impart a negative mesomeric (–M) effect. On the other hand, groups which do not contain π-bonds but which do possess a lone pair of electrons can donate this towards the rest of the molecule.[8] Hence, groups which contain a donatable lone pair of electrons are called +M groups. In the case of carbenes, when the α-substituent provides a +M effect, such as an amino group for instance, the nitrogen atom acts to donate its lone pair towards the empty p_π-orbital of the carbenic centre. Therefore, the p_π-orbital is raised in energy relative to the σ-orbital, giving a greater orbital energy separation, which favours singlet multiplicity and a bent geometry.[7b]

Steric effects can also be very important in determining carbene geometry, though this is typically only the case when electronic effects are limited. Bulky α-substituents can act to increase the carbene bond angle towards linearity due to steric clashing, and thus can act to confer triplet multiplicity on the carbenic centre.[7b]

1.4 *N*-Heterocyclic Carbenes (NHCs)

N-Heterocyclic carbenes (NHCs) are examples of diaminocarbenes, *i.e.* both of the α-substituents attached to the carbenic centre are amino groups. Many of the NHCs reported to date are 5-membered rings (see Figure 1.6 for archetypal examples) due to their stability and relative ease of synthesis, though examples of 6-, 7- and even 8-membered NHCs have been reported.[9] Due to their cyclic structure, they are constrained to having a bent geometry with an N-C-N bond angle of between 100-110°.[7b] Partly as a result of this geometrically imposed bent geometry, and partly due to the two α-amino substituents, which provide strong –I and +M effects, NHCs contain sp^2 hybridisation and singlet multiplicity at their carbenic centre, with a pair of electrons in the σ-orbital and an empty p_π-orbital.

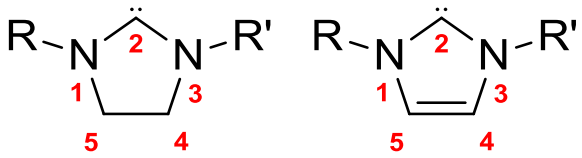

Figure 1.6 Generalised 5-membered NHC structures

The R-N-C-N-R bond of NHCs (and diaminocarbenes generally) is always planar,[7b] which implies that a significant degree of nitrogen lone pair delocalisation occurs into the empty p_π-orbital. Thus, the N-C-N bond specifically, possesses a significant degree of double bond character (Figure 1.7).

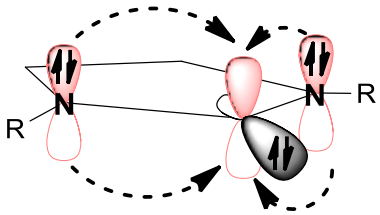

Figure 1.7 Delocalisation of nitrogen lone pair electron density into the p_{π}-orbital

As illustrated in Figure 1.6, the NHC ring can be fully saturated (left) or can contain a degree of unsaturation (right). Saturated 5-membered NHCs are known as imidazolidin-2-ylidenes, while their unsaturated counterparts are known as imidazol-2-ylidenes.[10] It may be assumed that imidazol-2-ylidenes are aromatic on the basis that they contain six π-electrons, which is in accordance with Hückel's rule of aromaticity. However, the aromaticity is not as pronounced as expected,[11] and it is important to note that the degree of aromaticity (or lack of therein) is not the major stabilising factor for NHCs. Indeed, imidazolidin-2-ylidenes (saturated) are stable and isolable, despite their lack of aromaticity.[7b] It is likely that the –I and +M effects provided by the two α-amino substituents confer the greatest stabilising effect on NHCs.

1.5 Metal-Carbene Bonding

A metal-carbene complex can be represented by the formula L_nM-CRR' (L = ancillary ligands, M = transition metal, R/R' = α-substituents). Typically, carbenes complexed to metals are classified as either Fischer-type or Schrock-type carbenes. This classification is based on the nature of the interaction between the metal and carbenic centre and therefore, more broadly, on the type of metal (oxidation state, group) and R/R' groups (π-donor or not) involved.

Fischer-type carbenes are often reported as bound to low oxidation state, electron-rich metal centres (*e.g.* Mo^0),[12] and contain an α-substituent with a lone pair of electrons, which can be donated into the p_{π}-orbital of the carbenic centre. Donation of the lone pair of electrons increases the orbital energy of the carbenic p_{π}-orbital (LUMO), thus making the π-electron density in the M-C bond more concentrated towards the metal, due to the metal d-orbital being lower in energy than the carbenic p_{π}-orbital.[7c, 13] The orbital interactions in Fischer-type carbene-metal complexes are illustrated below in Figure 1.8.

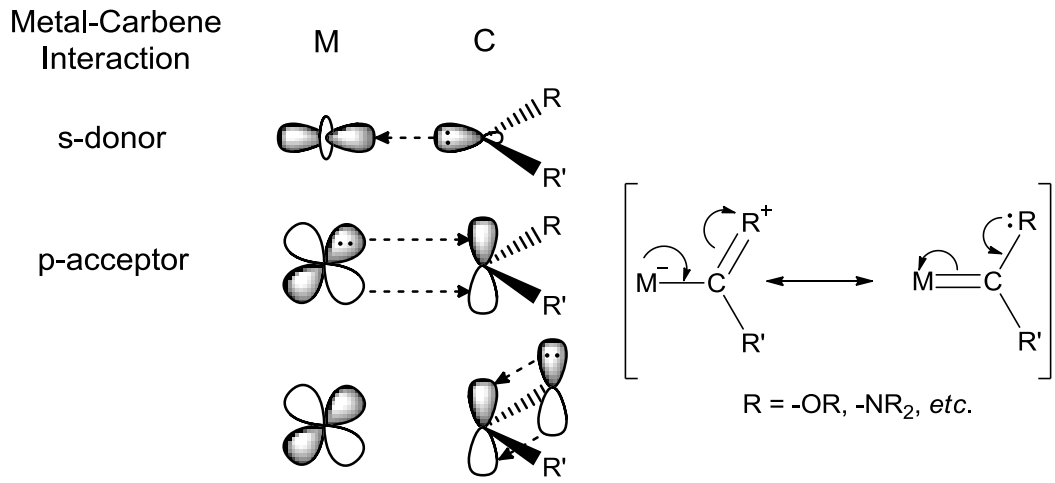

Figure 1.8 Orbital diagram and resonance structures representing the bonding in Fischer-type carbene-metal complexes[7c, 13]

Schrock-type carbenes are often found bound to higher oxidation state metals centres (*e.g.* Ti^{IV}),[14] and contain α-substituents incapable of providing a mesomeric effect; alkyl groups being an example. As a result, the carbenic p_π-orbital (LUMO) is lower in energy than the metal d-orbital allowing the π-electron density to be polarised towards the carbenic centre, making it nucleophilic.[7c, 13] The orbital interactions found in Schrock-type carbene-metal complexes are illustrated below (Figure 1.9).

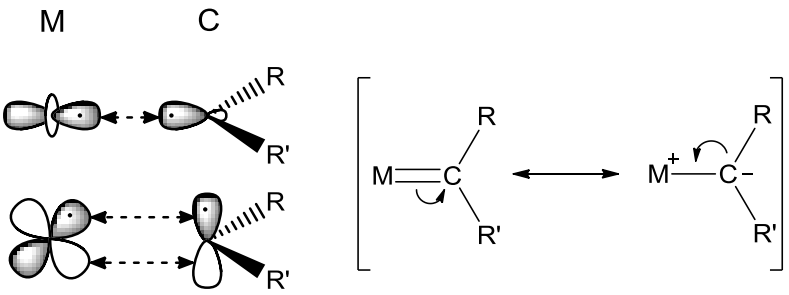

Figure 1.9 Orbital diagram and resonance structures representing the bonding in Schrock-type carbene-metal complexes[7c, 13]

N-Heterocyclic carbenes, unlike Fischer and Schrock-type carbenes, are relatively stable and do not necessarily have to be assembled in the coordination sphere of the metal. Metal-NHC bonding is most evocative of Fischer-type carbenes,[7c] though there are significant differences. Both of the α-substituents of NHCs are electron lone pair-bearing amine groups, which act to provide a strong +M effect, donating π-electron density towards the empty p_π-orbital of the carbenic centre. As a result, the carbenic p_π-orbital (LUMO) is elevated far beyond the metal d-orbital in energy, which means that π-backbonding from the metal to the carbenic centre is greatly reduced.[15] Thus, metal-NHC bonding occurs mainly *via* a σ-donor interaction (Figure 1.10). However, it should be noted that by judicious choice of the substituents attached to the backbone carbon atoms (labelled C4 and C5 – Figure 1.6) of the NHC ring, the ability of the

NHC to partake in π-backbonding from the metal centre can be increased. For example, by electron-deficient pyrimidine annulation of an NHC, the degree of π-backdonation from the metal centre to the NHC can be increased markedly.[16]

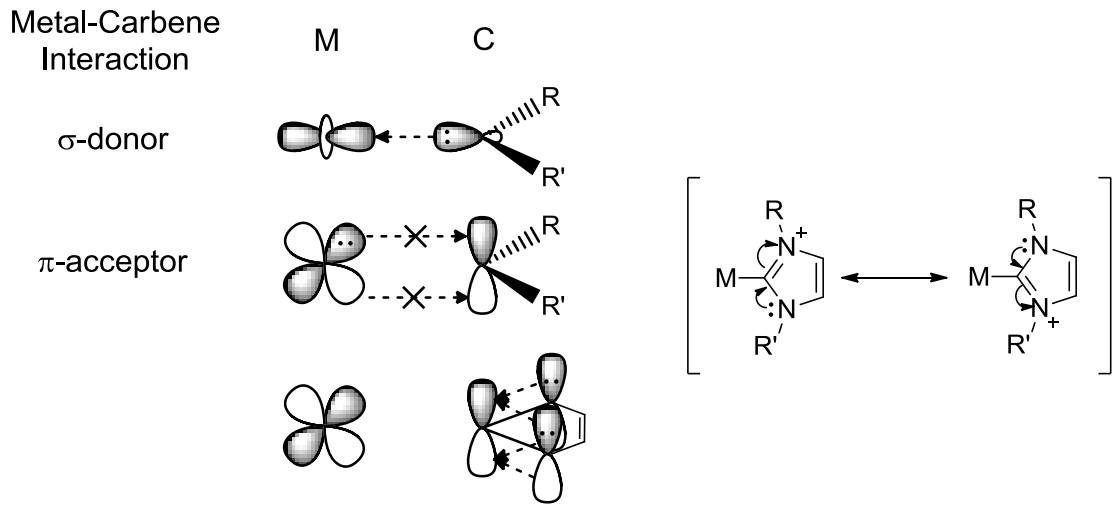

Figure 1.10 Orbital diagram and resonance structures representing the bonding in NHC-metal complexes[7c, 13]

NHCs are commonly considered as analogues of tertiary phosphine ligands in light of the extremely strong σ-donor capacity (and therefore nucleophilicity) of both classes of ligand.[17] They differ slightly with regards to π-backbonding ability though; π-backbonding generally being weak in NHCs[15] but present to a greater extent in phosphines. However, the substitution of tertiary phosphines for NHCs when forming a metal complex can produce several advantageous properties. One such property is that NHC ligands tend to exhibit stronger bonding to metals than phosphines, thus, the resulting metal-NHC complex displays greater thermal stability and undergoes decomposition much more slowly. NHCs also tend to be stronger σ-donors than phosphines, leading to increased electron density on the metal centre, which sometimes can confer superior catalytic activity on the resultant metal complex. Another advantage of using NHC ligands in place of phosphines is that they can be produced by facile syntheses, *in situ*, in high yields.[17]

1.6 Early Reports of *N*-Heterocyclic Carbenes

In 1962, Wanzlick noted the strong nucleophilicity of the carbene species that would later become known as *N*-heterocyclic carbenes, and suggested that this area of chemistry had much scope for further research.[18] Six years later, in 1968, Öfele and Wanzlick independently reported NHC complexes of d-block metals; Öfele a chromium complex (Scheme 1.1a)[19] and Wanzlick a mercury complex (Scheme 1.1b).[20] Both syntheses involved the *in situ* metallation of an imidazolium salt, which is an NHC precursor, with a basic metal reactant.[17]

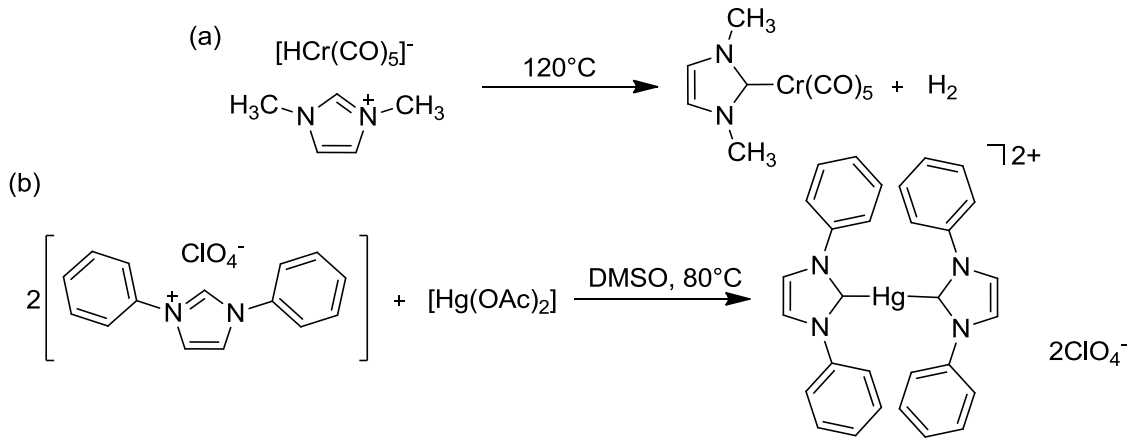

Scheme 1.1 The first metal-NHC complexes and their syntheses (a) Cr^0-NHC complex reported by Öfele[19] (b) Hg^{II}-NHC complex reported by Wanzlick[20]

Work continued on NHC chemistry, and in 1991 a major breakthrough occurred, with the isolation of the first stable free NHC by Arduengo *et al*..[21] An imidazol-2-ylidene bearing adamantyl *N*-substituents was synthesised by the deprotonation of the corresponding imidazolium salt by NaH (in the presence of a catalytic volume of dimethyl sulfoxide) in THF (Scheme 1.2), and could be isolated in the absence of water and oxygen.

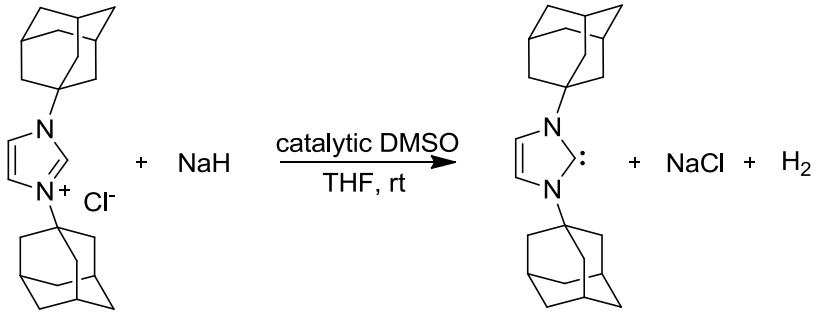

Scheme 1.2 Synthesis of the first stable free *N*-heterocyclic carbene[21]

More recently, there has been an explosion of interest in the chemistry of NHCs,[7a] which has incorporated novel synthetic routes for their synthesis, their individual properties as molecules and their coordination properties. This is embodied by the isolation and characterisation of a range of structurally diverse stable *N*-containing free carbenes including triazol-5-ylidenes,[22] imidazolidin-2-ylidenes,[23] acyclic diamino-2-ylidenes,[24] thiazol-2-ylidenes,[25] imidazol-5-ylidenes[26] and even alkylaminoylidenes.[27]

1.7 The Synthesis of Transition Metal-NHC Complexes

The transition metals vary profoundly in terms of their availability as reactive and soluble metal salts and their behaviour with potential ligands. This, along with the varied structural features and reactivity of NHC precursors, prevents there from being a universally effective method for transition metal-NHC complex synthesis. As a result, a wide range of synthetic routes have been

developed for the formation of transition metal-NHC complexes. The method chosen to synthesise a desired transition metal-NHC complex will therefore often depend on the transition metal and, indeed, NHC precursor involved, but will also sometimes depend simply on a researcher's personal experience and preference. As such, this section aims to guide the reader through the various synthetic methodologies reported to date, whilst giving examples of the successful implementation of these synthetic protocols.

1.7.1 Transmetallation from Ag^{I}

Arguably, the most widely used method for transition metal-NHC complex synthesis is *via* transmetallation of the NHC ligand from a Ag^{I}-NHC complex to a suitable metal precursor. In this instance, the Ag^{I}-NHC complex is acting, in effect, as a latent free NHC. Transmetallation of the NHC ligand from silver to another transition metal is able to occur due to the relatively low bond strength of Ag-NHC bonds compared to other transition metal-NHC bonds.[28] Thus, cleavage of the Ag^{I}-NHC bond and formation of a different transition metal-NHC bond is a thermodynamically favourable process. Furthermore, when the Ag^{I}-NHC complex or metal precursor contains a halide, the transmetallation process is accompanied by the formation of a silver halide, which owing to its high lattice enthalpy, precipitates immediately from solution. The formation and precipitation of silver halide during these reactions acts as an extremely strong thermodynamic driving force.

The first example of a Ag^{I}-NHC complex was reported by Arduengo *et al.* in 1993.[29] However, the transmetallation potential of these complexes did not become apparent until 1998, when Lin *et al.* described separate examples of transmetallation from a Ag^{I}-NHC complex onto both Au^{I} and Pd^{II} (Scheme 1.3).[30]

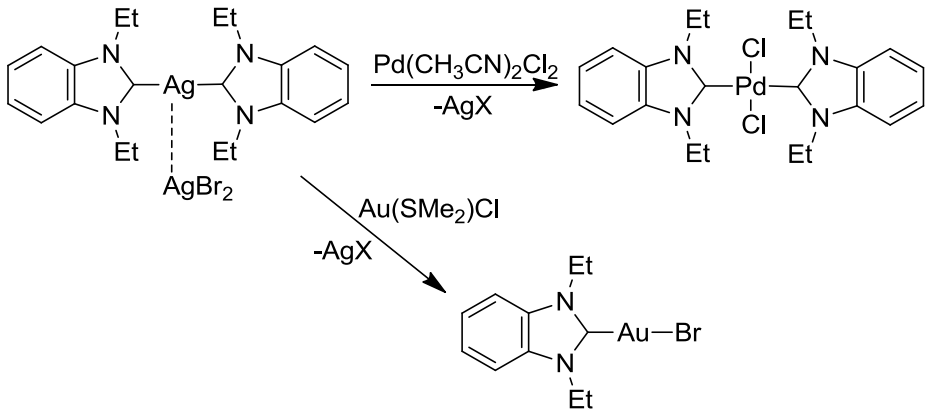

Scheme 1.3 Synthesis of Pd^{II}- and Au^{I}-NHC complexes from a Ag^{I}-NHC complex[30]

Since this initial report, the transmetallation from Ag^{I} route has been utilised a multitude of times for the synthesis of a vast range of NHC complexes, most of which contain mid-to-late transition metal ions.[31]

1.7.2 Transmetallation from Other Transition Metals

The transmetallation of an NHC ligand from other (*i.e.* not Ag^{I}) transition metals has been described by a number of research groups. The general premise is the same as for transmetallation from a Ag^{I}-NHC, in that the transmetallation reaction produces a compound with a stronger metal-NHC bond than that found in the starting material. Transmetallation from Cu^{I},[32] Ni^{II} [33] and Zr^{IV}-NHC [34] complexes amongst others has been reported, with an illustrative example being given below in Scheme 1.4.

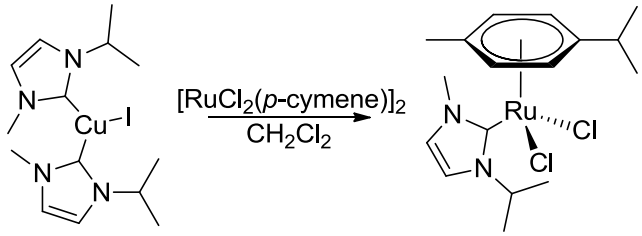

Scheme 1.4 Transmetallation of an NHC from a Cu^{I}-NHC complex to a Ru^{II} centre[32a]

1.7.3 Interaction with a Free NHC

Transition metal-NHC complexes can also be formed *via* the generation of a free NHC by reaction of an imidazolium salt with a strong base. Typical bases used for this reaction include NaH and ^{n}BuLi, which are examples of strong bases.[17] A strong base is required to form the free NHC, since the pK_a of an imidazolium is generally between 20 and 25. The free NHC, once formed, is highly nucleophilic, and thus must be kept under scrupulously anhydrous and anaerobic conditions to prevent decomposition. Once the free NHC has been formed, it may be isolated and characterised and then added to an appropriate transition metal compound to form the corresponding transition metal-NHC complex.

Scheme 1.5 depicts an example of the use of this method for the synthesis of a Rh^{I}-NHC complex of a C_2-symmetric ligand. First, the free NHC is formed by deprotonation of the starting imidazolium triflate salt using potassium *bis*(trimethylsilyl)amide as the base. Then, a Rh^{I} salt is added to a solution of the free carbene at low temperature in THF, to form the corresponding *cis*-chelated Rh^{I}-NHC complex shown.[35]

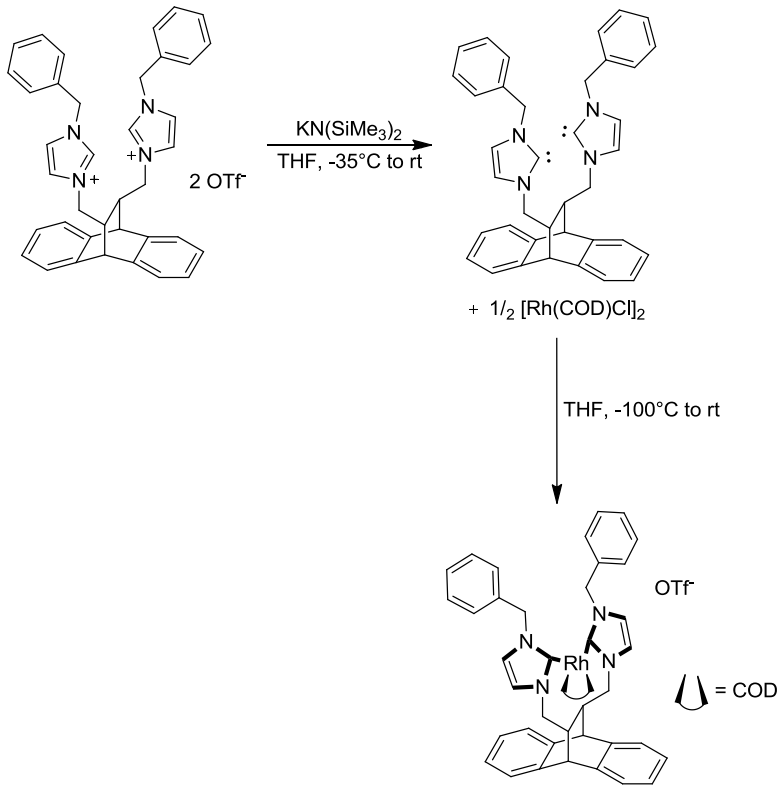

Scheme 1.5 Synthesis of a Rh^{I}-NHC complex *via* a free NHC[35]

The above example of transition metal-NHC complex synthesis *via* interaction of a metal salt with a free NHC is just one of perhaps hundreds of examples reported in the literature to date, which have described the synthesis of NHC complexes of metals from right across the transition metal series.[34, 36]

1.7.4 *In Situ* Deprotonation and Metallation

A related method of transition metal-NHC complex synthesis is the *in situ* deprotonation of the imidazolium salt, followed by metallation, meaning that the free NHC is not isolated. This method is useful in the respect that deprotonation can be effected by both strong bases (like those mentioned for the free NHC method), and weaker bases such as NEt_3 and K_2CO_3. The synthesis of a range of transition metal complexes has been described using this method,[37] with an example of its use being given in Scheme 1.6. This example depicts the synthesis of a Au^{I}-NHC complex *via* a protocol which was concurrently and independently reported by the groups of Gimeno[37d] and Cazin.[37a]

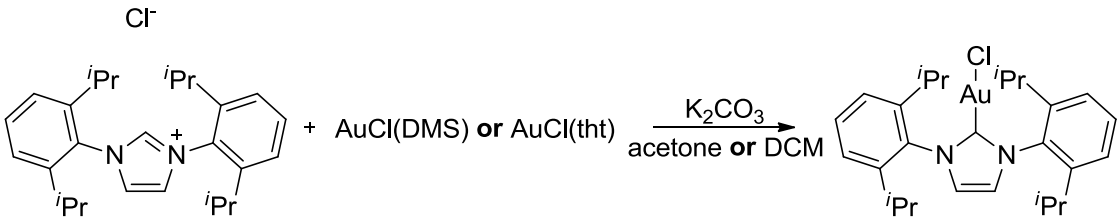

Scheme 1.6 Synthesis of Au^{I}-NHC complex by *in situ* deprotonation and metallation[37a, 37d]

1.7.5 *In Situ* Metallation with a Basic Metal Precursor

The first method of transition metal-NHC complex synthesis to be reported was that used by both Öfele and Wanzlick in 1968, when they independently synthesised NHC complexes of transition metals (Scheme 1.1).[19-20] Namely, it is the direct metallation of an imidazolium salt by a basic metal reactant. This method, like those described above, takes advantage of the relatively acidic nature of the imidazolium proton at the C2 position of the ring. The basic metal reactants tend to be oxides, acetates, alkoxides or amides.[38] For instance, Tulloch *et al.* reported the synthesis and characterisation of a novel pyridyl-substituted Cu^{I}-NHC complex using Cu_2O as the basic metallating reagent (Scheme 1.7).[38b] The reaction proceeded with a good yield and was the first example of the use of Cu_2O in this manner.

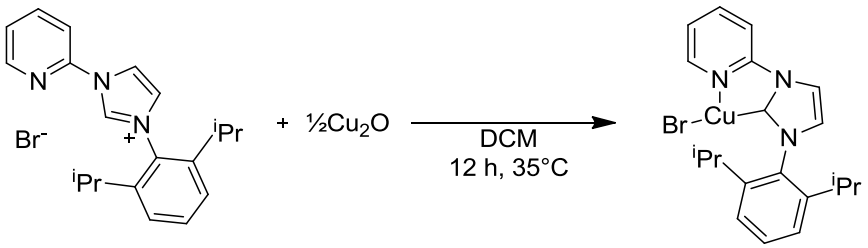

Scheme 1.7 Synthesis of a Cu^{I}-NHC complex using Cu_2O as both the base and metallating reagent[38b]

This method of metal-NHC synthesis can be applied not only to the late transition metals, but also to the lighter transition metals. Ohki *et al.* prepared a half sandwich Fe^{II}-NHC complex using an Fe^{II}-amide as the basic metallating reagent (Scheme 1.8).[39] The paramagnetic, coordinatively unsaturated, 16-electron complex formed is extremely air and moisture sensitive.

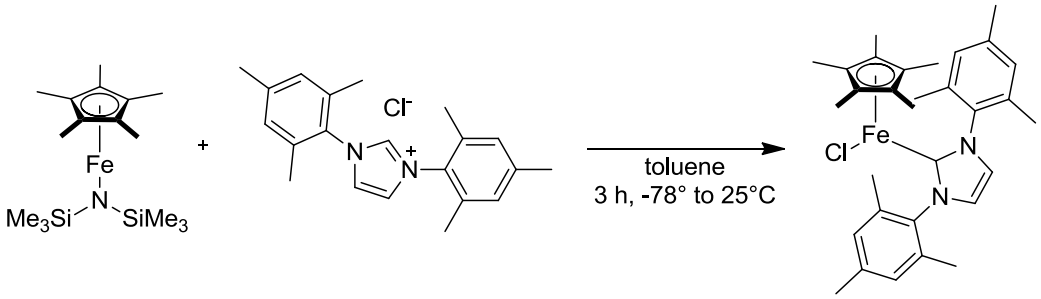

Scheme 1.8 Synthesis of an Fe^{II}-NHC complex using an Fe^{II}-amide[39]

1.7.6 Oxidative Addition

Transition metal-NHC complexes can be synthesised *via* oxidative addition of a C2-X (X = methyl, halide or H) bond to a low valent transition metal or metal hydride.[17, 40] For example, Albrecht *et al.* demonstrated the synthesis of an abnormally-bound Pd^{II}-NHC complex *via* the facile oxidative addition of a C4-I bond to a Pd^{0} starting material (Scheme 1.9).[40b]

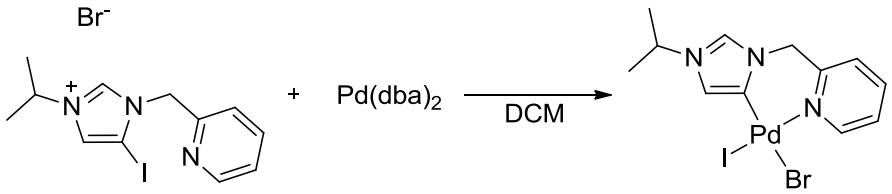

Scheme 1.9 Synthesis of a Pd^{II}-NHC *via* oxidative addition of a C-I bond to Pd^{0}[40b]

In related work, Peris *et al.* described the reaction of a *bis*-imidazolium precursor with an Ir^{I} starting material in the presence of the base NEt_3, initially to form an Ir^{I}-NHC complex where only one of the imidazoliums has been deprotonated and bound to the iridium. On standing in the absence of base, the C2-H bond of the unbound imidazolium undergoes oxidative addition to the iridium centre, forming the Ir^{III}-*bis*-NHC hydride complex (Scheme 1.10).[40a]

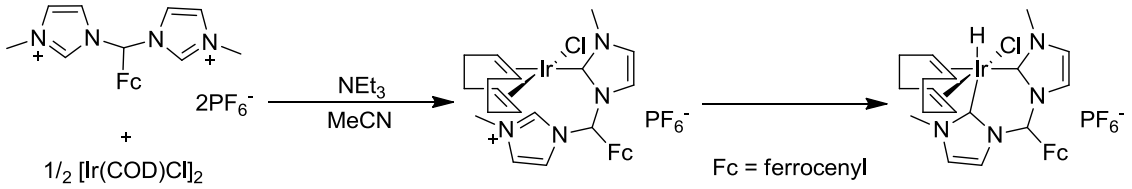

Scheme 1.10 Synthesis of a Ir^{III}-*bis*-NHC hydride complex through oxidative addition of a C2-H bond to an Ir^{I}-NHC complex[40a]

1.7.7 Insertion in to the C=C Bond of an Enetetraamine (Lappert Method)

The so-called Lappert method of transition metal-NHC complex synthesis involves the addition of an enetetraamine, effectively an imidazolidin-2-ylidene dimer, to a low valent transition metal to form an NHC complex. This method was first reported by Lappert *et al.* in the 1970's, where the synthesis of Cr, Fe, Rh, Ir, Ni, Pd, Pt and Au-NHC complexes was reported. Scheme 1.11 illustrates the formation of a Pt^{II}-NHC complex using this method.[41]

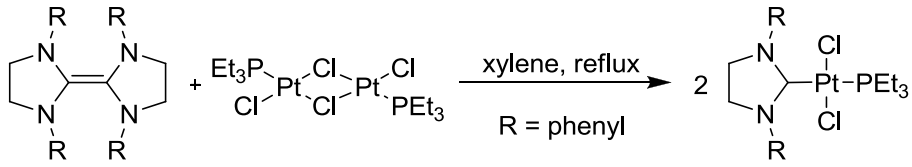

Scheme 1.11 Synthesis of a Pt^{II}-NHC complex using the Lappert method[41a]

1.7.8 Thermolysis and Metallation of a C2-Protected Precursor

Thermal elimination of H-X from the C2 position of an alcohol or chloroform-NHC adduct (a 'protected' form of the NHC) can yield a free NHC, which in the presence of a suitable metal precursor can form a transition metal-NHC complex. Grubbs *et al.* demonstrated the efficacy of this method when they used it to synthesise a Grubbs 2nd generation-type catalyst by initial elimination of methanol under vacuum from an alcohol-NHC adduct. This formed the free

NHC, which rapidly reacted with the Ru-based precursor, forming the desired product (Scheme 1.12).[42]

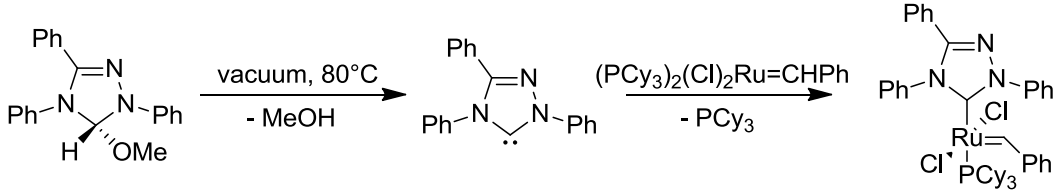

Scheme 1.12 Synthesis of a Grubbs 2nd generation-type catalyst using the thermal elimination of methanol[42]

1.7.9 Electrochemical Methods

A more unusual method for the synthesis of a transition metal-NHC complex was reported by Chen *et al.* at the start of 2011. An electrochemical process was used to form a variety of Cu^{I}, Cu^{II}, Ni^{II} and Fe^{II}-NHC complexes. Each of the electrochemical reactions occurs at room temperature in an undivided glass cell in acetonitrile. During the reaction, reduction of the imidazolium cation occurs at the cathode to form the free NHC, and releasing molecular hydrogen. Concurrently, oxidation of the metal of the (sacrificial) anode occurs, forming metal ions which are released. In solution, the free NHC and metal ion(s) combine, forming a stable metal-NHC complex (Scheme 1.13).[43]

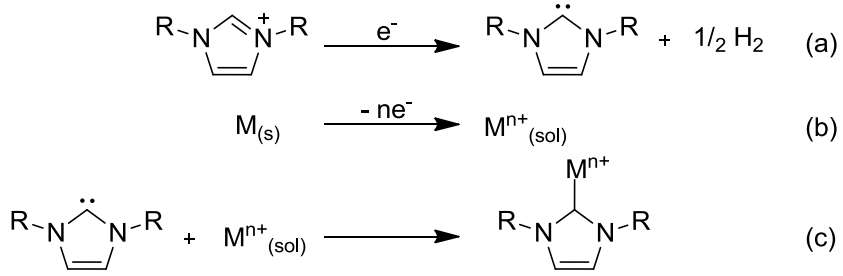

Scheme 1.13 Processes occurring at the cathode (a), anode (b) and in solution (c)[43]

This process of transition metal-NHC complex formation can be thought of as analogous to that using a strong base to form the free NHC. As with the strong base method, the solvent used during this method should be anhydrous and anaerobic, in order to prevent decomposition of the free NHC present in solution. Scheme 1.14 illustrates an example of this process.

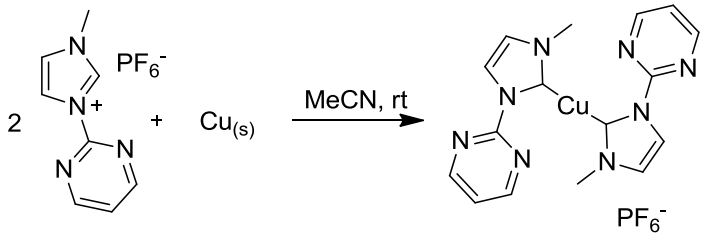

Scheme 1.14 Synthesis of a Cu^{I}-*bis*-NHC using an electrochemical procedure[43]

Notably, the electrochemical reduction of an imidazolium to form a free NHC had been reported previously by Gorodetsky *et al.* in 2004.[44] Subsequently, Feroci *et al.*[45] and Orsini *et al.*[46] amongst others have reported the electrochemical synthesis and use of free NHCs as strong bases in organic reactions. However, the application of this technique for the synthesis of transition metal-NHC complexes had not been published prior to the report of Chen *et al.*.[43]

1.7.10 Reaction of Imidazolium Salt with Metal Powders

Another unusual method for the synthesis of transition metal-NHC complexes was again reported by Chen *et al.* in 2009.[38a] A variety of metal complexes of pyridyl-substituted *N*-heterocyclic carbene complexes were synthesised by heating a metal powder and an imidazolium salt in acetonitrile in air for several days. Fe^{II}, Co^{II}, Ni^{II} and mixed-valent Cu-NHC complexes were all synthesised using this method. The Fe^{II} and Co^{II}-NHC complexes are particularly notable due to the fact that, though they are 14 and 15-electron complexes respectively, they are both air and moisture stable. The Fe^{II}-NHC and Co^{II}-NHC bonds are reported to be much shorter than previously characterised 16-18-electron Fe^{II} and Co^{II}-NHC complexes, presumably due to increased σ-electron donation to the electron-deficient metal centre from the NHC. Scheme 1.15 illustrates an example of a complex formed using this synthetic procedure.

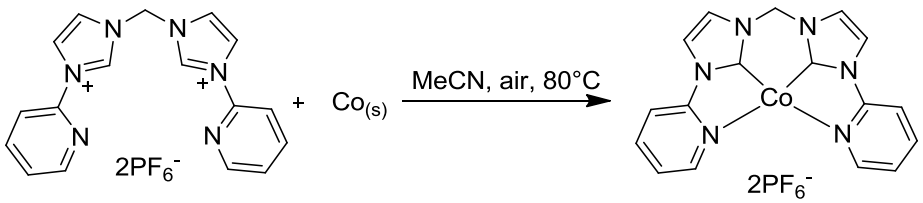

Scheme 1.15 Synthesis of a Co^{II}-NHC complex by the reaction of a metal powder with an imidazolium salt in air[38a]

1.7.11 Templated Synthesis from Isonitriles

The final method of transition metal-NHC complex synthesis to be described, is a templated synthetic protocol reported recently by Hashmi *et al.*.[47] In one paper, the synthesis of a range of Pd^{II}-NAC (*N*-acyclic carbene) and Pd^{II}-NHC complexes was described by reaction of a readily synthesised Pd^{II}-isonitrile complex with an amine or a 2-(chloroethyl)amine. An example of this synthetic protocol is illustrated in Scheme 1.16.

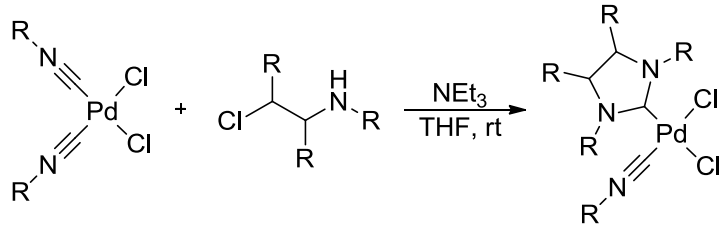

Scheme 1.16 Templated synthesis of a Pd^{II}-NHC complex from a Pd^{II}-isonitrile complex[47b]

1.8 Selected Examples of Transition Metal-NHC Complexes

The versatility of NHCs as ligands is clear when we consider that NHCs are known to form complexes with every transition metal element. The nature of the metal ions changes quite markedly across the d-block and thus normally, so does the structure of the NHC ligand employed to complex the metal.

The early transition metals are generally harder and more electropositive than the later transition metals. As a result, they typically interact most strongly with ligands containing alkoxide, aryloxide and amido donors; with the metal-ligand interaction containing a large ionic component. Thus, to synthesise stable metal-NHC complexes of these early transition metals, alkoxide,[48] aryloxide[49] or amido[50] anionic tethers are frequently used as substituents on the NHC, giving rise to a potentially multidentate ligand.[7a]

For instance, in work reported by Arnold *et al.*, alkoxide-tethered early transition metal-NHC complexes can be synthesised with the use of epoxides. During the synthesis, an *N*-substituted imidazole ring-opens the epoxide forming an alcohol tethered imidazolium salt. Subsequent deprotonation of the alcohol and imidazolium by reaction with a strong base such as ^{n}BuLi, KH, $LiN(SiMe_3)_2$ or $KN(SiMe_3)_2$, affords an alkali metal-NHC complex. These complexes can then allow the facile synthesis of early transition metal complexes *via* a transmetallation step. For example, the full synthesis of a Ti^{IV}-NHC complex as described by Arnold *et al.* is provided in Scheme 1.17.[7a, 48, 51]

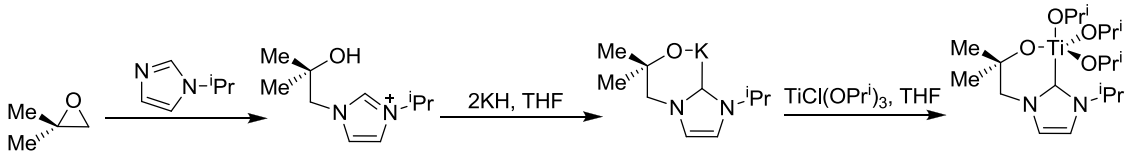

Scheme 1.17 Synthesis of a Ti^{IV}-NHC complex containing an alkoxide tether[7a, 48, 51]

The use of anionic tethers is not just limited to the early transition metals however. Transition metal-NHC complexes of the softer, late transition metals bearing anionic tethers are also known. For example, Douthwaite *et al.* described the synthesis of a Pd^{II}-NHC complex of a chiral phenoxyimine-tethered NHC ligand. Synthesis involves reaction of a chiral amine-

tethered imidazolium salt with a substituted 2-hydroxybenzaldehyde, leading to the chiral phenolimine-tethered imidazolium salt. Reaction of this precursor with a basic metal reagent, $Pd(OAc)_2$, leads to a [Pd(κ^3-*CNO*)Br]-type complex where the anionic phenoxide donor group is *trans* with respect to the NHC donor (Scheme 1.18).[52]

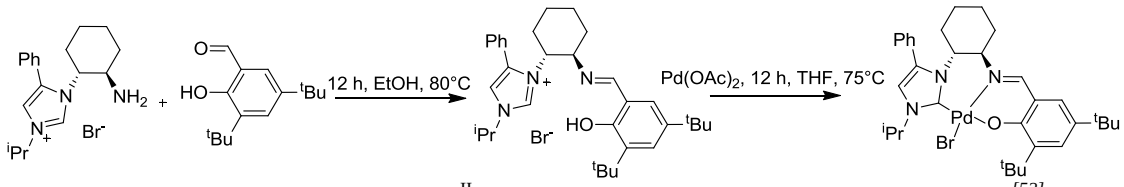

Scheme 1.18 Synthesis of a Pd^{II}-NHC complex containing an aryloxide tether[52]

It is important to highlight that there are numerous examples of transition metal-NHC complexes which do not contain anionic tethers, some of which have already been described. The strength of the interaction between the transition metal and NHC is often very high, particularly with respect to the late transition metals, thus rendering anionic tethers unnecessary to facilitate the formation of a stable transition metal-NHC complex. Indeed, many examples of complexes containing monodentate NHC ligands are known, a prime example of which is the Grubbs 2nd generation alkene metathesis catalyst (Fig 1.11). This complex is a highly active and functional group tolerant alkene metathesis catalyst; partly owing its efficacy to the inertness of the Ru-NHC bond, but also due to the strength of σ-electron donation by the NHC toward the Ru centre.[53]

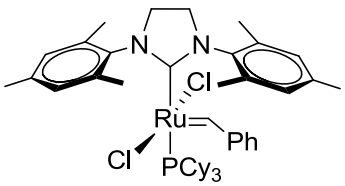

Figure 1.11 Grubbs 2nd generation alkene metathesis catalyst[53]

Multidentate NHC ligands are also widely known, for example, Kühn *et al*. recently reported examples of a number of chelating bidentate Rh^I-NHC complexes, which were tested for activity in a hydrosilylation reaction.[54] Synthesis of the imidazolium salt NHC precursors occurred *via* reaction of two equivalents of an *N*-substituted imidazole/benzimidazole/1,2,4-triazole with a dibromoalkane, and subsequent anion metathesis of Br^- with the non-coordinating PF_6^-. Complexation to the Rh centre occurred under basic conditions yielding the corresponding Rh^I-NHC complex. A typical example of the complexes formed is illustrated schematically in Scheme 1.19.

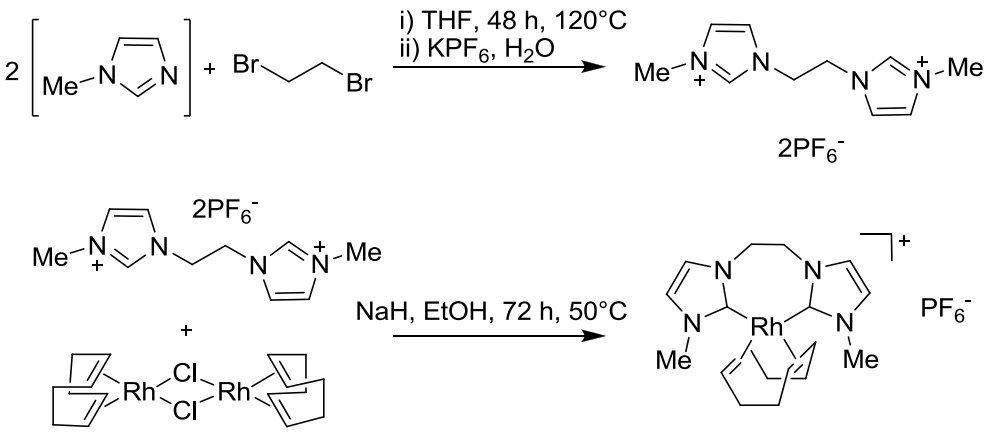

Scheme 1.19 Synthesis of a Rh^{I}-NHC complex where the NHC ligand is bidentate[54]

An elegant example of the potential stability afforded to metal complexes by coordination of NHC ligands is demonstrated in work by Peris and Crabtree *et al*.. In this work, a tridentate pincer-type ligand bearing two NHC donors and a pyridyl donor was complexed to a Pd^{II} centre, by reaction of $Pd(OAc)_2$ with an imidazolium salt under rather forcing conditions. The catalytic activity of the resulting complex was investigated in the ubiquitous Heck reaction, which is an example of a carbon-carbon bond forming reaction. The authors report that the complex is able to maintain Heck coupling activity under reflux in DEA (184°C) in air.[38c] Under these conditions, other comparative catalysts would tend to decompose, releasing palladium nanoparticles and ligand precursor. The synthesis of this catalyst and its structure is illustrated in the scheme below (Scheme 1.20).

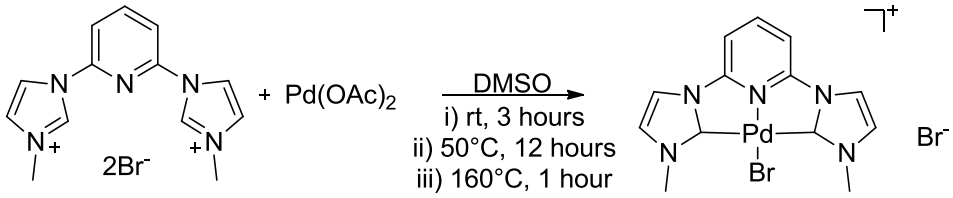

Scheme 1.20 Synthesis and structure of a thermally stable Pd^{II}-NHC Heck coupling catalyst[38c]

1.9 Copper-NHC Complexes

It might be argued that the chemistry of Cu-NHC complexes in general is less developed than that of the other group 11-NHC complexes.[55] However, in recent years the synthesis and use of Cu-NHC complexes in a variety of applications has become more attractive to researchers due to the significantly lower cost of copper compared to many of the other late transition metals.

Interest in coinage metal-NHC complexes, and specifically in Cu-NHC complexes, first began in 1993 with the isolation of the first example of a Cu^{I}-NHC complex by Arduengo *et al.*. This complex, a *bis*-NHC complex, was synthesised by interaction of two equivalents of the free

NHC, IMes (1,3-*bis*(2,4,6-trimethylphenyl)imidazol-2-ylidene), with one equivalent of the benzene solvate of Cu(CF_3SO_3) in tetrahydrofuran.[29]

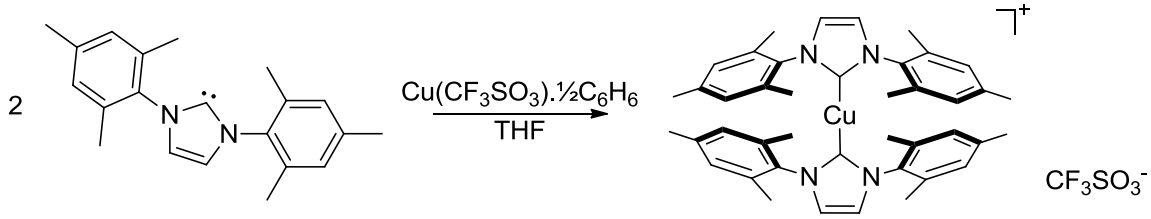

Scheme 1.21 Synthesis of the first example of a Cu-NHC complex[29]

Since this initial report, a vast array of structurally diverse Cu-NHC complexes has been reported, with perhaps hundreds of examples of Cu^{I}-NHC complexes, and a handful of examples of Cu^{II}-NHC complexes. The predominance of reports of Cu^{I}-NHC complexes over Cu^{II}-NHC complexes presumably reflects the more favourable nature of the 'soft-soft' interaction between an NHC donor and a Cu^{I} centre, when compared to a 'soft-intermediate' interaction between an NHC donor and a Cu^{II} centre.

Fascinatingly, a very recent report by Bertrand, Roesky, Kaim and Frenking *et al.* described the synthesis of two examples of Cu-NHC complexes containing copper in a formal oxidation state of zero.[56] The low valent, electron-rich Cu^{0} centre was found to be effectively stabilised by coordination of two cyclic (alkyl)(amino)carbenes (cAACs) to the Cu^{0} centre. The use of cAACs rather than conventional diaminocarbenes is vital, since cAACs are stronger σ-donors (due to having only one –I α-substituent) and thus form stronger bonds to metal centres. Furthermore, cAACs are more effective π-acceptors than diaminocarbenes (due to having only one +M α-substituent), and thus are more capable of relieving the build-up of electron density on the electron-rich Cu^{0} centre by accepting electron density in to their p_{π}-orbital. The synthesis of the Cu^{0}-NHC complex was achieved *via* a two-step procedure. Firstly, reaction of two equivalents of the free cAAC with CuI led to the formation of a Cu^{I}-*bis*-NHC complex. Then, reduction of this Cu^{I}-*bis*-NHC complex with metallic sodium in THF led to the formation of the Cu^{0}-NHC complex (Scheme 1.22).

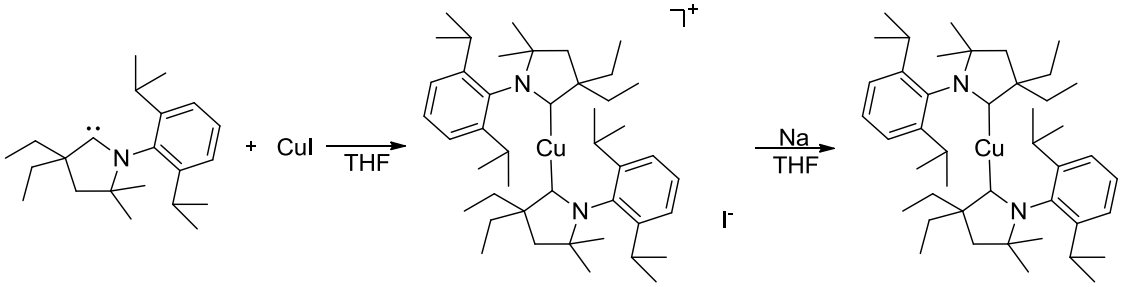

Scheme 1.22 Synthesis of the first example of a Cu^{0}-NHC complex[56]

Both the Cu^{I}-*bis*-NHC complex and Cu^{0}-*bis*-NHC complex (shown above) were fully characterised, including by X-ray diffraction analysis. The crystal structures of the two complexes revealed that, on reduction from Cu^{I} to Cu^{0}, a pronounced shortening of the Cu-$C_{carbene}$ bond occurs from between 1.95 – 1.92 Å in the Cu^{I}-*bis*-NHC complex, to between 1.87 – 1.86 Å in the Cu^{0}-*bis*-NHC complex. The molecular structure of the Cu^{0}-*bis*-NHC complex illustrated in Scheme 1.22 is given below (Figure 1.12).

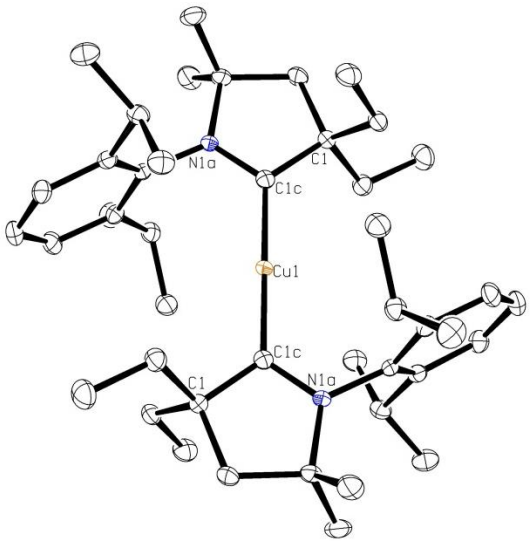

Figure 1.12 Molecular structure of a Cu^{0}-*bis*-NHC complex. Ellipsoids are drawn at the 50% probability level. H atoms have been omitted for clarity[56]

As mentioned earlier, the vast majority of reports, both on the synthesis and reactivity, of Cu-NHC complexes have involved copper in an oxidation state of one.[55] This is typified by the first reported synthesis of a Cu-NHC complex, which is shown in Scheme 1.21. Within the Cu^{I}-NHC complexes reported thus far, a major structural theme is the use of sterically very bulky *N*-substituents, such as 2,4,6-trimethylbenzene and 2,6-diisopropylbenzene. Bulky substituents such as these are used to afford the Cu^{I}-complex enhanced stability, by sterically protecting the carbene and metal centres. It has been noted that the use of much less bulky alkyl substituents, for example, accelerates the rate of decomposition of the resultant complex significantly, with hydrolysis appearing to be the most significant degradation pathway.[32a]

The stability of Cu^{I}-NHC complexes containing bulky *N*-substituents has seen their application as catalysts in a number of different transformations, the first example of which was reported in 2001 by Woodward *et al.*.[57] In this example, the addition of a catalytic quantity of the imidazolium salt, 1,3-*bis*(2,4,6-trimethylphenyl)imidazolidin-2-ylidene (SIMes), to a conjugate addition reaction (containing a copper source) was found to significantly enhance the rate of reaction. Since this early work, a number of examples of the use of well-defined Cu^{I}-NHC complexes containing sterically bulky NHC ligands in homogeneous catalytic processes have

been reported, including in the reduction of carbonyl compounds, in cyclopropanation reactions, in hydrosilylation reactions and in the [3 + 2] cycloaddition reaction of azides and alkynes.[58]

The Ullmann coupling reaction is, arguably, the prototypical Cu-catalysed process, having first been reported in 1901,[59] and having since been modified to encompass a range of cross-coupling reactions for the formation of C-C, C-N and C-O bonds to name but a few.[60] However, the use of NHC ligands to promote these important bond-forming reactions has been surprisingly rare, comprising only a handful of examples to date. Indeed, the first uses of NHC ligands in Ullmann-type chemistry were reported separately by Vicic *et al.* and Biffis *et al.* as late as 2008.[61] In the example reported by Vicic *et al.*, it was found that a well-characterised trifluoromethylated Cu^{I}-NHC complex could efficiently trifluoromethylate a range of aryl iodides under extremely mild reaction conditions, though the reactions were stoichiometric in the copper reagent, rather than catalytic. Scheme 1.23 illustrates an example of the use of this reaction.

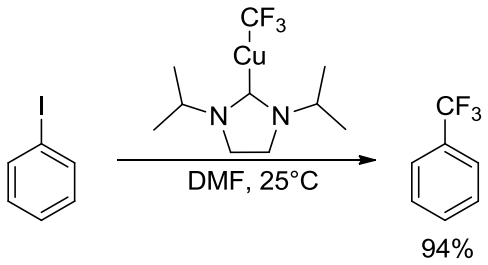

Scheme 1.23 Trifluoromethylation of iodobenzene using a Cu^{I}-NHC complex[61a]

On the other hand, Biffis *et al.* reported the catalytic application of a trinuclear Cu^{I}-NHC complex in a range of Ullmann-type coupling reactions, including the coupling of aryl halides with pyrazole, imidazole, 1,2,4-triazole and a range of phenols.[61c] Examples of some of these reactions, and the structure of the trinuclear complex, is provided in Scheme 1.24. The reactions reported generally illustrate the trend that Ullmann-coupling chemistry occurs most efficiently for aryl halides containing electron-withdrawing groups and that reactivity of the aryl halide follows the order I > Br > Cl.[60] Notably however, no examples of the reactions being performed in the absence of NHC ligand (but with a copper source) were reported, which begs the question of whether the NHC ligand is having any effect (positive or negative) at all on the efficiency of the reactions.

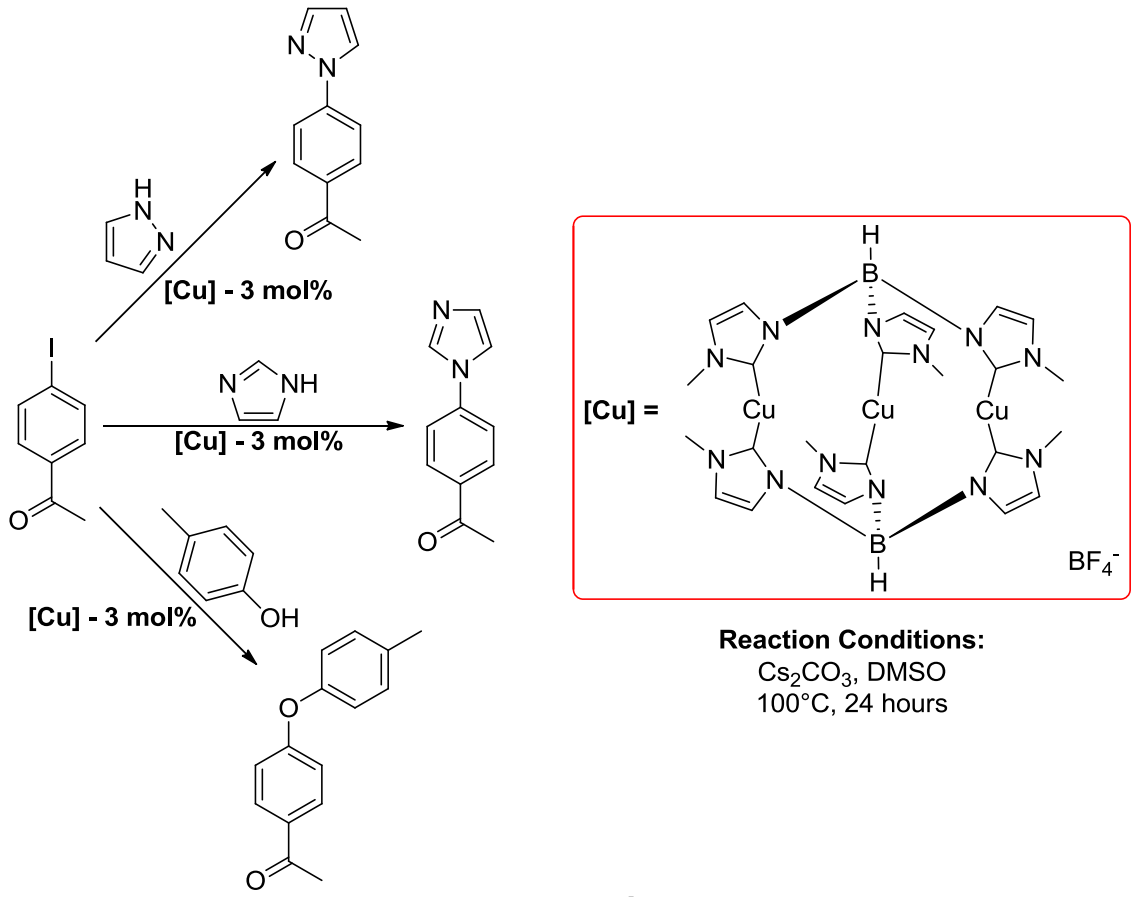

Scheme 1.24 Examples of the use of a trinuclear Cu^{I}-NHC complex in Ullmann-type coupling reactions[61c]

Since these first examples, two further reports of the use of trinuclear Cu^{I}-NHC complexes in Ullmann-type coupling reactions have been published by Biffis *et al.*, in 2009, and Whittlesey *et al.* in 2010.[62]

As described earlier, there are relatively few examples of well-characterised Cu^{II}-NHC complexes. Indeed, attempted formation of such complexes often meets with failure.[63] However, a couple of different strategies have been devised to help stabilise a Cu^{II}-NHC bond sufficiently to allow isolation of the resultant complex. For instance, Yun *et al.* reported the synthesis of a catalytically-active (in the 1,2- and 1,4-reduction of carbonyl compounds under hydrosilylation conditions) Cu^{II}-NHC complex with the use of stabilising acetate ligands.[64] Subsequently, Nechaev *et al.* reported the synthesis of a related range of acetate-stabilised Cu^{II}-NHC complexes, using sterically bulky *N*-substituents and 5-, 6- and 7-membered NHC rings.[63b] Interestingly, while Yun *et al.* report that their Cu^{II}-NHC complex is air stable, Nechaev *et al.* report that on exposure to atmospheric moisture, one of their complexes undergoes a ring-opening reaction of the NHC ligand to form a formamide.[63b, 64] Examples of the acetate-stabilised Cu^{II}-NHC complexes are given in Figure 1.13.

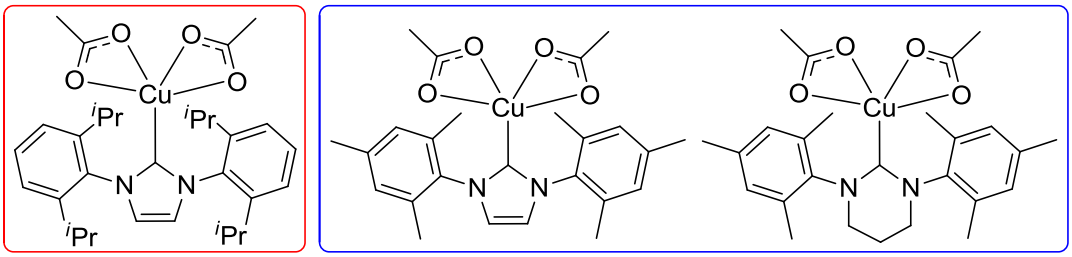

Figure 1.13 Acetate-stabilised structurally characterised Cu^{II}-NHC complexes reported by Yun *et al.* (red box)[64] and Nechaev *et al.* (blue box)[63b]

A related strategy for the stabilisation of Cu^{II}-NHC complexes is the use of a tethered anionic oxygen donor, such as an alkoxide, phenoxide or amidate. This strategy relies on the strength of the interaction between the hard oxygen donor and Cu^{II} centre maintaining the copper ion within the vicinity of the NHC, preventing complex degradation, even if NHC decoordination occurs. For example, Arnold *et al.* utilised an alkoxide tether to stabilise a copper centre, in what was the first structurally characterised example of a Cu^{II}-NHC complex (Figure 1.14).[65]

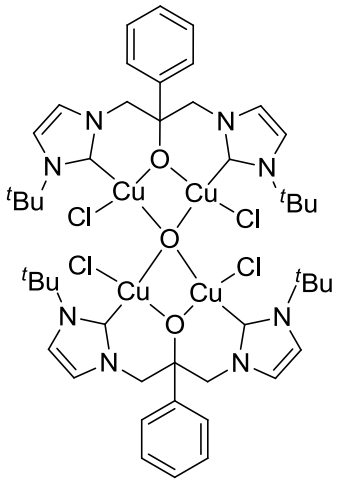

Figure 1.14 First structurally characterised example of a Cu^{II}-NHC complex[65]

In two separate reports, Hoveyda *et al.* have used the anionic tether approach for the synthesis of stable Cu^{II}-NHC complexes for use in enantioselective allylic alkylation reactions.[66] In a further report, Charette *et al.* found that coordination of the oxygen atom of an amidate *N*-substituent allowed the isolation of a square planar Cu^{II}-*bis*-NHC complex (Figure 1.15).[67] The use of tethered anionic nitrogen donors such as pyrazolates and carbazolides, for example, has also been shown to be capable of stabilising Cu^{II} centres.[43, 68]

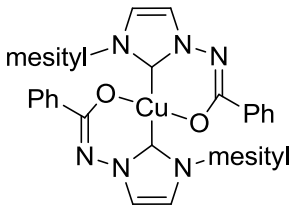

Figure 1.15 Anionic tether-stabilised Cu^{II}-*bis*-NHC complex[67]

Finally, two examples of well-characterised Cu^{II}-NHC complexes not containing either an acetate ligand or tethered anionic donor moiety have been reported. The first example, reported by Meyer *et al.* in 2003, contained a nitrogen-anchored *tris*-NHC ligand with the Cu^{II} centre proposed to be tetracoordinated.[69] The structure of this complex is provided in Chapter 5 (Figure 5.1). In the other example, the use of a pentadentate ligand containing four pyridyl donors was found to stabilise a Cu^{II} centre, with the resulting crystal structure revealing that the Cu^{II} centre contains an octahedral coordination geometry, with occupation of the sixth coordination site by an acetonitrile molecule.[70] The molecular structure of this compound is shown in Figure 1.16.

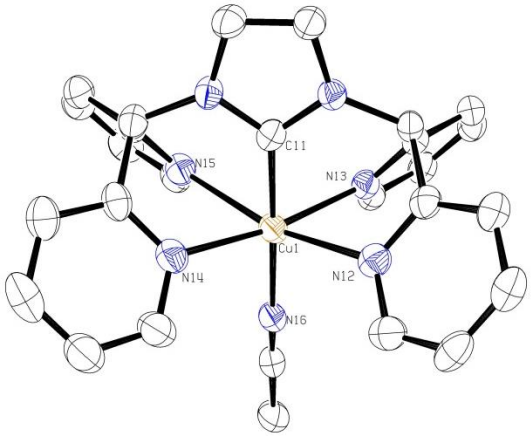

Figure 1.16 Molecular structure of a Cu^{II}-NHC complex. Ellipsoids are drawn at the 50% probability level. H atoms, tetrahydrofuran solvent and triflate anions have been omitted for clarity[70]

1.10 Project Aims

The initial aim of this project was to explore the versatility of the novel electrochemical technique for the synthesis of transition metal-NHC complexes first reported by Chen *et al.*.[43] In this first report, the synthesis of Cu^{I}, Cu^{II}, Ni^{II} and Fe^{II}-NHC complexes was reported, though the range of ligand precursors utilised was rather narrow, encompassing only pyridine-, pyrimidine- and pyrazole-tethered imidazolium salts. We sought to explore the broader applicability of this technique for the synthesis of Cu^{I}-NHC complexes encompassing a range of structurally divergent NHC ligands. For example, the synthesis of Cu^{I}-NHC complexes

containing the ubiquitous sterically demanding NHC ligands IMes (1,3-*bis*(2,4,6-trimethylphenyl)imidazol-2-ylidene) and IPr (1,3-*bis*(2,6-diisopropylphenyl)imidazol-2-ylidene) was to be attempted, in order to explore whether this electrochemical technique was suitable for use with these bulky ligand precursors. The synthesis of Cu^{I}-NHC complexes containing base sensitive and macrocyclic NHC ligands was also going to be tried, since the synthesis of these types of complexes using conventional synthetic techniques tends to be rather difficult.

We also aimed to explore unusual bonding and reactivity at Cu^{I} centres, with the specific intention of isolating a Cu^{I}-NHC complex containing a Cu^{I}-alkene interaction. This is particularly in light of the fact that Cu^{I}-NHC-alkene complexes are widely postulated as intermediates in certain Cu-catalysed reactions,[71] yet no structurally characterised example, to our knowledge, had previously been reported. A particularly encouraging report by Dias *et al.* appeared in early 2013, detailing the isolation of Cu^{I}-NHC-CO complexes;[72] carbon monoxide being considered not altogether dissimilar to an alkene in its interaction with a metal centre (σ-donor, π-acceptor). Our strategy for the synthesis of a Cu^{I}-NHC complex containing a Cu^{I}-alkene interaction was to tether an alkene on to the NHC ligand, thereby increasing the relative concentration of the alkene in the vicinity of the metal centre and thus, hopefully, encouraging an interaction between the two.

The synthesis and application of Cu^{I}-NHC complexes in a catalytic reaction was to be performed during the course of this project. The particular catalytic transformation chosen was an Ullmann-type etherification, in part due to the dearth of reports in the literature of the application of Cu^{I}-NHC complexes in this type of transformation.[61c, 62] Furthermore, since the catalytic cycle of an Ullmann-type coupling is likely to involve higher oxidation state copper species, the adventitious isolation of crystals of a number of different Cu^{II}-NHC complexes during the synthesis of pyridyl-tethered Cu^{I}-NHC complexes suggested that our pyridyl-tethered NHC ligands were competent at stabilising copper in variable oxidation states. We postulated that this ability to stabilise higher oxidation states of copper had the potential to vastly improve the performance of NHC ligands in an Ullmann-type coupling.

A final aim of this project was to rationally synthesise unusual examples of Cu^{II}-NHC complexes not bearing either a stabilising anionic tether or an acetate ligand. To the best of our knowledge, only one such example had ever been reported previously.[70] These complexes would be structurally characterised, where possible, allowing us to draw conclusions about the nature of interactions between NHC ligands and Cu^{II} centres. Furthermore, the oxidative decomposition of NHC ligands in the coordination sphere of copper was to be investigated using a combined experimental and computational approach, with the results helping to guide the future development of complexes resistant to such chemistry.

1.11 References

[1] D. Seyferth, *Organometallics* **2001**, *20*, 1488-1498.

[2] W. C. Zeise, *Annalen der Physik* **1831**, *97*, 497-541.

[3] The Nobel Prize in Chemistry 1912, *Nobelprize.org*, *Nobel Media AB 2013*, Web. 15 Jun 2014. http://www.nobelprize.org/nobel_prizes/chemistry/laureates/1912/

[4] The Nobel Prize in Chemistry 1963, *Nobelprize.org*, *Nobel Media AB 2013*, Web. 15 Jun 2014. http://www.nobelprize.org/nobel_prizes/chemistry/laureates/1963/

[5] The Nobel Prize in Chemistry 1973, *Nobelprize.org*, *Nobel Media AB 2013*, Web. 15 Jun 2014. http://www.nobelprize.org/nobel_prizes/chemistry/laureates/1973/

[6] The Nobel Prize in Chemistry 2005, *Nobelprize.org*, *Nobel Media AB 2013*, Web. 15 Jun 2014. http://www.nobelprize.org/nobel_prizes/chemistry/laureates/2005/

[7] a) S. T. Liddle, I. S. Edworthy, P. L. Arnold, *Chemical Society Reviews* **2007**, *36*, 1732-1744; b) D. Bourissou, O. Guerret, F. P. Gabbai, G. Bertrand, *Chemical Reviews* **2000**, *100*, 39-92; c) P. de Frémont, N. Marion, S. P. Nolan, *Coordination Chemistry Reviews* **2009**, *253*, 862-892.

[8] J. McMurry, *Organic Chemistry*, Third ed., Brooks/Cole Publishing Company, **1992**.

[9] a) J. J. Dunsford, K. J. Cavell, *Organometallics* **2014**, *33*, 2902-2905; b) C. J. E. Davies, M. J. Page, C. E. Ellul, M. F. Mahon, M. K. Whittlesey, *Chemical Communications* **2010**, *46*, 5151-5153; c) M. Iglesias, D. J. Beetstra, K. J. Cavell, A. Dervisi, I. A. Fallis, B. Kariuki, R. W. Harrington, W. Clegg, P. N. Horton, S. J. Coles, M. B. Hursthouse, *European Journal of Inorganic Chemistry* **2010**, *2010*, 1604-1607; d) M. J. Page, W. Y. Lu, R. C. Poulten, E. Carter, A. G. Algarra, B. M. Kariuki, S. A. Macgregor, M. F. Mahon, K. J. Cavell, D. M. Murphy, M. K. Whittlesey, *Chemistry – A European Journal* **2013**, *19*, 2158-2167.

[10] M. Liu, I. Yang, B. Buckley, J. K. Lee, *Organic Letters* **2010**, *12*, 4764-4767.

[11] a) C. Boehme, G. Frenking, *Journal of the American Chemical Society* **1996**, *118*, 2039-2046; b) C. Heinemann, T. Muller, Y. Apeloig, H. Schwarz, *Journal of the American Chemical Society* **1996**, *118*, 2023-2038.

[12] a) J. Barluenga, L. A. López, O. Löber, M. Tomás, S. García-Granda, C. Alvarez-Rúa, J. Borge, *Angewandte Chemie International Edition* **2001**, *40*, 3392-3394; b) E. O. Fischer, A. Maasböl, *Angewandte Chemie International Edition in English* **1964**, *3*, 580-581; c) D. I. Bezuidenhout, W. Barnard, B. van der Westhuizen, E. van der Watt, D. C. Liles, *Dalton Transactions* **2011**, *40*, 6711-6721; d) M. Fañanás-Mastral, F. Aznar, *Organometallics* **2009**, *28*, 666-668.

[13] D. F. Shriver, P. W. Atkins, C. H. Langford, *Inorganic Chemistry*, First ed., Oxford University Press, **1990**.

[14] a) R. R. Schrock, *Journal of the American Chemical Society* **1974**, *96*, 6796-6797; b) A. Perfetto, C. Costabile, P. Longo, F. Grisi, *Organometallics* **2014**, *33*, 2747-2759; c) V. M. Iluc, G. L. Hillhouse, *Journal of the American Chemical Society* **2014**, *136*, 6479-6488; d) J. T. Ciszewski, B. Xie, C. Cao, A. L. Odom, *Dalton Transactions* **2003**, 4226-4227.

[15] W. A. Herrmann, C. Köcher, *Angewandte Chemie International Edition in English* **1997**, *36*, 2162-2187.

[16] J. J. Hu, S.-Q. Bai, H. H. Yeh, D. J. Young, Y. Chi, T. S. A. Hor, *Dalton Transactions* **2011**, *40*, 4402-4406.

[17] P. L. Arnold, S. Pearson, *Coordination Chemistry Reviews* **2007**, *251*, 596-609.

[18] H. W. Wanzlick, *Angewandte Chemie International Edition in English* **1962**, *1*, 75-80.

[19] K. Öfele, *Journal of Organometallic Chemistry* **1968**, *12*, 42-43.

[20] H. W. Wanzlick, H. J. Schönherr, *Angewandte Chemie International Edition in English* **1968**, *7*, 141-142.

[21] A. J. Arduengo, R. L. Harlow, M. Kline, *Journal of the American Chemical Society* **1991**, *113*, 361-363.

[22] D. Enders, K. Breuer, G. Raabe, J. Runsink, J. H. Teles, J.-P. Melder, K. Ebel, S. Brode, *Angewandte Chemie International Edition in English* **1995**, *34*, 1021-1023.

[23] A. J. Arduengo, J. R. Goerlich, W. J. Marshall, *Journal of the American Chemical Society* **1995**, *117*, 11027-11028.

[24] R. W. Alder, P. R. Allen, M. Murray, A. G. Orpen, *Angewandte Chemie International Edition in English* **1996**, *35*, 1121-1123.

[25] A. J. Arduengo, J. R. Goerlich, W. J. Marshall, *Liebigs Annalen* **1997**, *1997*, 365-374.

[26] E. Aldeco-Perez, A. J. Rosenthal, B. Donnadieu, P. Parameswaran, G. Frenking, G. Bertrand, *Science* **2009**, *326*, 556-559.

[27] S. Solé, H. Gornitzka, W. W. Schoeller, D. Bourissou, G. Bertrand, *Science* **2001**, *292*, 1901-1903.

[28] I. J. B. Lin, C. S. Vasam, *Comments on Inorganic Chemistry: A Journal of Critical Discussion of the Current Literature* **2004**, *25*, 75-129.

[29] A. J. Arduengo, H. V. R. Dias, J. C. Calabrese, F. Davidson, *Organometallics* **1993**, *12*, 3405-3409.

[30] H. M. J. Wang, I. J. B. Lin, *Organometallics* **1998**, *17*, 972-975.

[31] a) Z. Wang, S. W. B. Ng, L. Jiang, W. J. Leong, J. Zhao, T. S. A. Hor, *Organometallics* **2014**, *33*, 2457-2466; b) V. Khlebnikov, A. Meduri, H. Mueller-Bunz, T. Montini, P. Fornasiero, E. Zangrando, B. Milani, M. Albrecht, *Organometallics* **2012**, *31*, 976-986; c) C. P. Newman, R. J. Deeth, G. J. Clarkson, J. P. Rourke, *Organometallics* **2007**, *26*, 6225-6233; d) F. Zhang, D. Ma, L. Duan, J. Qiao, G. Dong, L. Wang, Y. Qiu, *Inorganic*

Chemistry **2014**; e) A. l. Poulain, D. Canseco-Gonzalez, R. Hynes-Roche, H. Müller-Bunz, O. Schuster, H. Stoeckli-Evans, A. Neels, M. Albrecht, *Organometallics* **2011**, *30*, 1021-1029; f) S. Hameury, P. de Fremont, P.-A. R. Breuil, H. Olivier-Bourbigou, P. Braunstein, *Dalton Transactions* **2014**, *43*, 4700-4710; g) X.-Q. Xiao, G.-X. Jin, *Dalton Transactions* **2009**, 9298-9303.

[32] a) G. Venkatachalam, M. Heckenroth, A. Neels, M. Albrecht, *Helvetica Chimica Acta* **2009**, *92*, 1034-1045; b) M. R. L. Furst, C. S. J. Cazin, *Chemical Communications* **2010**, *46*, 6924-6925; c) X. Liu, R. Pattacini, P. Deglmann, P. Braunstein, *Organometallics* **2011**, *30*, 3302-3310; d) C. Chen, H. Qiu, W. Chen, *Journal of Organometallic Chemistry* **2012**, *696*, 4166-4172; e) J. Mormul, M. Steimann, U. Nagel, *European Journal of Inorganic Chemistry* **2014**, *2014*, 1389-1393.

[33] B. Liu, X. Liu, C. Chen, C. Chen, W. Chen, *Organometallics* **2011**, *31*, 282-288.

[34] G. T. S. Andavan, E. B. Bauer, C. S. Letko, T. K. Hollis, F. S. Tham, *Journal of Organometallic Chemistry* **2005**, *690*, 5938-5947.

[35] R. J. Lowry, M. T. Jan, K. A. Abboud, I. Ghiviriga, A. S. Veige, *Polyhedron* **2010**, *29*, 553-563.

[36] a) Y. Hoshimoto, Y. Hayashi, H. Suzuki, M. Ohashi, S. Ogoshi, *Organometallics* **2014**, *33*, 1276-1282; b) J. Huang, E. D. Stevens, S. P. Nolan, J. L. Petersen, *Journal of the American Chemical Society* **1999**, *121*, 2674-2678; c) E. Kühnel, I. V. Shishkov, F. Rominger, T. Oeser, P. Hofmann, *Organometallics* **2012**, *31*, 8000-8011.

[37] a) O. Santoro, A. Collado, A. M. Z. Slawin, S. P. Nolan, C. S. J. Cazin, *Chemical Communications* **2013**, *49*, 10483-10485; b) D. J. Nelson, A. Collado, S. Manzini, S. Meiries, A. M. Z. Slawin, D. B. Cordes, S. P. Nolan, *Organometallics* **2014**, *33*, 2048-2058; c) P. Huang, Y.-X. Wang, H.-F. Yu, J.-M. Lu, *Organometallics* **2014**, *33*, 1587-1593; d) R. Visbal, A. Laguna, M. C. Gimeno, *Chemical Communications* **2013**, *49*, 5642-5644; e) C. Gibard, H. Ibrahim, A. Gautier, F. Cisnetti, *Organometallics* **2013**, *32*, 4279-4283; f) C. Segarra, E. Mas-Marzá, M. Benítez, J. A. Mata, E. Peris, *Angewandte Chemie International Edition* **2012**, *51*, 10841-10845.

[38] a) B. Liu, Q. Xia, W. Chen, *Angewandte Chemie International Edition* **2009**, *48*, 5513-5516; b) A. A. D. Tulloch, A. A. Danopoulos, S. Kleinhenz, M. E. Light, M. B. Hursthouse, G. Eastham, *Organometallics* **2001**, *20*, 2027-2031; c) E. Peris, J. A. Loch, J. Mata, R. H. Crabtree, *Chemical Communications* **2001**, 201-202; d) J. A. Loch, M. Albrecht, E. Peris, J. Mata, J. W. Faller, R. H. Crabtree, *Organometallics* **2002**, *21*, 700-706; e) S. Gischig, A. Togni, *Organometallics* **2004**, *24*, 203-205; f) C. Romain, L. Brelot, S. Bellemin-Laponnaz, S. Dagorne, *Organometallics* **2010**, *29*, 1191-1198; g) F. E. Hahn, C. Holtgrewe, T. Pape, M. Martin, E. Sola, L. A. Oro, *Organometallics* **2005**,

24, 2203-2209; h) A. Raba, M. Cokoja, S. Ewald, K. Riener, E. Herdtweck, A. Pöthig, W. A. Herrmann, F. E. Kühn, *Organometallics* **2012**, *31*, 2793-2800.

[39] Y. Ohki, T. Hatanaka, K. Tatsumi, *Journal of the American Chemical Society* **2008**, *130*, 17174-17186.

[40] a) M. Viciano, E. Mas-Marzá, M. Poyatos, M. Sanaú, R. H. Crabtree, E. Peris, *Angewandte Chemie International Edition* **2005**, *44*, 444-447; b) A. Krüger, E. Kluser, H. Müller-Bunz, A. Neels, M. Albrecht, *European Journal of Inorganic Chemistry* **2012**, *2012*, 1394-1402; c) M. V. Baker, D. H. Brown, V. J. Hesler, B. W. Skelton, A. H. White, *Organometallics* **2006**, *26*, 250-252; d) S. Grundemann, M. Albrecht, A. Kovacevic, J. W. Faller, R. H. Crabtree, *Journal of the Chemical Society, Dalton Transactions* **2002**, 2163-2167; e) S. Caddick, F. G. N. Cloke, P. B. Hitchcock, J. Leonard, A. K. d. K. Lewis, D. McKerrecher, L. R. Titcomb, *Organometallics* **2002**, *21*, 4318-4319; f) D. S. McGuinness, K. J. Cavell, B. W. Skelton, A. H. White, *Organometallics* **1999**, *18*, 1596-1605; g) E. Kluser, A. Neels, M. Albrecht, *Chemical Communications* **2006**, 4495-4497.

[41] a) D. J. Cardin, B. Cetinkaya, E. Cetinkaya, M. F. Lappert, *Journal of the Chemical Society, Dalton Transactions* **1973**, 514-522; b) B. Cetinkaya, P. Dixneuf, M. F. Lappert, *Journal of the Chemical Society, Dalton Transactions* **1974**, 1827-1833.

[42] T. M. Trnka, J. P. Morgan, M. S. Sanford, T. E. Wilhelm, M. Scholl, T.-L. Choi, S. Ding, M. W. Day, R. H. Grubbs, *Journal of the American Chemical Society* **2003**, *125*, 2546-2558.

[43] B. Liu, Y. Zhang, D. Xu, W. Chen, *Chemical Communications* **2011**, *47*, 2883-2885.

[44] B. Gorodetsky, T. Ramnial, N. R. Branda, J. A. C. Clyburne, *Chemical Communications* **2004**, 1972-1973.

[45] M. Feroci, I. Chiarotto, M. Orsini, G. Sotgiu, A. Inesi, *Advanced Synthesis & Catalysis* **2008**, *350*, 1355-1359.

[46] M. Orsini, I. Chiarotto, G. Sotgiu, A. Inesi, *Electrochimica Acta* **2010**, *55*, 3511-3517.

[47] a) A. S. K. Hashmi, C. Lothschütz, C. Böhling, T. Hengst, C. Hubbert, F. Rominger, *Advanced Synthesis & Catalysis* **2010**, *352*, 3001-3012; b) A. S. K. Hashmi, C. Lothschütz, C. Böhling, F. Rominger, *Organometallics* **2011**, *30*, 2411-2417.

[48] D. Patel, S. T. Liddle, S. A. Mungur, M. Rodden, A. J. Blake, P. L. Arnold, *Chemical Communications* **2006**, 1124-1126.

[49] C. Romain, K. Miqueu, J.-M. Sotiropoulos, S. Bellemin-Laponnaz, S. Dagorne, *Angewandte Chemie International Edition* **2010**, *49*, 2198-2201.

[50] a) I. S. Edworthy, A. J. Blake, C. Wilson, P. L. Arnold, *Organometallics* **2007**, *26*, 3684-3689; b) S. A. Mungur, A. J. Blake, C. Wilson, J. McMaster, P. L. Arnold, *Organometallics* **2006**, *25*, 1861-1867.

[51] a) P. L. Arnold, M. Rodden, K. M. Davis, A. C. Scarisbrick, A. J. Blake, C. Wilson, *Chemical Communications* **2004**, 1612-1613; b) P. L. Arnold, M. Rodden, C. Wilson, *Chemical Communications* **2005**, 1743-1745.

[52] G. Dyson, J.-C. Frison, S. Simonovic, A. C. Whitwood, R. E. Douthwaite, *Organometallics* **2008**, *27*, 281-288.

[53] M. Scholl, S. Ding, C. W. Lee, R. H. Grubbs, *Organic Letters* **1999**, *1*, 953-956.

[54] S. K. U. Riederer, P. Gigler, M. P. Högerl, E. Herdtweck, B. Bechlars, W. A. Herrmann, F. E. Kühn, *Organometallics* **2010**, *29*, 5681-5692.

[55] J. C. Y. Lin, R. T. W. Huang, C. S. Lee, A. Bhattacharyya, W. S. Hwang, I. J. B. Lin, *Chemical Reviews* **2009**, *109*, 3561-3598.

[56] D. S. Weinberger, N. Amin Sk, K. C. Mondal, M. Melaimi, G. Bertrand, A. C. Stückl, H. W. Roesky, B. Dittrich, S. Demeshko, B. Schwederski, W. Kaim, P. Jerabek, G. Frenking, *Journal of the American Chemical Society* **2014**, *136*, 6235-6238.

[57] P. K. Fraser, S. Woodward, *Tetrahedron Letters* **2001**, *42*, 2747-2749.

[58] a) S. Díez-González, S. P. Nolan, *Synlett* **2007**, *2007*, 2158-2167; b) J. D. Egbert, C. S. J. Cazin, S. P. Nolan, *Catalysis Science & Technology* **2013**, *3*, 912-926.

[59] F. Ullmann, J. Bielecki, *Berichte der deutschen chemischen Gesellschaft* **1901**, *34*, 2174-2185.

[60] C. Sambiagio, S. P. Marsden, A. J. Blacker, P. C. McGowan, *Chemical Society Reviews* **2014**, *43*, 3525-3550.

[61] a) G. G. Dubinina, H. Furutachi, D. A. Vicic, *Journal of the American Chemical Society* **2008**, *130*, 8600-8601; b) G. G. Dubinina, J. Ogikubo, D. A. Vicic, *Organometallics* **2008**, *27*, 6233-6235; c) C. Tubaro, A. Biffis, E. Scattolin, M. Basato, *Tetrahedron* **2008**, *64*, 4187-4195.

[62] a) A. Biffis, C. Tubaro, E. Scattolin, M. Basato, G. Papini, C. Santini, E. Alvarez, S. Conejero, *Dalton Transactions* **2009**, 7223-7229; b) C. E. Ellul, G. Reed, M. F. Mahon, S. I. Pascu, M. K. Whittlesey, *Organometallics* **2010**, *29*, 4097-4104.

[63] a) A. Grandbois, M.-È. Mayer, M. Bédard, S. K. Collins, T. Michel, *Chemistry – A European Journal* **2009**, *15*, 9655-9659; b) E. L. Kolychev, V. V. Shuntikov, V. N. Khrustalev, A. A. Bush, M. S. Nechaev, *Dalton Transactions* **2011**, *40*, 3074-3076.

[64] J. Yun, D. Kim, H. Yun, *Chemical Communications* **2005**, 5181-5183.

[65] P. L. Arnold, M. Rodden, K. M. Davis, A. C. Scarisbrick, A. J. Blake, C. Wilson, *Chemical Communications* **2004**, 1612-1613.

[66] a) A. O. Larsen, W. Leu, C. N. Oberhuber, J. E. Campbell, A. H. Hoveyda, *Journal of the American Chemical Society* **2004**, *126*, 11130-11131; b) J. J. Van Veldhuizen, J. E. Campbell, R. E. Giudici, A. H. Hoveyda, *Journal of the American Chemical Society* **2005**, *127*, 6877-6882.

[67] C. Y. Legault, C. Kendall, A. B. Charette, *Chemical Communications* **2005**, *0*, 3826-3828.

[68] a) B. Liu, B. Liu, Y. Zhou, W. Chen, *Organometallics* **2010**, *29*, 1457-1464; b) D. I. Bezuidenhout, G. Kleinhans, G. Guisado-Barrios, D. C. Liles, G. Ung, G. Bertrand, *Chemical Communications* **2014**, *50*, 2431-2433.

[69] X. Hu, I. Castro-Rodriguez, K. Meyer, *Journal of the American Chemical Society* **2003**, *125*, 12237-12245.

[70] J. M. Smith, J. R. Long, *Inorganic Chemistry* **2010**, *49*, 11223-11230.

[71] a) D. S. Laitar, E. Y. Tsui, J. P. Sadighi, *Organometallics* **2006**, *25*, 2405-2408; b) V. Lillo, M. R. Fructos, J. Ramírez, A. A. C. Braga, F. Maseras, M. M. Díaz-Requejo, P. J. Pérez, E. Fernández, *Chemistry – A European Journal* **2007**, *13*, 2614-2621.

[72] C. Dash, A. Das, M. Yousufuddin, H. V. R. Dias, *Inorganic Chemistry* **2013**, *52*, 1584-1590.

Chapter 2

Electrochemical Synthesis of Neutral and Cationic Cu^{I}-NHC Complexes Bearing either Bulky or Non-Bulky Monodentate Ligands

2.1 Introduction

Monocationic copper (Cu^{I}) is a soft transition metal ion and thus tends to interact strongly with soft donor groups, such as *N*-heterocyclic carbenes (NHCs). The stability of a Cu^{I}-NHC bond means that the presence of other donor groups on the NHC ligand is not required to generate stable complexes.

The initial aim of this project was to prepare a variety of bulky and non-bulky monodentate NHC-precursors and effect their coordination to Cu^{I} using a novel electrochemical synthetic technique.

2.2 Ligand Synthesis

2.2.1 Bulky NHC Ligand Precursors

So-called 'bulky' NHC ligands are those which possess a large degree of steric crowding around the carbenic centre. The degree of steric crowding results largely from the nature of the 'R' substituents attached to the nitrogen atoms of the NHC. Aryl substituents, particularly those bearing a 2,6-substitution pattern, provide a significant degree of steric crowding and thus are commonly incorporated in to NHC ligands. Bulky NHCs are typically much more easily isolated as the corresponding free carbene compared to non-bulky NHCs, as typified by the first free carbene to be isolated, which bore adamantyl *N*-substituents.[1] Furthermore, a high degree of steric bulk around the carbene centre can kinetically stabilise the resultant transition metal-NHC complex, as will be illustrated later in the case of Cu^{I}-NHC complexes.

The synthesis of a series of diazabutadienes, which are precursors to bulky NHCs, was based on two synthetic procedures reported by Nolan *et al.*.[2] 2,6-Diisopropylphenyl-, 2,6-dimethylphenyl- and 2,4,6-trimethylphenyl-substituted symmetrical diazabutadienes (compounds **P1-P3**) were prepared by the reaction of two equivalents of the appropriate aromatic amine with glyoxal, a simple dialdehyde, in the presence of a catalytic amount of acid (Scheme 2.1). The reactions were performed by dissolving the aromatic amine in either methanol or ethanol, adding the glyoxal and formic acid (catalyst) and stirring at room temperature. The product, a bis-secondary aldimine, forms as a bright yellow solid very quickly

after the addition of all of the reagents, and can be purified easily by washing with the reaction solvent. The vibrant colour of the products arises due to the extended π-conjugation present within the molecules. The reactions to produce compounds **P1**-**P3** all proceed in moderate yields (46-64%).

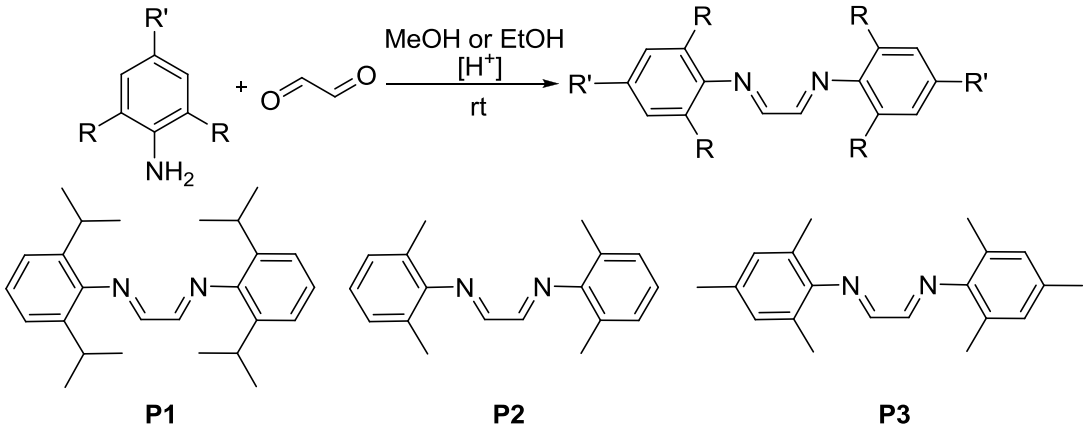

Scheme 2.1 Synthesis of diazabutadiene ligand precursors

The diazabutadienes (compounds **P1**-**P3**) are produced following two consecutive Mannich reactions. Addition of the first aromatic amine to glyoxal is illustrated in Figure 2.1, where the aromatic amine is aniline. During the reaction, protonation of the glyoxal occurs initially, forming a hydroxycarbenium ion, which then undergoes nucleophilic attack by the amine nitrogen, eventually leading to the release of a molecule of water. The final step of the reaction forms the desired secondary aldimine functional group and regenerates the proton catalyst.

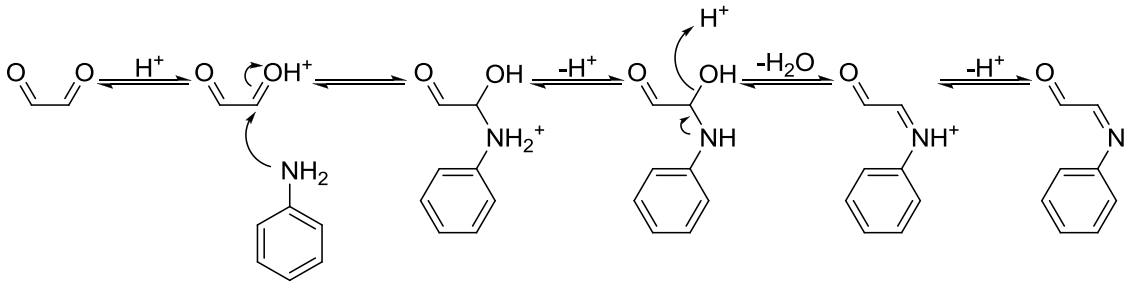

Figure 2.1 Mannich reaction between glyoxal and aniline

Analysis of the products of these reactions by ^{1}H and $^{13}C\{^{1}H\}$ NMR spectroscopy, high-resolution MS and elemental analysis provided clear evidence that compounds **P1**-**P3** had formed cleanly. For example, the aldimine proton (N=CH) is clearly observed as a singlet at approximately 8.1 ppm in the ^{1}H NMR spectra of compounds **P1**-**P3** (in $CDCl_3$), this signal being absent from the ^{1}H NMR spectra of the starting materials. Also, $[M + H]^+$ fragments for all three compounds were observed and measured *via* high-resolution MS.

The synthesis of the bulky imidazolium salt ligand precursors was also based on two synthetic procedures reported by Nolan *et al.*.[2] 1,3-*Bis*-(2,6-diisopropylphenyl)imidazolium, 1,3-*bis*-

(2,6-dimethylphenyl)imidazolium and 1,3-*bis*-(2,4,6-trimethylphenyl)imidazolium salts were all prepared with chloride counter-anions (compounds **L1-L3**, Scheme 2.2).

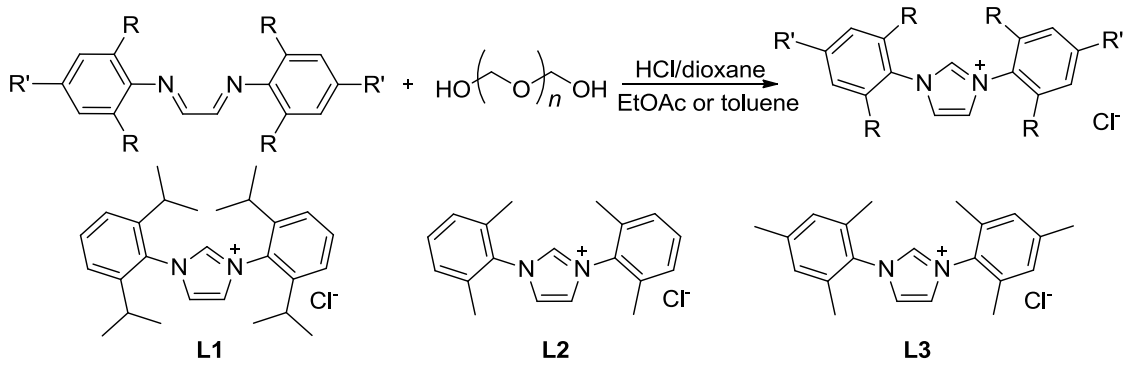

Scheme 2.2 Synthesis of imidazolium salt ligand precursors **L1-L3**

The reaction occurs with the addition of diazabutadiene to paraformaldehyde in the presence of an excess of HCl (in dioxane, 4 mol dm^{-3}). In all three cases, following addition of the reagents, a brown mixture containing the product formed. Since the pure product should be a white, crystalline solid, a number of side-reactions are proposed to occur. During the synthesis of compound **L1**, a different synthetic protocol was followed in comparison to **L2** and **L3**, which could account for the higher yield of compound **L1** obtained (61% *vs*. 53% and 10%). The key differences proposed are, that the reagents were combined at 0°C during production of **L1**, as opposed to about 50°C during synthesis of **L2** and **L3**. This factor seems to reduce the rate of the side-reactions to a much greater extent compared to the desired reaction to form the product. This is evidenced by the much slower appearance of a brown colour to the mixture, and that the resulting solid formed is much paler in colour. The other key difference is that during the synthesis of **L1**, the HCl and paraformaldehyde were precombined and added to the stirring diazabutadiene dropwise. Finally, the diisopropyl-substituted diazabutadiene precursor to compound **L1** is much more sterically hindered than the other two diazabutadienes and thus is much less prone to hydrolysis reactions, for example, which could account for some of the side-products. Hintermann[3] proposed a mechanism for the reaction of the diazabutadiene with paraformaldehyde in the presence of HCl, which is given in Figure 2.2.

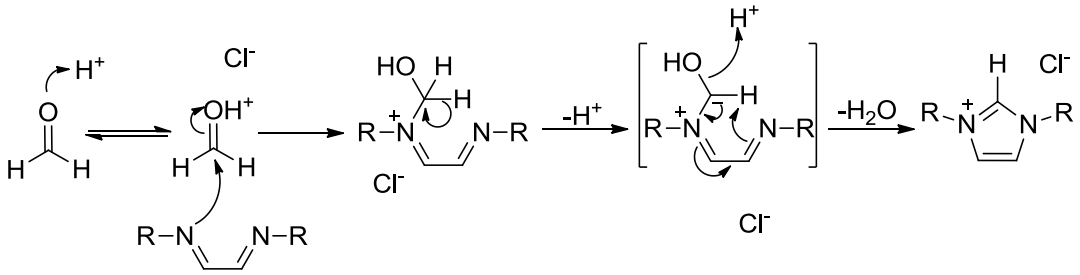

Figure 2.2 Reaction of diazabutadiene with formaldehyde

During this reaction, nucleophilic attack on the hydroxycarbenium ion by the diazabutadiene occurs forming an iminium salt. Loss of a proton from the iminium salt forms an ylidic species, which then undergoes 1,5-dipolar cyclisation to form the imidazolium chloride salt.

Formation of the desired imidazolium chlorides (**L1**-**L3**) was demonstrated using ^{1}H and $^{13}C\{^{1}H\}$ NMR spectroscopy, high-resolution MS and elemental analysis. Most notably, the aldimine proton (N=CH) singlet signal at approximately 8.1 ppm in the ^{1}H NMR spectrum (in $CDCl_3$) of the starting diazabutadienes has disappeared. Instead, a single singlet above 10.9 ppm (in $CDCl_3$ or CD_2Cl_2) appears, which corresponds to the C2 proton of the imidazolium. Figure 2.3 provides a comparison between the ^{1}H NMR spectra of a diazabutadiene and its imidazolium chloride product.

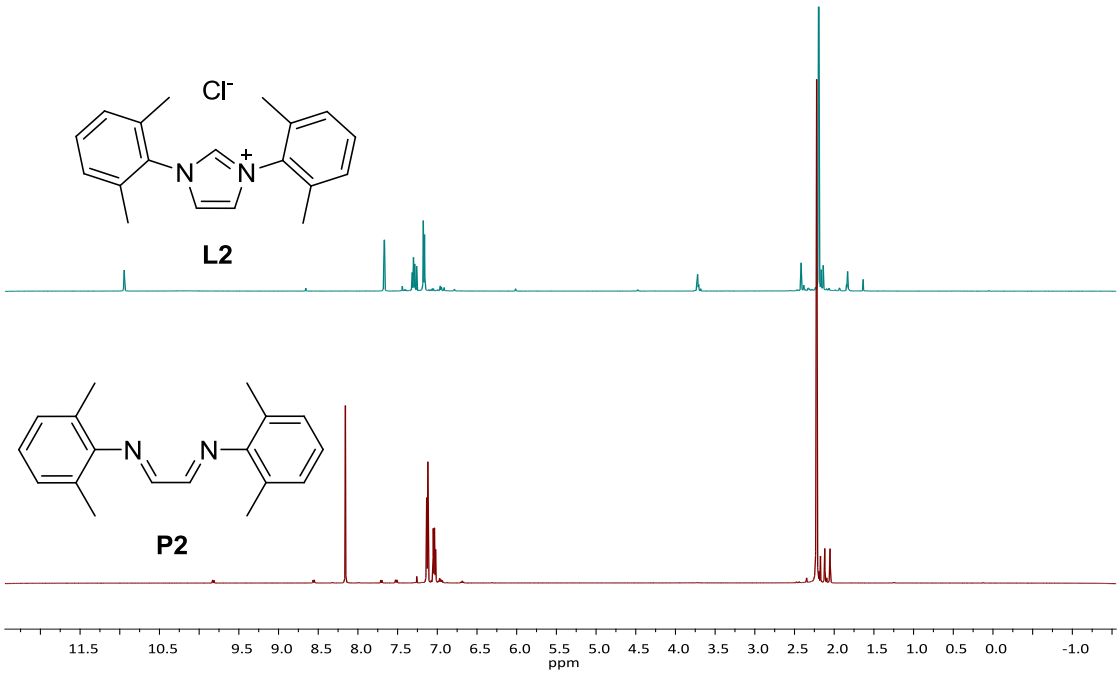

Figure 2.3 ^{1}H NMR spectra of NHC precursor **L2** (*top*) versus diazabutadiene **P2** (*bottom*)

The signal for the C2 proton of imidazolium salts, particularly imidazolium halides, is shifted significantly downfield. One of the reasons for this is the strong hydrogen bonding interaction between the C2 proton, which acts as the H-bond donor, and the counter-anion, which acts as the H-bond acceptor. This H-bonding interaction causes the C2 proton to experience a large deshielding effect, thus making it resonate downfield. H-Bonding interactions are typically more significant/stronger between the C2 proton and halide anions, than between the C2 proton and non-coordinating anions (*e.g.* PF_6^-). This explains why, in general, the C2 proton resonance occurs at lower field for imidazolium halide salts than for imidazolium hexafluorophosphate salts, for example.

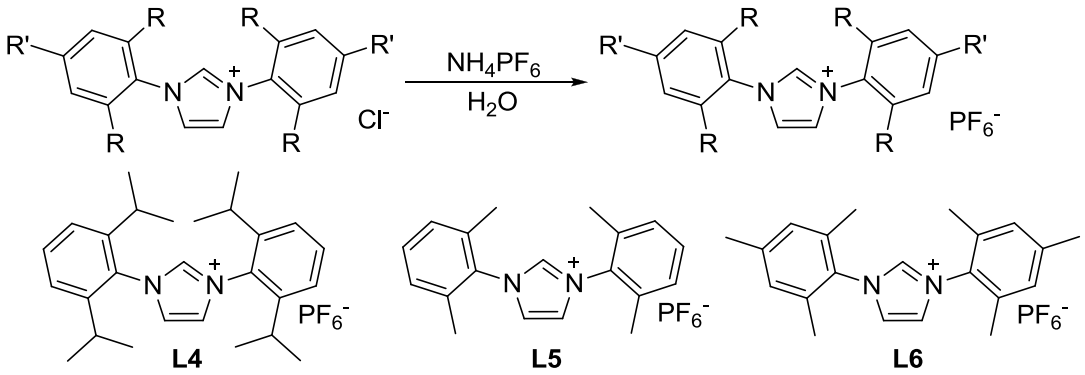

Scheme 2.3 Salt metathesis reaction to form imidazolium PF_6^- salts **L4**-**L6**

Salt metathesis reactions of NHC precursors **L1**-**L3** with NH_4PF_6 in water yielded the desired anion-exchanged products (**L4**-**L6**). Slow addition of 5 equivalents of an aqueous solution of NH_4PF_6 to an aqueous solution of **L1**-**L3** induces the precipitation of **L4**-**L6** as white solids, which can be purified by filtering and washing with water. The formation of the desired anion-exchanged products was evident in the differing solubilities of the starting imidazolium chloride and the product, an imidazolium hexafluorophosphate, and also by ^{1}H NMR spectroscopy.

2.2.2 Non-Bulky NHC Ligand Precursors

Non-bulky NHC ligands are those which bear small/flexible *N*-substituents. Such substituents provide little steric protection of the carbene centre, which renders the corresponding free carbene much more reactive towards dimerisation/decomposition. Furthermore, it would be anticipated that certain transition metal-NHC complexes, such as Cu^I-NHC complexes, formed from such ligands would also be more susceptible to decomposition.

One of the least bulky NHC precursors available is 1-methyl-3-ethylimidazolium chloride (**L7**). This material is available commercially and thus it was not necessary to synthesise it.

1-Methyl-3-benzylimidazolium bromide (**L8**) is a known NHC precursor. In this study, it was isolated as a colourless oil in good yield by the reaction of benzyl bromide with *N*-methylimidazole in anhydrous tetrahydrofuran. ^{1}H NMR data was in agreement with that previously reported.[4] A salt metathesis reaction of **L8** with NH_4PF_6 in water produced colourless crystals of 1-methyl-3-benzylimidazolium hexafluorophosphate (**L9**) after recrystallisation from acetone/diethyl ether. Vapour diffusion of pentane in to a concentrated solution of the ligand in dichloromethane produced colourless plate crystals which were suitable for X-ray diffraction analysis (Figure 2.4).

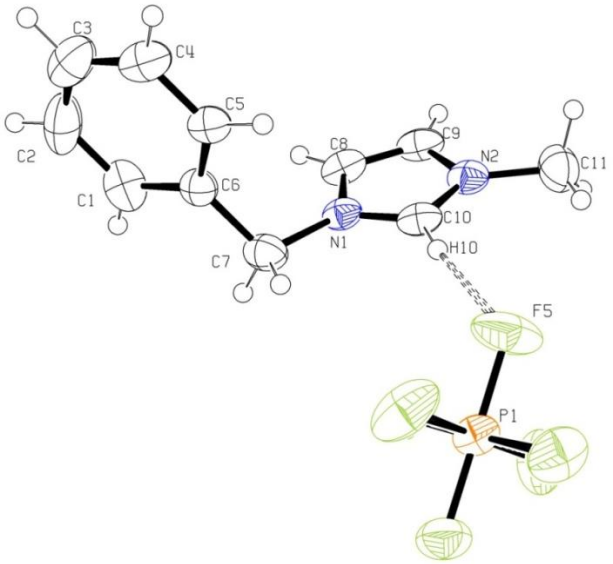

Figure 2.4 Molecular structure of **L9**. Ellipsoids are drawn at the 50% probability level

Table 2.1 Selected bond distances (Å) and angles (deg) for **L9**			
N(1)-C(10)	1.323(3)	N(1)-C(10)-N(2)	108.8(2)
N(2)-C(10)	1.324(3)	C(10)-H(10)---F(5)	168.03
N(1)-C(8)	1.375(3)	P(1)-F(5)---H(10)	119.70
N(2)-C(9)	1.370(4)		
C(8)-C(9)	1.344(4)		
H(10)---F(5)	2.218		

The solid-state structure of **L9** shows very little of note other than a hydrogen bonding interaction between the imidazolium C2 proton and a neighbouring fluorine atom (on the hexafluorophosphate counter-anion). Hydrogen bonding in imidazolium salts is well documented and has been the subject of a recent review.[5] Hydrogen bonds have a strong preference for H-bond donor linearity when compared to van der Waals' interactions, for example, and this is observed here with a near-linear C-H---F angle of 168°. Furthermore, H-bond acceptor directionality can be important, and frequently corresponds with the position of electron lone pairs on the H-bond acceptor atom. In this case, the P-F---H angle of 120° accords with the approximate positions of the fluorine lone pairs.[6] An important point to note however, is that the H atoms were not located on the diffraction map, but were placed on their carrier atoms using a riding model with constrained bond lengths and angles. Thus, a lengthy and detailed discussion of the metrics of the presumed hydrogen bonding interaction is not appropriate.

The symmetrical NHC precursor 1,3-dibenzylimidazolium bromide (**L10**) was obtained from another student.

The benzimidazolium analogues of **L10**, 1,3-dibenzylbenzimidazolium bromide (**L11**) and 1,3-dibenzylbenzimidazolium hexafluorophosphate (**L12**), were synthesised to demonstrate the application of the electrochemical synthetic protocol with benzannulated NHC precursors. 1,3-Dibenzylbenzimidazolium bromide (**L11**) was prepared according to a literature procedure[7] in excellent yield by reacting benzimidazole with two equivalents of benzyl bromide in acetonitrile at room temperature, in the presence of the base potassium carbonate, for 2 days. The simple salt metathesis reaction of **L11** with NH_4PF_6 in methanol yielded 1,3-dibenzylbenzimidazolium hexafluorophosphate (**L12**) (Scheme 2.4).

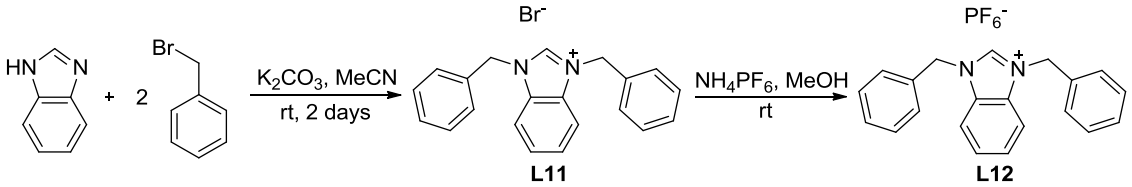

Scheme 2.4 Synthesis of 1,3-dibenzylbenzimidazolium NHC precursors (**L11** and **L12**)

Finally, two imidazolium-linked *meta*-xylyl cyclophanes (**L13A** and **L13B**) were synthesised for application in the electrochemical system. The synthesis of **L13A**, a cyclophane bromide, was achieved by initial reaction of the commercially available starting material α,α'-dibromo-*m*-xylene with two equivalents of imidazole following a literature procedure, to produce α,α'-diimidazole-*m*-xylene (**P13**).[8] Then, reaction of one equivalent of α,α'-diimidazole-*m*-xylene with another equivalent of α,α'-dibromo-*m*-xylene in acetone at room temperature formed cyclophane bromide **L13A** in moderate yield.[8] A salt metathesis reaction was performed on **L13A** to form the cyclophane hexafluorophosphate **L13B**. This reaction was particularly desirable given the almost complete insolubility of **L13A** in acetonitrile (the metal complexation solvent). **L13B** on the other hand is freely soluble in acetonitrile. The synthesis of **L13A** and **L13B** is illustrated in Scheme 2.5.

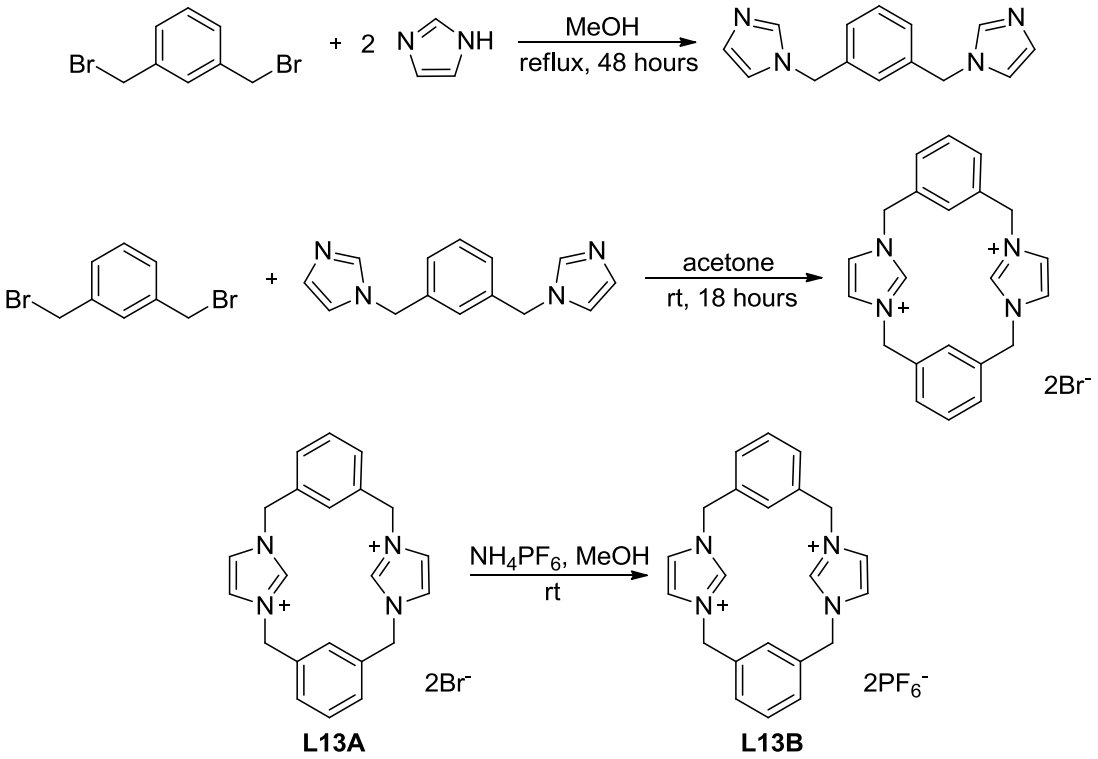

Scheme 2.5 Synthesis of cyclophane NHC precursors (**L13A** and **L13B**)

2.3 Electrochemical Synthesis

The method used to synthesise the complexes described *vide infra* is an electrochemical technique originally reported by Liu *et al.* in 2011.[9] This electrochemical approach utilises the redox-active nature of imidazoliums, in order to generate free NHCs *in situ*. This method can therefore be seen in some respects as akin to the technique of using a strong base, such as NaH or ^{n}BuLi, to generate the free NHC by deprotonation of the 'acidic' C2 proton. As with the strong base method, the solvent used during the electrochemical procedure should be anhydrous and anoxic, in order to prevent decomposition of the free NHC present in solution. During the electrochemical reaction, the imidazolium is reduced at the cathode, releasing molecular hydrogen (theoretically the only by-product) and forming the free NHC (Scheme 2.6a). At the same time, oxidation of the metal comprising the anode occurs, releasing metal ions in to solution (Scheme 2.6b). In solution, the free NHC(s) and metal ion(s) combine, forming the metal-NHC complex. (Scheme 2.6c).[9]

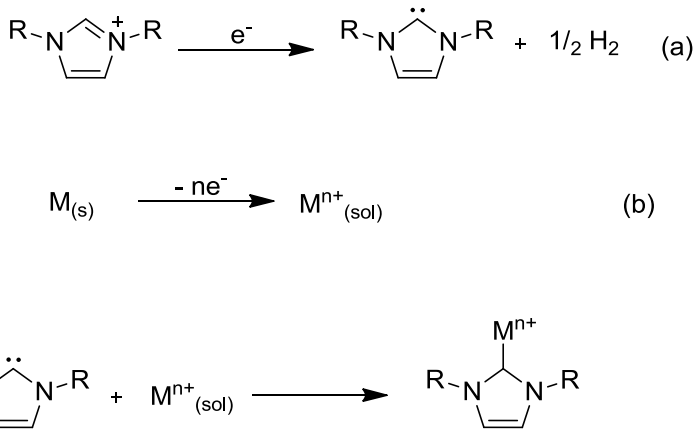

Scheme 2.6 Processes occurring at the cathode (a), anode (b) and in solution (c)[9]

Notably, the electrochemical reduction of an imidazolium to form a free NHC had been reported previously by Gorodetsky *et al.* as far back as 2004.[10] Subsequently, Feroci *et al.*[11] and Orsini *et al.*[12] amongst others have reported the synthesis and use of free NHCs as strong neutral bases in organic reactions. Despite this, the formation of TM-NHC complexes *via* the electrogeneration of free NHCs was not reported until 2011.

2.3.1 Electrochemical Synthesis of Cu^{I}-NHC Complexes

In the article published by Liu *et al.*,[9] the electrochemical synthesis of Cu^{I}, Cu^{II}, Ni^{II} and Fe^{II}-NHC complexes in acetonitrile was reported. The reactions seemed to proceed most efficiently during the generation of Cu^{I}-NHC complexes and as such, Cu^{I} complexes will form the initial targets of this project.

The efficiency with which Cu^{I}-NHC complexes are synthesised electrochemically could be due to the fact that the acetonitrile solvent strongly stabilises Cu^{I} towards disproportionation/oxidation, as is evident in the ease of isolation of Cu^{I}-acetonitrile (*e.g.* $[Cu(MeCN)_4]PF_6$) adducts.[13] A further reason for targeting Cu^{I}-NHC complexes is that it has been demonstrated that transmetallation of the NHC ligand from Cu^{I}-NHCs to other transition metals can occur, in a manner similar to Ag^{I}-NHCs.[14] This increases the potential application of the synthesised Cu^{I}-NHC complexes.

As mentioned previously, the initial stages of this project have involved the synthesis of Cu^{I}-NHC complexes. Hence, copper plates were used as both the anode and cathode and acetonitrile was used as the reaction solvent for the reasons outlined previously. An electrolyte is not required during the reactions due to the ability of the imidazolium salt to act as not only the reactant, but also the electrolyte. The reactions are performed at room temperature in a standardised way. Initially, the imidazolium salt is added to a flask and dried *in vacuo*. Then, anhydrous acetonitrile is added to the flask dissolving the imidazolium salt. The acetonitrile is

degassed by bubbling with argon for at least 1 hour. Next, the electrodes are inserted in to the flask, purged with argon and inserted in to the reaction mixture. A potential is applied such that a constant current of 50 - 60 mA flows throughout the reaction. The reactions are monitored by ^{1}H NMR spectroscopy (for the more air/moisture stable complexes) and the reaction is halted after the reaction is over 95% complete (*i.e*. less than 5% of the starting material left). The reaction work-up depends on which starting imidazolium has been used.

Before performing each reaction, the theoretical reaction time is calculated using the equation in Figure 2.5. Most reactions take longer than the theoretical time. In the experimental section, the reactions are quoted in terms of 'Q', *i.e*. how much more charge passed than the theoretical amount required.

$Q = nFN$	Q = total charge [C or A s]
	n = number of electrons transferred
	F = Faraday's constant [C mol^{-1}]
$t = Q / I$	N = moles of starting material [mol]
	I = current [A]
$\therefore t = nFN / I$	t = time [s]

Figure 2.5 Faraday's law – calculation of theoretical reaction time

The NHC precursors synthesised for this work were chosen for a number of reasons, including how common they are and how easy they are to make. This is because the first part of the project has been an investigation in to the versatility of the electrochemical reaction system. Their ubiquity in NHC chemistry has already been illustrated in the introduction to this work and their synthesis was discussed *vide ante*, and was shown to be reasonably efficient.

The previously reported Cu^{I}-NHC complexes **C1**, **C2** and **C3A** were synthesised electrochemically to demonstrate that the electrochemical technique is suitable for making transition metal complexes of bulky NHC ligands. Furthermore, since they have been applied in catalysis,[15] cleaner, cheaper and more efficient routes to their synthesis are always desirable. Dimethyl- or diisopropyl-substitution at the 2 and 6 positions of the phenyl *N*-substituents mean that once formed, these ligands' carbene centres are sterically crowded and thus protected from decomposition. Electrolysis of NHC precursors **L1**, **L2** and **L3** for 3Q, 4Q and 2Q respectively yielded the Cu^{I}-NHC complexes **C1**, **C2** and **C3A** as slightly off-white to white solids following work-up. The white colour (no electronic transitions in the visible region of the spectrum) strongly indicated that the complexes formed were indeed Cu^{I}-NHC complexes, as opposed to Cu^{II}-complexes or Cu^{II} decomposition products. Monocationic copper has a full d-orbital (d^{10} configuration), therefore, d-d transitions cannot occur with Cu^{I} complexes. Also, due to the full d-orbital, LMCT transitions are not generally possible for Cu^{I} complexes. Where colour does sometimes arise in Cu^{I} complexes, it can be *via* a MLCT transition. In complexes **C1**, **C2** and **C3A**, neither of the ligands (an NHC and a chloride) possess a low-lying LUMO in to which an

electronic transition from a metal can occur during an MLCT transition. Therefore, the Cu^{I} complexes **C1**, **C2** and **C3A** are not coloured.

The ^{1}H and $^{13}C\{^{1}H\}$ NMR spectra of complexes **C1**, **C2** and **C3A** matched those previously reported.[16] Analysis of Cu^{I}-NHC complexes by ^{1}H NMR spectroscopy reveals the disappearance of the resonance for the C2 proton of the imidazolium ring. This is strongly characteristic of the formation of a carbene. The spectra of complexes **C1**, **C2** and **C3A** (recorded in $CDCl_3$ or d_6-acetone) also show that there is only one ligand environment, as expected. The $^{13}C\{^{1}H\}$ NMR spectra provided even more compelling evidence that Cu^{I}-NHC complexes have been formed, with the appearance of downfield resonances at 180.9, 179.0 and 179.3 ppm respectively for complexes **C1**, **C2** and **C3A**, corresponding to the copper-bound C2 atom. The exact identity of complexes **C1**, **C2** and **C3A** was further confirmed by elemental analysis. The Cu^{I}-NHC complexes **C1**, **C2** and **C3A** are illustrated in Figure 2.6.

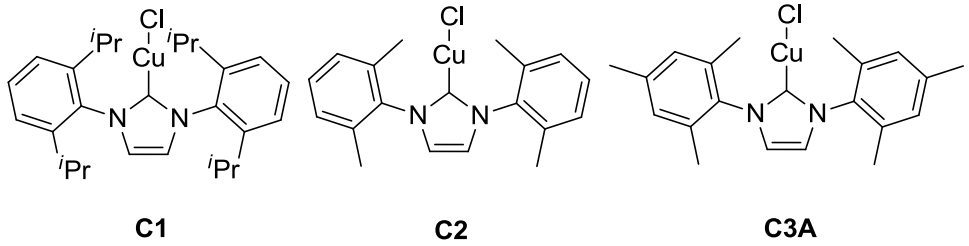

Figure 2.6 Complexes **C1**, **C2** and **C3A**

A range of different geometries about the metal centre in Cu^{I} complexes are known; some of the more common being linear, tetrahedral and trigonal. This lack of preference for a particular coordination geometry reflects the d^{10} electron configuration and thus absence of ligand field effects. The tendency of Cu^{I} to often form linear complexes may be in part due to the closeness in energies of the 3d, 4s and 4p orbitals causing spd hybridisation effects, which act to create two collinear spd-hybridised orbitals. Steric and geometric constraints imposed by the ligand also have an effect on the metal centre geometry. Since ligand precursors **L1**, **L2** and **L3** are very bulky, it would be difficult for any more than two of these to be accommodated around the Cu^{I} centre.

The NMR spectra (both ^{1}H and $^{13}C\{^{1}H\}$) of **C2** and **C3A** are different, depending on whether the spectra are recorded in d_6-DMSO or $CDCl_3$. The spectra in $CDCl_3$ indicate the presence of only one ligand environment, thus being consistent with the presence of only one Cu^{I} species in solution, most likely the linear heteroleptic [Cu(NHC)Cl]-type complex. However, when deuterated DMSO is used as the NMR solvent, a new set of ligand resonances appear. The ^{1}H NMR spectrum of **C3A** illustrates the two groups of resonances, which are labelled **A** and **B** in Figure 2.7, and have a ratio of about 2.5:1 (**A**:**B**) at room temperature.

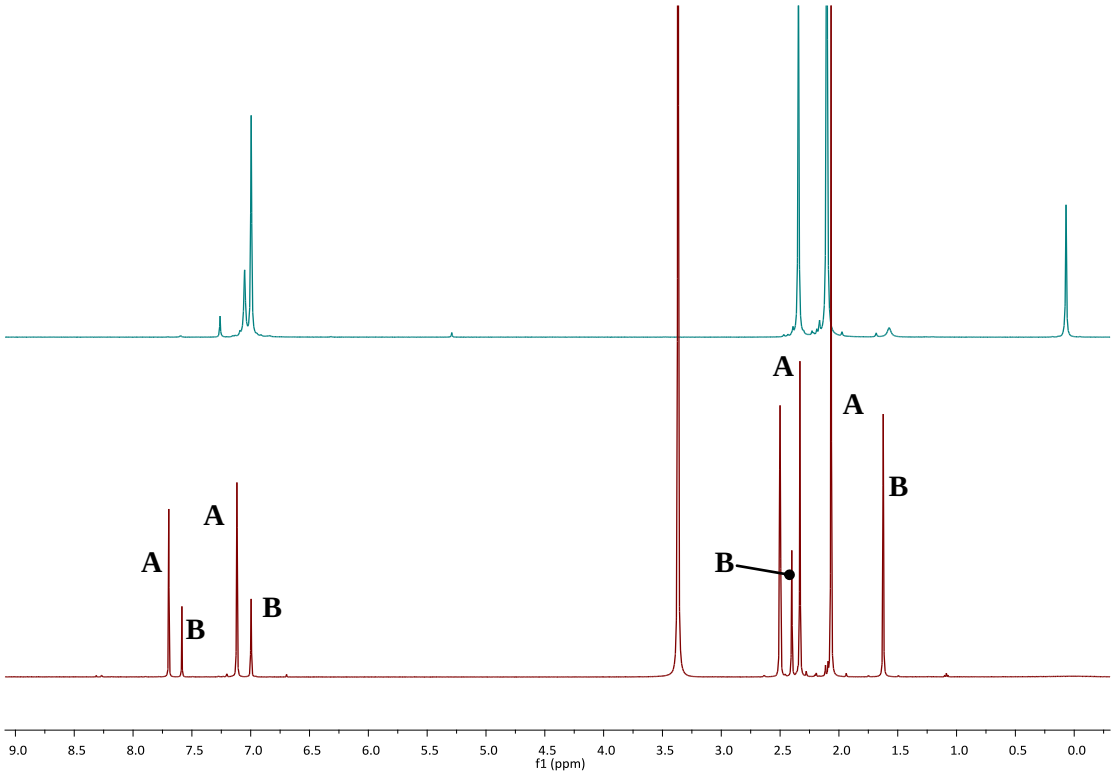

Figure 2.7 ^{1}H NMR spectra of complex **C3A** in d_6-DMSO (*bottom*) and $CDCl_3$ (*top*)

The non-integral ratio of the two sets of resonances (2.5:1) in d_6-DMSO suggests that the two different ligand environments are unlikely to be part of the same molecule. Thus, the two sets of resonances must belong to two different Cu^{I}-NHC species. One would propose that the two different species present in d_6-DMSO solutions of **C3A** are the neutral [Cu(NHC)Cl] complex and the ionic $[Cu(NHC)_2]^{+}CuCl_2^{-}$ complex (Figure 2.8). This assignment is based on previous studies of NHC exchange in Ag^{I}-NHC complexes, where both neutral [Ag(NHC)Cl] and ionic $[Ag(NHC)_2]^{+}AgCl_2^{-}$ species are observed to exist in equilibrium with each other. More polar solvents, such as dimethylsulfoxide, were also shown to favour the formation of the ionic complex versus the neutral complex.[17] This could explain why the two species are observed in d_6-DMSO, which would stabilise an ionic complex, but not in the far less polar $CDCl_3$.

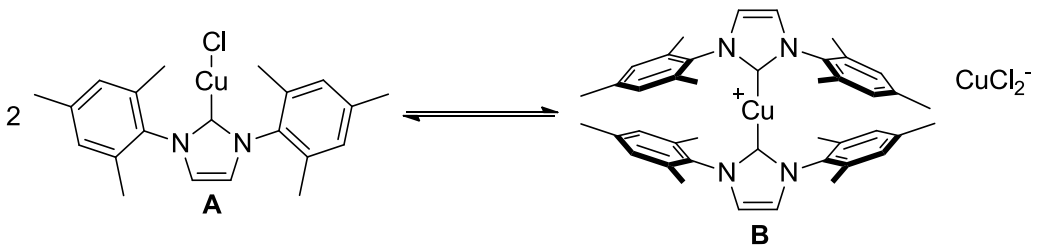

Figure 2.8 Proposed equilibrium between a [Cu(NHC)Cl]-type complex and a $[Cu(NHC)_2]^{+}CuCl_2^{-}$-type complex

Assignment of the two sets of resonances to either the neutral or ionic complex in the spectrum of **C3A** in d_6-DMSO is made using the assignments of similar Ag^I-NHCs during previous studies.[17a] The dominant species (**A**) in d_6-DMSO appears to be the neutral [Cu(NHC)Cl] complex with the minor species (**B**) being the ionic $[Cu(NHC)_2]^+CuCl_2^-$ complex. Most of the resonances of **A** and **B** occur at similar chemical shifts, indicating that the protons for the neutral and ionic complexes are in similar chemical environments. The largest difference in chemical shift between the equivalent protons of **A** and **B** occurs for the *ortho*-methyl protons of the aromatic rings. The *ortho*-methyl protons of **B (**$[Cu(NHC)_2]^+CuCl_2^-$) are shifted significantly upfield (1.62 ppm) compared to those of **A** ([Cu(NHC)Cl]), which resonate at 2.07 ppm. This upfield shift could be ascribed to the shielding effect provided by an interaction between the *ortho*-methyl protons of one aromatic ring with the ring current of the aromatic ring of the other NHC ligand. This interaction is illustrated in Figure 2.9, and is made possible by rotation about the N-$C_{(substituent)}$ bond. Clearly, no such interaction is possible for a [Cu(NHC)Cl]-type complex.

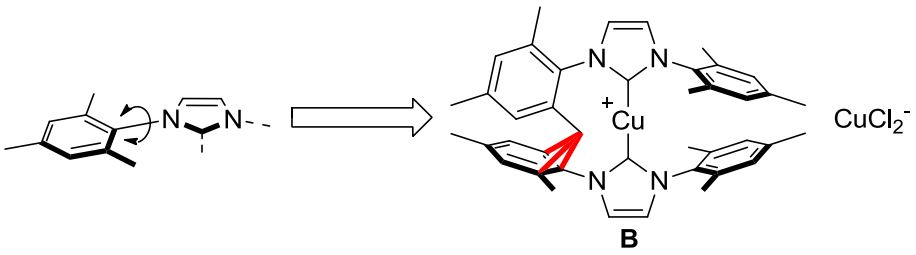

Figure 2.9 Shielding of *ortho*-methyl protons in a $[Cu(NHC)_2]^+CuCl_2^-$ complex

Variable temperature NMR studies were performed on **C3A** in d_6-DMSO to establish how the equilibrium between **A** and **B** would be altered on heating. The NMR sample of **C3A** was heated from ambient temperature (22°C) to 99°C with ^{1}H NMR spectra being collected at 10°C intervals. A small change was observed in the ratio of **A** to **B** on heating the sample. At room temperature, the ratio of the two sets of resonances, **A** and **B** is 2.5:1. Heating the sample to 99°C increased the proportion of **B**, giving a ratio of **A** to **B** of 2:1. No broadening or coalescence of the resonances of **A** and **B** occurs upon heating. This indicates that even at high temperatures, NHC-exchange between Cu^I-centres (which is required for the equilibrium between **A** and **B**) is slow on the NMR timescale. This allows both species to be observable by ^{1}H NMR spectroscopy.

The equilibrium between neutral [Ag(NHC)Cl]-type and ionic $[Ag(NHC)_2]^+AgCl_2^-$-type species has been studied in a recent report,[17b] as alluded to previously, where it was concluded, using evidence from variable concentration studies and DFT calculations, that NHC-exchange (and thus interconversion between [Ag(NHC)Cl] and $[Ag(NHC)_2]^+AgCl_2^-$) occurred *via* an associative mechanism. DFT calculations illustrated that a considerable steric clash occurs in the transition state between two of the *N*-substituents. The energetic cost of such a clash would

clearly be minimised if the *N*-substituents were methyl groups, for example, as opposed to mesityl groups, as in the case of **C3A**. This steric clash in the NHC-exchange transition state may explain why for **C3A**, exchange between **A** and **B** is slow on the NMR timescale, even at elevated temperatures.

As discussed *vide ante*, salt metathesis reactions were performed on ligand precursors **L1**-**L3** to form the imidazolium hexafluorophosphate salts **L4**-**L6**. Electrolysis of **L4**-**L6** for 10, 5 and 14Q respectively produced the previously reported Cu^{I}- *bis*NHC complexes **C4** and **C6** and the novel Cu^{I}- *bis*NHC complex **C5** (Scheme 2.7).

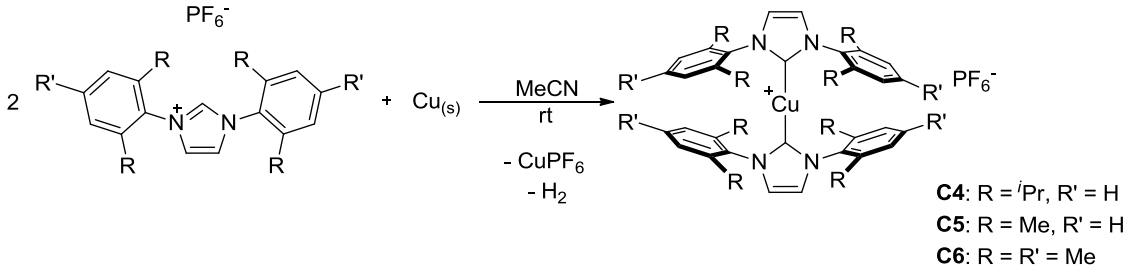

Scheme 2.7 Electrochemical synthesis of complexes **C4**-**C6**

The complexes **C4**-**C6** were isolated as off-white to white solids. The ^{1}H and $^{13}C\{^{1}H\}$ NMR spectra of **C4** and **C6** matched those described previously.[18] **C5** was isolated as an off-white solid in 37% yield. The product was characterised by ^{1}H and $^{13}C\{^{1}H\}$ NMR spectroscopy, high-resolution MS and elemental analysis. ^{1}H NMR spectroscopy reveals the loss of the low field resonance of the imidazolium hexafluorophosphate **L5** (9.56 ppm in d_6-acetone) on formation of the complex **C5**. A further significant difference between the ^{1}H NMR spectrum of the starting material, **L5**, and the product, **C5**, is the marked upfield shift of the *ortho*-methyl protons of the aromatic rings upon complexation (from 2.29 ppm in **L5** to 1.78 ppm in **C5**). This occurs due to the aromatic ring current shielding effect described earlier. Finally, a notable difference in the chemical shift values of the imidazole backbone (C4 and C5) protons is present when comparing the ^{1}H NMR spectra of **L5** and **C5**. On complexation, the resonance of the backbone protons shifts from 8.27 ppm (**L5**) to 7.52 ppm (**C5**). A comparison of the ^{1}H NMR spectra of **L5** and **C5** is given in Figure 2.10. A low field resonance at 178.1 ppm in d_6-acetone in the $^{13}C\{^{1}H\}$ NMR spectrum of **C5** is further verification of the formation of the desired Cu^{I}-NHC complex.

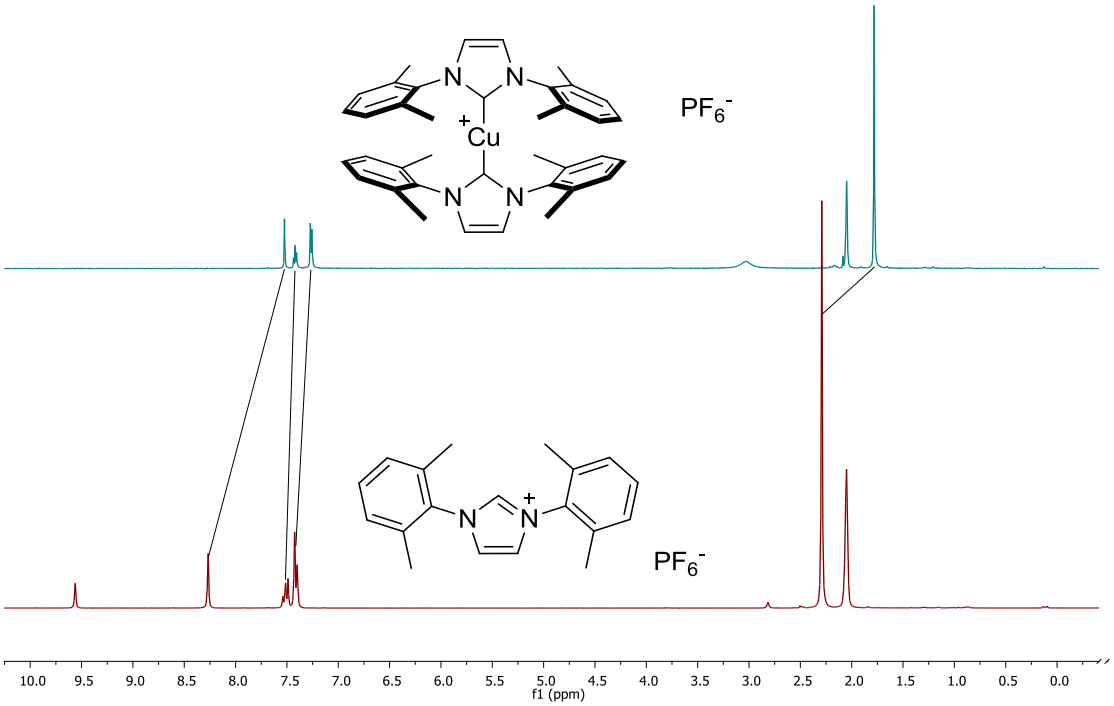

Figure 2.10 ^{1}H NMR spectra of complex **L5** (*bottom*) versus **C5** (*top*) in d_6-acetone

It was possible to obtain single crystals of **C5** suitable for X-ray diffraction analysis by the vapour diffusion of diethyl ether in to a concentrated solution of **C5** in acetone. **C5** crystallises in the monoclinic crystal system and was solved in the space group $P2_1/n$ (Figure 2.11).

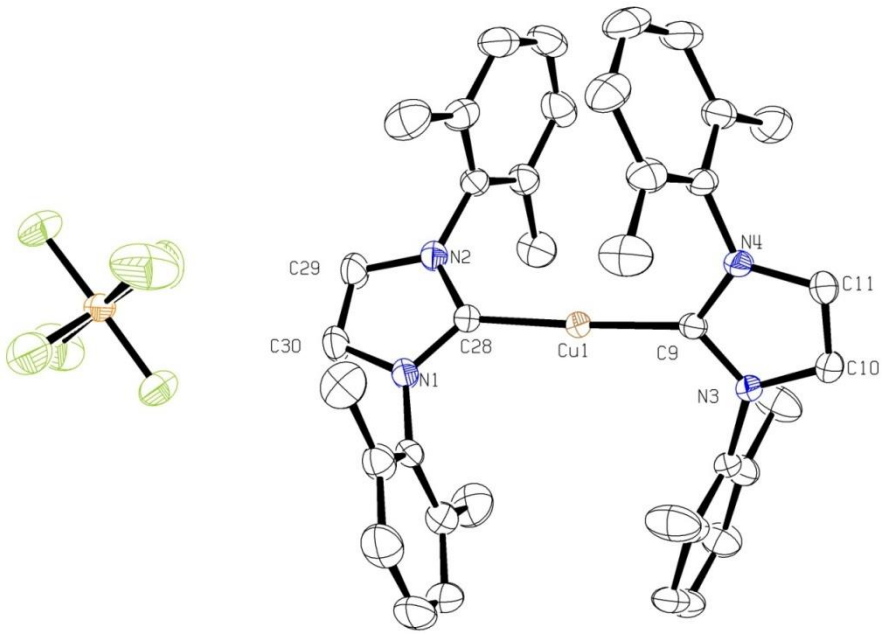

Figure 2.11 Molecular structure of **C5**. Ellipsoids are drawn at the 50% probability level. H atoms are omitted for clarity

Table 2.2 Selected bond distances (Å) and angles (deg) for **C5**

C(9)-Cu(1)	1.8918(17)	C(9)-Cu(1)-C(28)	177.55(7)
C(28)-Cu(1)	1.8873(17)	N(3)-C(9)-N(4)	104.21(14)
N(3)-C(9)	1.353(2)	N(1)-C(28)-N(2)	104.03(14)
N(4)-C(9)	1.358(2)	N(1)-C(28)-C(9)-N(3)	44.2
N(1)-C(28)	1.359(2)	N(2)-C(28)-C(9)-N(4)	48.4
N(2)-C(28)	1.354(2)		

The molecular structure of **C5** is provided (Figure 2.11) along with a table of relevant bond angles, bond lengths and torsional angles (Table 2.2). As expected, and in line with similar previously reported complexes,[18b] the coordination geometry about the Cu^{I} centre is near-linear with a bond angle of 177.55°. The Cu-C bond lengths of 1.89 Å are typical for Cu^{I}-NHC complexes. No Cu-C bond lengthening is encountered in the structure due to steric clashing between the ligands. This is presumably due to the fact that the aryl *N*-substituents are able to twist away from the plane defined by the imidazole. In fact, the plane of the aryl groups is almost orthogonal to that of the imidazole groups. Since a σ-donor interaction is thought to be the major bonding contribution to Cu^{I}-NHC bonds (with little contribution from a π-backbonding interaction), the two NHC ligands of **C5** are also able to twist with respect to each other in order to relieve steric congestion. Torsion angles of 44.2° and 48.2° between the NHC ligands illustrates the twisting of the two NHC ligands with respect to each other.

1-Methyl-3-ethylimidazolium chloride (**L7**) has been the least bulky NHC precursor used in the electrochemical reaction system. Electrolysis of **L7** for 2Q yielded an orange oil (**C7**) after work-up. A white solid was expected as the product for this reaction. It is suggested that contamination of the final product by copper salts and ligand oxidation/breakdown products leads to the appearance of the product as an orange oil rather than a white solid. This contamination has proved difficult to remove, especially given the extreme air/moisture sensitivity of **C7**, rendering conventional purification techniques, such as column chromatography, useless. Exposure of **C7** to the atmosphere quickly leads to the formation of an intractable green oil. Repeated attempts at crystallisation of **C7** proved futile. However, ^{1}H NMR and $^{13}C\{^{1}H\}$ NMR spectroscopy as well as high-resolution MS has been able to provide some evidence as to the exact nature of **C7**. ^{1}H NMR spectroscopy reveals the loss of the C2 proton resonance, a typical indication that metal complexation has been successful. The presence of only one set of ligand resonances in $CDCl_3$ in the ^{1}H and $^{13}C\{^{1}H\}$ NMR spectra demonstrates the presence of one ligand environment in the complex. A characteristic low field resonance at 176.0 ppm in the $^{13}C\{^{1}H\}$ NMR spectrum of **C7** shows that the product is almost

definitely a Cu^{I}-NHC complex. The strongest clue as to the exact nature of **C7** is provided by high-resolution MS, where the dominant fragment is a *bis*NHC fragment, $[Cu(NHC)_2]^+$. This fragment could be formed easily by loss of a Cu-bound Cl anion. Thus, the proposed structure of **C7** is that of a trigonal Cu^{I} centre bound by two NHC ligands and one chloride ligand (Figure 2.12). The huge disparity in ligand bulk between 1-methyl-3-ethylimidazolium chloride (**L7**) and 1,3-bis(2,6-diisopropylphenyl)imidazolium chloride (**L1**), for example, helps explain how two NHC ligands might be accommodated around the Cu^{I} centre in **C7**, but only one NHC ligand can be accommodated around the Cu^{I} centre in **C1**.

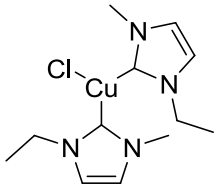

Figure 2.12 Proposed structure of **C7**

Trigonal Cu^{I}-*bis*NHC complexes similar to **C7** have been prepared previously. For example, Albrecht *et al.*[14a] prepared a Cu^{I} complex bearing two 1-methyl-3-isopropylimidazol-2-ylidene ligands and an iodide ligand. This complex is illustrated in Figure 2.13.

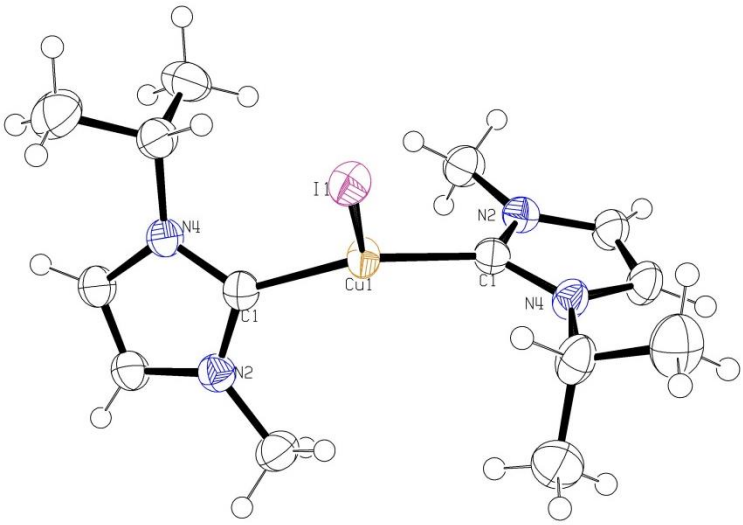

Figure 2.13 Trigonal Cu^{I}-NHC complex prepared by Albrecht *et al.*[14a]

Electrolysis of 1-methyl-3-benzylimidazolium bromide (**L8**) for 2Q produced the complex, **C8**, as colourless crystals in a 67% yield. **C8** was subject to characterisation by ^{1}H NMR spectroscopy, which revealed the loss of the characteristic C2 proton resonance of imidazolium salts. Analysis by $^{13}C\{^{1}H\}$ NMR spectroscopy in $CDCl_3$ demonstrated the appearance of a resonance at 178.7 ppm, characteristic of a Cu^{I}-bound carbenic carbon atom. Elemental analysis revealed the empirical formula of **C8** to be $C_{11}H_{12}BrCuN_2$, implying that the complex contains

one NHC and one bromide ligand per Cu centre. Single crystals of **C8** suitable for X-ray diffraction analysis were grown by the slow evaporation of a concentrated solution of **C8** in tetrahydrofuran. **C8** crystallises in the monoclinic crystal system and was solved in the space group $P2_1/n$ (Figure 2.14).

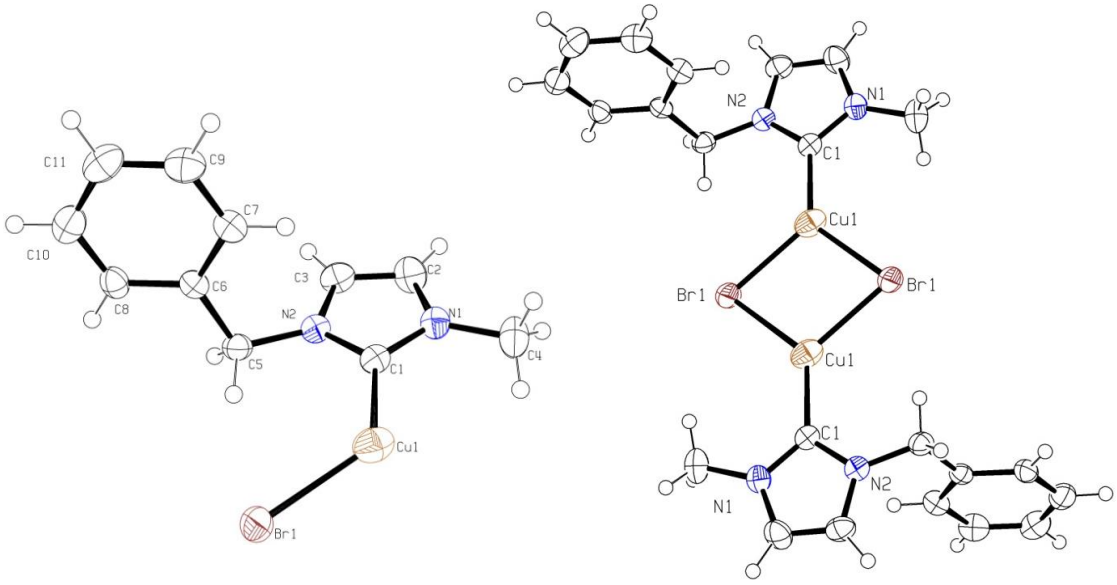

Figure 2.14 Molecular structure of **C8** (asymmetric unit (*left*) and dimer (*right*)). Ellipsoids are drawn at the 50% probability level

Table 2.3 Selected bond distances (Å) and angles (deg) for **C8**

C(1)-Cu(1)	1.932(6)	C(1)-Cu(1)-Br(1)	131.31(18)
Cu(1)-Br(1)	2.4249(11)	C(1)-Cu(1)-Br(1)'	127.94(18)
Cu(1)-Br(1)'	2.4506(13)	Br(1)-Cu(1)-Br(1)'	100.75(4)
C(1)-N(1)	1.380(8)	N(1)-C(1)-N(2)	104.5(5)
C(1)-N(2)	1.363(7)		
Cu(1)---Cu(1)'	3.109		

C8 crystallises as a dimer with the two Cu^I centres of the dimer possessing a distorted trigonal planar geometry. The dimer is held together by two μ^2-Br atoms giving an asymmetric $[Cu_2Br_2]$ core. [Ag(NHC)X] and [Cu(NHC)X]-type complexes frequently crystallise as dimers when the NHC bears less sterically-hindering *N*-substituents, with numerous examples being present in the literature.[15b, 17b, 19] The lack of preference of Cu^I for a single coordination geometry (*e.g.* linear in **C5** and trigonal planar in **C8**) reflects the d^{10} electron configuration and thus lack of ligand field effects for Cu^I complexes.

The formation of a dimer in the solid state could explain the marked elongation of the Cu-Br bonds in **C8**. Cu-Br bonds of structurally characterised linear [Cu(NHC)Br] complexes are often in the region of approximately 2.20 Å.[15b] However, the Cu-Br bonds in the asymmetric [Cu_2Br_2] core of **C8** are 2.42 Å and 2.45 Å in length respectively. This elongation possibly results from the increase in the coordination number of the Cu centres from 2 to 3 upon dimerisation. The increased coordination number presumably means that a build-up of electron density at the metal centre occurs, which can be relieved by a lengthening of the Cu-Br bonds and the concomitant decrease in orbital overlap and electron donation which that brings.

The Cu-C bond length of 1.93 Å is fairly typical for Cu^I-NHC complexes, which are typically in the range of 1.87 - 1.96 Å.[15b, 20] The distance between the two Cu centres of the dimer, at 3.11 Å, is well outside of the sum of the van der Waals radii (2.80 Å), and thus there is unlikely to be any cuprophilic interaction at all between the Cu centres. On examination of the extended crystal structure, close contacts are observed between the bromides and a CH_2 proton of a benzyl group of a neighbouring dimer. This close contact, at 2.91 Å, falls well within the sum of the van der Waals radii (3.05 Å).

Electrolysis of the anion-exchanged salt of **L8**, 1-methyl-3-benzylimidazolium hexafluorophosphate **(L9)**, for 5Q yielded the *bis*-NHC complex (**C9**) as colourless crystals following work-up, in a 58% yield (Figure 2.15).

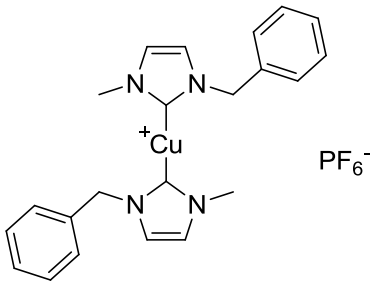

Figure 2.15 Structure of complex **C9**

Characterisation by the conventional means, ^1H and $^{13}C\{^1H\}$ NMR spectroscopy and high-resolution MS, conclusively demonstrated the successful synthesis of **C9**. Disappearance of the lowest field resonance in the ^1H NMR spectrum (imidazolium proton) and appearance of a low field resonance in the $^{13}C\{^1H\}$ NMR spectrum at 179.1 ppm (in CD_3CN) was apparent. Furthermore, the overwhelmingly dominant fragment in the high-resolution mass spectrum was **C9** minus the hexafluorophosphate anion ($[M - PF_6]^+$).

Substitution of the methyl group of **L8** with a benzyl group gives the symmetrical NHC precursor 1,3-dibenzylimidazolium bromide (**L10**). Electrolysis of **L10** in acetonitrile for 2Q yielded the complex **C10** following work-up. Loss of the imidazolium proton resonance in the

^{1}H NMR spectrum and appearance of a resonance at 177.9 ppm in $CDCl_3$ indicated the formation of a Cu^I-NHC complex. To date, accurate elemental analysis of **C10** has not been possible, presumably due to the presence of copper salt contaminants which have proved not particularly facile to remove under air/moisture-free conditions. However, single crystals of **C10** suitable for X-ray diffraction analysis were able to be grown by the vapour diffusion of diethyl ether in to a concentrated solution of **C10** in tetrahydrofuran. **C10** crystallises in the triclinic crystal system and was solved in the space group $P\bar{1}$ (Figure 2.16).

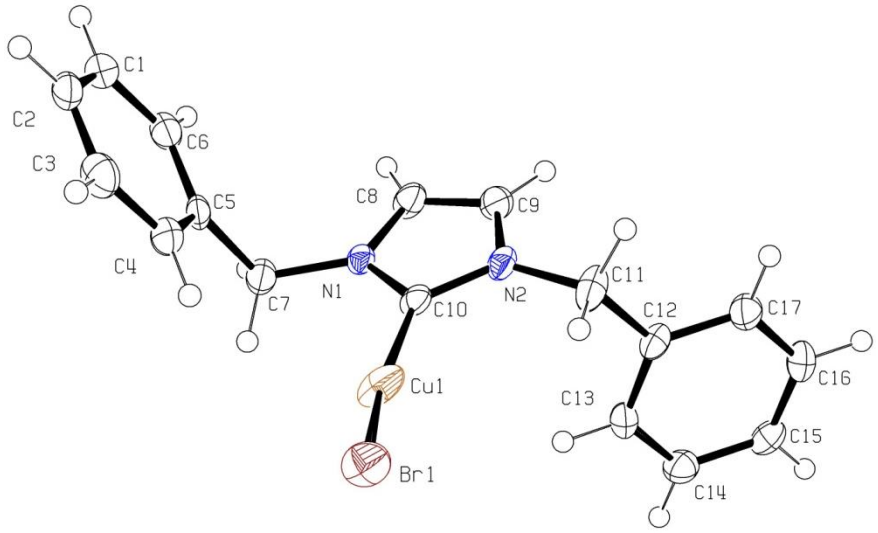

Figure 2.16 Molecular structure of **C10**. Ellipsoids are drawn at the 50% probability level

Table 2.4 Selected bond distances (Å) and angles (deg) for **C10**			
C(1)-Cu(1)	1.894(3)	C(10)-Cu(1)-Br(1)	162.21(11)
Cu(1)-Br(1)	2.2574(6)	N(1)-C(10)-N(2)	103.5(3)
C(10)-N(1)	1.352(4)	N(2)-C(10)-Cu(1)-Br(1)	42.3(5)
C(10)-N(2)	1.363(5)		

At first appearance, **C10** crystallises as a simple approximately linear two-coordinate complex. Both Cu-C (1.89 Å) and Cu-Br (2.26 Å) bond distances are typical for linear Cu^I-NHC complexes.[15b] The C-Cu-Br bond angle of 162.21° is a little unusual for this type of complex, given its pronounced departure from perfect linearity. It is especially unusual given that the *N*-substituents are non-bulky benzyl groups, which can bend away from the carbene/metal centre, as shown in Figure 2.16. However, examination of the extended crystal structure reveals a possible explanation for the deviation from linearity exhibited by **C10** (Figure 2.17).

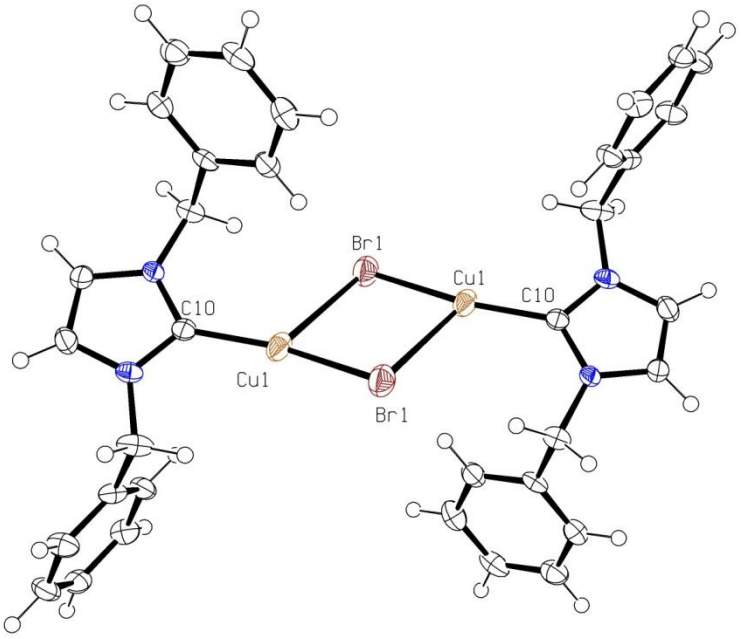

Figure 2.17 Molecular structure of apparent dimer of **C10**. Ellipsoids are drawn at the 50% probability level

Table 2.5 Selected bond distances (Å) and angles (deg) for **C10** 'dimer'

Cu(1)-Br(1)	2.2574(6)	C(10)-Cu(1)-Br(1)	162.21(11)
Cu(1)-Br(1)' or Cu(1)'-Br(1)	3.1644(3)	C(10)-Cu(1)-Br(1)'	111.24
		Br(1)-Cu(1)-Br(1)'	86.14
		Cu(1)-Br(1)-Cu(1)'	93.86

Association of neighbouring CuBr groups results in the formation of what appears to be a dimer in the solid state, the centre of which lies on an inversion centre. However, the distance between the neighbouring CuBr units, at 3.16 Å, is very long, falling just within the sum of the van der Waals radii (3.25 Å). This would tend to imply that the Cu-Br bonding interaction holding the dimer together is weak at best. It is easy to envisage that this structure, while not a true dimer, represents an intermediate in the process of dimerisation during crystallisation. A partially dimeric structure, not too dissimilar to **C10,** has been reported previously by Raubenheimer *et al*..[21] The extended crystal structure also reveals a number of other close contacts in the solid state, including π-proton interactions between one of the backbone NHC protons and a neighbouring aromatic ring (H---π distance of 2.73 Å).

The benzannulated derivatives of **L10** are 1,3-dibenzylbenzimidazolium bromide (**L11**) and 1,3-dibenzylbenzimidazolium hexafluorophosphate (**L12**), the anion-exchanged salt of **L11**.

Benzannulation of the backbone of an NHC provides a small degree of extra bulk, but mainly acts to tune the electronic properties of the NHC ligand. Benzimidazol-2-ylidenes, despite being unsaturated, are known to possess spectroscopic and structural characteristics more akin to the saturated imidazol-2-ylidenes. For instance, the free NHCs of both benzimidazol-2-ylidenes and imidazolidin-2-ylidenes rapidly dimerise (when bearing small *N*-substituents) to form the corresponding enetetraamine.[22]

Electrolysis of **L11** and **L12** for 1.5Q and 11Q respectively, led to the formation of the anticipated neutral [Cu(NHC)Br]-type complex, **C11**, and cationic $[Cu(NHC)_2]^+PF_6^-$-type complex (**C12**). Both complexes were isolated as white crystalline solids in good yields (68 and 65%). Characterisation by ^{1}H NMR and $^{13}C\{^1H\}$ NMR spectroscopy as well as high-resolution MS and elemental analysis was performed for both compounds to confirm their structure and purity.

Single crystals of both **C11** and **C12** suitable for X-ray diffraction analysis were grown by the vapour diffusion of pentane in to a concentrated solution of either **C11** or **C12** in dichloromethane. Both **C11** and **C12** crystallise in the triclinic crystal system and both were solved in the space group $P\bar{1}$ (Figure 2.18).

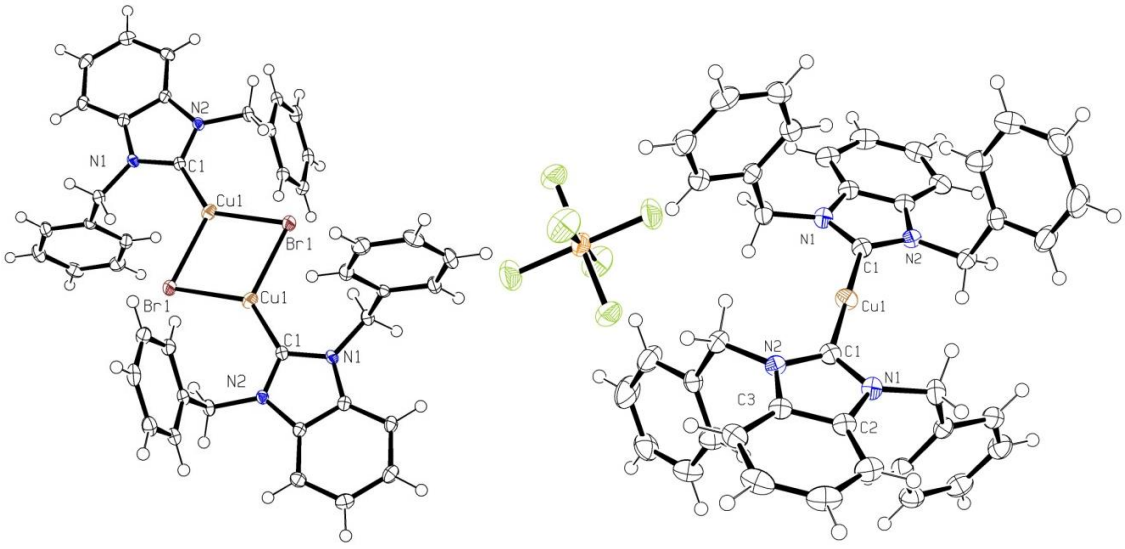

Figure 2.18 Molecular structures of **C11** (*left*) and **C12** (*right*). Asymmetric units not illustrated. Ellipsoids are drawn at the 50% probability level

Table 2.6 Selected bond distances (Å) and angles (deg) for **C11** and **C12**

	C11	**C12**		**C11**	**C12**
C(1)-Cu(1)	1.914(3)	1.9066(15)	C(1)-Cu(1)-C(1)'	-	180.00(7)
Cu(1)-Br(1)	2.4183(5)	-	C(1)-Cu(1)-Br(1)	134.16(8)	-
Cu(1)-Br(1)'	2.5073(5)	-	C(1)-Cu(1)-Br(1)'	125.58(8)	-
C(1)-N(1)	1.369(3)	1.3523(19)	N(1)-C(1)-N(2)	104.9(2)	105.82(12)
C(1)-N(2)	1.365(3)	1.3522(19)			

C11 crystallises as a centrosymmetric dimer with an inversion centre in the middle of the asymmetric $[Cu_2Br_2]$ core. The asymmetry of the central $[Cu_2Br_2]$ core is illustrated by the quite substantially differing Cu-Br bond lengths of 2.42 and 2.51 Å and C-Cu-Br bond angles of 134.16 and 125.58°. The asymmetry presumably arises due to packing effects in the extended crystal lattice. The Cu-Br bond lengths of **C11**, at 2.42 and 2.51 Å, are very comparable to those of the dimer (**C8**), described earlier (2.42 Å and 2.45 Å). Examination of the extended crystal structure reveals a number of π-based interactions including π-π stacking and π-proton interactions. This is perhaps not surprising given that there are six aromatic rings per dimer. [Cu(NHC)X]-type complexes where the NHC is a benzimidazolin-2-ylidene have been synthesised previously, and have been reported to crystallise as halide-bridged dimers.[23]

The cationic $[Cu(NHC)_2]^+PF_6^-$-type complex (**C12**) also crystallises as a centrosymmetric structure with a perfectly linear geometry at the Cu^I centre (180.00°). The two NHC ligands are in virtually the same plane, with a very small torsional angle of 4.6° separating them. This adds credence to the suggestion that the benzyl substituents are non-bulky, since there is obviously little steric requirement for the ligands to twist with respect to each other. As with **C11**, a number of possible π-π stacking and π-proton interactions are evident in the extended crystal structure, along with F---H interactions.

The cyclophane bromide NHC precursor **L13A** is almost entirely insoluble in acetonitrile. However, performing a salt metathesis reaction on **L13A** produces the cyclophane hexafluorophosphate NHC precursor **L13B**, which is freely soluble in acetonitrile. Electrolysis of **L13B** for 5.5Q produced **C13**, which has the formula $[Cu(NHC)]_2^{2+}2PF_6^-$. Silver and gold complexes derived from **L13B** have been prepared previously,[24] which are isostructural to **C13**. It should be noted, however, that the synthesis of the silver and gold analogues using normal chemical methods required much more forcing conditions than are used in the electrochemical system.

As described earlier in the chapter, electrochemical reactions are monitored by withdrawing small aliquots from the reaction mixture at certain values of 'Q' and recording the ^{1}H NMR spectra of the aliquots. Complete disappearance of the low field resonance (imidazolium proton) indicates that the reaction has reached completion. Usually, when the NMR spectra from over the course of the reaction are overlayed, they show only depletion of the starting material and appearance of a single product. In the case of **C13**, this is illustrated in Figure 2.19, below. The disappearance of the starting material (red square) is clearly evident, along with the concomitant formation of the product (blue circle).

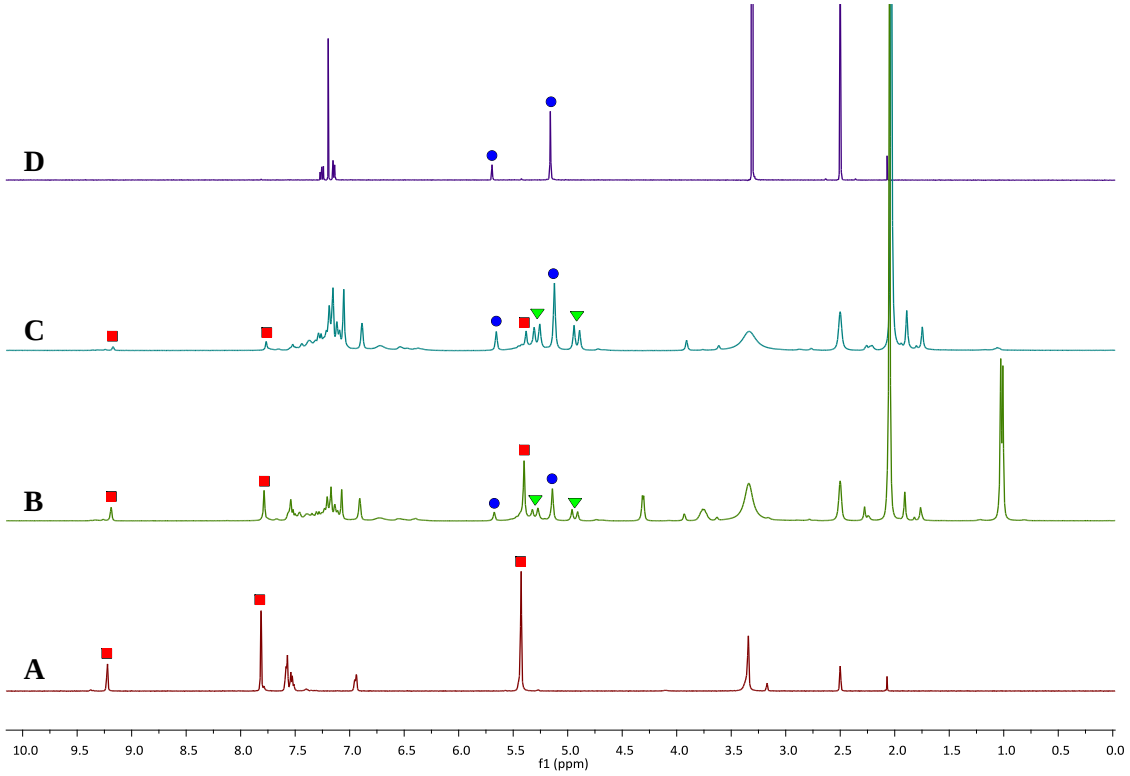

Figure 2.19 ^{1}H NMR spectra obtained in d_6-DMSO during the electrolysis of **L13B**. Starting material (**A**), during the reaction (**B** and **C**) and product (**D**)

Notably, a group of new resonances (green triangle) appear during the reaction, which are not present in either the starting material or the product. The AX-type resonances, which have a $^{2}J_{H\text{-}H}$ coupling of 15.2 Hz, correspond to two inequivalent benzylic proton environments. Since the benzylic protons of the product (blue circle) are equivalent in the ^{1}H NMR spectrum in d_6-DMSO, this new set of resonances must belong to an intermediate in the formation of the product (**C13**). Based on literature precedent, the structure of the intermediate in this reaction (green triangle) is proposed below (Figure 2.20).[24a, 25]

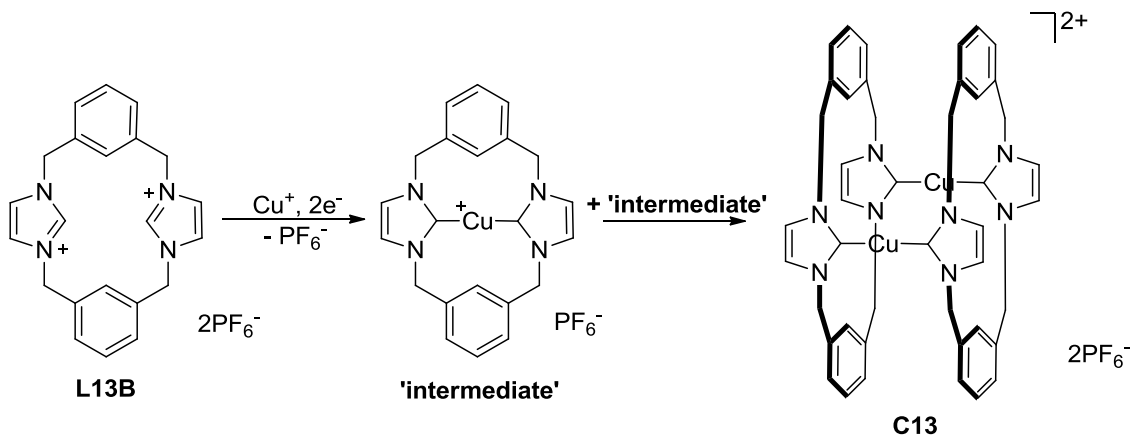

Figure 2.20 Formation of **C13** from **L13B** *via* an NMR-detectable intermediate

A Hg^{II} complex reported by Baker *et al*.[25] bound to the NHC derived from **L13B** was isolated as a $[Hg(NHC)]^{2+}2PF_6^-$ complex (Figure 2.21), analogous to the intermediate illustrated above. The ^1H NMR spectrum of the Hg^{II}-NHC complex displays the same characteristic AX-type pattern of resonances observed in the spectra obtained during the reaction to form **C13**.

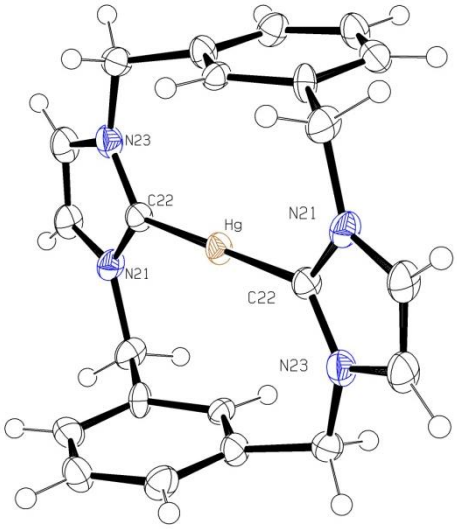

Figure 2.21 Hg^{II}-NHC complex reported by Baker *et al*.[25] Ellipsoids are drawn at the 50% probability level. PF_6^- anions are omitted for clarity

It is anticipated that the 'intermediate' shown above (Figure 2.20) is the kinetic product of the electrochemical reaction, but that **C13** is the thermodynamic product and thus the isolable product following completion of the electrolysis and work-up. It is proposed that the relative instability of the 'intermediate' with respect to **C13** is as a result of the unusually long Cu-C bonds that would be present in the 'intermediate', if indeed it is structurally analogous to the Hg^{II}-NHC complex above. The C-Hg bond distances are 2.05 Å, which is not overly long for an NHC bound to a larger Hg^{2+} cation,[25] but which would be unusually long for an NHC bound to the much smaller Cu^+ cation, where bond lengths are typically in the range of 1.87 - 1.96 Å.[15b,

[20] To achieve a Cu^{I}-C bond length in this region, significant and presumably energetically unfavourable distortion of the ligand would have to occur.

C13 was isolated as a white crystalline solid following work-up in 71% yield. The complex was subject to full characterisation by ^{1}H NMR and $^{13}C\{^{1}H\}$ NMR spectroscopy, high-resolution MS and elemental analysis. NMR spectra of **C13** were obtained in both CD_3CN and d_6-DMSO (Figure 2.22). Surprisingly, the benzylic protons are equivalent in the more polar solvent d_6-DMSO (*bottom*), but become inequivalent in CD_3CN, resonating as an AB pattern of doublets. This implies that the cyclophane is conformationally rigid on the NMR timescale in CD_3CN, hence giving rise to the AB pattern, but that it is conformationally fluxional on the NMR timescale in d_6-DMSO, thus producing a singlet signal. An interesting feature of both spectra is the chemical shift of the C2 proton of the aromatic rings, which resonates at approximately 5.7 ppm in both solvents. This marked upfield shift compared to the other aromatic protons (C4, C5 and C6) is thought to be due to this proton residing within the applied magnetic field-opposing region of the aromatic ring current of the two parallel NHC rings.[24] Inspection of the molecular structure of **C13** (Figure 2.23) gives this theory some credence.

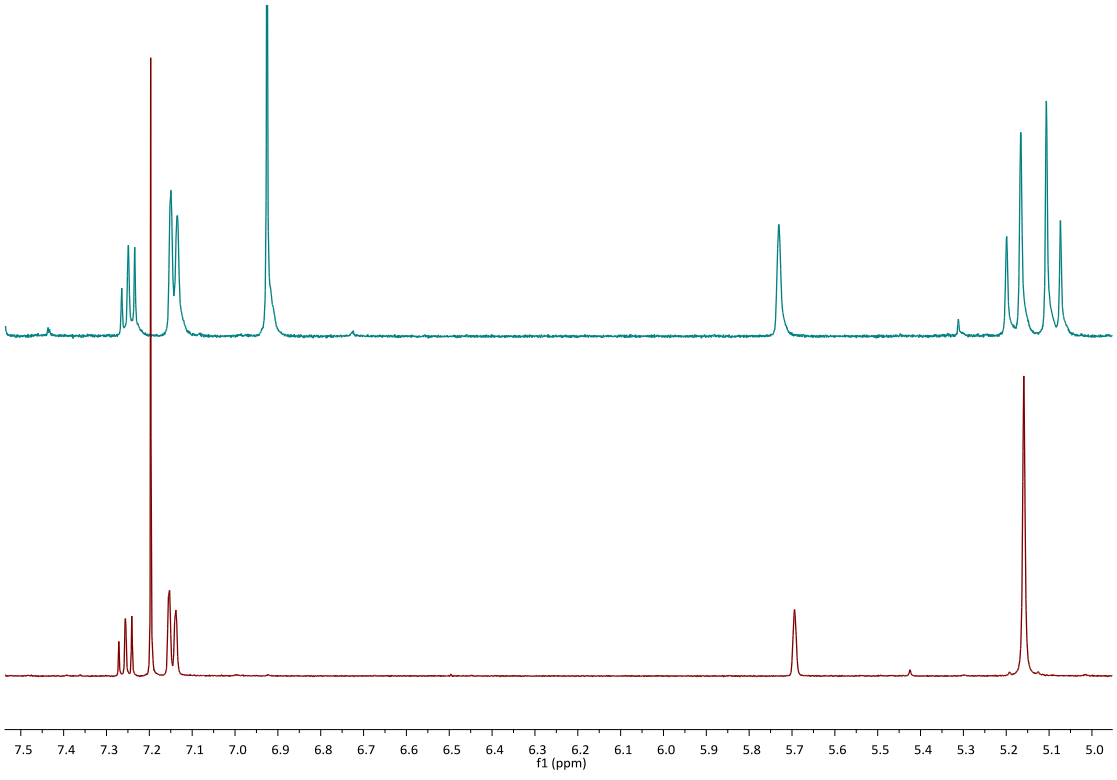

Figure 2.22 ^{1}H NMR spectra of **C13** in d_6-DMSO (bottom) and CD_3CN (top)

Single crystals of **C13** suitable for X-ray diffraction analysis were grown by the vapour diffusion of diethyl ether in to a concentrated solution of **C13** in acetonitrile. **C13** crystallises in the monoclinic crystal system and was solved in the space group $P2_1/c$ (Figure 2.23).

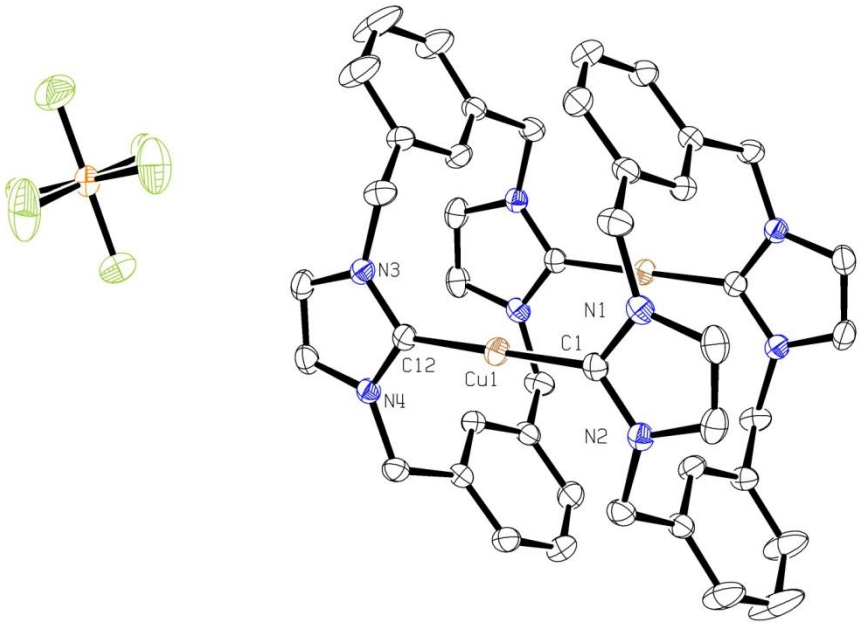

Figure 2.23 Molecular structure of **C13**. Ellipsoids are drawn at the 50% probability level. H atoms and one PF_6^- are omitted for clarity

Table 2.7 Selected bond distances (Å) and angles (deg) for **C13**

C(1)-Cu(1)	1.8966(17)	C(1)-Cu(1)-C(12)	178.45(7)
C(12)-Cu(1)	1.8952(17)	N(1)-C(1)-N(2)	104.14(14)
N(1)-C(1)	1.355(2)	N(3)-C(12)-N(4)	103.99(14)
N(2)-C(1)	1.351(2)		
N(3)-C(12)	1.351(2)		
N(4)-C(12)	1.355(2)		

The solid state structure of **C13** is analogous to silver and gold complexes previously reported. The benzyl groups are arranged such that they point towards the Cu centres on one side and away from them on the other. The Cu-C bond distances, at 1.90 Å, are fairly typical for Cu^I-NHC complexes. Furthermore, the C-Cu-C bond angle of 178.45° is only a slight deviation from perfect linearity, which is as you would expect for this type of complex.

2.4 Conclusions

Cu^I-NHC complexes have become increasingly popular in the field of organometallic chemistry due to their wide range of potential applications, including in catalysis, biomedicine and as transmetallating agents for the synthesis of other transition metal-NHC complexes. The

relatively low cost of copper, in comparison to palladium or gold for example, only adds to the appeal of copper compounds in these roles.

It has been demonstrated that a novel electrochemical synthetic technique can be applied to the synthesis of both novel and previously characterised Cu^{I}-NHC complexes. Complexes have been synthesised with a range of *N*-substituents include bulky aryl groups and much less bulky benzyl and alkyl groups. By obsequiously adhering to the electrochemical procedure which has been developed, moderate to good yields of the desired Cu^{I}-NHC complex could be produced during every reaction.

The electrochemical procedure has allowed the selective synthesis of both neutral and cationic complexes, depending on the choice of starting imidazolium salt. The use of imidazolium halide (coordinating anion) starting materials led to the exclusive synthesis of neutral [Cu(NHC)X]-type complexes. This represents the first reported example of the synthesis of [Cu(NHC)X]-type complexes using an electrochemical procedure. The use of imidazolium hexafluorophosphate (non-coordinating anion) starting materials led to the exclusive synthesis of cationic $[Cu(NHC)_2]^{+}PF_6^{-}$-type complexes.

2.5 Future Work

Future work in this area will involve extending the electrochemical methodology to other transition metals. Copper's group 11 congeners, silver and gold, would seem like obvious targets for the application of this technique, especially given their similar chemical characteristics to copper. Indeed, preliminary screening *via* electrolysis of an acetonitrile solution of **L3** using a gold wire anode and a copper plate cathode led to the conversion of **L3** to a mix of Au^{I}-NHC complexes (IMes-Au-Cl and $[Au(IMes)_2]^{+}AuCl_2^{-}$). This initial result is promising, and represents the first reported example of the electrochemical synthesis of a Au^{I}-NHC complex. It would also be pertinent to try other members of the 1st row transition metal series in the electrochemical system, including iron, cobalt and nickel, metals whose relative low cost also makes them attractive for use in catalysis.

The application of the novel Cu^{I}-NHC complexes synthesised during this work in catalysis is perhaps another area worthy of further exploration. Cu^{I}-NHC complexes have been demonstrated to have significant roles in click chemistry, hydrosilylation, amination (*e.g.* Ullman coupling) and reduction of carbonyl compounds.[15b, 20b, 26]

2.6 References

[1] A. J. Arduengo, R. L. Harlow, M. Kline, *Journal of the American Chemical Society* **1991**, *113*, 361-363.

[2] a) L. Jafarpour, E. D. Stevens, S. P. Nolan, *Journal of Organometallic Chemistry* **2000**, *606*, 49-54; b) X. Bantreil, S. P. Nolan, *Nat. Protocols* **2011**, *6*, 69-77.

[3] L. Hintermann, *Beilstein Journal of Organic Chemistry* **2007**, *3*, 22.

[4] J. Haider, K. Kunz, U. Scholz, *Advanced Synthesis & Catalysis* **2004**, *346*, 717-722.

[5] K. Dong, S. Zhang, *Chemistry – A European Journal* **2012**, *18*, 2748-2761.

[6] T. Steiner, *Angewandte Chemie International Edition* **2002**, *41*, 48-76.

[7] S. Patil, J. Claffey, A. Deally, M. Hogan, B. Gleeson, L. M. Menéndez Méndez, H. Müller-Bunz, F. Paradisi, M. Tacke, *European Journal of Inorganic Chemistry* **2010**, *2010*, 1020-1031.

[8] M. V. Baker, M. J. Bosnich, D. H. Brown, L. T. Byrne, V. J. Hesler, B. W. Skelton, A. H. White, C. C. Williams, *The Journal of Organic Chemistry* **2004**, *69*, 7640-7652.

[9] B. Liu, Y. Zhang, D. Xu, W. Chen, *Chemical Communications* **2011**, *47*, 2883-2885.

[10] B. Gorodetsky, T. Ramnial, N. R. Branda, J. A. C. Clyburne, *Chemical Communications* **2004**, 1972-1973.

[11] M. Feroci, I. Chiarotto, M. Orsini, G. Sotgiu, A. Inesi, *Advanced Synthesis & Catalysis* **2008**, *350*, 1355-1359.

[12] M. Orsini, I. Chiarotto, G. Sotgiu, A. Inesi, *Electrochimica Acta* **2010**, *55*, 3511-3517.

[13] J. R. Black, W. Levason, M. Webster, *Acta Crystallographica Section C* **1995**, *51*, 623-625.

[14] a) G. Venkatachalam, M. Heckenroth, A. Neels, M. Albrecht, *Helvetica Chimica Acta* **2009**, *92*, 1034-1045; b) M. R. L. Furst, C. S. J. Cazin, *Chemical Communications* **2010**, *46*, 6924-6925.

[15] a) H. Jang, A. R. Zhugralin, Y. Lee, A. H. Hoveyda, *Journal of the American Chemical Society* **2011**, *133*, 7859-7871; b) S. Díez-González, E. C. Escudero-Adan, J. Benet-Buchholz, E. D. Stevens, A. M. Z. Slawin, S. P. Nolan, *Dalton Transactions* **2010**, *39*, 7595-7606; c) H. Lebel, M. Davi, S. Díez-González, S. P. Nolan, *The Journal of Organic Chemistry* **2006**, *72*, 144-149.

[16] a) S. Okamoto, S. Tominaga, N. Saino, K. Kase, K. Shimoda, *J. Organomet. Chem.* **2005**, *690*, 6001-6007; b) V. Jurkauskas, J. P. Sadighi, S. L. Buchwald, *Organic Letters* **2003**, *5*, 2417-2420.

[17] a) M. Iglesias, D. J. Beetstra, J. C. Knight, L.-L. Ooi, A. Stasch, S. Coles, L. Male, M. B. Hursthouse, K. J. Cavell, A. Dervisi, I. A. Fallis, *Organometallics* **2008**, *27*, 3279-

3289; b) H.-L. Su, L. M. Perez, S.-J. Lee, J. H. Reibenspies, H. S. Bazzi, D. E. Bergbreiter, *Organometallics* **2012**, *31*, 4063-4071.

[18] a) S. Díez-González, N. M. Scott, S. P. Nolan, *Organometallics* **2006**, *25*, 2355-2358; b) S. Díez-González, E. D. Stevens, N. M. Scott, J. L. Petersen, S. P. Nolan, *Chemistry – A European Journal* **2008**, *14*, 158-168.

[19] J. C. Y. Lin, R. T. W. Huang, C. S. Lee, A. Bhattacharyya, W. S. Hwang, I. J. B. Lin, *Chemical Reviews* **2009**, *109*, 3561-3598.

[20] a) N. P. Mankad, T. G. Gray, D. S. Laitar, J. P. Sadighi, *Organometallics* **2004**, *23*, 1191-1193; b) S. Díez-González, E. D. Stevens, S. P. Nolan, *Chemical Communications* **2008**, 4747-4749.

[21] H. G. Raubenheimer, S. Cronje, P. J. Olivier, J. G. Toerien, P. H. van Rooyen, *Angewandte Chemie International Edition in English* **1994**, *33*, 672-673.

[22] F. E. Hahn, L. Wittenbecher, D. Le Van, R. Fröhlich, *Angewandte Chemie International Edition* **2000**, *39*, 541-544.

[23] W. J. Humenny, S. Mitzinger, C. B. Khadka, B. K. Najafabadi, I. Vieira, J. F. Corrigan, *Dalton Transactions* **2012**, *41*, 4413-4422.

[24] a) M. V. Baker, D. H. Brown, R. A. Haque, B. W. Skelton, A. H. White, *Dalton Transactions* **2004**, 3756-3764; b) P. J. Barnard, M. V. Baker, S. J. Berners-Price, B. W. Skelton, A. H. White, *Dalton Transactions* **2004**, 1038-1047.

[25] M. V. Baker, D. H. Brown, R. A. Haque, P. V. Simpson, B. W. Skelton, A. H. White, C. C. Williams, *Organometallics* **2009**, *28*, 3793-3803.

[26] a) S. Díez-González, S. P. Nolan, *Synlett* **2007**, *2007*, 2158,2167; b) C. Munro-Leighton, S. A. Delp, E. D. Blue, T. B. Gunnoe, *Organometallics* **2007**, *26*, 1483-1493.

Chapter 3

Structural Diversity of Cu^{I}-NHC Complexes: Ligand Tuning Facilitates Isolation of the First Structurally Characterised Cu^{I}-NHC Containing a Cu^{I}-Alkene Interaction

3.1 Introduction

Ethylene, the simplest alkene, plays a pivotal role in the life cycle of plants, including during fruit ripening. Perception of ethylene by plants is thought to be made possible by the presence of a Cu^{I} cofactor, which reversibly binds ethylene, allowing the occurrence of a cellular response.[1] Furthermore, the reversible binding of alkenes to Cu^{I} centres is thought to be a vital step in a variety of Cu^{I}-catalysed reactions, including alkene aziridination[2] and cyclopropanation[3] reactions.

The binding of alkenes to metal centres (including Cu^{I}) can be described using the Dewar-Chatt-Duncanson model.[4] This involves donation of π-bonding electrons from the alkene to a vacant orbital of appropriate symmetry on the metal centre (σ-donor component). At the same time, back-donation of electron density from a filled metal orbital to the antibonding π*-orbital on the alkene occurs. Both of these effects typically lead to an increase in the bond length of the alkene, due to decreased π-bonding electron density and increased π*-antibonding electron density. The Dewar-Chatt-Duncanson model of metal-alkene bonding is illustrated diagrammatically in Figure 3.1.

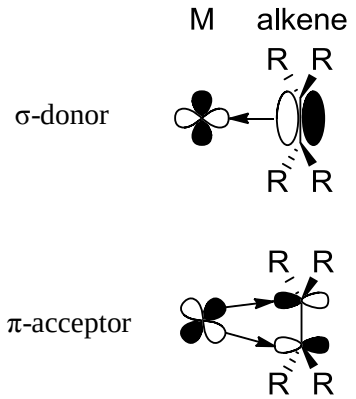

Figure 3.1 The metal-alkene interaction

To date, a number of structurally characterised Cu^{I}-alkene complexes have been reported, [5] many of which contain a chelating *N*-donor ligand such as *tris*(pyrazolyl)borate.[5c, 5g] However, there have been no reported Cu^{I}-NHC complexes containing a Cu^{I}-alkene interaction to our

knowledge. To this end, attempts were made to synthesise a Cu^{I}-NHC complex containing an alkene interaction, which would allow a greater understanding of the nature of the Cu^{I}-alkene interaction, and fine tuning of the ligands for use in catalytic processes which rely on alkene coordination to a Cu^{I} centre.

3.2 Synthesis and Cu^{I} Complexes of Non-Bulky Allyl-Containing Ligands

3.2.1 Ligands

A possible strategy for accessing NHC-Cu^{I}-alkene complexes is to tether an alkene to the NHC ligand. By doing this, the effective concentration of the alkene is increased within the vicinity of the metal centre, thus making highly labile coordination more possible to observe. Thus, a range of ligands bearing either one or two *N*-allyl tethers were synthesised, where the electronic and steric properties were varied by further *N*-substitution of the NHC or by backbone benzannulation.

Ligand precursor **L14** (1,3-diallylbenzimidazolium bromide) was prepared using a modified literature procedure. [6] Reaction of an excess of allyl bromide with benzimidazole in acetonitrile with sodium hydrogen carbonate as the base, led to the formation of **L14** in moderate yield. Analysis of **L14** by ^{1}H and $^{13}C\{^{1}H\}$ NMR spectroscopy and high-resolution MS (operating in ESI+ mode) provided data which was in firm agreement with that already reported. In particular, a low field resonance at 11.41 ppm (500 MHz, $CDCl_3$) is strongly indicative of the formation of a (benz)imidazolium halide compound. Cooling of a saturated acetonitrile solution to -30°C led to the isolation of **L14** as large off-white crystals.

Imidazolium salt **L15** (1-allyl-3-methylimidazolium bromide) was also prepared according to literature procedure.[7] Allyl bromide was slowly added to stirring 1-methylimidazole in the absence of solvent, producing a highly exothermic reaction. The salt (**L15**) was isolated as a brown oil in quantitative yield following work-up. Again, the product was characterised by ^{1}H and $^{13}C\{^{1}H\}$ NMR spectroscopy, high-resolution MS and elemental analysis. All analytical data was in agreement with precedent.

Ligand precursor **L16** is the non-benzannulated analogue of **L14** and again was prepared using literature procedure.[7] The synthesis of **L16** is illustrated in Scheme 3.1.

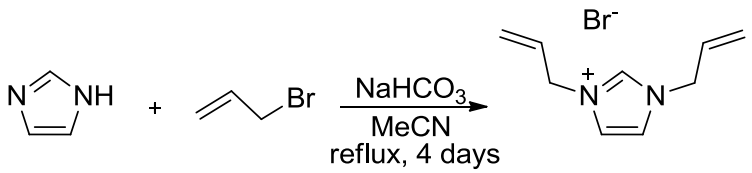

Scheme 3.1 Synthesis of ligand precursor **L16**

Analytically pure **L16** was obtained as a golden-yellow oil in reasonable yield after filtration and removal of the volatiles *in vacuo*. Analysis of **L16** by ^{1}H and $^{13}C\{^{1}H\}$ NMR spectroscopy, high-resolution MS and elemental analysis gave incontrovertible evidence of the successful formation of the imidazolium salt, and was in agreement with previously reported data.

3.2.2 Complexes

Cu^{I}-NHC complexes can be synthesised using a range of methods including (i) deprotonation of an imidazolium salt using a strong base followed by coordination to a metal, (ii) transmetallation from the corresponding Ag^{I}-NHC, (iii) deprotonation and coordination *in situ* of the imidazolium salt with a basic metal precursor (*e.g.* Cu_2O) and (iv) electrochemical reduction of the imidazolium and metal coordination using the technique described in Chapter 2.[8]

Initial attempts at complexation of ligand precursors **L14** – **L16** were made *via* deprotonation with a strong base, the base in question being potassium *tert*-butoxide (*tert*-butanol pK_a = approximately 19). This technique finds widespread use in the literature to synthesise Cu^{I}-NHC complexes.[9] Reaction of **L15** with 1.3 equivalents of potassium *tert*-butoxide and a slight excess of CuBr in anhydrous/degassed tetrahydrofuran at room temperature gave an oily brown solid after work-up. The resultant NMR spectra of the crude product were surprisingly complex, and indicated the presence of three different products. Examination of the ^{1}H NMR spectrum illustrated the complete loss of a resonance corresponding to the imidazolium proton, suggesting that all three products were Cu^{I}-NHC complexes. This was unambiguously confirmed by the $^{13}C\{^{1}H\}$ NMR spectrum, which showed three low field resonances at 177.7, 177.8 and 178.7 ppm (126 MHz, $CDCl_3$), typical of Cu^{I}-bound carbenic carbon atoms (Figure 3.2).

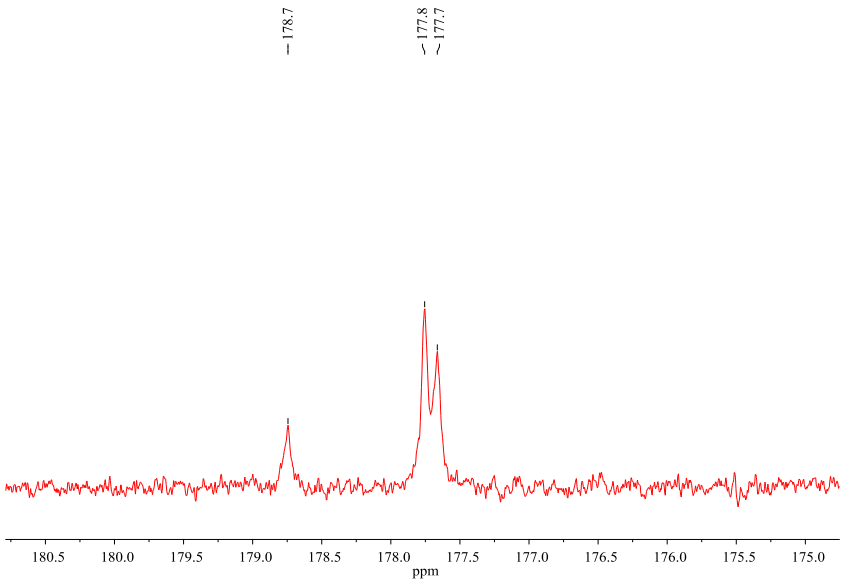

Figure 3.2 Carbenic carbon resonances of the products formed by the reaction of **L15** with potassium *tert*-butoxide and a slight excess of CuBr (126 MHz, $CDCl_3$)

Close examination of the ^{1}H, $^{13}C\{^{1}H\}$, ^{1}H-^{1}H COSY and $^{13}C\{^{1}H\}$ dept135 NMR spectra provided convincing evidence that the three products formed were the desired product, and two allyl rearrangement products (Figure 3.3).

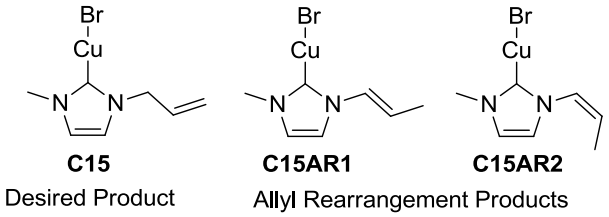

Figure 3.3 Products formed by the reaction of **L15** with potassium *tert*-butoxide and a slight excess of CuBr

The two allyl rearrangement products (**C15AR1** and **C15AR2**) are most likely formed by a prototropic isomerisation process caused by the potassium *tert*-butoxide base.[10] Separation of the desired product from the two allyl rearrangement products was not possible due to the air/moisture sensitive nature of the Cu^{I}-NHC complexes, which precludes purification by column chromatography for example. However, slow evaporation of a solution of the three products in tetrahydrofuran yielded a small number of clear needles which were suitable for X-ray diffraction analysis. The crystals were found to belong to the orthorhombic crystal system and the structural solution was performed in the space group *Cmca* (Figure 3.4).

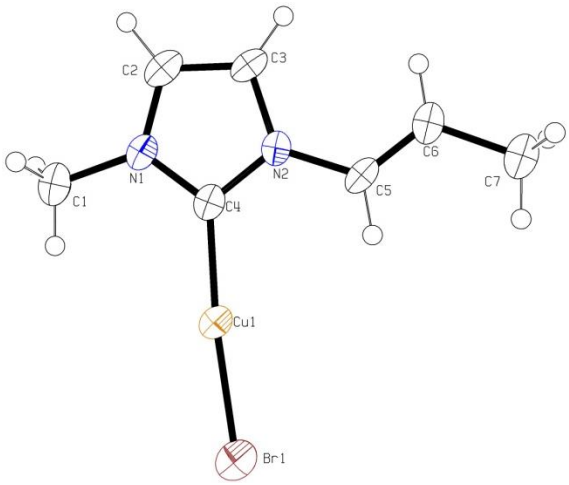

Figure 3.4 Molecular structure of the *trans* allyl rearrangement product (**C15AR1**). Ellipsoids are drawn at the 50% probability level

Table 3.1 Selected bond distances (Å) and angles (deg) of the *trans* allyl rearrangement product (**C15AR1**)

C(4)-Cu(1)	1.896(9)	C(4)-Cu(1)-Br(1)	174.6(3)
Cu(1)-Br(1)	2.188(2)	N(1)-C(4)-N(2)	104.6(7)
N(1)-C(4) / N(2)-C(4)	1.34(1) / 1.36(1)		
C(5)-C(6)	1.32(1)		
C(6)-C(7)	1.54(1)		

After the structural solution was performed, it was clear that the crystallised material was one of the predicted allyl rearrangement products (**C15AR1**). This is shown by the pronounced shortening of the C5-C6 bond (to 1.32 Å) and the lengthening of the C6-C7 bond (1.54 Å). Furthermore, the entire ligand itself is almost perfectly planar, which again suggests that an allyl rearrangement has occurred. The bond lengths observed are within the ranges typically observed for this type of complex. For example, the C-Cu bond (1.90 Å) falls well within the 1.87 – 1.96 Å range usually encountered.[9c, 11] Also, the Cu-Br bond length, at 2.19 Å, is a value typical for a linear 2-coordinate Cu^{I}-NHC complex. It is perhaps a little surprising that this molecule does not crystallise as a $(\mu\text{-Br})_2$-bridged dimer, especially as the two *N*-substituents can be considered as sterically non-bulky. The crystallisation of Cu^{I}-NHC complexes as $(\mu\text{-Br})_2$-bridged dimers was observed in Chapter 2.

Since the deprotonation of an imidazolium salt using a strong base seems to be unsuitable for the formation of Cu^{I}-NHC complexes bearing allyl tethers, another method of metal complexation was required. Deprotonation and coordination *in situ* of the imidazolium salt with a basic metal precursor (Cu_2O in this case) was examined to see if it was a more suitable method to use with the apparently base-sensitive allyl-tethered ligand precursors. The formation of Cu^{I}-NHC complexes using Cu_2O as both the base and metallating reagent has proved successful in a number of cases.[12]

Reaction of ligand precursor **L14** with an excess of Cu_2O in anhydrous dichloromethane at reflux produced a white solid following work-up (**C14**). Analysis of the product by ^{1}H NMR spectroscopy revealed the disappearance of the low field imidazolium proton of the starting material and the presence of only one carbenic product, whose resonances (including the allyl protons) are slightly shifted from those of **L14**. In addition, a broad resonance at 186.1 ppm in the $^{13}C\{^{1}H\}$ NMR spectrum of **C14** strongly suggests that the product is a Cu^{I}-NHC complex. This was confirmed by high-resolution MS and elemental analysis. The growth of single crystals suitable for X-ray diffraction analysis was accomplished by the slow evaporation of a

concentrated solution of **C14** in chloroform. **C14** crystallises in the triclinic crystal system and the structural solution was performed in the space group $P\bar{1}$ (Figure 3.5).

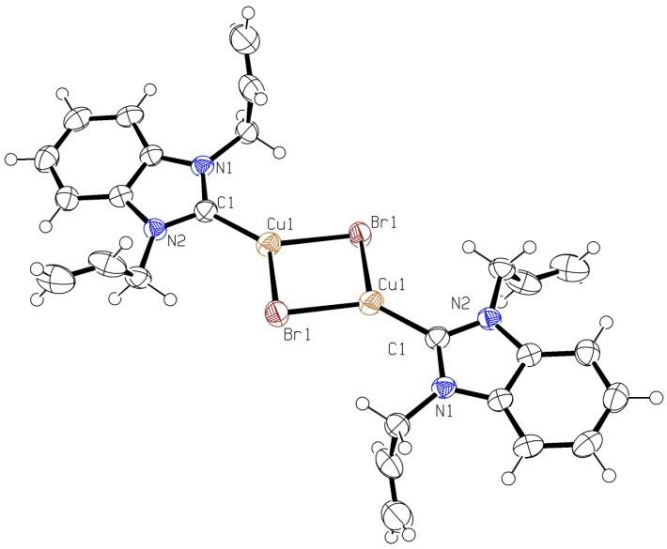

Figure 3.5 Molecular structure of **C14**. Ellipsoids are drawn at the 50% probability level

Table 3.2 Selected bond distances (Å) and angles (deg) for **C14**

C(1)-Cu(1)	1.908(2)	C(1)-Cu(1)-Br(1)	130.48(9)
Cu(1)-Br(1)	2.4404(6)	C(1)-Cu(1)-Br(1)'	127.34(9)
Cu(1)-Br(1)'	2.4562(5)	N(1)-C(1)-N(2)	104.9(2)
N(1)-C(1) / N(2)-C(1)	1.356(3) / 1.358(3)		

C14 crystallises as a centrosymmetric $(\mu\text{-Br})_2$-bridged dimer. The central $(CuBr)_2$ core is slightly asymmetric, with Cu-Br bond lengths of 2.44 and 2.46 Å respectively. The $(CuBr)_2$ core forms a plane with a torsion angle of approximately 24° with respect to the plane defined by the benzimidazol-2-ylidene ring. The Cu-C bond length, at 1.91 Å, is entirely normal for this type of complex. Notably, there is absolutely no indication of a Cu^I-alkene interaction in this complex, with the closest Cu^I-alkene contact occurring at 4.60 Å.

The clean formation of a Cu^I complex of **L15** using a strong base (potassium *tert*-butoxide) and a slight excess of CuBr was unsuccessful, as described previously. However, reaction of **L15** with Cu_2O under similar conditions to those used for the synthesis of **C14** led to the formation of **C15**, which was obtained as a white solid in 50% yield following work-up. The loss of the low field imidazolium proton resonance was observed in the ^1H NMR spectrum, as well as the appearance of a low field resonance (178.1 ppm) in the $^{13}C\{^1H\}$ NMR spectrum (75 MHz, $CDCl_3$), suggesting a Cu^I-NHC complex had been formed. The coordination of the alkene to the

Cu^{I} centre is not indicated by ^{1}H NMR spectroscopy, due to little change in the chemical shift of the allylic protons of **C15** versus **L15** being observed. To confirm this, single crystals suitable for X-ray diffraction analysis were grown by the slow evaporation of a concentrated solution of the product in dichloromethane. **C15** was found to crystallise in the monoclinic crystal system, and the structural solution was performed in the space group $P2_1/c$ (Figure 3.6).

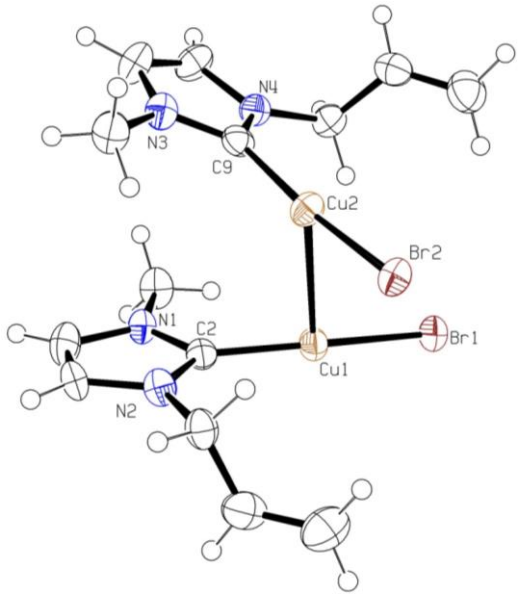

Figure 3.6 Molecular structure of **C15**. Ellipsoids are drawn at the 50% probability level

Table 3.3 Selected bond distances (Å), angles (deg) and torsion angles (deg) for **C15**

Cu(1)-Cu(2)	2.740(2)	C(2)-Cu(1)-Br(1)	167.7(3)
C(2)-Cu(1) / C(9)-Cu(2)	1.911(9) / 1.91(1)	C(9)-Cu(2)-Br(2)	169.8(3)
Cu(1)-Br(1) / Cu(2)-Br(2)	2.275(1) / 2.282(2)	Br(1)-Cu(1)-Cu(2)-Br(2)	-77.14(6)
N(1)-C(2) / N(2)-C(2)	1.37(2) / 1.38(1)		
N(3)-C(9) / N(4)-C(9)	1.37(1) / 1.37(1)		

Compound **C15** crystallises as a dimer with a highly unusual ligand-unsupported cuprophilic interaction (Cu---Cu = 2.74 Å). Ligand-unsupported cuprophilic interactions are less common than their argentophilic and aurophilic analogues, though several examples have been described in the literature.[13] It is evident from the solid state structure that distortion of the C-Cu-Br bonds (to 169.8° and 167.7°) away from linearity occurs, presumably as a result of the cuprophilic interaction. The two bromides of the dimer are inclined away from each other, with a Br-Cu-Cu-Br torsion angle of 77°. Cu-C bond lengths of 1.91 and 1.92 Å are within the usual range for Cu^{I}-NHC complexes, as are the Cu-Br bond lengths (both 2.28 Å). This indicates that

the cuprophilic interaction does not significantly modify the electronic properties of the Cu^{I} centres. Aside from the cuprophilic interaction, no other notable interactions (including π-stacking, π-H interactions, H-bonding) are observable in the solid state, including alkene coordination to the metal centre.

Ligand precursor **L16** (1,3-diallylimidazolium bromide) reacted cleanly (by ^{1}H NMR spectroscopy) with Cu_2O in dichloromethane to furnish complex **C16**, which surprisingly was obtained as a pale yellow oil. Crystallisation was attempted under a number of different conditions, but unfortunately no solid was ever obtained. However, elemental analysis of the complex suggested a 1:1 ratio of NHC:CuBr, and thus the probable structure is illustrated below (Figure 3.7).

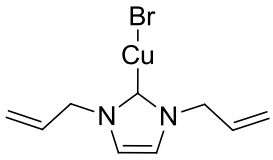

Figure 3.7 Complex **C16**

The characterisation data obtained (both solid state and solution-based analysis) for Cu^{I}-NHC complexes **C14** – **C16** provides no evidence of alkene coordination to the metal centre. The crystal structures of **C14** and **C15** illustrate distant approaches of the alkene to the metal centre, and the ^{1}H NMR and $^{13}C\{^{1}H\}$ NMR spectra give no significant shift in the resonances of the ^{1}H and ^{13}C nuclei, which would be expected on alkene coordination to the metal centre and the concomitant lengthening/weakening of the C=C bond. A noteworthy feature of the solid state structures of **C15AR1**, **C14** and **C15** is the variation in the coordination geometry about the Cu^{I} centre, *i.e*. linear 2-coordinate, trigonal planar 3-coordinate and cuprophilically-linked distorted linear 2-coordinate. Subtle differences in the steric and electronic properties of these ligands have led to significant differences in the solid state, which belies the labile nature of the Cu^{I} cation and its d^{10} electron configuration.

Since coordination of the alkene to the metal centre was not observable in these complexes which bear non-bulky ligands, it was decided to alter the steric properties (and to a lesser extent the electronic properties) of the ligands. By doing this, it was hoped that the formation of $(\mu\text{-halide})_2$-bridged dimers and cuprophilic interactions could be prevented, perhaps keeping a coordination site free on the metal centre for alkene binding.

3.3 Synthesis and Cu^{I} Complexes of Bulky Allyl-Containing Ligands

3.3.1 Ligands

Unsymmetrical ligand precursors **L17** (1-mesityl-3-allylimidazolium bromide) and **L18** (1-(2-methoxyphenyl)-3-allylimidazolium bromide) were both synthesised using a two-step procedure reported previously in the literature.[14] Initially, the mono-substituted imidazole (*N*-mesitylimidazole, **P17**, or *N*-(2-methoxyphenyl)imidazole, **P18**) is generated *via* a four component condensation reaction in acetic acid (Scheme 3.2). The desired products can be obtained as either light brown or yellow solids with reasonable purity.

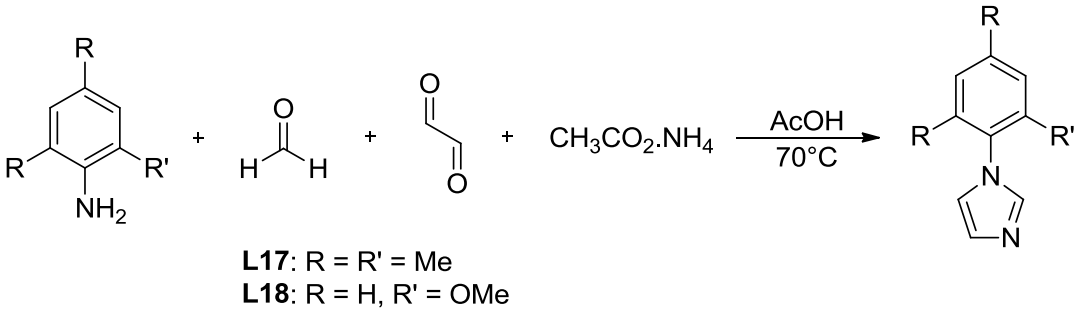

Scheme 3.2 Synthesis of precursors to **L17** and **L18**

The reactions proceed in poor to moderate yields (6 – 39%), despite much higher yields being reported in the literature. The low yields reflect the number of side reactions occurring and by-products being formed, which is evident by the extremely dark colour the reaction mixture goes after addition of all of the reagents. Performing the reactions at lower temperature (*e.g.* room temperature) led only to the formation of the undesired symmetrical diazabutadienes.

After isolating the mono-substituted imidazoles, reaction of these with allyl bromide in acetonitrile at room temperature led to the formation of analytically pure **L17** and **L18** in excellent yield (95% and 89% respectively). Ligand precursors **L17** and **L18** are illustrated in Figure 3.8.

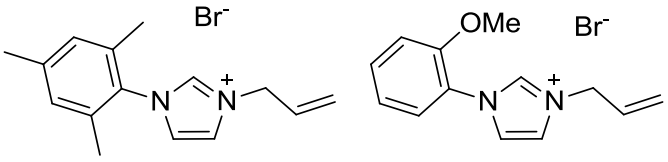

Figure 3.8 Ligand precursors **L17** (left) and **L18** (right)

L17 and **L18** were both fully characterised using ^{1}H and $^{13}C\{^{1}H\}$ NMR spectroscopy, high-resolution MS and elemental analysis. Imidazolium proton resonances at 10.43 (500 MHz, $CDCl_3$) and 10.55 ppm (500 MHz, $CDCl_3$), for **L17** and **L18** respectively, were strongly indicative that the desired products had formed. Single crystals of **L17** suitable for X-ray diffraction analysis were grown by the vapour diffusion of diethyl ether in to a concentrated

acetonitrile solution. The crystals obtained were of poor quality, although they allowed the overall structure to be elucidated (Figure 3.9).

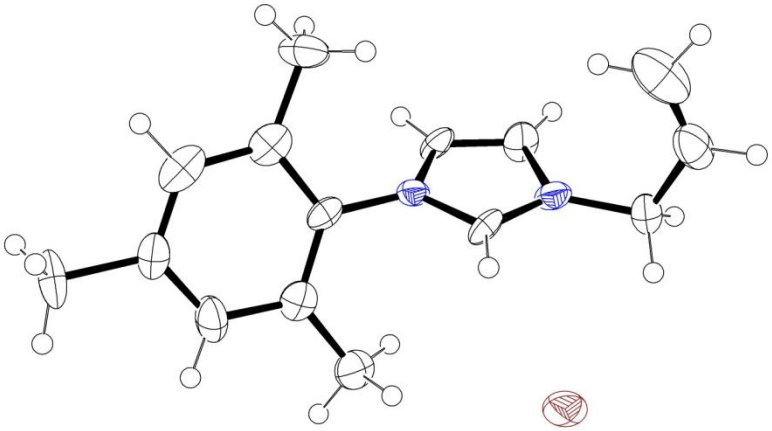

Figure 3.9 Molecular structure of **L17**. Ellipsoids are drawn at the 50% probability level

Due to the poor quality of the data obtained, it is not appropriate to discuss in detail the observed bond lengths/angles when the s.u.s for these are so high. The data does however reveal that **L17** exhibits the expected structure, with the mesityl ring orientated out of the plane defined by the imidazolium ring. A possible hydrogen bond is also observed between the imidazolium C2 proton and a neighbouring bromide anion.

Unlike ligand precursors **L14** – **L16**, **L17** and **L18** contain one bulky *N*-substituent (mesityl or 2-methoxyphenyl), which may act to help kinetically stabilise the resultant Cu^{I} complexes, making these less prone to decomposition.

3.3.2 Complexes

Given the success of the reactions between ligand precursors **L14** – **L16** and Cu_2O, reaction of Cu_2O was attempted with the bulkier ligand precursors **L17** and **L18**. Reaction of **L17** with Cu_2O at reflux in anhydrous dichloromethane in the presence of 4Å molecular sieves led to the formation of **C17** (Scheme 3.3).

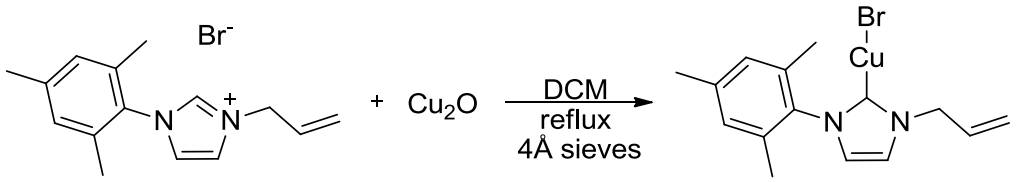

Scheme 3.3 Synthesis of complex **C17**

Analysis of **C17** by ^{1}H NMR spectroscopy indicated the loss of the imidazolium proton, and slight shifts in the resonances of the other ligand protons were suggestive of successful complexation to a metal centre. Moreover, a low field resonance at 179.0 ppm (75 MHz, $CDCl_3$) in the $^{13}C\{^{1}H\}$ NMR spectrum suggests carbenic coordination to Cu^{I}. An overlay of the ^{1}H NMR spectra of **L17** and **C17** is provided below (Figure 3.10).

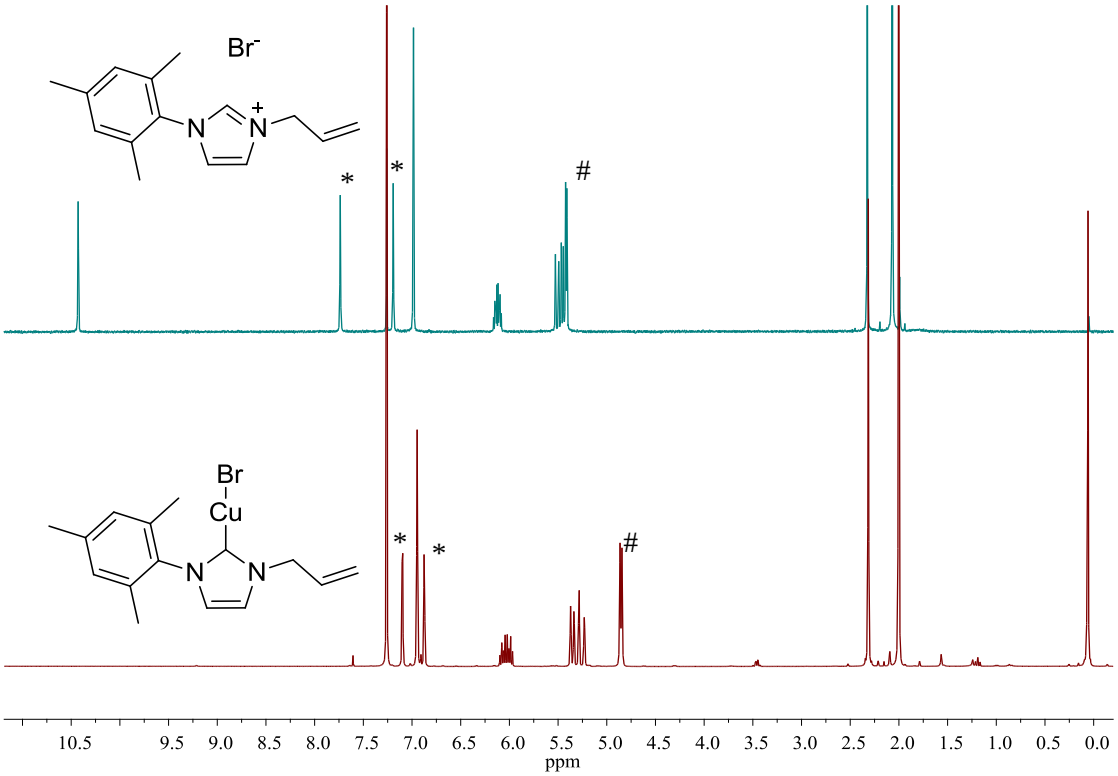

Figure 3.10 ^{1}H NMR spectra of **L17** (top) versus **C17** (bottom) (300 MHz, $CDCl_3$)

The shifts in the resonances of the ligand protons upon complexation to the Cu^{I} centre are most pronounced for the NHC backbone protons (indicated by * above) and the methylene protons (indicated by # above) of the allyl substituent. It is also notable that little change is seen in the chemical shift of the alkenic protons in the complex versus the starting material (Figure 3.11). It would be anticipated that if the alkene were coordinating to the metal centre, a marked upfield shift in the alkene protons would occur, due to the decreased π-bonding electron density and increased π*-antibonding electron density in the alkene double bond brought about by metal coordination.

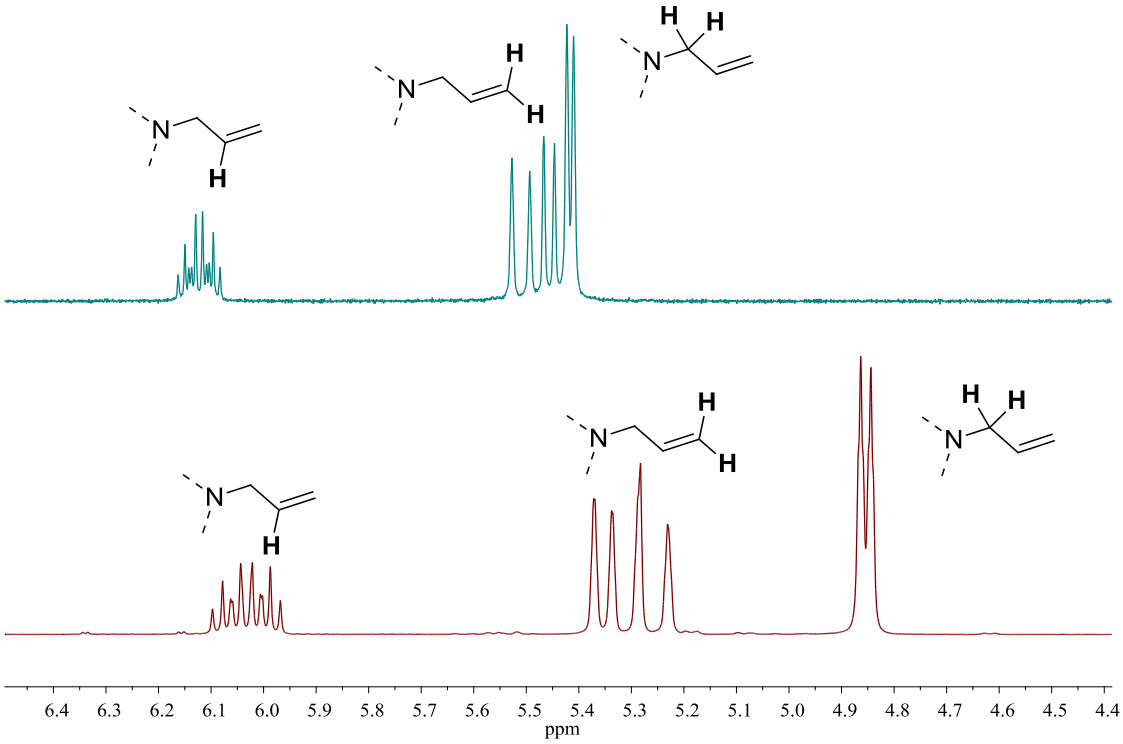

Figure 3.11 ^{1}H NMR spectra of the allylic protons of **L17** (top) versus **C17** (bottom) (300 MHz, $CDCl_3$)

It was possible to obtain single crystals of **C17** suitable for X-ray diffraction analysis by the vapour diffusion of pentane in to a concentrated solution of the complex in either dichloromethane or tetrahydrofuran. Complex **C17** was found to crystallise in the triclinic crystal system, with the structural solution being performed in the space group $P\bar{1}$ (Figure 3.12).

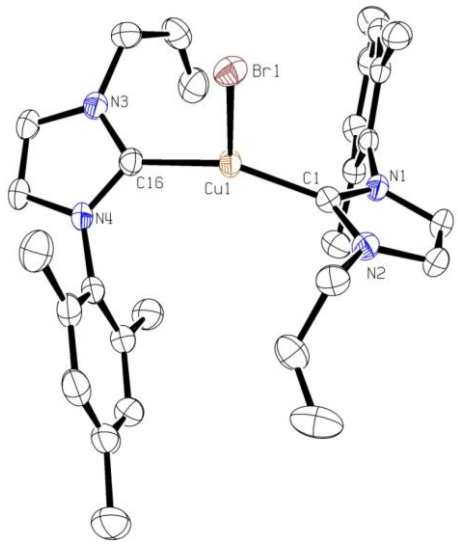

Figure 3.12 Molecular structure of **C17**. Ellipsoids are drawn at the 50% probability level. H atoms are omitted for clarity

Table 3.4 Selected bond distances (Å) and angles (deg) for **C17**

Cu(1)-Br(1)	2.6156(4)	C(1)-Cu(1)-C(16)	151.09(7)
C(1)-Cu(1)	1.933(2)	C(1)-Cu(1)-Br(1)	105.60(5)
C(16)-Cu(1)	1.936(2)	C(16)-Cu(1)-Br(1)	103.25(5)

C17 crystallises with a rather unusual distorted trigonal coordination geometry as a $CuBrL_2$-type complex. This type of complex has been observed in only two other examples.[9a, 15] This is somewhat unexpected, especially given that elemental analysis gives a ratio of 1:1 (NHC:CuBr). It is suggested that transmetallation occurs during crystallisation giving 1 mole equivalent of the $CuBrL_2$-type complex and 1 mole equivalent of CuBr. The trigonal geometry is surprising, considering the steric bulk of the mesityl wingtip groups. The bulky mesityl groups must act to widen the C-Cu-C bond angle (151.1°), which in turn decreases the C-Cu-Br bond angles (103.3° and 105.6°) and also forces the bromide further from the Cu^I centre (Cu-Br = 2.62 Å) in order to relieve steric congestion. This value for the Cu-Br bond length is rather long compared to literature precedent, and may also be caused to some extent by the strong σ-donor effect of the two NHCs coordinated to the Cu^I centre, which acts to increase electron density at the metal centre and thus weaken the interaction between the bromide and metal centre. The C-Cu bond lengths, at 1.93 and 1.94 Å, are slightly elongated with respect to the values observed previously in this chapter, though compare favourably with those reported previously by Albrecht (1.930(2) Å)[9a] and Lavoie (1.935(3) Å).[15] In agreement with the ^1H and $^{13}C\{^1H\}$ NMR spectroscopic data obtained for **C17**, the solid state structure supports the assertion that there is no interaction between the alkene and metal centre. The closest approach of the alkene to the metal centre occurs at a distance of 3.65 Å, which is well outside of the sum of the van der Waals' radii.

Ligand precursor **L18** contains a 2-methoxyphenyl *N*-substituent, which not only adds a degree of steric protection to the carbene centre, but also provides the possibility of acting as a labile donor to a metal centre. Furthermore, the methyl ether exerts a strong +M effect on the phenyl ring and thus, potentially, on the NHC ring as well. Reaction of **L18** with Cu_2O at reflux in anhydrous dichloromethane in the presence of 4Å molecular sieves led to the formation of **C18**. Complex **C18** was fully characterised using a combination of ^1H and $^{13}C\{^1H\}$ NMR spectroscopy, high-resolution MS and elemental analysis, all of which were consistent with the formation of a CuBrL-type Cu^I complex. Indeed, single crystals suitable for X-ray diffraction analysis could be obtained by the slow evaporation of a concentrated solution of the product in dichloromethane. Complex **C18** crystallised in the orthorhombic crystal system and the structural solution was performed in the chiral space group $P2_12_12_1$ (Figure 3.13).

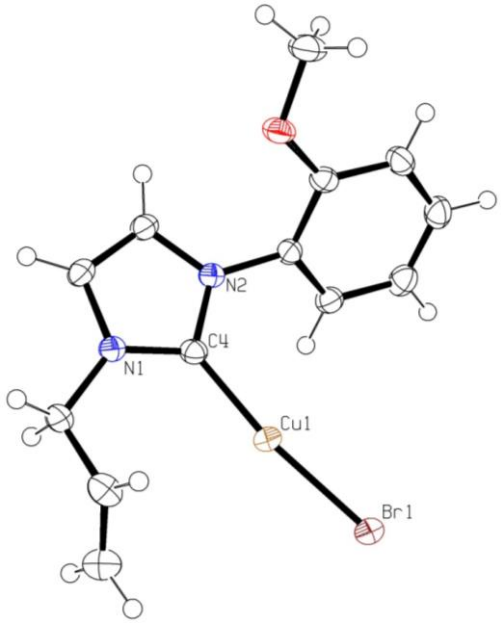

Figure 3.13 Molecular structure of **C18**. Ellipsoids are drawn at the 50% probability level

Table 3.5 Selected bond distances (Å) and angles (deg) for **C18**

Cu(1)-Br(1)	2.2822(3)	C(4)-Cu(1)-Br(1)	172.08(5)
C(4)-Cu(1)	1.918(2)	N(1)-C(4)-N(2)	103.7(1)
N(1)-C(4)	1.373(2)		
N(2)-C(4)	1.383(2)		

The Cu^{I} centre in **C18** is 2-coordinate with an approximately linear geometry (172.1°). The C-Cu and Cu-Br bond lengths, at 1.92 and 2.28 Å, are within typical ranges for this type of complex. The 2-methoxyphenyl ring is twisted with respect to the plane defined by the NHC ring by approximately 47°. This would act to prohibit π-overlap between the methoxyphenyl and NHC rings resulting in the highly π-electron donating OMe group having little electronic effect on the NHC. One of the alkenic carbon atoms lies in relatively close proximity to the copper centre (3.00 Å), though it is unlikely that an interaction between the two is present; this is more likely a crystal packing effect.

As with complexes **C14** – **C16**, neither **C17** nor **C18** provide compelling evidence of an interaction between the alkene and Cu^{I} centre. The steric properties of the ligands of **C14** – **C18** have been varied significantly, but this has not facilitated any interaction. The addition of ancillary donors and variation of electronic properties of the NHC ligands has not thus far been attempted. To this end, the ligand precursors described below were appended with 2-pyridyl *N*-substituents. It was anticipated this would modulate both the electronic properties of the NHC,

but also provide the opportunity for metal chelation. The complexes formed from these ligands are fascinating in their own right, moreover, they allowed the isolation of the first example of a structurally characterised Cu^{I}-NHC containing a Cu^{I}-alkene interaction.

3.4 Synthesis and Cu^{I} Complexes of Pyridyl Allyl-Containing Ligands

3.4.1 Ligands

Imidazolium salt **L19** (1-(2-pyridyl)-3-allylimidazolium bromide) contains added steric bulk in the form of a 2-pyridyl *N*-substituent. Not only does the 2-pyridyl substitution offer extra steric protection, it also offers the possibility of **L19** acting as a chelating ligand by binding to the metal centre through both its carbenic carbon and its pyridyl nitrogen.

The synthesis of **L19**, like that for ligand precursors **L17** and **L18**, involves two synthetic steps. However, the first step in this case proceeds *via* an Ullmann coupling reaction, where imidazole is coupled to 2-bromopyridine using potassium carbonate as the base and catalytic amounts of copper iodide and DL-proline (Scheme 3.4).[16]

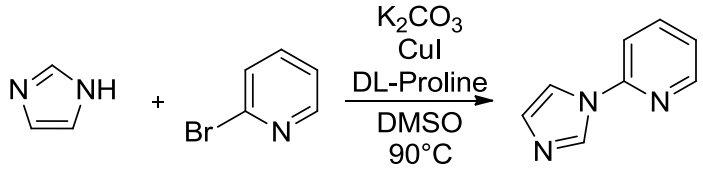

Scheme 3.4 Ullmann coupling to form 1-(2-pyridyl)imidazole (**P19**)

The Ullmann coupling reaction proceeds efficiently, yielding the coupled product as a colourless oil (which slowly crystallises) in 71% yield following purification by column chromatography.

Despite the presence of two nucleophilic nitrogen atoms in 1-(2-pyridyl)imidazole (**P19**), reaction with an excess of allyl bromide at reflux in diisopropyl ether led to the clean formation of the imidazolium salt, **L19**, in high yield (Figure 3.14).

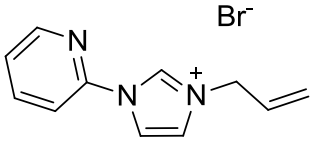

Figure 3.14 Ligand precursor **L19**

L19 was fully characterised by ^{1}H and $^{13}C\{^{1}H\}$ NMR spectroscopy, high-resolution MS and elemental analysis. An extremely low field (even for an imidazolium halide) resonance at 11.76 ppm (300 MHz, $CDCl_3$) corresponding to the imidazolium proton indicates formation of the desired product. Furthermore, single crystals suitable for X-ray diffraction analysis were grown by layering diethyl ether over a concentrated solution of the product in chloroform. **L19**

crystallises in the monoclinic crystal system and the structural solution was performed in the space group $P2_1/c$ (Figure 3.15).

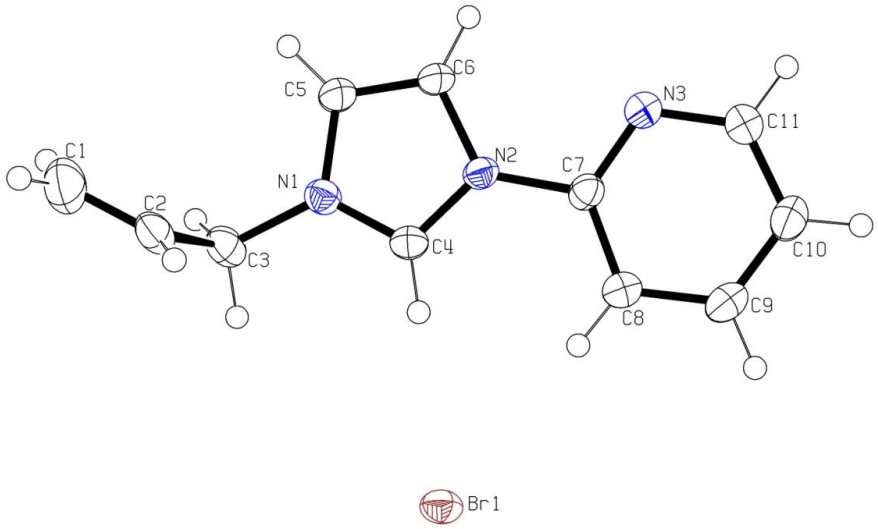

Figure 3.15 Molecular structure of **L19**. Ellipsoids are drawn at the 50% probability level

Table 3.6 Selected bond distances (Å), angles (deg) and torsion angles (deg) for **L19**

N(1)-C(4)	1.336(2)	N(1)-C(4)-N(2)	108.4(1)
N(2)-C(4)	1.357(2)	C(4)-N(2)-C(7)-N(3)	0.3(2)
N(2)-C(7)	1.448(2)		
N(1)-C(3)	1.494(2)		
C(1)-C(2)	1.330(3)		
C(4)---Br(5)	3.36		

The pyridyl and imidazolium rings of **L19** lie almost coplanar in the solid state which acts to increase π-overlap between the two. The significant π-overlap between the two aromatic systems perhaps helps to explain the significant low field shift of the imidazolium proton (11.76 ppm). The electron-deficient pyridyl ring acts to withdraw electron density from the N-C-N π-system, resulting in deshielding of the imidazolium proton. A H-bonding interaction occurs between the imidazolium proton and the bromide anion, which presumably acts to deshield the imidazolium proton yet further. Pronounced π-overlap between the imidazolium and pyridine rings is manifested in the shortening of the N2-C7 bond (1.45 Å) versus the N1-C3 bond (1.49 Å). The pyridyl nitrogen atom (N3) and an imidazolium backbone proton (on C6) appear to interact with the same atoms of a neighbouring unit forming a weakly H-bonded pair. Furthermore, there appears to be a strong anion-π interaction between the N-C-N π-cloud and a

neighbouring bromide anion which, at 3.36 Å, falls well below the sum of the van der Waals' radii (Figure 3.16). Anion-π interactions are much less common than cation-π interactions.[17] This interaction is seemingly facilitated by the electron-poor (positively charged) N-C-N bond of the imidazolium, which is even more electron-poor than normal due to the effect of the electron-withdrawing pyridyl attached to the N2 nitrogen.

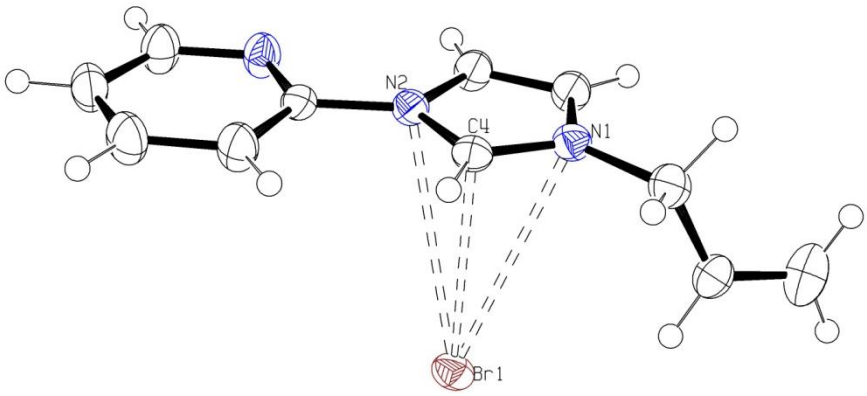

Figure 3.16 Anion-π interaction observed in **L19**

A symmetrical analogue of **L19** was synthesised (**L20**) to examine the effect of a potential extra NHC donor on Cu^{I} binding. Like **L19**, **L20** was synthesised following a two-step procedure involving an Ullmann coupling followed by reaction with allyl bromide. Initially, reaction of 2 equivalents of imidazole with 2,6-dibromopyridine using potassium carbonate as the base and catalytic amounts of copper iodide and DL-proline led to the formation of 2,6-*bis*(1-imidazolyl)pyridine (**P20**).[16] Then, reaction of 2,6-*bis*(1-imidazolyl)pyridine (**P20**) with allyl bromide in acetonitrile led to the formation of **L20** (Figure 3.17).

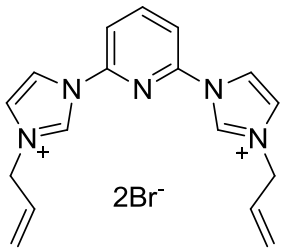

Figure 3.17 Ligand precursor **L20**

Ligand precursor **L20** was fully characterised using ^{1}H and $^{13}C\{^{1}H\}$ NMR spectroscopy, high-resolution MS and elemental analysis. Single crystals of **L20** suitable for X-ray diffraction analysis were grown by the vapour diffusion of diethyl ether in to a concentrated acetonitrile solution. **L20** crystallises in the triclinic crystal system and the structural solution was performed in the space group $P\bar{1}$ (Figure 3.18).

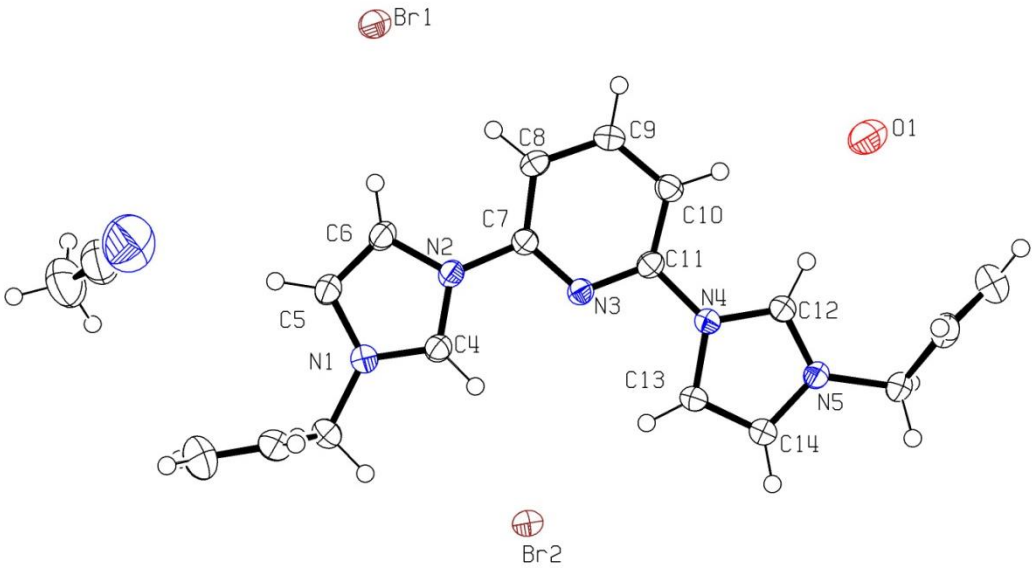

Figure 3.18 Molecular structure of **L20**. Ellipsoids are drawn at the 50% probability level

Table 3.7 Selected bond distances (Å) and angles (deg) for **L20**

N(1)-C(4) / N(5)-C(12)	1.332(3) / 1.334(3)	N(1)-C(4)-N(2)	108.2(2)
N(2)-C(4) / N(4)-C(12)	1.348(3) / 1.355(3)	N(4)-C(12)-N(5)	107.7(2)
C(4)---Br(2)	3.286		

L20 crystallises with one molecule of water (the protons could not be located on the diffraction map) and one molecule of acetonitrile in the asymmetric unit. Again, the pyridyl and imidazolium rings lie almost co-planar, which helps to maximise π-orbital overlap. A number of H-bonding interactions are also evident in the solid state structure. For example, the protons attached to C4 and C13 form H-bonds to a bromide anion located between them. Another H-bond occurs between the imidazolium proton attached to C12 and a neighbouring water molecule (O1). A H-bonding chain is present in the solid-state structure, which is propagated through H-bonds between the water molecules and Br1. Again, there is strong evidence for the presence of a rare anion-π interaction between the N2-C4-N1 π-cloud and Br2 (C4---Br2 = 3.29 Å).

3.4.2 Complexes

Reaction of Cu_2O with ligand precursors **L14** – **L18** led to the formation of analytically pure Cu^I complexes **C14** – **C18**. Thus, the use of Cu_2O as both the base and metallating reagent for the formation of complexes from the ligand precursors (**L19** and **L20**) described above seemed like a prudent choice. However, reaction of **L19** with Cu_2O at reflux in dichloromethane in the

presence of 4Å molecular sieves led to the isolation, after work-up, of an intractable green oil. The oil is assumed to be the decomposition product(s) of the target compound, and thus no analytical data was obtained. It is suggested, that reaction of Cu_2O with **L19** initially leads to the formation of some of the desired product, which then rapidly decomposes in the presence of trace air/moisture.

Therefore, another approach for the synthesis of the desired CuBrL-type Cu^I complex was needed. Thus, **L19** was treated with 1 equivalent of CuBr in the presence of an excess of Cs_2CO_3 in anhydrous acetonitrile at 50°C. The Cs_2CO_3 is too weak a base to cause allylic rearrangement reactions to occur, but is strong enough (and relatively soluble) so that deprotonation of **L19** can occur to form the Cu^I complex. Upon heating, the reaction mixture rapidly turned a pale yellow colour from colourless, potentially indicating that metal complexation was occurring. After work-up, a yellow solid was obtained (**C19A**) which was fully characterised by ^1H and $^{13}C\{^1H\}$ NMR spectroscopy, high-resolution MS and elemental analysis. ^1H NMR spectroscopy revealed the complete loss of the low field imidazolium proton resonance, and a broad low field resonance at 183.7 ppm (126 MHz, CD_3CN) in the $^{13}C\{^1H\}$ NMR spectrum of **C19A** strongly suggested that a Cu^I complex had been formed.

Elemental analysis shows that, instead of a CuBrL-type complex, **C19A** was in fact a *bis*-NHC $CuBrL_2$-type complex. This is also hinted at in the high-resolution MS, where the dominant molecular ion corresponds to $[Cu(NHC)_2]^+$. However, great care should be taken when interpreting the ESI+ mass spectra of Cu^I-NHC complexes, since their labile nature can lead to ligand scrambling resulting in the appearance of *bis*-NHC species in samples of pure *mono*-NHC compounds. This ligand scrambling behaviour is well documented for Ag^I-NHC complexes.[18] The possible structure of complex **C19A** is illustrated in Figure 3.19.

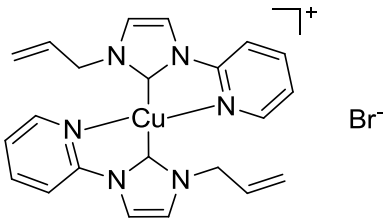

Figure 3.19 Proposed structure of **C19A**

Complex **C19A** is proposed to be an ionic complex (as shown above) on the basis of its poor solubility in dichloromethane, chloroform and tetrahydrofuran but its slightly better solubility in the more polar acetonitrile. Furthermore, a similar complex to **C19A** bearing diisopropylphenyl groups instead of allyl groups and a hexafluorophosphate anion instead of a bromide anion has been prepared and structurally characterised previously.[9a] Unfortunately, single crystals suitable for X-ray diffraction analysis have thus far not been obtained and so the exact structure of **C19A** cannot be confirmed unambiguously.

As discussed *vide ante*, complex **C19A** is in all likelihood a $CuBrL_2$-type complex rather than the desired CuBrL-type complex. Therefore, a different approach was needed to access the seemingly elusive CuBrL-type complex of ligand precursor **L19**. Transmetallation from the corresponding Ag^I-NHC complex is a method of transition metal-NHC complex synthesis which frequently meets with success where other methods fail. It relies on the usually excellent reactivity of Ag_2O with imidazolium salts to form Ag^I-NHC complexes and also on the relatively weak Ag^I-NHC bond, which allows smooth transfer of the NHC to another transition metal ion (*e.g.* Cu^I). Moreover, the Ag^I-NHC complex formed in the first step of the synthesis is air and moisture stable (though light sensitive), so can be handled and purified easily in air and kept on the bench for extended periods of time.

Reaction of an excess of Ag_2O with **L19** in anhydrous dichloromethane in the presence of 4Å molecular sieves led to the formation of a dark suspension, which, after filtration, removal of the solvent and recrystallisation yielded the Ag^I-NHC complex **C19B** (Scheme 3.5).

Scheme 3.5 Synthesis of Ag^I-NHC complex **C19B**

Characterisation of **C19B** by ^1H NMR spectroscopy indicated the loss of the imidazolium proton resonance, and formation of the Ag^I-NHC complex was confirmed by the $^{13}C\{^1H\}$ NMR spectrum which showed a low field resonance at 181.6 ppm (75 MHz, $CDCl_3$). Since silver has two naturally occurring isotopes, ^{107}Ag and ^{109}Ag, both of which have a nuclear spin of ½, it would be anticipated that coupling between the carbenic carbon and silver would occur. This would give rise to the carbenic carbon resonance being split in to a doublet of doublets. However, coupling is very often not observed in Ag^I-NHC complexes including in the example of **C19B**.[18] It has been suggested that this is a manifestation of the fluxional behaviour of Ag^I-NHC complexes, with respect to ligand exchange, on the NMR timescale.[19] In order to confirm connectivity in complex **C19B** and to understand the nature of the transmetallating species for the NHC transfer to Cu^I (described later), single crystals of **C19B** suitable for X-ray diffraction analysis were grown by the vapour diffusion of diethyl ether in to a concentrated solution of the complex in chloroform. **C19B** was observed to crystallise in the monoclinic crystal system and the structural solution was performed in the space group $P2_1/n$ (Figure 3.20).

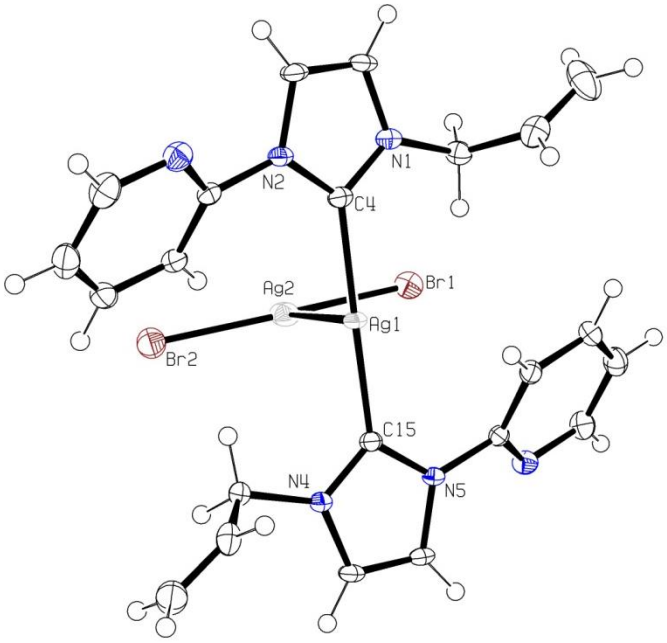

Figure 3.20 Molecular structure of **C19B**. Ellipsoids are drawn at the 50% probability level

Since Figure 3.20 is provided only to show overall connectivity, a lengthy discussion of the bonding parameters within the structure is unnecessary. However, it is shown that **C19B** crystallises as a well-known $[AgNHC_2]^+AgBr_2^-$-type complex, where the C-Ag-C bond lies almost perpendicularly to the Br-Ag-Br bond. The two silver centres are linked by a weak argentophilic interaction.

Given the decomposition observed during the reaction of **L19** with Cu_2O, it was deemed judicious to perform the transmetallation from **C19B** to Cu^I under strictly inert conditions since the resultant Cu^I-NHC complex was likely to be highly sensitive to air/moisture. As such, the **C19B** complex was dissolved in anhydrous, degassed dichloromethane in a glovebox. With stirring, an excess of solid CuBr was added to the solution. The colour of the solution very quickly turned yellow, and a pale yellow solid formed (AgBr). After stirring at room temperature, the highly insoluble AgBr and excess CuBr could be removed by filtration and the solvent removed from the solution to yield a yellow crystalline solid (**C19C**). Complex **C19C** was found to be highly air/moisture sensitive, particularly in solution, and decomposes rapidly upon exposure to ambient conditions giving a green solution and eventually an intractable green oil. However, characterisation of complex **C19C** was possible by ^{1}H NMR spectroscopy, high-resolution MS and elemental analysis. The ^{1}H NMR spectrum of **C19C** showed that the resonances of many of the ligand protons were broadened considerably in comparison to **C19B** and indeed **C19A**. The protons most affected by the spectral broadening included all but one of the pyridyl protons, the backbone NHC protons and the allylic methylene protons. One of the pyridyl protons and the alkenic protons retain reasonably sharp resonances (Figure 3.21).

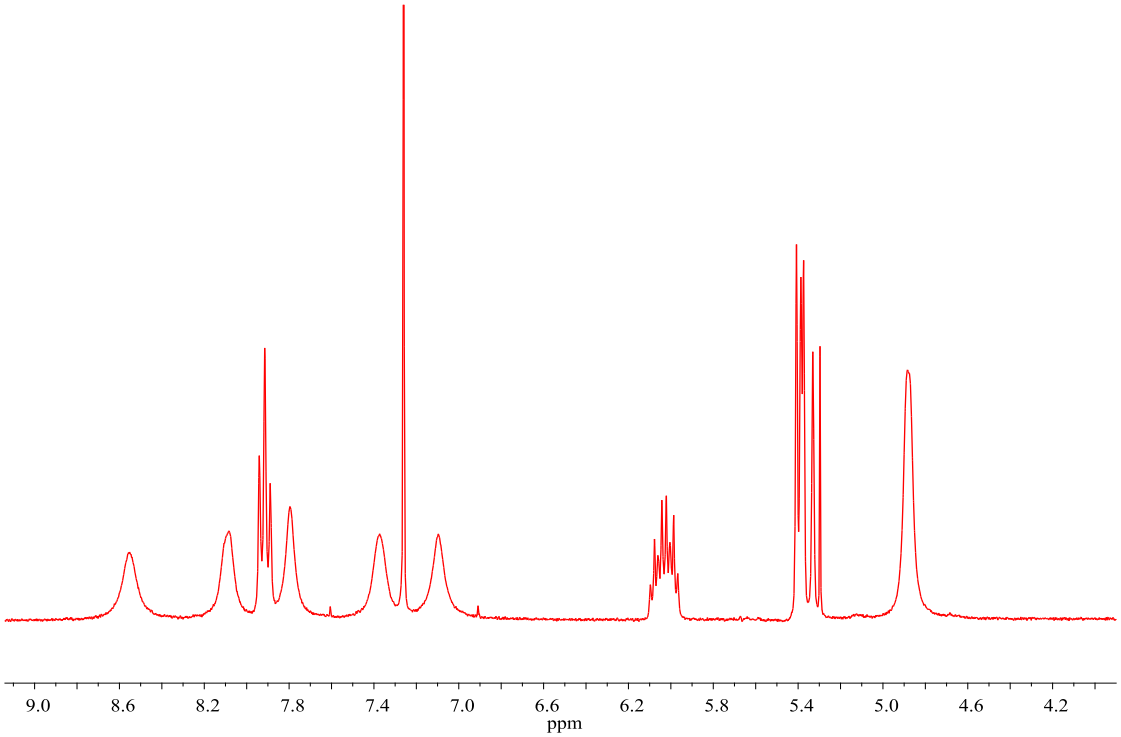

Figure 3.21 ^{1}H NMR spectrum (4 - 9 ppm region) of **C19C** (300 MHz, $CDCl_3$)

A similar NMR spectrum has been reported previously for a similar complex by Danopoulos.[12a] Danopoulos attributes the broadening to non-rigidity in solution, although also suggests that an equilibrium involving *mono*- and *bis*-NHC complexes could be contributing to broadening. It is notable that in Figure 3.21, the protons whose resonances are most broadened are those in closest proximity to the metal coordination environment (*i.e.* nearest the carbenic carbon and pyridyl nitrogen). The protons most affected by the broadening are marked in Figure 3.22.

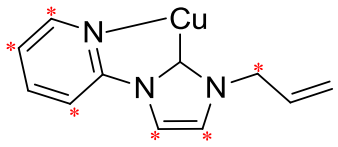

Figure 3.22 Proton environments affected by spectral broadening (marked by *)

On this basis, it is proposed that the spectral broadening is caused by coordinative lability at the Cu^{I} centre, which may invoke *mono*- and *bis*-NHC complexes as well as *mono*-NHC dimers. Indeed, from a slightly different ligand, Danopoulos was able to characterise two different complexes (a dimer and a polymer) in the solid state which could be formed selectively by varying the crystallisation conditions.[12a] If these two species existed in solution and exchange between them was fast on the NMR timescale, a broadened spectrum would result, just as is observed for **C19C**.

Elemental analysis on a sample of **C19C** strongly indicated that the target CuBrL-type complex had been successfully formed. To confirm this unequivocally, single crystals suitable for X-ray diffraction analysis were grown on standing of a dilute solution of the product in a mixture of dichloromethane and pentane (1:2). **C19C** was found to crystallise in the monoclinic crystal system and the structural solution was performed in the space group $P2_1/n$ (Figure 3.23).

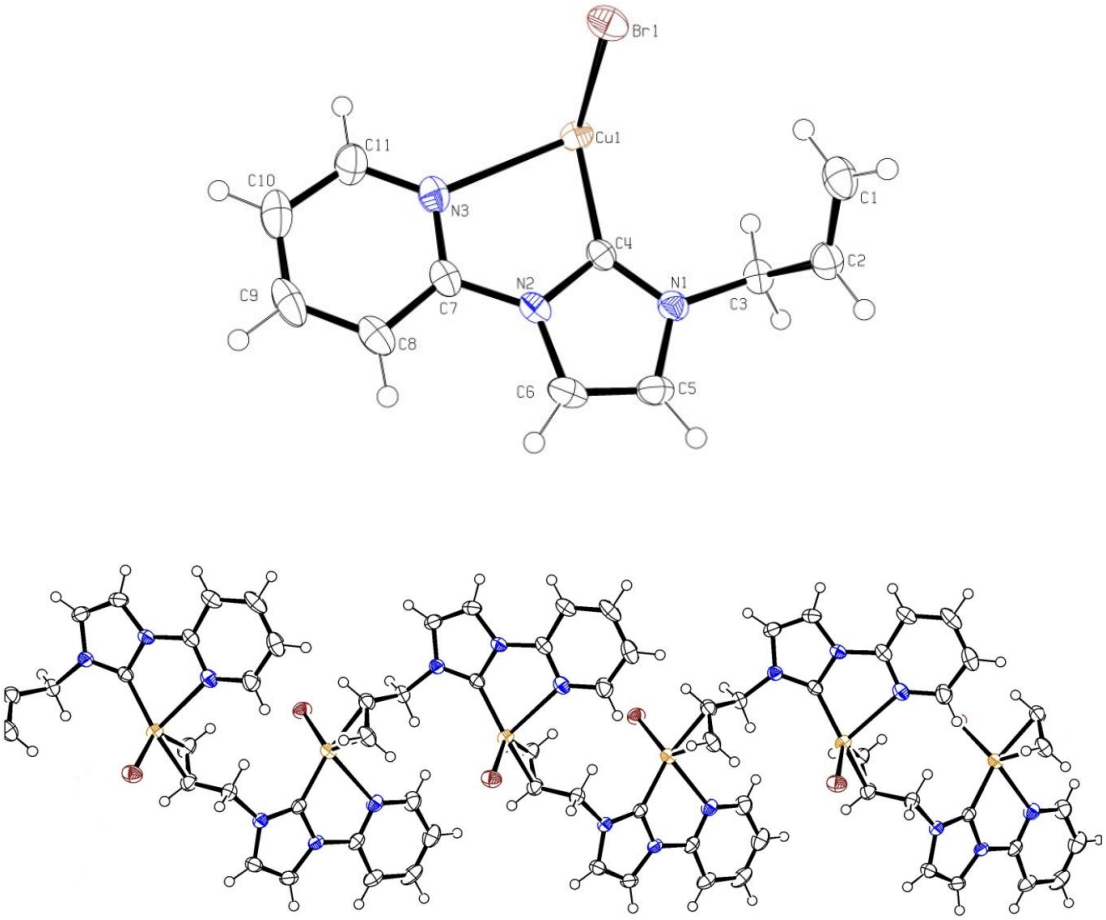

Figure 3.23 Molecular structure of **C19C**. Ellipsoids are drawn at the 50% probability level. The asymmetric unit is shown (top) along with a section of the 1-D chain (bottom)

Table 3.8 Selected bond distances (Å) and angles (deg) for **C19C** (those for **L19** are included for comparison)

	L19	**C19C**		**L19**	**C19C**
Cu(1)-Br(1)	-	2.4388(5)	C(4)-Cu(1)-alk*	-	130.74
C(4)-Cu(1)	-	1.971(2)	alk*-Cu(1)-Br(1)	-	115.30
N(3)-Cu(1)	-	2.497(2)	Br(1)-Cu(1)-C(4)	-	112.60(7)
C(1)-Cu(1)	-	2.096(3)	C(4)-Cu(1)-N(3)	-	74.90(9)
C(2)-Cu(1)	-	2.099(3)	alk*-Cu(1)-N(3)	-	105.51
alk*-Cu(1)	-	1.984	Br(1)-Cu(1)-N(3)	-	101.49(5)
C(1)-C(2)	1.330(3)	1.366(4)	N(1)-C(4)-N(2)	108.4(1)	103.6(2)
N(1)-C(4)	1.336(2)	1.362(3)			
N(2)-C(4)	1.357(2)	1.388(3)			

(* = denotes centre of alkene double bond)

C19C crystallised as a 1-dimensional polymer propagated by coordination of the Cu^{I} centre of one unit to the alkene of a neighbouring unit. This represents the first example of alkene coordination to a Cu^{I}-NHC complex. It is interesting to note that while alkene coordination to the Cu^{I} centre is observed in the solid state, noticeable shifts in the resonances of the alkenic ^{1}H and ^{13}C nuclei were not observed in their respective NMR spectra, indicating that alkene coordination to the metal centre is highly labile. The coordination geometry around the copper centre is probably best described as distorted trigonal pyramidal; with the alkene, carbenic carbon and bromide occupying the basal positions (bond angles of 130.74°, 115.30° and 112.60°) and the pyridyl nitrogen occupying the apical position. Significant distortion of an idealised trigonal pyramidal geometry occurs, in part, due to the geometric restriction imposed by the 5-membered chelate ring, which has a bite angle of 74.9° as defined by the C-Cu-N angle. The chelate ring itself is essentially planar. Notably long bonds are observed between the NHC and copper centre (1.97 Å) and between the pyridyl nitrogen and copper (2.50 Å), which may be a consequence of the copper centre trying to optimise orbital overlap with both donors. The Cu-Br bond, at 2.44 Å, is relatively long with respect to the terminal Cu-Br bonds described for complexes **C15** and **C18** (2.28 / 2.28 and 2.28 Å) but compares well with the bridging Cu-Br bonds of **C14** (2.44 and 2.46 Å). This lengthening may result from a need to reduce steric

clashing around the 4-coordinate Cu^{I} centre, and also the possible increase in electron density at the Cu^{I} centre by having three other donor moieties bound to the metal centre.

As mentioned above, alkene coordination to the metal centre is observed in complex **C19C**. Alkene coordination results in a pronounced lengthening of the alkenic C-C bond from 1.33 Å (**L19**) to 1.37 Å (**C19C**). This lengthening was anticipated since metal coordination acts to decrease π-bonding electron density and increase π*-antibonding electron density about the alkenic C-C bond, thus resulting in a reduction in the overall bond order of the C-C double bond. The coordination of the alkene to the metal centre appears to have been facilitated by the addition of the pyridyl group to the NHC ligand, which acts as both an ancillary donor and also as a modifier of the electronic properties of the NHC donor. With this in mind, it is unsurprising then that many of the structurally characterised Cu^{I}-alkene complexes reported thus far contain chelating *N*-donor ligands such as *tris*(pyrazolyl)borate.[5c, 5g] The exact role of the pyridyl in enabling alkene coordination to the metal centre in this case is unclear however; it may be altering the properties of the Cu^{I} centre directly by coordination to it, or it may be indirectly affecting the Cu^{I} centre by modifying the donor ability of the NHC (decreasing the energy of the LUMO).

A symmetrical *bis*-NHC analogue of **L19** was synthesised (**L20**). This was done to examine the effect of an extra NHC donor on Cu^{I} coordination and hence on interaction between the Cu^{I} centre and alkenes. It was decided to attempt the complexation of **L20** to Cu^{I} using the procedure described for the synthesis of **C19A**, rather than going *via* the Ag^{I}-NHC complex, since *bis*-imidazolium salts are known to require more forcing conditions when reacting with Ag_2O,[20] and since the solubility of **L20** is poor in chlorinated solvents, which are typically used for Ag_2O reactions.

Reaction of **L20** with two equivalents of CuBr and an excess of Cs_2CO_3 in anhydrous acetonitrile at 50°C immediately led to the formation of a yellow suspension. After filtration, the solvent was removed *in vacuo* to give a Cu^{I}-NHC complex (**C20A**) as a yellow solid. The solubility of the product was reasonably poor, although ^{1}H and $^{13}C\{^{1}H\}$ NMR spectra with good signal to noise ratios could be obtained at elevated temperatures (333.6 K) with a large number of scans. The ^{1}H NMR spectrum illustrates the presence of only one ligand environment and also the loss of the imidazolium proton. Unlike the ^{1}H NMR spectrum of **C19C**, the spectrum of **C20A** is sharp, perhaps indicating that the complex is less labile than **C19C**. The $^{13}C\{^{1}H\}$ NMR spectrum of **C20A** shows a characteristic low field resonance at 181.9 ppm (126 MHz, CD_3CN, 333.6 K), indicating the formation of a Cu^{I}-NHC complex. The high-resolution mass spectrum of **C20A** was dominated by a peak at m/z 354.08, which was found to correspond to a $[Cu_2(NHC)_2]^{2+}$ fragment. However, elemental analysis of a sample of **C20A** strongly suggested that it was a $Cu_3Br_3L_2$-type complex. In order to identify the complex **C20A** unambiguously,

single crystals suitable for X-ray diffraction analysis were obtained by the cooling of a saturated solution of the product from 333 K to ambient temperature in anhydrous acetonitrile. **C20A** was found to crystallise in the monoclinic crystal system, and the structural solution was performed in the space group *C*2/*c* (Figure 3.24). From this data, it is evident that the solid state structure is in firm agreement with the formulation of the product ($Cu_3Br_3L_2$), provided by elemental analysis.

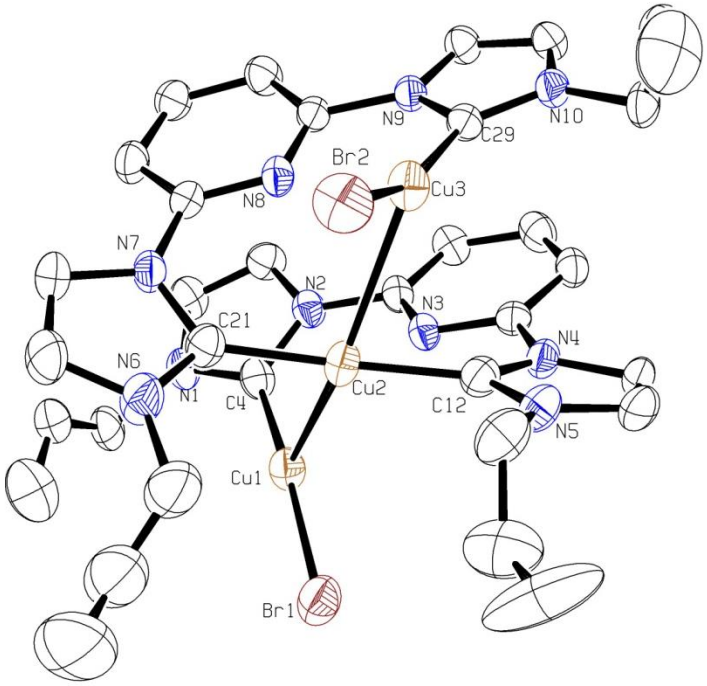

Figure 3.24 Molecular structure of **C20A**. Ellipsoids are drawn at the 50% probability level. H atoms, a bromide anion and a co-crystallised acetonitrile molecule are omitted for clarity

Table 3.9 Selected bond distances (Å) and angles (deg) for **C20A**

Cu(1)-Br(1)	2.2838(8)	C(4)-Cu(1)-Br(1)	171.0(2)
C(4)-Cu(1)	1.912(5)	C(12)-Cu(2)-C(21)	164.6(2)
C(12)-Cu(2)	1.935(5)	C(29)-Cu(3)-Br(2)	156.9(2)
C(21)-Cu(2)	1.936(5)		
Cu(3)-Br(2)	2.3072(9)		
C(29)-Cu(3)	1.920(5)		
Cu(1)-Cu(2)	2.867(1)		
Cu(2)-Cu(3)	2.781(1)		

C20A was found to crystallise as a ligand-supported cuprophilic trimer. Cuprophilic trimers slightly similar to **C20A** have been described previously in the literature,[21] although many of these occur as C_3-symmetric triangular Cu^I clusters.[22] The geometries (excluding possible cuprophilic interactions) about all three of the Cu^I centres are best described as distorted linear, with bond angles of 171.0°, 164.6° and 156.9° respectively. The C-Cu and Cu-Br bond lengths are within typical ranges for Cu^I-NHC complexes. The distances between the three Cu^I centres are 2.87 Å and 2.78 Å, and thus possibly represent weak cuprophilic interactions. It is notable in the structure that pyridyl coordination does not occur, with the closest pyridyl-Cu^I interaction occurring between Cu3 and N8 at a distance of 2.64 Å. This presumably results from the conformational restriction imposed by the ligand on the positions of the Cu^I centres (*i.e.* away from the pyridyl nitrogens), but may also result from the withdrawal of electron density away from the pyridyl nitrogen atoms by the NHC rings, making the pyridyls poorer donors. Twisting of the NHC rings with respect to the pyridyl rings occurs to varying degrees (torsion angles of between 10.3° - 31.8°), which would act to decrease π-overlap between the NHC and pyridyl rings. Possibly as a result of the lack of coordination by the pyridyls to the Cu^I centre in **C20A**, no alkene coordination is observed; it appears that all three Cu^I centres are coordinatively saturated in this complex.

An explanation for the dominant ion in the high resolution mass spectrum of **C20A** being a $[Cu_2(NHC)_2]^{2+}$ fragment was obtained by the serendipitous crystallisation of **C20B**. Complex **C20B** crystallised during the slow evaporation of a sample of **C20A** exposed to air/moisture and was found to crystallise in the triclinic crystal system. The structural solution was performed in the space group $P\bar{1}$ (Figure 3.25).

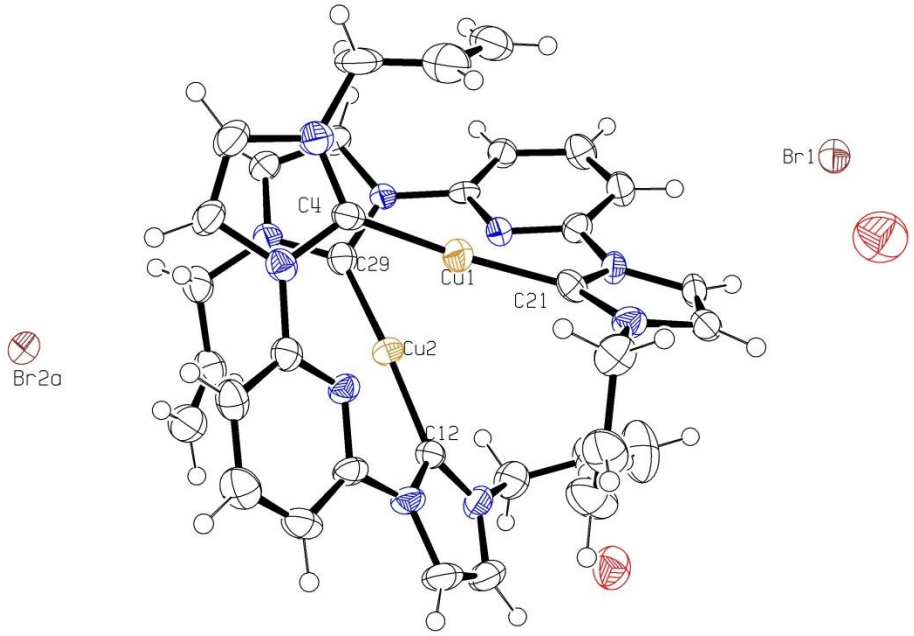

Figure 3.25 Molecular structure of **C20B**. Ellipsoids are drawn at the 50% probability level

It is clear from Figure 3.25 that exposure of samples of **C20A** to air/moisture results in the 'breakdown' of **C20A**, forming the helicate **C20B**. This is why only a $[Cu_2(NHC)_2]^{2+}$ fragment was observed in the mass spectrum. It is a somewhat surprising result, especially given the tendency of Cu^I-NHC complexes bearing non-bulky *N*-substituents (*i.e.* allyl) to decompose, reforming imidazolium salts and unidentifiable Cu^{II}-containing detritus. The formation of **C20B** over imidazolium-containing decomposition products, for instance, suggests that the 16-membered metallacycle contained within **C20B** is highly stable, even on prolonged exposure to air and moisture.

3.5 Conclusions

The tremendous structural diversity observed in the chemistry of Cu^I has been frequently demonstrated throughout this chapter. 2-, 3- and 4-coordinate Cu^I complexes have been synthesised with linear, trigonal, T-shaped and trigonal pyramidal geometries to name but a few. This kind of rampant coordinative variation is explained by the lability of the closed-shell d^{10} Cu^I cation and has consequences for the use of Cu^I complexes in catalysis.

Furthermore, by significant variation of the *N*-substituents, the first structurally characterised Cu^I-NHC complex containing a Cu^I-alkene interaction has been obtained. This complex indicates that a strong interaction between an *N*-donor ligand and the Cu^I centre, along with the NHC itself, is vital in facilitating alkene coordination. Such knowledge will help to guide the development of Cu^I-NHC complexes for use in catalytic processes, which rely heavily on alkene coordination to the Cu^I centre.

3.6 Future Work

Future work in this area should focus on modifying the pyridyl-containing ligand precursors to produce complexes with greater air stability, but which are still capable of alkene coordination. Testing of such complexes in reactions which rely on alkene coordination, such as alkene aziridination and cyclopropanation could then be performed. Furthermore, the binding of carbon monoxide by these complexes (σ-donor, π-acceptor ligands, akin to alkenes) could also be examined, since reversible CO-binding Cu^I complexes have the potential to be used in gas purification.

It was noticed that the decomposition of **C19C** led to the formation of a small number of green crystals, which could be analysed by single crystal X-ray diffraction analysis. The structure obtained was that of a highly unusual Cu^{II}-NHC complex. With this in mind, the synthesis of a range of Cu^{II}-NHC complexes could be attempted, and comparison of these with the analogous Cu^I-NHC complexes in Cu-catalysed cross-coupling processes (*e.g.* Ullmann coupling) could be

attempted. Such a study could help shed light on the nature of the active species in these coupling reactions, and guide future Cu-catalyst development.

3.7 References

[1] F. I. Rodríguez, J. J. Esch, A. E. Hall, B. M. Binder, G. E. Schaller, A. B. Bleecker, *Science* **1999**, *283*, 996-998.

[2] P. Brandt, M. J. Södergren, P. G. Andersson, P.-O. Norrby, *Journal of the American Chemical Society* **2000**, *122*, 8013-8020.

[3] A. G. Jarvis, A. C. Whitwood, I. J. S. Fairlamb, *Dalton Transactions* **2011**, *40*, 3695-3702.

[4] a) M. J. S. Dewar, *Bull. Soc. Chim. Fr.* **1951**, 71-79; b) J. Chatt, L. A. Duncanson, *Journal of the Chemical Society (Resumed)* **1953**, *0*, 2939-2947.

[5] a) B. J. Bellott, G. S. Girolami, *Organometallics* **2009**, *28*, 2046-2052; b) J. J. Allen, A. R. Barron, *Dalton Transactions* **2009**, *0*, 878-890; c) C. Martín, J. M. Muñoz-Molina, A. Locati, E. Alvarez, F. Maseras, T. R. Belderrain, P. J. Pérez, *Organometallics* **2010**, *29*, 3481-3489; d) G. Doyle, K. A. Eriksen, D. VanEngen, *Organometallics* **1985**, *4*, 830-835; e) J. S. Thompson, J. F. Whitney, *Acta Crystallographica Section C* **1984**, *40*, 756-759; f) V. A. K. Adiraju, J. A. Flores, M. Yousufuddin, H. V. R. Dias, *Organometallics* **2012**, *31*, 7926-7932; g) H. V. R. Dias, H.-L. Lu, H.-J. Kim, S. A. Polach, T. K. H. H. Goh, R. G. Browning, C. J. Lovely, *Organometallics* **2002**, *21*, 1466-1473.

[6] F. H. Ekkehardt Hahn, C.; Pape, T., *Zeitschrift für Naturforschung B* **2004**, *59b*, 1051-1053.

[7] F. Ekkehardt Hahn, B. Heidrich, T. Pape, A. Hepp, M. Martin, E. Sola, L. A. Oro, *Inorganica Chimica Acta* **2006**, *359*, 4840-4846.

[8] B. Liu, Y. Zhang, D. Xu, W. Chen, *Chemical Communications* **2011**, *47*, 2883-2885.

[9] a) G. Venkatachalam, M. Heckenroth, A. Neels, M. Albrecht, *Helvetica Chimica Acta* **2009**, *92*, 1034-1045; b) S. Díez-González, E. D. Stevens, N. M. Scott, J. L. Petersen, S. P. Nolan, *Chemistry – A European Journal* **2008**, *14*, 158-168; c) S. Diez-Gonzalez, E. C. Escudero-Adan, J. Benet-Buchholz, E. D. Stevens, A. M. Z. Slawin, S. P. Nolan, *Dalton Transactions* **2010**, *39*, 7595-7606.

[10] V. A. Anisimova, I. E. Tolpygin, *Russian Journal of Organic Chemistry* **2011**, *47*, 1346-1353.

[11] a) N. P. Mankad, T. G. Gray, D. S. Laitar, J. P. Sadighi, *Organometallics* **2004**, *23*, 1191-1193; b) S. Diez-Gonzalez, E. D. Stevens, S. P. Nolan, *Chemical Communications* **2008**, 4747-4749.

[12] a) A. A. D. Tulloch, A. A. Danopoulos, S. Kleinhenz, M. E. Light, M. B. Hursthouse, G. Eastham, *Organometallics* **2001**, *20*, 2027-2031; b) C. A. Citadelle, E. L. Nouy, F. Bisaro, A. M. Z. Slawin, C. S. J. Cazin, *Dalton Transactions* **2010**, *39*, 4489-4491; c) J. Chun, H. S. Lee, I. G. Jung, S. W. Lee, H. J. Kim, S. U. Son, *Organometallics* **2010**, *29*, 1518-1521.

[13] a) R. D. Köhn, G. Seifert, Z. Pan, M. F. Mahon, G. Kociok-Köhn, *Angewandte Chemie International Edition* **2003**, *42*, 793-796; b) A. Sundararaman, L. N. Zakharov, A. L. Rheingold, F. Jakle, *Chemical Communications* **2005**, *0*, 1708-1710; c) J.-P. Zhang, Y.-B. Wang, X.-C. Huang, Y.-Y. Lin, X.-M. Chen, *Chemistry – A European Journal* **2005**, *11*, 552-561; d) G. M. Chiarella, D. Y. Melgarejo, A. Rozanski, P. Hempte, L. M. Perez, C. Reber, J. P. Fackler Jr, *Chemical Communications* **2010**, *46*, 136-138.

[14] G. Occhipinti, V. R. Jensen, K. W. Törnroos, N. Å. Frøystein, H.-R. Bjørsvik, *Tetrahedron* **2009**, *65*, 7186-7194.

[15] A. C. Badaj, S. Dastgir, A. J. Lough, G. G. Lavoie, *Dalton Transactions* **2010**, *39*, 3361-3365.

[16] H.-Y. Gong, B. M. Rambo, E. Karnas, V. M. Lynch, J. L. Sessler, *Nature Chemistry* **2010**, *2*, 406-409.

[17] B. L. Schottel, H. T. Chifotides, K. R. Dunbar, *Chemical Society Reviews* **2008**, *37*, 68-83.

[18] J. C. Garrison, W. J. Youngs, *Chemical Reviews* **2005**, *105*, 3978-4008.

[19] H. M. J. Wang, I. J. B. Lin, *Organometallics* **1998**, *17*, 972-975.

[20] A. A. D. Tulloch, A. A. Danopoulos, S. Winston, S. Kleinhenz, G. Eastham, *Journal of the Chemical Society, Dalton Transactions* **2000**, 4499-4506.

[21] B. Liu, Q. Xia, W. Chen, *Angewandte Chemie International Edition* **2009**, *48*, 5513-5516.

[22] a) B. Liu, Y. Zhang, D. Xu, W. Chen, *Chemical Communications* **2011**, *47*, 2883-2885; b) V. J. Catalano, L. B. Munro, C. E. Strasser, A. F. Samin, *Inorganic Chemistry* **2011**, *50*, 8465-8476; c) C. Chen, H. Qiu, W. Chen, *Journal of Organometallic Chemistry* **2012**, *696*, 4166-4172.

Chapter 4

Pyridyl-Tethered NHCs: Application of Cu^{I} Complexes in Ullmann-Type Etherification and Crystallisation of their Atmospheric Oxidation Products

4.1 Introduction

During the course of the studies performed on the pyridyl-substituted Cu^{I}-NHC complexes (described in Chapter 3), it was observed that exposure of solutions of these complexes to atmospheric conditions very often led to the formation of green solutions, from which green or blue crystals could be obtained. These crystals were found to be rare examples of Cu^{II}-NHC complexes. This is in stark contrast to other Cu^{I}-NHC complexes (*i.e.* those not containing pyridyl donors), where exposure to atmospheric conditions tends to lead to ligand demetallation and re-formation of an imidazolium salt, along with highly insoluble Cu^{II}-containing species. With this apparent stabilisation of organo-Cu^{II} species in mind, a library of pyridyl-substituted imidazolium salts (Figure 4.1) and their respective Cu^{I}-complexes were synthesised and their competence in Ullmann-type etherification reactions tested. Ullmann-type coupling was chosen, since the mechanism by which it occurs involves higher oxidation state organo-copper species.[1] However, the exact mechanism by which Ullmann-type coupling chemistry proceeds is still debated within the literature, with evidence for both a radical pathway (Cu^{I}/Cu^{II})[2] and a conventional oxidative addition/reductive elimination pathway (Cu^{I}/Cu^{III}).[3]

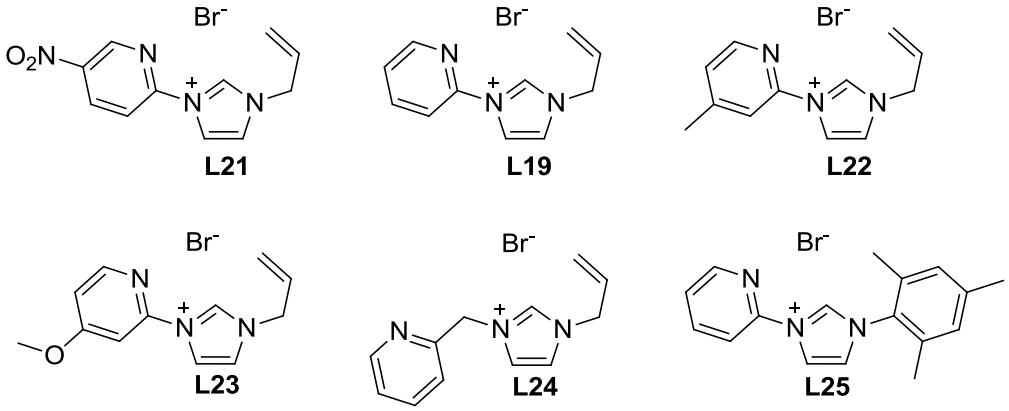

Figure 4.1 Target ligand set for testing in Ullmann-type coupling

4.2 Ligand and Cu^{I}-NHC Complex Synthesis

4.2.1 5-Nitropyridyl-Substituted NHC

The ligand precursor **L21** was synthesised, where the pyridyl ring has been appended with a nitro group in the 5-position (*para*-substituted with respect to the imidazolium ring). By placing the nitro group in the 5-position, it is able to exert a strong –M effect on the imidazolium ring which could alter the electronic properties of the resulting NHC complex. Furthermore, the strong –I effect provided by the nitro group may also act to make the pyridine more weakly basic (and thus a poorer donor to a metal centre).

L21 was synthesised using a two-step procedure. Firstly, 1-(2-(5-nitro)pyridyl)imidazole (**P21**) was synthesised *via* the nucleophilic aromatic substitution reaction between sodium imidazolide and 2-bromo-5-nitropyridine in anhydrous dimethylformamide.[4] This was followed by reaction of **P21** with an excess of allyl bromide in acetonitrile at reflux. **L21** was obtained as off-white needles in an overall yield of 86% (for both steps). The synthetic procedure is outlined in Scheme 4.1.

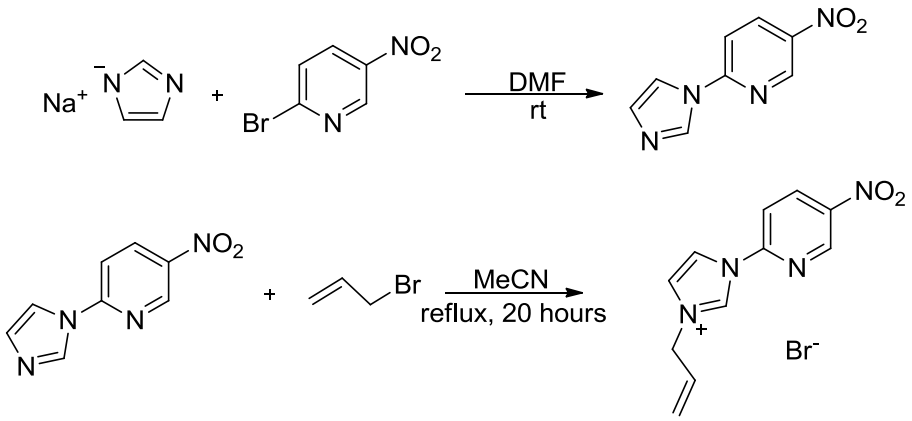

Scheme 4.1 Synthesis of **L21**

After successful isolation of ligand precursor **L21**, characterisation by ^{1}H and $^{13}C\{^{1}H\}$ NMR spectroscopy, high-resolution MS and elemental analysis was performed. A low field resonance was observed at 12.22 ppm (300 MHz, DMSO) in the ^{1}H NMR spectrum, strongly indicative of the formation of an imidazolium halide. Also, the high resolution mass spectrum of **L21** was dominated by a peak at m/z 231.1, corresponding to the $[M - Br]^{+}$ fragment. X-Ray diffraction analysis of **L21** was possible with single crystals obtained by the vapour diffusion of diethyl ether in to a concentrated solution of the product in acetonitrile. **L21** crystallises in the triclinic crystal system and the structural solution was performed in the space group $P\bar{1}$ (Figure 4.2).

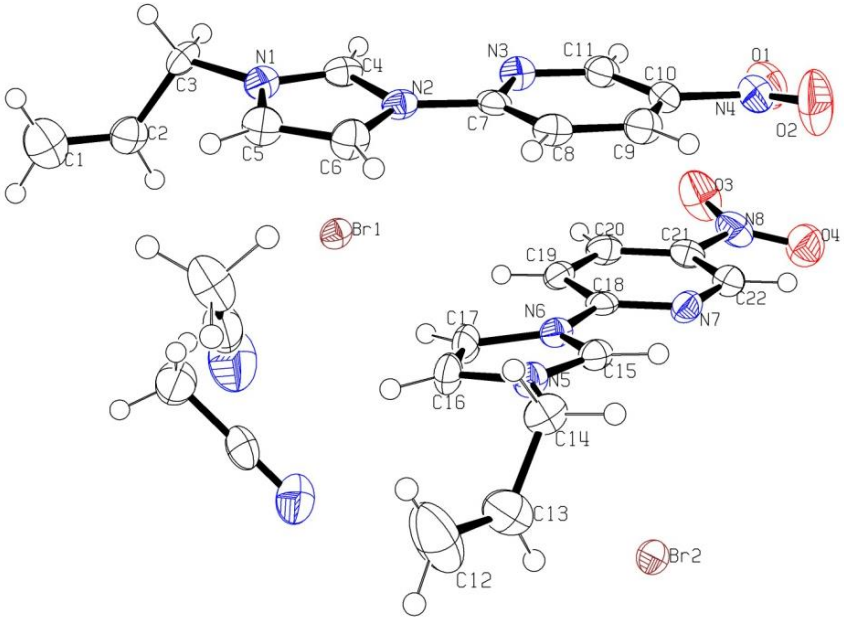

Figure 4.2 Molecular structure of **L21**. Ellipsoids are drawn at the 50% probability level

Table 4.1 Selected bond distances (Å) and angles (deg) for **L21**

N(1)-C(4) / N(5)-C(15)	1.338(4) / 1.339(5)	N(1)-C(4)-N(2)	108.5(3)
N(2)-C(4) / N(6)-C(15)	1.363(5) / 1.370(5)	N(5)-C(15)-N(6)	107.8(3)
N(2)-C(7) / N(6)-C(18)	1.447(4) / 1.459(5)		
N(1)-C(3) / N(5)-C(14)	1.507(4) / 1.509(5)		
C(4)---Br(1) / C(15)---Br(2)	3.315 / 3.309		

L21 crystallises with two imidazolium bromides and two molecules of acetonitrile in the asymmetric unit. The nitropyridyl and imidazolium rings lie almost co-planar with a torsion angle of approximately 6 – 7°. The nitro groups are also offset slightly with respect to the pyridyl rings, by 12 – 14°. A large number of short contacts (shorter than the sum of the van der Waals' radii) are evident between several hydrogen atoms of the pyridyl and imidazolium rings and neighbouring bromide anions. Anion-π interactions are also evident within the structure, occurring between bromide anions and the C2 carbon of both imidazolium rings at distances of 3.31 and 3.32 Å respectively. Another interesting feature, is that there appears to be a difference in bond lengths about the N-C-N of the imidazolium rings (Figure 4.3).

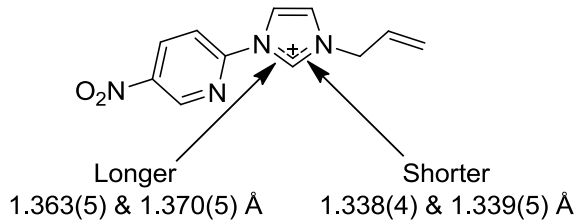

Figure 4.3 Imidazolium N-C-N bond lengths in **L21**

While only a small difference, it appears to be significant. The reason for this difference could be due to electron withdrawal by the nitropyridine unit affecting the imidazolium nitrogen closest to it, reducing its π-electron density, which in turn reduces the π-electron density that it has available to donate across the N-C-N moiety. Thus, there is reduced π-electron density in the N-C bond closest to the pyridyl, which is manifested in the lengthening of this bond.

Reaction of an excess of Ag_2O with **L21** in anhydrous dichloromethane in the presence of 4Å molecular sieves led to the formation of a dark suspension. After filtration, washing of the solid with a large volume of solvent and removal of the solvent *in vacuo*, an off-white solid was produced (**C21A**). The Ag^I-NHC complex **C21A** was found to be rather insoluble, but analysis by ^1H NMR spectroscopy was possible, and indicated loss of the imidazolium proton resonance. Reaction of **C21A** with an excess of CuBr in anhydrous dichloromethane at room temperature led to the formation of an orange/yellow solution after filtration to remove AgBr and unreacted CuBr (Scheme 4.2). Slow addition of anhydrous pentane to the solution led to the rapid crystallisation of a red solid (**C21B**), which was collected and dried.

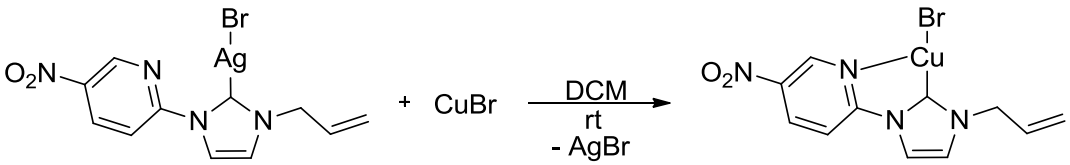

Scheme 4.2 Synthesis of **C21B**

Full characterisation of **C21B** by ^1H and $^{13}C\{^1H\}$ NMR spectroscopy, high-resolution MS and elemental analysis indicated the presence of analytically pure CuBrL-type complex. Slight broadening of certain resonances was observed in the ^1H NMR spectrum of **C21B**. Single crystals suitable for X-ray diffraction analysis were grown by the slow evaporation of a concentrated solution of **C21B** in acetonitrile. Complex **C21B** crystallised in the orthorhombic crystal system and the structural solution was performed in the space group *Pccn* (Figure 4.4).

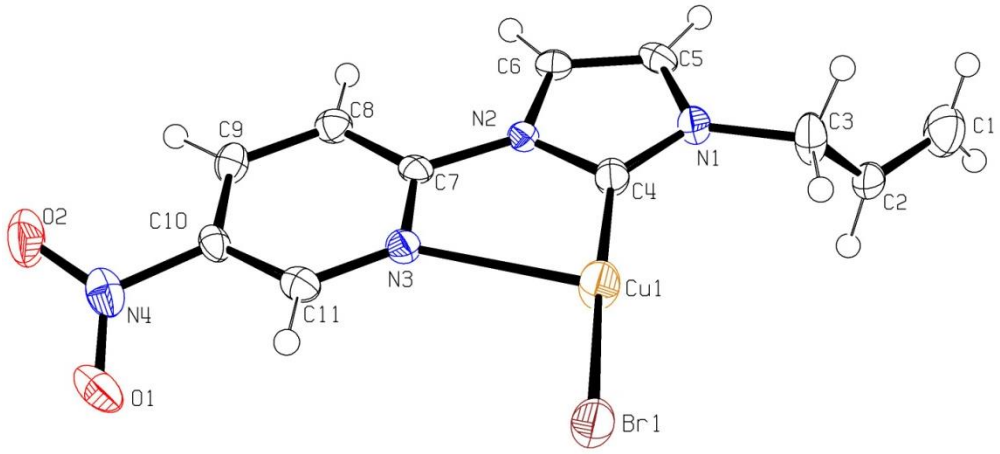

Figure 4.4 Molecular structure of **C21B**. Ellipsoids are drawn at the 50% probability level

Table 4.2 Selected bond distances (Å) and angles (deg) for **C21B**

Cu(1)-Br(1)	2.2851(5)	C(4)-Cu(1)-Br(1)	176.82(8)
C(4)-Cu(1)	1.907(3)	C(4)-Cu(1)-N(3)	74.7(1)
N(3)-Cu(1)	2.562(2)	N(3)-Cu(1)-Br(1)	108.32(5)
N(1)-C(4)	1.361(3)	N(1)-C(4)-N(2)	103.2(2)
N(2)-C(4)	1.394(4)		

Complex **C21B** crystallised as a monomer with the coordination environment around the Cu^{I} centre best described as distorted T-shaped. A similar coordination environment has been reported previously by Danopoulos.[5] The C-Cu and Cu-Br distances, at 1.91 and 2.29 Å respectively, are entirely within the range expected for linear 2-coordinate CuBrL-type complexes, as is the C-Cu-Br bond angle (176.8°). The N-Cu bond length on the other hand is extremely long (2.56 Å), implying the presence of a weak interaction at best between the pyridyl nitrogen and Cu^{I} centre. The fact that this bond is lengthened suggests that the primary effect of adding the nitro group has been to inductively withdraw electron density away from the pyridyl nitrogen atom, making it a poorer donor to the metal centre. This is interesting, considering the fact that the nitro group is *para*-substituted with respect to the NHC ring, and thus should exert a considerable π-electron withdrawing effect on it.

4.2.2 Pyridyl-Substituted NHC

The synthesis and characterisation of the ligand precursor **L19** and its associated Cu^{I} complex (**C19C**) was described in Chapter 3. It was found that exposure of a solution in dichloromethane of complex **C19C** to low oxygen levels yielded a small number of poor quality green needles amongst the yellow crystals of complex **C19C**, some of which were suitable for X-ray

diffraction analysis. The crystals were found to belong to the triclinic crystal system, with the structural solution being performed in the space group $P\bar{1}$ (Figure 4.5).

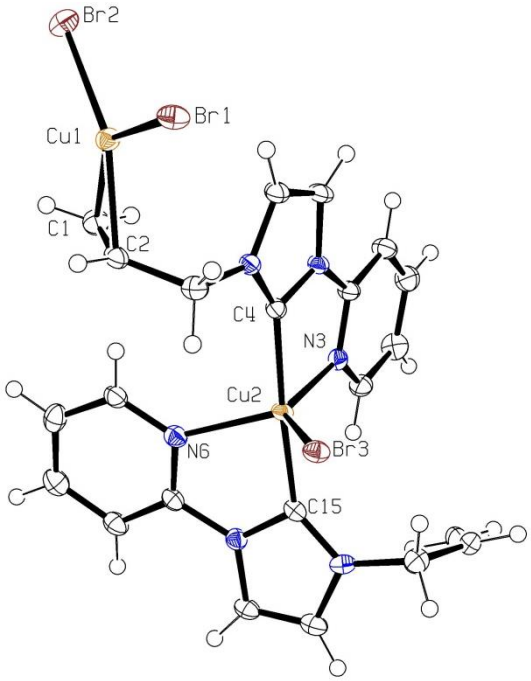

Figure 4.5 Molecular structure of **C19D**. Ellipsoids are drawn at the 50% probability level

Table 4.3 Selected bond distances (Å) and angles (deg) for **C19D**

Cu(1)-Br(1)	2.3628(7)	C(4)-Cu(2)-C(15)	175.3(2)
Cu(1)-Br(2)	2.3452(7)	Br(3)-Cu(2)-N(3)	134.57(9)
Cu(2)-Br(3)	2.5152(7)	Br(3)-Cu(2)-N(6)	117.88(8)
Cu(2)-C(4)	1.977(4)	N(3)-Cu(2)-N(6)	107.5(1)
Cu(2)-C(15)	1.981(4)	Br(1)-Cu(1)-Br(2)	108.86(3)
Cu(2)-N(3)	2.164(3)		
Cu(2)-N(6)	2.181(3)		
Cu(1)-alk*	1.962		
C(1)-C(2)	1.357(6)		

(* denotes centre of alkene double bond)

C19D was found to be an interesting mixed Cu^{II}-Cu^{I} NHC complex. The structure illustrates the presence of two chelating NHC units and a bromide around the Cu^{II} centre, with the structure being charge-balanced by an alkene-coordinated $CuBr_2^-$ unit. The coordination geometry around the Cu^{II} centre can be described as slightly distorted trigonal bipyramidal, with the NHC donors occupying the apical positions and the pyridyl donors and a bromide occupying the equatorial

plane. This distortion from idealised trigonal bipyramidal geometry probably arises, in part, as a result of the relatively narrow bite angle of the chelating pyridyl-NHC ligand (approximately 78°). The C-Cu bond lengths, at 1.98 Å, are at the upper end of the small number of values reported in the literature, which fall between 1.91 and 2.01 Å respectively.[6] This relative lengthening of the C-Cu bonds is potentially a result of the significant structural trans influence imparted by the strong σ-donor NHC ligands on each other. The Cu^{I} centre (Cu1) is found in a trigonal planar environment (if considering the centroid of the alkene donor).

Upon exposure of a solution of Cu^{I} complex **C19C** in chloroform to atmospheric conditions, followed by crystallisation from the vapour diffusion of pentane in to the solution of **C19C** in chloroform, a small number of poor quality green needles were again produced. After determining the unit cell of the crystals, they were observed to be different to the Cu^{II} complex described above (**C19D**), and thus a data collection was performed. The crystals were found to belong to the monoclinic crystal system, with the structural solution being performed in the space group $P2_1/c$ (Figure 4.6).

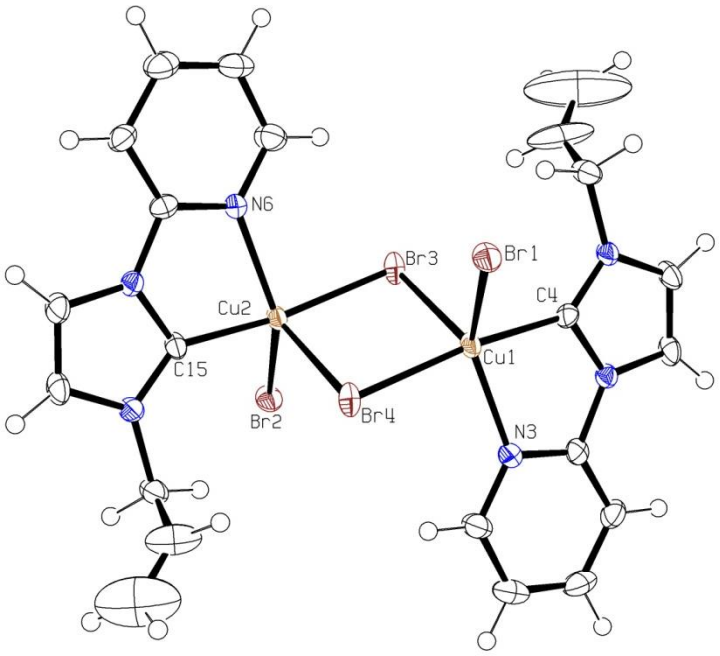

Figure 4.6 Molecular structure of **C19E**. Ellipsoids are drawn at the 50% probability level. Four molecules of co-crystallised chloroform are omitted for clarity

Table 4.4 Selected bond distances (Å) and angles (deg) for **C19E**

Cu(1)-Br(1)	2.4826(8)	C(4)-Cu(1)-Br(4)	169.5(1)
Cu(2)-Br(2)	2.4805(8)	Br(1)-Cu(1)-N(3)	136.6(1)
Cu(1)-C(4)	1.957(5)	Br(1)-Cu(1)-Br(3)	107.67(3)
Cu(2)-C(15)	1.959(5)	Br(3)-Cu(1)-N(3)	115.6(1)
Cu(1)-N(3)	2.115(4)		
Cu(2)-N(6)	2.126(4)		
Cu(1)-Br(3)	2.587(1)		
Cu(1)-Br(4)	2.346(1)		

Complex **C19E** was found to have crystallised as a (μ-halide)$_2$-bridged dimer. The bridging halides were found to be substitutionally disordered (labelled as Br3 and Br4 in Figure 4.6), containing a mixture of chloride and bromide. It is anticipated that the chloride originates from impurities in the wet chloroform solvent. Interestingly, the terminally bound halides were not found to be substitutionally disordered, comprising only bromide. The geometry around the two Cu^{II} centres can again be described as slightly distorted trigonal bipyramidal. The coordination sphere of the Cu^{II} centre comprises the NHC and a bridging halide in the apical positions. The equatorial positions contain a terminal halide, a bridging halide and the pyridyl. The C-Cu bond lengths of 1.96 Å compare extremely well with literature precedent, but are a little shorter than those observed in complex **C19D**, possibly reflecting the weaker trans influence of the bridging halide compared to the NHC donor.

The isolation and X-ray crystallographic analysis of Cu^{II} complexes **C19D** and **C19E** (albeit, only small amounts were made) illustrated that pyridyl-appended NHC ligands are highly effective in stabilising higher oxidation states of copper. It is possible that this ability is important in Ullmann-type coupling chemistry, where the presence of higher oxidation organo-copper species during the catalytic cycle is widely predicted.

4.2.3 4-Methylpyridyl-Substituted NHC

The p-methyl-substituted pyridyl ligand precursor, **L22**, was synthesised using a very similar protocol to ligand precursor **L19**. Initially, an Ullmann-type coupling of 2-bromo-4-methylpyridine with imidazole was performed using an established procedure (to form **P22**).[7] Then, reaction of the coupled product with an excess of allyl bromide at reflux in acetonitrile cleanly afforded the imidazolium salt, **L22**, as an off-white solid after work-up. Full

characterisation of **L22** was performed, including single crystal X-ray diffraction analysis. Single crystals were obtained by the vapour diffusion of pentane in to a concentrated solution of the product in chloroform. **L22** was found to crystallise in the triclinic crystal system, with the structural solution being performed in the space group $P\bar{1}$ (Figure 4.7).

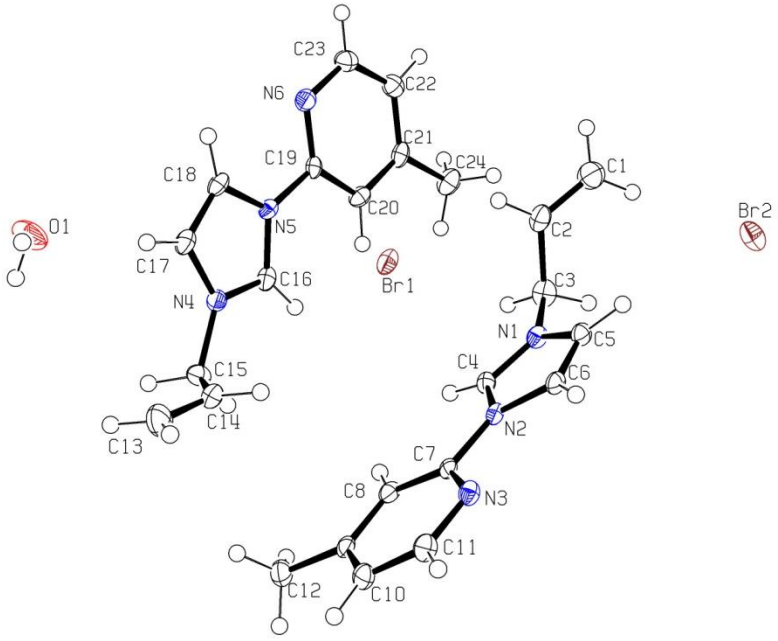

Figure 4.7 Molecular structure of **L22**. Ellipsoids are drawn at the 50% probability level

The crystal structure of ligand precursor **L22** is provided to illustrate connectivity rather than for a lengthy discussion of bond metrics. However, it is clear from the structure above, that there are two imidazolium bromide moieties and one water molecule in the asymmetric unit. One of the bromides (Br2) and the water molecule form a 1D hydrogen-bonded zigzag which propagates throughout the structure. The other bromide (Br1) appears to be involved in two anion-π interactions with the neighbouring π-clouds of the imidazolium rings (N1-C4-N2 and N4-C16-N5) and two hydrogen bonds with neighbouring imidazolium protons (H4 and H16).

Similarly to ligand precursor **L21**, reaction of an excess of Ag_2O with **L22** in anhydrous dichloromethane in the presence of 4Å molecular sieves led to the formation of a dark suspension, which gave a white solid after work-up (**C22A**). The Ag^I-NHC complex **C22A** was fully characterised using ^1H and $^{13}C\{^1H\}$ NMR spectroscopy, high-resolution MS and elemental analysis. Loss of the imidazolium resonance in the ^1H NMR spectrum as well as the appearance of a low field resonance at 181.1 ppm (75 MHz, $CDCl_3$) in the $^{13}C\{^1H\}$ NMR spectrum indicated the successful formation of a Ag^I-NHC complex. Furthermore, single crystal X-ray diffraction analysis of **C22A** unambiguously elucidated the solid state structure of **C22A**. The crystal used in the analysis was obtained by the vapour diffusion of pentane in to a concentrated solution of the product in chloroform. **C22A** was found to crystallise in the monoclinic crystal system with the structural solution being performed in the space group *C2/c* (Figure 4.8).

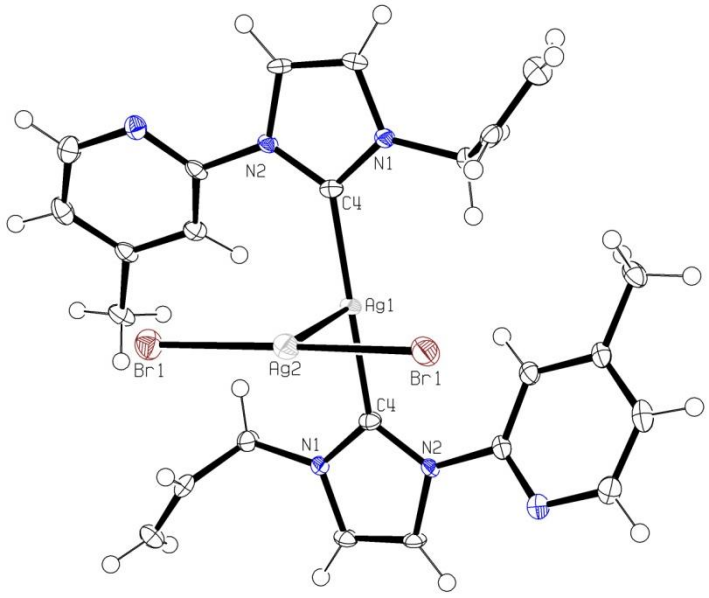

Figure 4.8 Molecular structure of **C22A**. Ellipsoids are drawn at the 50% probability level

Table 4.5 Selected bond distances (Å) and angles (deg) for **C22A**

Ag(1)-C(4)	2.089(3)	C(4)-Ag(1)-C(4)	179.0(1)
Ag(1)-Ag(2)	3.0405(6)	C(4)-Ag(1)-Ag(2)	90.51(9)
Ag(2)-Br(1)	2.4443(3)	Br(1)-Ag(1)-Br(1)	175.61(2)

Analogously to the Ag^{I} complex of ligand precursor **L19** (described in the previous chapter), **C22A** crystallised as a $[Ag(NHC)_2]AgBr_2$-type complex, with a possible argentophilic interaction (3.04 Å) between the two independent Ag^{I} centres. The C-Ag bond length, at 2.09 Å, is typical of Ag^{I}-*bis*NHC complexes with halogeno anions (2.08(1) Å).[8]

Treatment of the Ag^{I} complex **C22A** with an excess of CuBr in dichloromethane led to the formation of a yellow solid following work-up. Full characterisation of the yellow solid (**C22B**), including elemental analysis, indicated the formation of a Cu^{I}-NHC complex with the formulation [Cu(NHC)Br]. The ^{1}H NMR spectrum was found to be significantly broadened, similarly to the spectra of **C21B** and **C19C**. Single crystals suitable for X-ray diffraction analysis were grown on standing of a chloroform/hexane (1:2) solution of the product. **C22B** crystallised in the monoclinic crystal system, and a structural solution was obtained in the space group $P2_1/c$ (Figure 4.9).

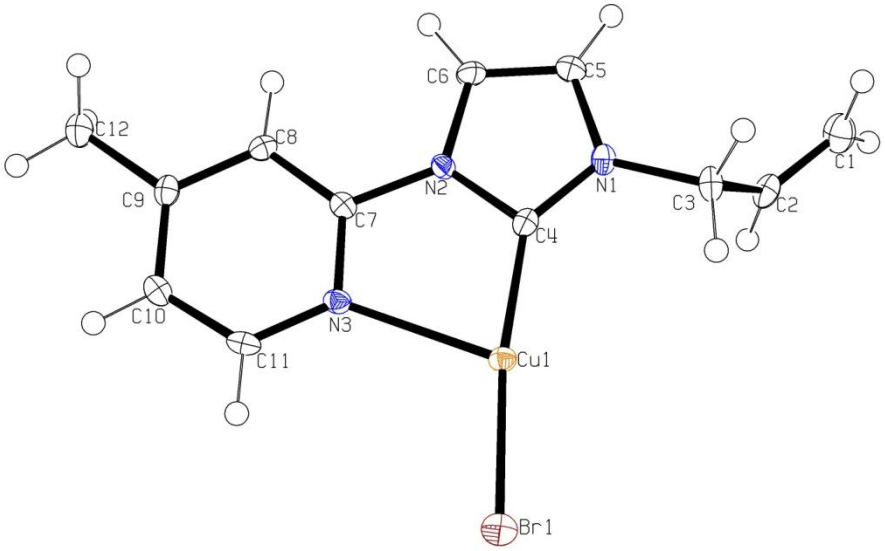

Figure 4.9 Molecular structure of **C22B**. Ellipsoids are drawn at the 50% probability level

Table 4.6 Selected bond distances (Å) and angles (deg) for **C22B**

Cu(1)-Br(1)	2.2527(6)	C(4)-Cu(1)-Br(1)	171.78(12)
C(4)-Cu(1)	1.899(4)	C(4)-Cu(1)-N(3)	78.23(14)
N(3)-Cu(1)	2.338(3)	N(3)-Cu(1)-Br(1)	109.99(8)
N(1)-C(4)	1.351(5)	N(1)-C(4)-N(2)	103.3(3)
N(2)-C(4)	1.377(5)		

Given the observation of an alkene-Cu^{I} interaction in the crystal structure of **C19C** (described in the previous chapter), it was anticipated that **C22B** would crystallise in a similar manner (as the only difference is a methyl group). However, the geometry about the Cu^{I} centre in complex **C22B**, like **C19B**, is best described as distorted T-shaped (and devoid of an alkene-Cu^{I} interaction). This indicates that the nature of alkene-Cu^{I} interactions is more complicated than first thought. The Cu-C and Cu-Br bond lengths in **C22B** are comparable to those in **C21B**, whereas the Cu-N bond length in this complex (2.34 Å) is considerably shorter than the nitro-pyridyl example (2.56 Å). This perhaps reflects the increased pyridyl σ-donor strength on moving from 3-nitro to 4-methylpyridine.

Exposure of a pure sample of **C22B** to low levels of O_2 followed by crystallisation by the vapour diffusion of diethyl ether in to a concentrated solution of **C22B** in acetonitrile yielded a very small number of dark blue block crystals amongst the yellow crystals. The blue crystals were of suitable quality for X-ray diffraction analysis. The blue crystals were found to belong to the monoclinic crystal system, with the structural solution being performed in the space group $P2_1/n$ (Figure 4.10).

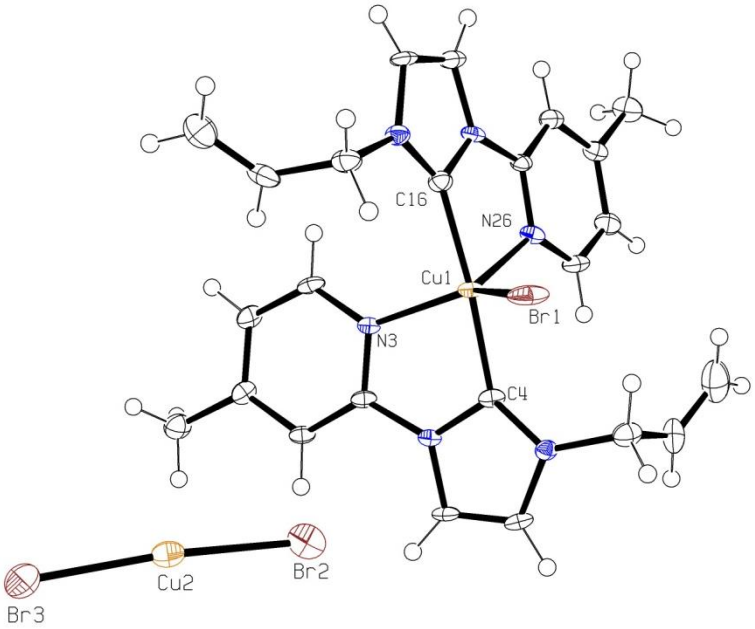

Figure 4.10 Molecular structure of **C22C**. Ellipsoids are drawn at the 50% probability level

Table 4.7 Selected bond distances (Å) and angles (deg) for **C22C**

Cu(1)-Br(1)	2.5057(9)	C(4)-Cu(1)-C(16)	175.2(2)
Cu(2)-Br(2)	2.174(1)	Br(1)-Cu(1)-N(3)	134.3(1)
Cu(2)-Br(3)	2.202(1)	Br(1)-Cu(1)-N(26)	119.6(1)
Cu(1)-C(4)	1.981(6)	N(3)-Cu(1)-N(26)	106.0(2)
Cu(1)-C(16)	1.982(6)	Br(2)-Cu(2)-Br(3)	174.14(5)
Cu(1)-N(3)	2.127(5)		
Cu(1)-N(26)	2.192(5)		

The structure of **C22C**, like **C19D**, was found to contain both a Cu^{II} and a Cu^{I} centre. Similarly to complexes **C19D**, the coordination sphere of the Cu^{II} centre contains two chelating NHC units and a bromide. The cationic Cu^{II} environment is charge-balanced by a non-coordinated linear (174°) $CuBr_2^-$ unit. The bond lengths and angles are very comparable to those observed in **C19D**, as might be expected on the basis of the similarity between the two chelating NHC ligands.

4.2.4 4-Methoxypyridyl-Substituted NHC

Ligand precursor **L23** was synthesised *via* a two-step protocol similarly to ligand precursors **L19**, **L21** and **L22**. However, the first step in the synthesis of **L23** was not an Ullmann coupling (as it was for **L19** and **L22**), since the requisite starting material (2-bromo-4-methoxypyridine)

is extremely expensive. Instead, a literature procedure utilising 4-methoxypyridine *N*-oxide and 1,1′-sulfonyldiimidazole (much cheaper starting materials) in a nucleophilic aromatic substitution reaction was attempted.[9] Reaction of these two reagents in toluene at 100°C for 2 hours led to the successful formation of the desired product (**P23**), which was obtained as a pale oil following work-up (Scheme 4.3).

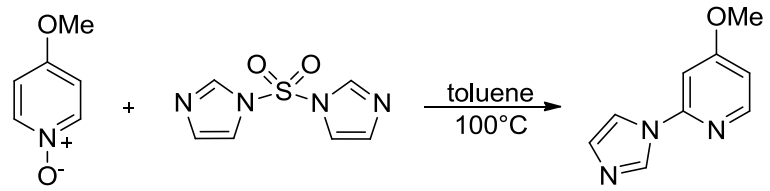

Scheme 4.3 Synthesis of **P23**

The product of the above reaction was then reacted with an excess of allyl bromide in acetonitrile to give ligand precursor **L23** as an off-white solid in excellent yield (91%). **L23** was subject to full characterisation by the standard methods. As with ligand precursors **L19**, **L21** and **L22**, reaction of **L23** with Ag_2O in dichloromethane quickly and cleanly led to the formation of an Ag^I-NHC complex (**C23A**), as evidenced by the characterisation data obtained (^1H and $^{13}C\{^1H\}$ NMR spectroscopy, high-resolution MS and elemental analysis).

As might be expected, the Ag complex of **L23** (**C23A**), was competent in the NHC transmetallation reaction with CuBr, forming the Cu^I-NHC complex in excellent yield after work-up. The Cu^I-NHC complex (**C23B**) was obtained as a yellow solid, which was fully characterised. Comparison of the ^1H NMR spectra of the Ag^I-NHC complex (**C23A**) and its Cu^I analogue (**C23B**) demonstrates quite a marked difference in behaviour between the two complexes in solution (Figure 4.11).

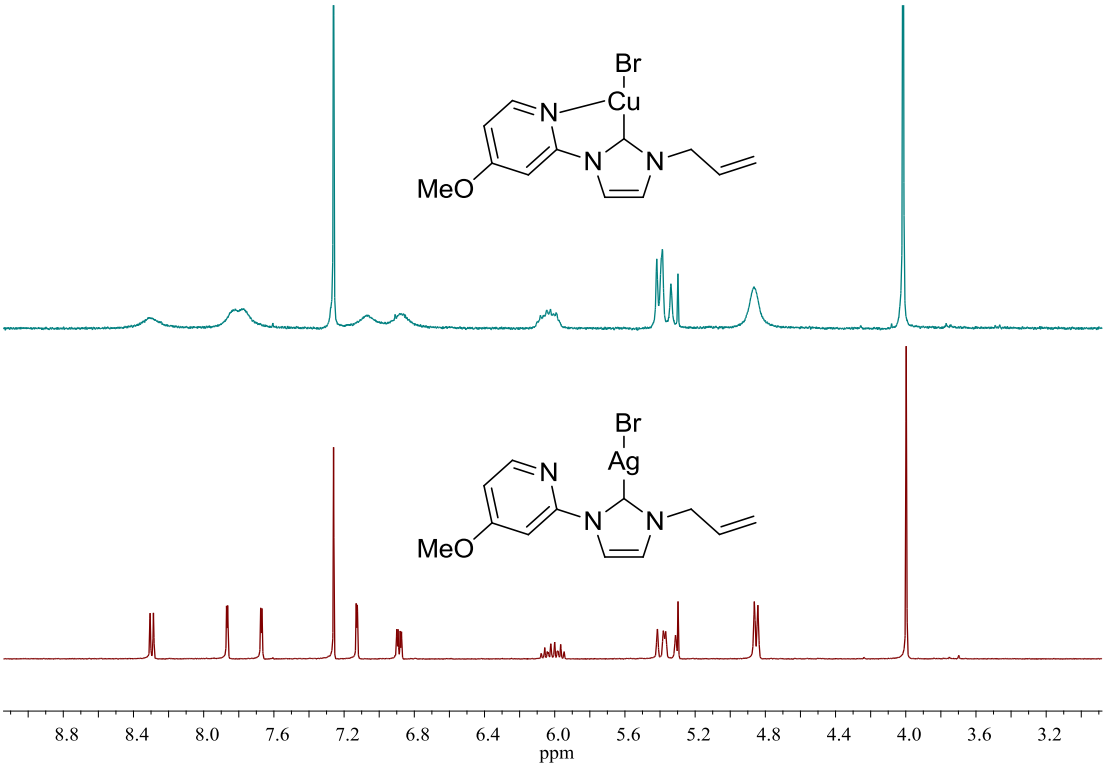

Figure 4.11 ^{1}H NMR spectra of the Ag^{I} complex, **C23A**, (bottom) and Cu^{I} complex, **C23B**, (top)

Crystallisation of **C23B** yielded two polymorphs, seemingly dependent on the crystallisation conditions used. Yellow needles were obtained on standing of a solution of **C23B** in dichloromethane/hexane (1:3), which were found to belong to the triclinic crystal system, with the structural solution being performed in the space group $P\bar{1}$ (Figure 4.12a - **C23B'**). Yellow polyhedral crystals on the other hand were obtained on standing of a solution of **C23B** in dichloromethane/diethyl ether (1:4). These crystals were found to belong to the monoclinic crystal system and the structural solution was performed in the space group $P2_1/n$ (Figure 4.12b - **C23B''**).

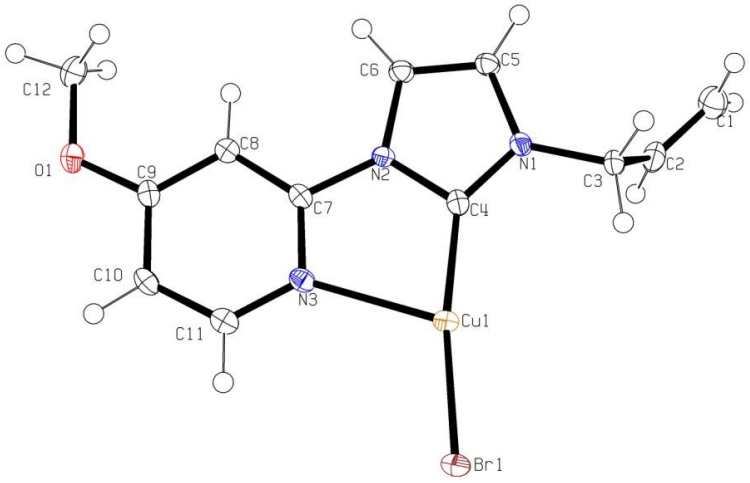

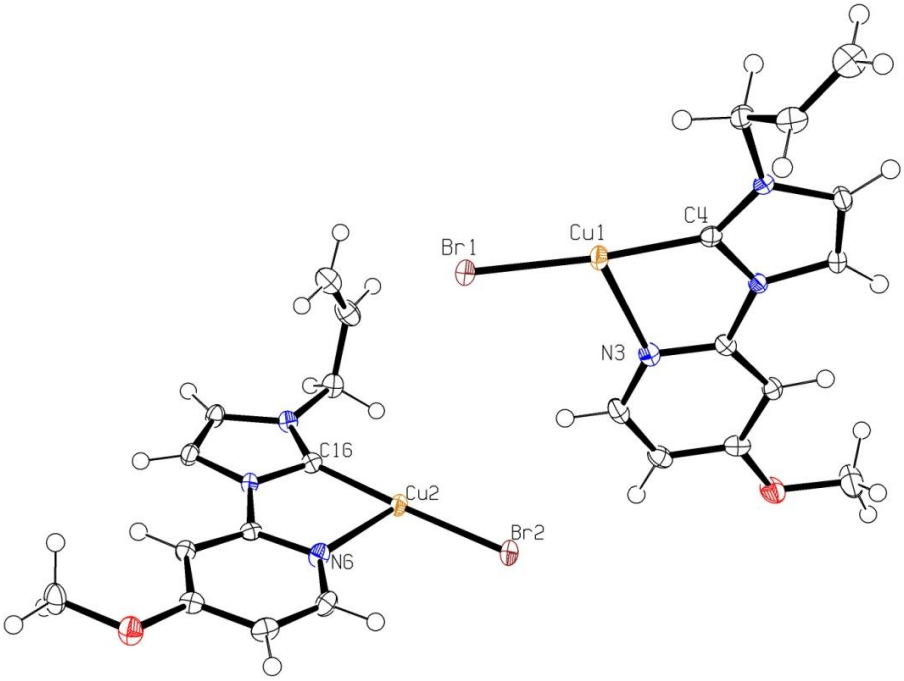

Figure 4.12a (top) and **Figure 4.12b** (bottom) Molecular structure(s) of **C23B**. Ellipsoids are drawn at the 50% probability level

Table 4.8 Selected bond distances (Å) and angles (deg) for **C23B**

	C23B'	**C23B''**	**C23B''**
Cu(1)-Br(1)/Cu(2)-Br(2)	2.2716(3)	2.2738(4)	2.2642(4)
C(4)-Cu(1)/C(16)-Cu(2)	1.905(2)	1.904(2)	1.899(3)
N(3)-Cu(1)/N(6)-Cu(2)	2.307(2)	2.335(2)	2.257(2)
C(4)-Cu(1)-Br(1) / C(16)-Cu(2)-Br(2)	169.28(7)	168.45(7)	173.72(8)

It is clear from the data in Table 4.8 that the three crystallographically independent Cu^{I}-NHC molecules in the two polymorphs have very comparable bond metrics, as would be expected. All three molecules crystallise with a distorted T-shape geometry about the Cu^{I} centre. The C-Cu and Cu-Br bond lengths observed for **C23B** are again very comparable to **C21B**, **C19C** and **C22B**. The Cu-N bond length (average = 2.30 Å) of **C23B** is much shorter than that of **C21B** (2.56 Å) and slightly shorter than that of **C22B** (2.34 Å), which presumably indicates that addition of the methoxy group to the pyridyl ring has slightly increased the σ-donor strength of the pyridyl nitrogen atom. This is logical on consideration of one of the possible resonance forms of 4-methoxypyridine, where the pyridyl nitrogen atom contains a formal negative charge (Figure 4.13).

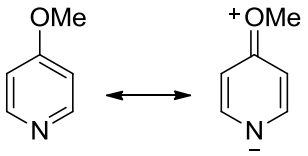

Figure 4.13 Two possible resonance forms of 4-methoxypyridine

4.2.5 Picolyl-Substituted NHC

The synthesis of ligand precursor **L24** proved to be extremely straightforward. The HBr salt of 2-bromomethylpyridine was added to a vigorously stirring solution of 1-allylimidazole and K_2CO_3 in acetonitrile. After stirring this suspension for 24 hours and removing the K_2CO_3 by filtration, the product was obtained as a pale yellow oil in quantitative yield. **L24** was subject to full characterisation, including by ^{1}H NMR spectroscopy, which illustrated the presence of an imidazolium salt, with a low field resonance at 10.60 ppm (300 MHz, $CDCl_3$).

Reaction of ligand precursor **L24** with Ag_2O in dichloromethane led to the formation of the corresponding Ag^I complex (**C24A**), which was isolated as a sticky white solid. The Ag^I complex (**C24A**) was used to form a Cu^I complex without further purification. Reaction of the Ag^I complex with an excess of CuBr in dichloromethane led to the formation of the Cu^I complex, **C24B**, which was isolated as a pale yellow solid following work-up. The complex was fully characterised by the usual means. Crystals of **C24B** could be obtained by the vapour diffusion of diethyl ether in to a concentrated solution of the product in dichloromethane. The crystals however, were of generally poor quality (intergrown/twinned). A very small single fragment was eventually isolated but owing to its size, the data collection was performed using the more intense Cu Kα radiation (λ = 1.5418 Å). The vast majority of X-ray diffraction data collected for the rest of this work was collected using Mo Kα radiation (λ = 0.7107 Å). The complex **C24B** was found to crystallise in the monoclinic crystal system and the structural solution was performed in the space group $P2_1/n$ (Figure 4.14).

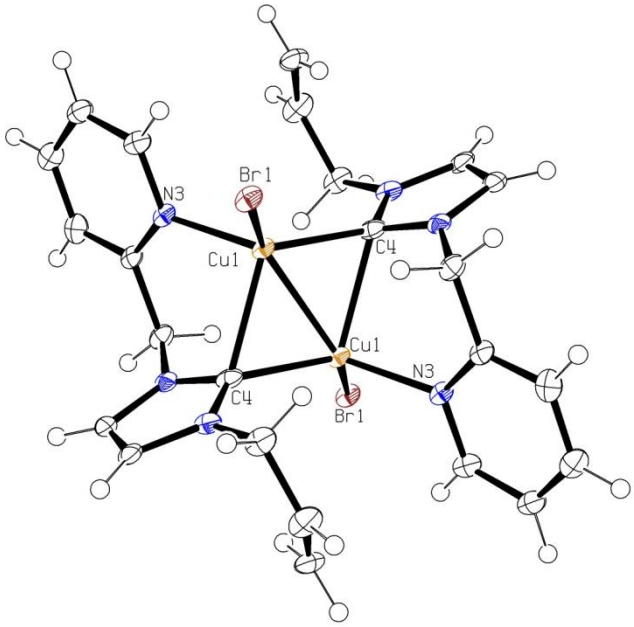

Figure 4.14 Molecular structure of **C24B**. Ellipsoids are drawn at the 50% probability level

Table 4.9 Selected bond distances (Å) and angles (deg) for **C24B**

Cu(1)-Br(1)	2.4623(8)	Br(1)-Cu(1)-C(4)	109.5(1)
Cu(1)---Cu(1')	2.4010(8)	Br(1)-Cu(1)-C(4')	109.7(1)
Cu(1)-C(4)	2.011(4)	Br(1)-Cu(1)-N(3)	106.0(1)
Cu(1)-C(4')	2.284(5)	N(3)-Cu(1)-C(4)	125.4(2)
Cu(1)-N(3)	2.053(3)	N(3)-Cu(1)-C(4')	92.3(2)
		C(4)-Cu(1)-C(4')	112.4(2)

Surprisingly, complex **C24B** crystallised as an unusual bridging NHC-containing dimer, where the bridging NHCs are presumably supported by the presence of the ancillary pyridyl donor group. Bridging NHCs are rather rare in Cu^{I} chemistry, with only a few examples having been reported to date.[10] As a result of the bridging nature of the NHC ligands, the Cu-C bond lengths (2.01 and 2.28 Å) are much longer than those of terminally bound NHCs, which are typically between 1.87 and 1.96 Å, with the carbenic centre of each NHC being quite notably closer to one Cu^{I} centre than the other.[10c] Also, as a result of the bridging NHCs, the two Cu^{I} centres have been brought in to rather close proximity (Cu-Cu distance = 2.40 Å). This particularly short Cu-Cu bond length indicates the presence of a cuprophilic interaction. It is not known whether the solid state structure accurately represents the speciation in solution. However, since one of the methylene resonances (py-CH_2-NHC) has not been split in to diastereotopic protons

(as would be expected if **C24B** was conformationally rigid on the NMR timescale), then it is likely that the complex is labile on the NMR timescale.

Bridging NHCs were the subject of recent DFT work by Hor *et al*..[10b] It was observed that the energetic difference between the addition of a bridging or terminal NHC to a $[Cu_2(\mu\text{-}I)_2(NHC)_2]$-type system was within experimental error, suggesting that bridging NHCs can form very stable complexes. It was also found, that bridging NHCs are more similar to CO than phosphines in their interactions with metal centres. This is because the bridging NHC is a better π-acceptor and can thus benefit from the increased π-backbonding from the two Cu^I centres that it bridges.

During the course of studies on complex **C19C**, a number of canary-yellow crystals were obtained on slow evaporation of a solution of **C19C** in the presence of excess CuBr. The crystals were initially assumed to be the 1D polymer described in the previous chapter. However, X-ray diffraction analysis of these crystals (complex **C19F**) revealed that they belonged to a different crystal system (triclinic), hence a data collection was performed. The structural solution was performed in the space group $P\bar{1}$ (Figure 4.15). Similarly to complex **C24B**, the NHC ligands were found to be bridging, rather than terminal.

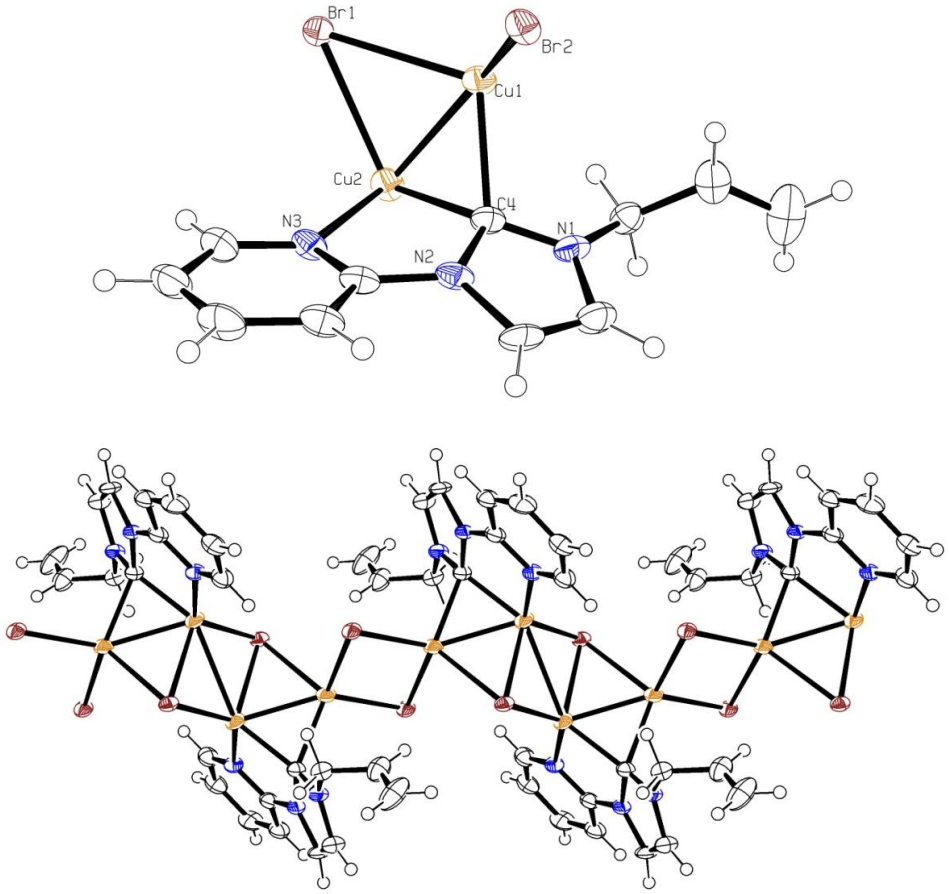

Figure 4.15 Molecular structure of **C19F**. Ellipsoids are drawn at the 50% probability level. The asymmetric unit is shown (top) along with a section of the 1D chain formed (bottom)

Table 4.10 Selected bond distances (Å) for **C19F**

Cu(1)-Br(2)	2.442(1)	Cu(1)---Cu(2)	2.441(1)
Cu(1)- Br(2')	2.4980(7)	Cu(2)---Cu(2)	2.827(1)
Cu(1)-Br(1)	2.681(1)	Cu(1)-C(4)	2.098(6)
Cu(2)-Br(1)	2.379(1)	Cu(2)-C(4)	2.044(6)
Cu(2)-Br(1')	2.619(1)	Cu(2)-N(3)	2.110(4)

As mentioned above, complex **C19F** is a 1D polymer containing unusual bridging NHCs. The occurrence of bridging NHCs is again probably facilitated by the presence of an ancillary pyridyl donor. The Cu-C bond lengths are more similar (2.10 and 2.04 Å) than those observed in **C24B** (2.01 and 2.28 Å), illustrating the more symmetrical nature of the bridge in complex **C19F**. Again, the bridging nature of the NHC ligand has acted to bring the two crystallographically independent Cu^{I} centres in to close proximity (2.44 Å), allowing the formation of a cuprophilic interaction.

The crystallographic observation of bridging NHC ligands in both **C24B** and **C19F** indicates that this type of bonding is perhaps more prevalent in Cu^{I} chemistry than previously thought. Such species may represent key intermediates in Cu^{I}-NHC catalysed processes, especially amongst those where the ligand contains ancillary nitrogen-based donors.

4.2.6 1-Pyridyl-3-Mesityl-Substituted NHC

Unlike ligand precursors **L19** and **L21** - **L24**, **L25** does not contain a pendant allyl group tethered to the imidazolium ring. Instead, **L25** contains a very bulky mesityl group, which is known to afford considerable steric protection to the carbenic centre. However, like ligand precursors **L19** and **L21** - **L24**, **L25** does contain a pyridyl group, which may help to stabilise higher oxidation state organo-copper species during a catalytic cycle. Ligand precursor **L25** was synthesised using a previously reported procedure starting from *N*-mesitylimidazole (**P17**) and 2-bromopyridine.[11] The reaction was performed as a 'dry melt', whereby the two reactants were heated with stirring in the absence of solvent in a closed flask at 160°C for 10 hours. After this time, the previously molten mixture had solidified. Repeated recrystallisation of the solid from chloroform/diethyl ether gave the pure imidazolium salt product, **L25**, as an off-white solid in excellent yield. During the reaction, it was imperative that the flask used was fully submerged in the heating medium (silicone oil) to reduce evaporation/sublimation and loss of the reactants from the reaction mixture. The reaction to produce **L25** proceeds *via* a nucleophilic aromatic substitution reaction, and is illustrated below (Scheme 4.4).

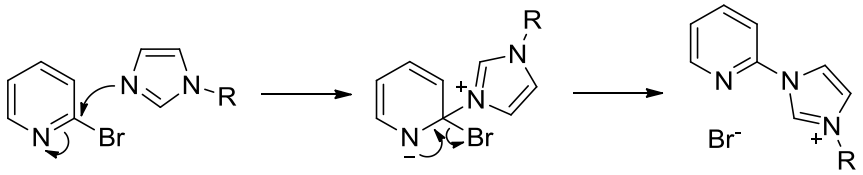

Scheme 4.4 Mechanism of ligand precursor **L25** synthesis

Single crystal X-ray diffraction analysis of **L25** unambiguously confirmed the connectivity of the compound (Figure 4.16).

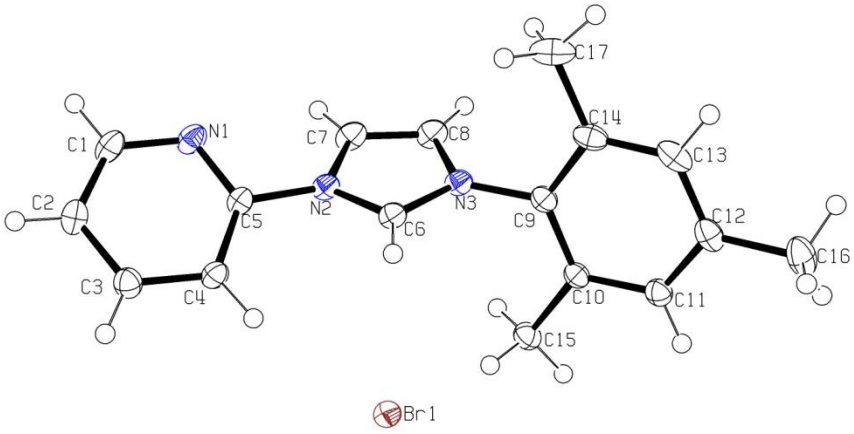

Figure 4.16 Molecular structure of **L25**. Ellipsoids are drawn at the 50% probability level

In contrast to the other structurally characterised pyridyl-containing imidazolium halides described elsewhere in this work, the structure of **L25** contains no evidence of anion-π interactions between the bromide anion and electron-deficient imidazolium N-C-N π-cloud. Such interactions are likely precluded by the presence of the bulky mesityl group adjacent to the imidazolium ring. However, a hydrogen bond between the imidazolium proton and bromide exists; such interactions being ubiquitous features of structurally characterised imidazolium halides.

Reaction of ligand precursor **L25** with Ag_2O to form an Ag^I complex (**C25A**) required slightly more forcing conditions (heating at reflux) than those used to form the analogous complexes of ligand precursors **L19** and **L21** - **L24**. The Ag^I complex of **L25** (**C25A**) was used to form the Cu^I complex using the same procedure as described previously in this chapter. The Cu^I complex, **C25B**, was obtained as a yellow crystalline solid following work-up. Elemental analysis and ^1H NMR spectroscopy of a sample of **C25B** suggested that the desired complex had formed and was pure. Interestingly, crystallisation of a sample of **C25B** yielded crystals with apparently different morphologies, dependent on the crystallisation solvent system used. Vapour diffusion of pentane in to a concentrated solution of **C25B** in chloroform yielded yellow block crystals (**C25B'**), which were found to belong to the monoclinic crystal system. The structural solution of the crystals of **C25B'** was performed in the space group $P2_1/c$ (Figure 4.17). Vapour diffusion of diethyl ether in to a sample of **C25B** in acetonitrile also yielded

block crystals belonging to the monoclinic crystal system (**C25B''**). These crystals however, were found to have a C-centred lattice, with the structural solution being performed in the space group *C2/c* (Figure 4.18).

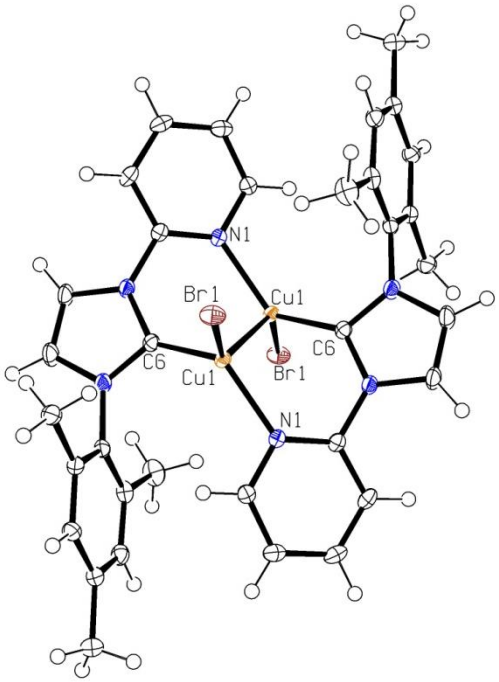

Figure 4.17 Molecular structure of **C25B'**. Ellipsoids are drawn at the 50% probability level

Table 4.11 Selected bond distances (Å) and angles (deg) for **C25B'**

Cu(1)-Br(1)	2.4142(3)	Br(1)-Cu(1)-C(6)	113.48(5)
Cu(1)---Cu(1')	2.5247(3)	Br(1)-Cu(1)-N(1)	109.83(4)
Cu(1)-C(6)	1.933(2)	C(6)-Cu(1)-N(1)	127.47(7)
Cu(1)---C(6')	2.834		
Cu(1)-N(1)	2.037(2)		

Complex **C25B'** was found to crystallise as a dimer in a manner akin to **C24B**. In this case however, the NHC ligands are terminal rather than bridging, as is evident in the Cu1-C6' distance (2.83 Å). As a result of the dimeric structure of **C25B'**, the pyridyl and NHC rings are not co-planar (as they are in the other structures), with a torsion angle of approximately 35°. A similar dimeric structure has been observed previously with an oxazolinyl-NHC complex.[12] The Cu-C and Cu-Br bond lengths are fairly typical of this type of complex. The dimeric nature of this complex has again brought the Cu^{I} centres in to fairly close proximity (2.52 Å), possibly leading to a cuprophilic interaction.

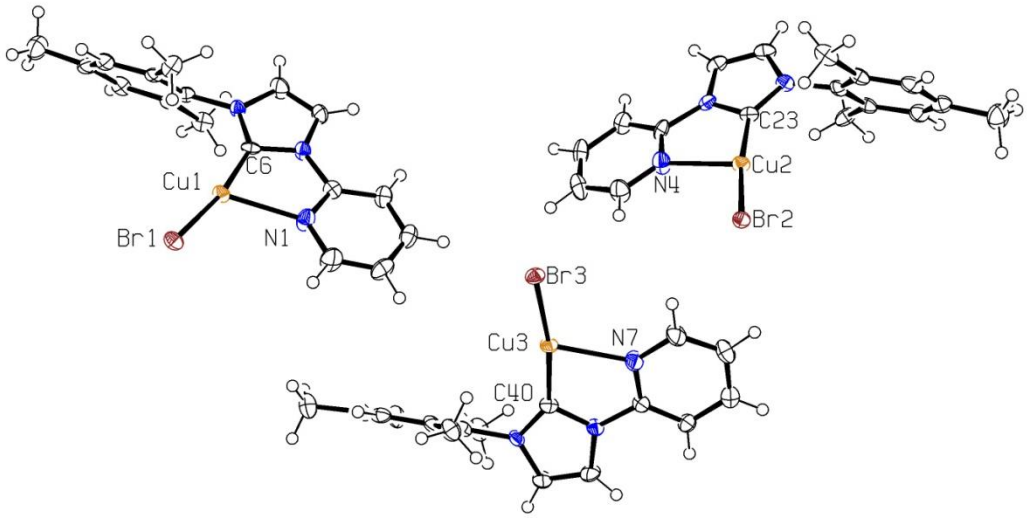

Figure 4.18 Molecular structure of **C25B''**. Ellipsoids are drawn at the 50% probability level

Table 4.12 Selected bond distances (Å) and angles (deg) for **C25B''**

Cu-Br	2.277(1), 2.285(1), 2.777(1)	Br-Cu-C	170.4(2), 171.4(2), 169.8(2)
Cu-C	1.911(7), 1.923(8), 1.909(8)	Br-Cu-N	109.8(2), 109.2(2), 109.7(2)
Cu-N	2.294(7), 2.305(7), 2.289(7)	C-Cu-N	79.2(3), 78.8(3), 79.5(3)

Similarly to complexes **C21B**, **C22B** and **C23B**, the crystals of **C25B''** were found to contain Cu^{I} in a distorted T-shaped coordination environment. This rare geometry arises as a result of the constraints imposed on the Cu^{I} centre by the rigid pyridyl-substituted NHC ligand. The asymmetric unit of **C25B''** comprises three independent Cu^{I}-NHC molecules, all of which possess similar (and fairly typical) bond metrics, as shown above (Table 4.12).

The crystallographic elucidation of two different polymorphs of complex **C25B**, formed under only slightly different conditions, adds credence to the idea that these complexes are quite labile in solution and can interconvert between different forms rapidly. This interconversion behaviour and the existence of unusual geometries around the Cu^{I} centre, is presumably facilitated by the d^{10} electron configuration of Cu^{I}, and thus lack of geometric preference.

4.3 The Ullmann reaction

Heteroatom alkylation and arylation reactions make up the largest class of chemical transformations used by pharmaceutical companies for the synthesis of drug candidate molecules.[13] As such, the development of these reactions to encompass a wider range of more highly functionalised and 'difficult' substrates is extremely desirable. Currently, palladium-based catalysts are often used for such transformations, though the decidedly lower cost of

copper would make this metal an appealing prospect for pharmaceutical companies, if its catalytic activity could be significantly improved.

The use of copper in catalysis was first reported in the Ullmann reaction by Fritz Ullmann in 1901, where a variety of aryl halides were coupled together using stoichiometric amounts of copper powder.[14] Since then, the term 'Ullmann reaction' has been used to encompass a wide variety of Cu-catalysed coupling reactions for the formation not just of C-C bonds, but for heteroatom alkylation and arylation reactions as well.

Given the undoubted importance then, of Ullmann coupling chemistry, and with a library of well-defined Cu^{I}-NHC complexes in hand, it was decided to evaluate the catalytic efficacy of these complexes in an Ullmann coupling reaction. This would be of particular interest, since the use of Cu^{I}-NHC complexes in Ullmann-type coupling chemistry has thus far been limited to only a handful of examples.[15] Of these limited examples, two involved the use of the ubiquitous SIMes and SI*i*Pr complexes of Cu^{I} as aryl-trifluoromethylating agents, while the other three reports examined the use of tripodal NHC complexes (without ancillary donors) in C-C, C-N and/or C-O bond forming reactions.

4.3.1 Ullmann-Type Etherification - Initial Screening

Historically, Ullmann coupling reactions have often required large, even stoichiometric amounts of copper and rather harsh reaction conditions. Furthermore, the reaction often only works efficiently if electron-poor aryl halides (activated with respect to Ullmann couplings) are used, which limits the applicability of this type of transformation. To this end, it was our intention to develop a catalytic system which uses sub-stoichiometric amounts of copper catalyst, is active under relatively mild conditions (<100°C) and is able to couple electron-rich aryl halides.

The reaction chosen for initial catalytic screening, was the arylation of the cheap and commercially available reagent 3,5-dimethylphenol with the Ullmann-deactivated reagent 4-iodoanisole. This reaction was to be performed at reflux in acetonitrile with caesium carbonate used as the base (Scheme 4.5).

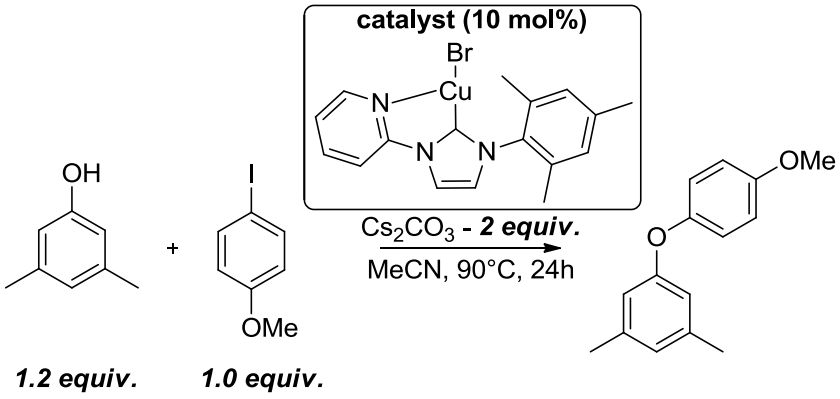

Scheme 4.5 Ullmann-type etherification reaction used for catalyst screening

The catalyst chosen for the initial screening was one of the preformed and well characterised complexes described earlier, namely, complex **C25B**. The catalytic screening was performed by adding the four solid reagents (3,5-dimethylphenol, 4-iodoanisole, caesium carbonate and complex **C25B**) to a small ampoule and degassing/drying these *in vacuo*. To these was added anhydrous acetonitrile, with the resulting suspension being heated at reflux (90°C) for 24 hours. After 24 hours, the reaction was allowed to cool to room temperature and the crude mixture filtered through celite. Removal of the solvent *in vacuo* yielded a crude solid, which was analysed by ^{1}H NMR spectroscopy (Figure 4.19).

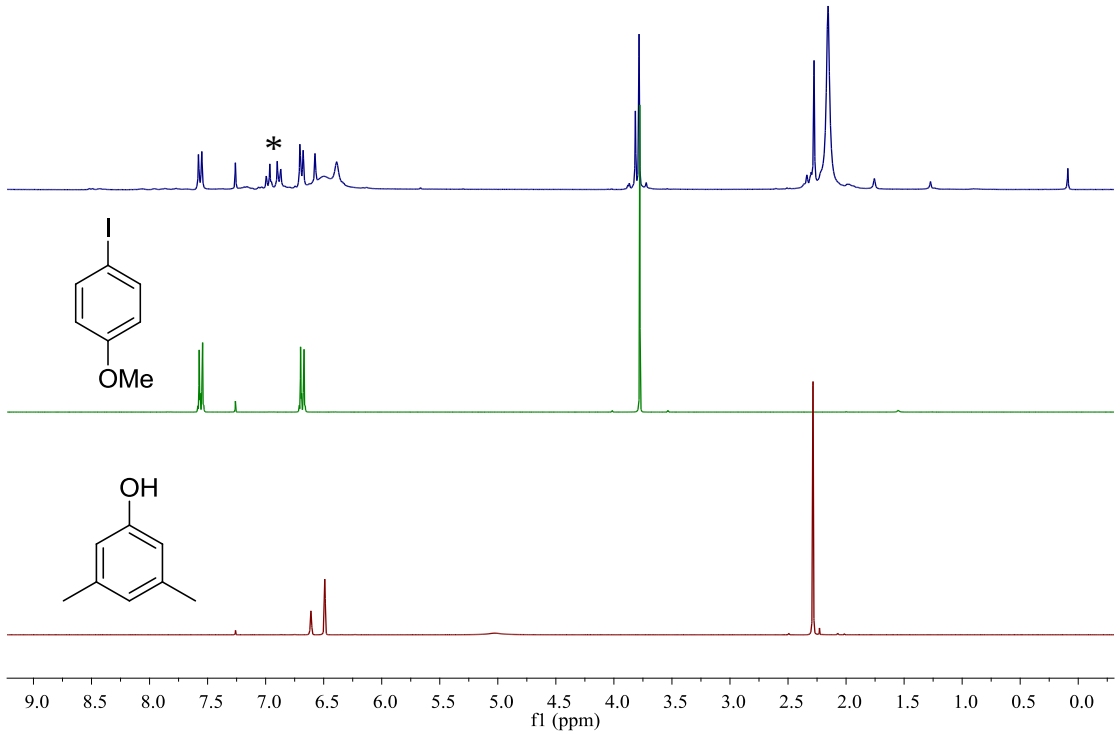

Figure 4.19 ^{1}H NMR spectra of the 3,5-dimethylphenol (bottom), 4-iodoanisole (centre) and crude reaction mixture (top)

Examination of the overlain NMR spectra in Figure 4.19 illustrates that as well as there being starting material remaining in the reaction mixture, there also appears to be a significant quantity of coupled-product (aromatic resonances of the product indicated by *). In fact, a conversion of 44% is suggested by comparison of the integrations of the product and starting material. This was encouraging, since it suggests that these complexes display significant activity in what is normally a very challenging coupling.

4.3.2 Ullmann-Type Etherification - Parallel Screening

With the promising result described above in mind, it was decided to first assess the catalytic activity of a range compounds, which would serve as standards/bases for comparison. These include just the ligand precursors on their own (no Cu source), to check that the mechanism by

which any coupling occurs is not organocatalytic in nature. Cuprous iodide would also be tested in the absence of any ligand precursor, to determine whether the NHC ligands have a beneficial effect on catalysis. Finally, the catalytic competency of the common Cu^{I} complexes [Cu(IMes)Cl] and $[Cu(IMes)_2]PF_6$ (synthesised using the electrochemical technique) would be measured, to establish whether the addition of a pyridyl ancillary donor to an NHC would improve catalytic performance. The results of these initial experiments are provided below in Table 4.13. It should be noted that unlike the initial screening experiment, the catalytic experiments described for the remainder of this chapter were performed in a carousel reactor.

Entry	Catalyst (10 mol%)	Yield (%)[a]
1	None	0
2	**L21**	0
3	**L25**	0
4	CuI	20
5	[Cu(IMes)Cl]	15
6	$[Cu(IMes)_2]PF_6$	6

Table 4.13 Reaction conditions: 1.2 mmol 3,5-dimethylphenol, 1.0 mmol 4-iodoanisole, 2.0 mmol Cs_2CO_3,'catalyst', 5 ml MeCN, 90°C, 24 hours. [a] Yields were determined by GC using *p*-cymene as an internal standard

On examination of the data contained in Table 4.13, it is abundantly clear that in the absence of both a copper source and a ligand precursor (entry 1), no detectable coupling occurs between the phenol and aryl halide. On addition of 10 mol% of either ligand precursor **L21** or **L25** (entries 2 and 3), the result was the same as that for entry 1, *i.e*. no coupling. This strongly suggests that the mechanism by which this coupling occurs is definitely not organocatalytic in nature, and that having a source of copper in the reaction is vital. Coupling did however occur in the ligandless reaction (this is slightly misleading, as acetonitrile is an excellent ligand for Cu^{I}), entry 4. The use of 10 mol% of CuI in the absence of any ligand precursor led to a relatively modest yield of the coupled product (20% (by GC)). Use of the IMes-containing pre-formed complexes [Cu(IMes)Cl] and $[Cu(IMes)_2]PF_6$ (entries 5 and 6) again led to coupling of the phenol and aryl halide (15% and 6% respectively), though the yields of both were lower than that achieved by just CuI alone. This suggests that rather than enhancing the catalytic activity of the copper centre, the coordination of these sterically demanding ligands to copper actually significantly impairs its catalytic performance. There are two possible reasons for this; firstly, that the steric bulk of the ligand acts to prevent the copper centre achieving higher coordination numbers, which would be necessary if the Ullmann coupling proceeds *via* an oxidative

addition/reductive elimination pathway. Secondly, that due to the absence of a harder ancillary donor on the IMes ligand, oxidation of the Cu^{I} centre to either Cu^{II} or Cu^{III} during catalysis would result in immediate decoordination of the ligand leaving a catalytically-poor naked copper centre (similar to the use of only CuI as the catalyst - entry 4 in Table 4.13). Intriguingly, comparison of the two IMes complexes ([Cu(IMes)Cl] and $[Cu(IMes)_2]PF_6$) shows that the mono-NHC complex is somewhat more catalytically active than the *bis*NHC complex. Again, this may be due to steric effects (one bulky ligand versus two bulky ligands around the copper centre) or decoordination effects (the copper centre is probably more easily leached in to solution from [Cu(IMes)Cl] than from $[Cu(IMes)_2]PF_6$). The yield of coupled product produced by [Cu(IMes)Cl] (15%) compares well with an example reported in the literature, where 4-methylphenol was coupled with 4-iodoanisole using 10 mol% of the catalyst [Cu(IPr)Cl] and similar conditions to those used for this catalyst screening experiment (yield = 9%).[15c]

Before the preformed complexes were investigated in the Ullmann coupling of 3,5-dimethylphenol with 4-iodoanisole, *in situ* generated catalysts were first examined, using 10 mol% of the ligand precursor (**L19** and **L21** - **L25**) and 10 mol% of CuI. By doing this, it would be possible to compare the activities of the *in situ* formed catalysts with the activities of the preformed and well characterised complexes, which would potentially provide some clues as to the nature of the catalytically active species in these reactions. Also, two other copper sources were tested: $CuBr_2$, a Cu^{II} source, and $[Cu(MeCN)_4]PF_6$, a non-halide-containing Cu^{I} source.

Entry	Catalyst (10 mol%)	Yield (%)[a]
4	CuI	20
7	**L21** + CuI	14
8	**L19** + CuI	32
9	**L22** + CuI	27
10	**L23** + CuI	34
11	**L24** + CuI	42
12	**L25** + CuI	17
13	**L21** + $CuBr_2$	12
14	**L21** + $[Cu(MeCN)_4]PF_6$	13

Table 4.14 Reaction conditions: 1.2 mmol 3,5-dimethylphenol, 1.0 mmol 4-iodoanisole, 2.0 mmol Cs_2CO_3,'catalyst', 5 ml MeCN, 90°C, 24 hours. [a] Yields were determined by GC using *p*-cymene as an internal standard

Table 4.14 gives the yields of coupled product obtained from the *in situ* generated catalysts (entries 7 - 14), and the yield obtained from CuI as the catalyst (entry 4) for comparison. It can be seen that the *in situ* generated complexes derived from ligand precursors **L19** and **L22 - L24** display superior catalytic activity than that of just CuI alone. Conversely, the catalysts derived from **L21** and **L25** were not as effective as CuI in the coupling reaction. Ligand precursor **L21** (nitropyridyl-substituted imidazolium) displayed the lowest activity of all those tested, with yields of 14% (with CuI), 12% ($CuBr_2$) and 13% ($[Cu(MeCN)_4]PF_6$) achieved. This is potentially a consequence of the weak coordination of the pyridyl-nitrogen to the copper centre (Cu-N distance is 2.56 Å in complex **C21B**), which results in little stabilisation of higher oxidation state copper species during the catalytic cycle by the pyridyl donor. As a result, a coupled product yield of 14% is observed, which compares very well with that achieved by another linear, 2-coordinate heteroleptic Cu^I complex, [Cu(IMes)Cl] (15%). Comparison of the yields given in entries 7, 13 and 14 (**L21** + either CuI, $CuBr_2$ or $[Cu(MeCN)_4]PF_6$) suggests that, surprisingly, the nature of the copper source seems to make little to no difference to the yield of coupled product obtained at the end of the reaction. As a result, we would postulate that a catalytically competent species (most likely a Cu^I complex) can be generated quickly during the reaction, regardless of the starting oxidation state of the copper centre.

The *in situ* generated catalyst derived from the sterically demanding ligand precursor **L25**, performed only slightly better than that of either **L21** or [Cu(IMes)Cl], achieving a yield of 17 %. Although a potentially stabilising pyridyl substituent is present, which would help to stabilise higher oxidation state copper species during the catalytic cycle, the steric bulk of the ligand provided by the mesityl group seems to be preventing efficient catalysis. This is exemplified by comparison of entries 8 and 12 in Table 4.14. Both ligand precursors (**L19** and **L25**) contain an unsubstituted pyridyl, whereas ligand precursor **L19** contains a pendant allyl in place of the mesityl group found on **L25**. Thus, electronically speaking at least, there should be little difference between the two ligands. The biggest difference between the two ligands should be their steric bulk, with the small allyl group of **L19** versus the bulky mesityl of **L25**. We can see that by comparison of the data in Table 4.14, the *in situ* generated catalyst derived from **L19** is almost two times more catalytically active (32% yield) than the catalyst derived from **L25** (17%). Thus, it is likely that reductions in steric bulk around the copper centre help to increase the activity of the resultant complex with respect to Ullmann coupling chemistry. However, a stabilising contribution to the catalyst from the allyl substituent cannot be ruled out.

As described earlier, the *in situ* generated complexes derived from ligand precursors **L19** and **L22 - L24** display superior catalytic activity than that of just CuI alone. This suggests that for this reaction, a good pyridyl donor and a lack of steric bulk around the copper centre seem to be vital for efficient catalysis. The most catalytically active *in situ* generated complex (42% yield) derives from ligand precursor **L24**, which contains one allyl *N*-substituent and one 2-picolyl *N*-

substituent. The added flexibility of the 2-picolyl substituent of **L24** versus the 2-pyridyl substituents of **L19**, **L22** and **L23** appears to play a significant role in facilitating catalysis. This is surprising on consideration of chelate ring stability, where 5-membered chelate rings (such as those found in **C19C**, **C22B** and **C23B**) are typically thought to be more stable than 6-membered chelate rings (**C24B**) on entropic grounds.[16]

So that some information about the nature of the active catalytic species can be discerned, the preformed complexes **C21B**, **C19C**, **C22B**, **C23B**, **C24B** and **C25B** were examined in the Ullmann coupling of 3,5-dimethylphenol and 4-iodoanisole (Table 4.15).

Entry	Catalyst (10 mol%)	Yield (%)[a]
4	CuI	20
15	**C21B**	12
16	**C19C**	33
17	**C22B**	27
18	**C23B**	33
19	**C24B**	38
20	**C25B**	21

Table 4.15 Reaction conditions: 1.2 mmol 3,5-dimethylphenol, 1.0 mmol 4-iodoanisole, 2.0 mmol Cs_2CO_3,'catalyst', 5 ml MeCN, 90°C, 24 hours. [a] Yields were determined by GC using *p*-cymene as an internal standard

Table 4.15 gives the yields of coupled product obtained from the preformed, well-characterised complexes **C21B**, **C19C**, **C22B**, **C23B**, **C24B** and **C25B**. It is clear again that complexes **C19C**, **C22B**, **C23B** and **C24B** give superior yields compared to just CuI alone, whereas **C21B** and **C25B** perform similarly/slightly worse than CuI. In fact, the yields obtained from the *in situ* generated catalysts compare extremely well with those obtained from the preformed catalysts (Figure 4.20).

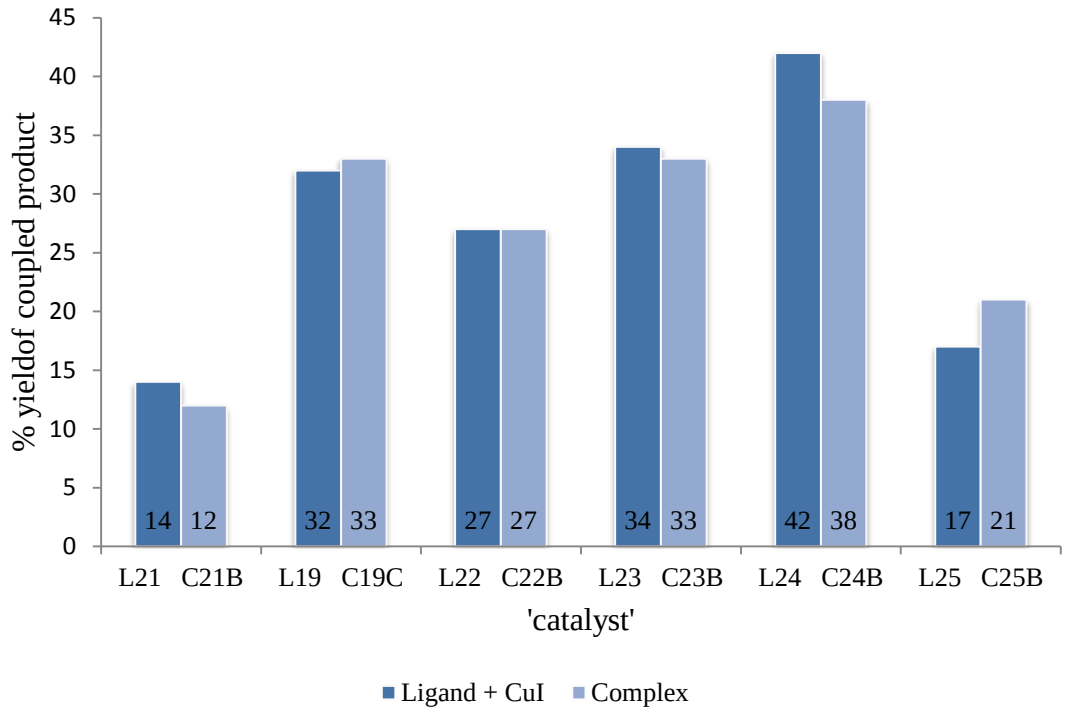

Figure 4.20 Comparison of Ullmann coupling yields obtained from *in situ* generated catalysts and preformed catalysts

Figure 4.20 illustrates that the yields of coupled product obtained from the *in situ* generated catalysts versus the preformed catalysts are very similar in all cases. This strongly suggests that the active catalyst (presumably a *mono*-NHC complex) for each ligand is identical, irrespective of whether the catalyst is preformed or not.

With the knowledge that the catalyst derived from ligand precursor **L24** gives rise to the highest yield of coupled product, the optimisation of reaction conditions using this precursor was attempted. The amounts and thus ratios of ligand precursor to CuI and base to CuI were altered to examine what effect, if any, this would have. The reaction conditions used, including temperature, reaction duration and type of base were all identical to those used in the previous parallel screening experiments. Table 4.16 summarises the yields of coupled product obtained at various ratios of ligand precursor to CuI and base to CuI.

Entry	**L24**:CuI Ratio	Cs_2CO_3:CuI Ratio	Yield (%)[a]
22	2:1	20:1	52
11	1:1	20:1	42
23	0.5:1	20:1	37
24	1:1	40:1	58
25	2:1	40:1	42

Table 4.16 Reaction conditions: 1.2 mmol 3,5-dimethylphenol, 1.0 mmol 4-iodoanisole, 2.0 or 4.0 mmol Cs_2CO_3, 0.1 mmol CuI, 0.2, 0.1 or 0.05 mmol **L24**, 5 ml MeCN, 90°C, 24 hours. [a] Yields were determined by GC using *p*-cymene as an internal standard

Entries 22, 11 and 23 provide a comparison of the yields obtained when the ratio of ligand precursor to CuI is varied. It is evident that at increased ligand precursor to CuI ratios, *e.g*. 2:1 (0.2 mmol **L24**: 0.1 mmol CuI), the yield of coupled product increases. For example, upon increasing the ligand precursor to CuI ratio from 0.5:1 to 1:1 to 2:1, the yield increases from 37% to 42% to 52%. The increased yield obtained by increasing the ligand precursor to CuI ratio is in contrast to previous reports in the literature, where a 1:1 ligand to copper ratio was found to be sufficient for efficient catalysis to occur.[17] This suggests that either, the *bis*-NHC complex of ligand precursor **L24** is more catalytically active in this coupling reaction than the *mono*-NHC complex. Alternatively, and probably more likely, the *mono*-NHC complex is more catalytically active, and thus having an excess of ligand in the reaction mixture allows rapid reformation of the active catalyst in the event of ligand demetallation.

Comparison of entries 11 and 24 illustrates the effect of increasing the ratio of base to copper (at a 1:1 ratio of ligand precursor to CuI). Doubling the amount of base relative to the amount of copper (entry 24) gives a coupled product yield of 58%, which was the highest yield observed during the course of these studies. Thus, it appears that increasing the amount of base helps to more effectively recycle the active catalyst during the reaction, hence the increased yield. The mechanism by which this occurs is not known, though it may involve the increased base being able to more effectively remove halide anions from the copper centre during the catalytic cycle, allowing regeneration of an active catalyst. Alternatively, the added base may help re-deprotonate the ligand precursor if it becomes protonated during the catalytic cycle, helping maintain the high concentration of active catalyst during the reaction. Intriguingly, at increased ligand precursor to CuI ratios (2:1 - entries 22 and 25), doubling the amount of base has the opposite effect, decreasing the yield of coupled product (52% versus 42%).

Using the optimised conditions (1.2 mmol 3,5-dimethylphenol, 1.0 mmol 4-iodoanisole, 4.0 mmol Cs_2CO_3, 0.1 mmol CuI, 0.1 mmol **L24**, 5 ml MeCN, 90°C, 24 hours), the reaction was

repeated under strictly inert conditions, *i.e.* thoroughly dried and degassed solvents, reagents and reaction vessel). The yield of coupled product obtained under these strictly inert conditions (57%) compares very favourably with the yield obtained under standard conditions (58%). This finding is encouraging if this complex was to be used in industrial processes, since its catalytic performance is just as efficient regardless of whether the reaction is performed under inert or non-inert conditions.

Finally, under the same conditions as those used in entry 11 (Tables 4.14 and 4.16), the rate of product formation over time was monitored in order to probe the kinetics of the reaction and possible catalyst deactivation towards the end of the experiment. The reaction was monitored over time by withdrawing aliquots from the reaction mixture at set intervals and analysing these by GC. Figure 4.21 demonstrates the results of this study.

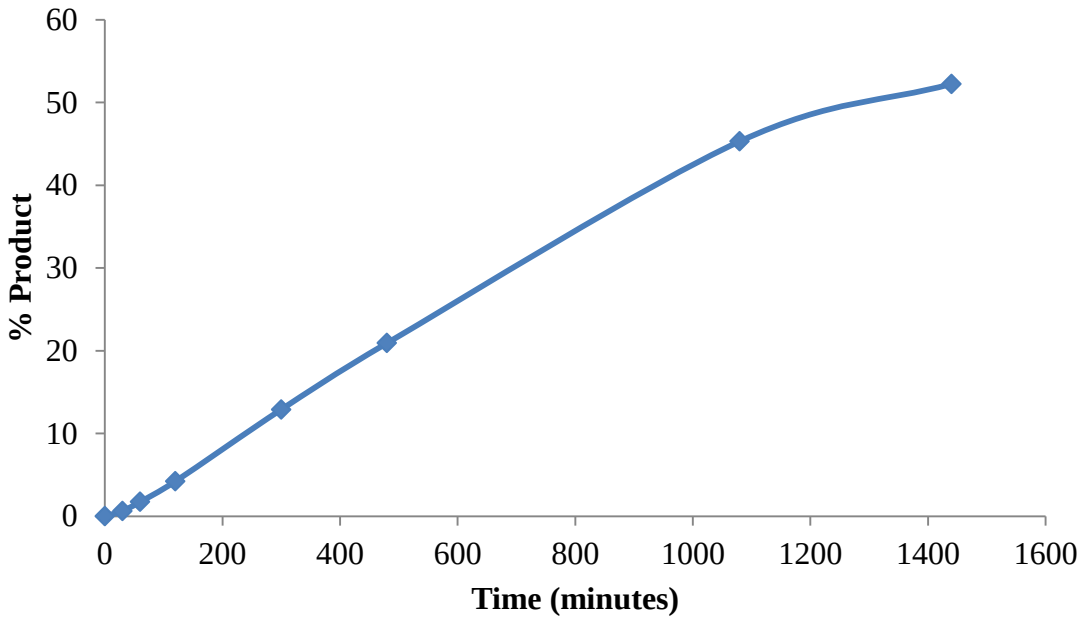

Figure 4.21 Evolution of product over time in the Ullmann coupling of 3,5-dimethylphenol and 4-iodoanisole

Figure 4.21 shows the production of Ullmann-coupled product over time. It is clear on examination of the chart that the reaction has a slight induction period (between 0 - 30 minutes), which is then followed by a period of steady production of product. Finally, after approximately 18 hours (1080 minutes), the production of the coupled product noticeably begins to slow down. This presumably indicates that the catalyst is being lost in a decomposition process. However, it is also clear from Figure 4.21 that product is still being produced, even after 24 hours, albeit at a much slower rate.

4.4 Conclusions

A range of pyridyl-tethered NHC ligand precursors and their respective copper complexes have been described during the course of this chapter. Most of these were rationally designed, synthesised and crystallised, though a small number owe their isolation and crystallographic characterisation to serendipity. Many of the pyridyl-tethered NHC ligands have demonstrated the rare ability of being able to stabilise both Cu^{I}, and Cu^{II} centres, a property which is likely to be of particular relevance during the design of cheaper, more efficient copper-based catalysts for industry. Furthermore, it has been established that the pyridyl ancillary donor can help stabilise unusual bridging NHC complexes (of Cu^{I}), perhaps suggesting that these ligands are more like carbon monoxide than phosphines in their interactions with metal centres.

The ligand precursors and complexes synthesised during this chapter were screened in a challenging Ullmann coupling reaction. It was hoped that the ability of these ligands to stabilise higher oxidation state organo-Cu species would be highly important during the catalytic cycle. Indeed, it was found that yields of coupled product were dramatically increased by the addition of ligand to the coupling reaction, versus copper iodide alone. A maximum yield of 58% was achieved under optimised reaction conditions with a 2-picolyl-substituted NHC precursor and copper iodide. This yield is unprecedentedly high for NHC-based copper catalysts in difficult Ullmann coupling reactions.

4.5 Future Work

There is plenty of scope for future workers to continue with and build on the results obtained for this chapter. For example, it would be advisable for future workers to begin modification of ligand precursor **L24** (the most catalytically active) by, for example, adding electron-donating and electron-withdrawing groups on to the pyridyl ring to examine the way in which the electronic properties of the pyridyl affect catalysis. The nature of the NHC ring itself should be varied, for instance, by replacing the 'normal' 5-membered NHC with a benzimidazolium-derived NHC or an 'abnormal' 5-membered NHC, to examine how the σ-donor strength of the NHC influences the catalytic activity at the copper centre. The steric properties of the ligand should be varied, to prove or disprove the theory that increased steric bulk around the copper centre leads to an inhibition of catalysis.

The reaction conditions of the Ullmann coupling itself could be modified by future workers to examine, for example, if caesium carbonate is the most effective base for this transformation. The solvent used could also be changed; the use of dimethyl sulfoxide instead of acetonitrile may allow the reaction to be performed at temperatures higher than 90°C, which may lead to a significant enhancement in overall yield.

4.6 References

[1] a) A. J. Hickman, M. S. Sanford, *Nature* **2012**, *484*, 177-185; b) A. Casitas, X. Ribas, *Chemical Science* **2013**, *4*, 2301-2318.

[2] S. E. Creutz, K. J. Lotito, G. C. Fu, J. C. Peters, *Science* **2012**, *338*, 647-651.

[3] H.-Z. Yu, Y.-Y. Jiang, Y. Fu, L. Liu, *Journal of the American Chemical Society* **2010**, *132*, 18078-18091.

[4] M. J. McPhillie, R. Trowbridge, K. R. Mariner, A. J. O'Neill, A. P. Johnson, I. Chopra, C. W. G. Fishwick, *ACS Medicinal Chemistry Letters* **2011**, *2*, 729-734.

[5] A. A. D. Tulloch, A. A. Danopoulos, S. Kleinhenz, M. E. Light, M. B. Hursthouse, G. Eastham, *Organometallics* **2001**, *20*, 2027-2031.

[6] a) P. L. Arnold, M. Rodden, K. M. Davis, A. C. Scarisbrick, A. J. Blake, C. Wilson, *Chemical Communications* **2004**, *0*, 1612-1613; b) A. O. Larsen, W. Leu, C. N. Oberhuber, J. E. Campbell, A. H. Hoveyda, *Journal of the American Chemical Society* **2004**, *126*, 11130-11131; c) C. Y. Legault, C. Kendall, A. B. Charette, *Chemical Communications* **2005**, *0*, 3826-3828; d) J. J. Van Veldhuizen, J. E. Campbell, R. E. Giudici, A. H. Hoveyda, *Journal of the American Chemical Society* **2005**, *127*, 6877-6882; e) J. Yun, D. Kim, H. Yun, *Chemical Communications* **2005**, *0*, 5181-5183; f) B. Liu, B. Liu, Y. Zhou, W. Chen, *Organometallics* **2010**, *29*, 1457-1464; g) E. L. Kolychev, V. V. Shuntikov, V. N. Khrustalev, A. A. Bush, M. S. Nechaev, *Dalton Transactions* **2011**, *40*, 3074-3076.

[7] H.-Y. Gong, B. M. Rambo, E. Karnas, V. M. Lynch, J. L. Sessler, *Nature Chemistry* **2010**, *2*, 406-409.

[8] J. C. Garrison, W. J. Youngs, *Chemical Reviews* **2005**, *105*, 3978-4008.

[9] J. M. Keith, *The Journal of Organic Chemistry* **2007**, *73*, 327-330.

[10] a) S. Gischig, A. Togni, *Organometallics* **2004**, *24*, 203-205; b) X. Han, L.-L. Koh, Z.-P. Liu, Z. Weng, T. S. A. Hor, *Organometallics* **2010**, *29*, 2403-2405; c) S. Diez-Gonzalez, E. C. Escudero-Adan, J. Benet-Buchholz, E. D. Stevens, A. M. Z. Slawin, S. P. Nolan, *Dalton Transactions* **2010**, *39*, 7595-7606; d) C. Chen, H. Qiu, W. Chen, *Journal of Organometallic Chemistry* **2012**, *696*, 4166-4172; e) V. J. Catalano, L. B. Munro, C. E. Strasser, A. F. Samin, *Inorganic Chemistry* **2011**, *50*, 8465-8476.

[11] S. Grundemann, M. Albrecht, A. Kovacevic, J. W. Faller, R. H. Crabtree, *Journal of the Chemical Society, Dalton Transactions* **2002**, 2163-2167.

[12] N. Schneider, V. César, S. Bellemin-Laponnaz, L. H. Gade, *Journal of Organometallic Chemistry* **2005**, *690*, 5556-5561.

[13] J. S. Carey, D. Laffan, C. Thomson, M. T. Williams, *Organic & Biomolecular Chemistry* **2006**, *4*, 2337-2347.

[14] F. Ullmann, J. Bielecki, *Berichte der deutschen chemischen Gesellschaft* **1901**, *34*, 2174-2185.

[15] a) C. Tubaro, A. Biffis, E. Scattolin, M. Basato, *Tetrahedron* **2008**, *64*, 4187-4195; b) C. E. Ellul, G. Reed, M. F. Mahon, S. I. Pascu, M. K. Whittlesey, *Organometallics* **2010**, *29*, 4097-4104; c) A. Biffis, C. Tubaro, E. Scattolin, M. Basato, G. Papini, C. Santini, E. Alvarez, S. Conejero, *Dalton Transactions* **2009**, 7223-7229; d) G. G. Dubinina, J. Ogikubo, D. A. Vicic, *Organometallics* **2008**, *27*, 6233-6235; e) G. G. Dubinina, H. Furutachi, D. A. Vicic, *Journal of the American Chemical Society* **2008**, *130*, 8600-8601.

[16] A. L. Gavrilova, B. Bosnich, *Chemical Reviews* **2004**, *104*, 349-384.

[17] A. Ouali, J.-F. Spindler, A. Jutand, M. Taillefer, *Advanced Synthesis & Catalysis* **2007**, *349*, 1906-1916.

Chapter 5

Rational Synthesis and Decomposition of Higher Oxidation State Cu-NHC Complexes: Consequences for Catalysis

5.1 Introduction

The chemistry of organo-Cu^{I} complexes is reasonably well explored and understood in the literature, with numerous examples of coordination to Cu^{I} by alkyl,[1] aryl,[2] alkenyl,[3] alkynyl,[4] carbonyl,[5] cyano[6] and carbenic[7] functional groups having been reported. Indeed, the isolation and characterisation of Cu^{I}-NHC complexes has formed a significant proportion of the work described so far in this thesis.

The prevalence of C-Cu^{I} bonds is not a surprise, especially when considering the complementary nature of the 'soft-soft' interaction between the Cu^{I} cation and carbon donor. This favourable interaction has been utilised innumerable times, both in nature (for example, ethylene binding in plants),[8] as well as in synthetic chemistry (for instance, Ullmann-type coupling reactions,[9] conjugate addition reactions[10] and CO binding and sequestration).[11]

Well characterised higher oxidation state (Cu^{II} and Cu^{III}) organo-copper chemistry is somewhat more scarce however, with an obvious mismatch between the intermediate/hard Cu^{II} or Cu^{III} cations and soft carbon donors. A few examples of characterised Cu^{II}-NHC complexes have been reported to date, with the first appearing in 2003 (though this example was not characterised by X-ray diffraction analysis). In this instance, the Cu^{II} centre is probably tetracoordinated by a chelating nitrogen-anchored *tris*-NHC ligand (Figure 5.1).[12]

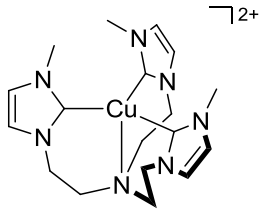

Figure 5.1 Proposed structure of the first characterised Cu^{II}-NHC complex[12]

Since then, other examples have appeared where typically, the NHC ligand possesses an anionic ancillary donor such as an alkoxide, phenoxide or amide.[13] Alternatively, acetate ligands have been shown to stabilise Cu^{II}-NHC complexes sufficiently to allow characterisation, though such complexes tend to undergo ring-opening upon exposure to moisture (Figure 5.2).[14]

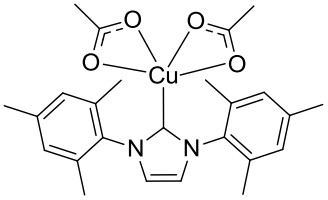

Figure 5.2 Acetate-stabilised Cu^{II}-NHC complex[14b]

The pyridyl-tethered ligand set (Figure 5.3) described in the previous chapter has demonstrated the ability to stabilise Cu^{II} centres, as evidenced by the adventitious crystallisation of a number of Cu^{II}-NHC complexes. With this in mind, the rational synthesis of Cu^{II}-NHC complexes containing pyridyl- and picolyl-tethered ligands was attempted in order to better understand their structure, stability and reactivity. During these studies, it became apparent that under certain circumstances, decomposition of the NHC ligands occurs. This potentially has enormous implications for the use of Cu-NHC complexes in catalysis, specifically; those catalytic processes which invoke higher oxidation state copper species.

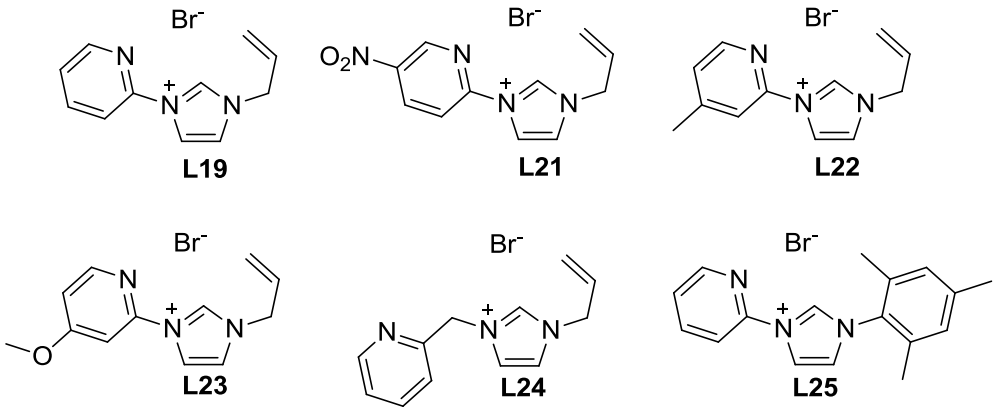

Figure 5.3 Pyridyl-tethered ligand set

5.2 Synthesis of Cu^{II}-NHC Complexes

5.2.1 Synthesis of [Cu(NHC)X_2]-Type Complexes

The synthesis and characterisation of ligand precursor **L21** (nitro-substituted precursor) and its corresponding Cu^{I} complex was described in the previous chapter. The presence of the nitro-substituent on the pyridyl ring led to a marked decrease in the basicity of the pyridyl nitrogen atom (and hence, σ-donor strength), which was manifested in the lengthening of the Cu^{I}-N bond (from 2.34 Å in **C22B** to 2.56 Å in **C21B**). Since the ability of this ligand set to stabilise a Cu^{II} centre (as illustrated in Chapter 4) is likely to be due to the presence of an effective pyridyl donor, initial attempts at synthesising Cu^{II}-NHC complexes did not involve ligand precursor **L21**. Instead, ligand precursors **L19**, **L22** and **L23** were used, which contain much more basic pyridyl donors.

As discussed earlier, there are a limited number of examples of Cu^{II}-NHC complexes rationally synthesised and characterised in the literature. Of these, the most commonly employed synthetic methodology is transmetallation from either a Li^{I} [13a] or Ag^{I}-NHC complex [13b, 13c, 15] to a Cu^{II} salt. Alternatively, reaction of a free carbene (either preformed or generated *in situ*) with a Cu^{II} salt [12, 14, 16] or Cu^{I} salt in air [17] can be used to generate the desired complex. Bearing in mind the base sensitivity of allyl-tethered imidazolium salts, which was exemplified by an allylic rearrangement reaction of **L15** under strongly basic conditions (Chapter 3), the free carbene route for the synthesis of Cu^{II}-NHC complexes derived from ligand precursors **L19**, **L22** and **L23** is unlikely to be of much utility. Hence, the Ag^{I}-NHC transmetallation route would appear to be a more sensible route for the synthesis of Cu^{II}-NHC complexes from these NHC precursors.

Reaction of ligand precursor **L19** with Ag_2O cleanly afforded the corresponding Ag^{I}-NHC complex (**C19B**), whose characterisation data and solid-state structure was described in Chapter 3. Reaction of the Ag^{I}-NHC complex (**C19B**) with one equivalent of $CuBr_2$ at ambient temperature in anhydrous dichloromethane gave the desired Cu^{II}-NHC complex (**C19G**) in a moderate 57% yield, following work-up (Scheme 5.1).

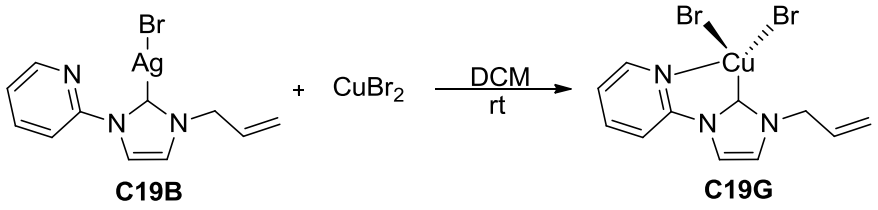

Scheme 5.1 Synthesis of Cu^{II}-NHC complex **C19G**

The so-formed dark green complex was subject to characterisation by elemental analysis and single crystal X-ray diffraction analysis. Dark green block crystals suitable for X-ray diffraction analysis were grown *via* the vapour diffusion of diethyl ether in to a concentrated solution of the product in dichloromethane. Complex **C19G** was found to crystallise in the monoclinic crystal system, with the structural solution being performed in the space group *C2/c* (Figure 5.4). Analysis by NMR spectroscopy is precluded by the paramagnetism of the Cu^{II} centre. Unfortunately, an accurate mass of the molecular ion could not be obtained *via* high-resolution mass spectrometry either, presumably due to decomposition and ligand scrambling during ionisation in the spectrometer.

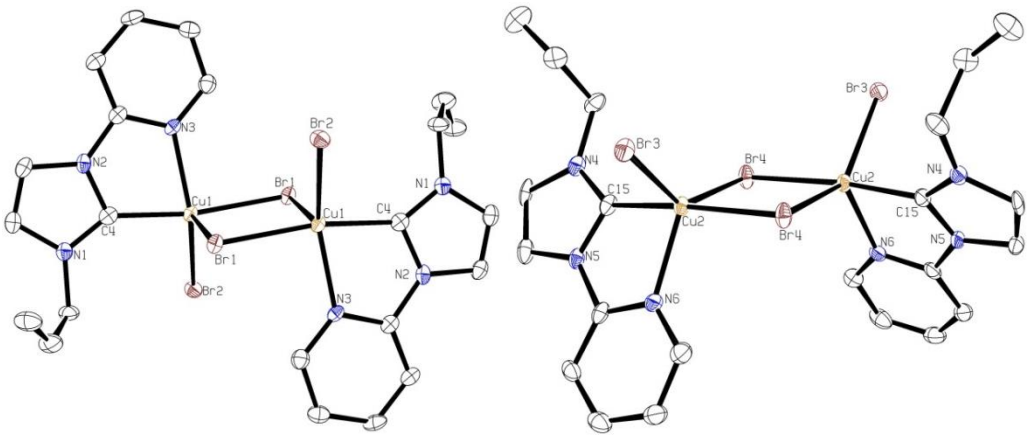

Figure 5.4 Molecular structure of **C19G** showing crystallographically independent *trans* (left) and *cis* (right) $(\mu\text{-Br})_2$-bridged dimers. Ellipsoids are drawn at the 50% probability level. H atoms and co-crystallised solvent have been omitted for clarity

Table 5.1 Selected bond distances (Å) and angles (deg) for **C19G**

	***trans* dimer**	***cis* dimer**
C(4)-Cu(1) / C(15)-Cu(2)	1.981(4)	1.934(5)
N(3)-Cu(1) / N(6)-Cu(2)	2.133(4)	2.135(4)
Br(2)-Cu(1) / Br(3)-Cu(2)	2.4474(7)	2.4492(7)
Br(1)-Cu(1) / Br(4)-Cu(2)	2.6653(8)	2.5600(7)
Br(1*)-Cu(1) / Br(4*)-Cu(2)	2.4608(7)	2.4325(8)
C(4)-Cu(1)-Br(1*) / C(15)-Cu(2)-Br(4*)	171.0(1)	173.4(1)
Br(2)-Cu(1)-N(3) / Br(3)-Cu(2)-N(6)	144.2(1)	106.2(1)
Br(1)-Cu(1)-N(3) / Br(4)-Cu(2)-N(6)	102.9(1)	116.2(1)
Br(1)-Cu(1)-Br(2) / Br(4)-Cu(2)-Br(3)	112.85(2)	137.38(3)

(***** denotes bridging halide *trans* to NHC donor)

The asymmetric unit of **C19G** contains two halves of two crystallographically independent $(\mu\text{-Br})_2$-bridged dimers and 1.5 molecules of co-crystallised dichloromethane. The complete dimers are illustrated in Figure 5.4, while the co-crystallised dichloromethane has been omitted for clarity. The crystallisation of two independent dimers (both a *cis* and a *trans* dimer) is in contrast to the structure of **C19E** (obtained by atmospheric oxidation of **C19C** in Chapter 4), which contains only a *trans* dimer.

The coordination geometry about both of the crystallographically independent Cu^{II} centres is best described as distorted trigonal bipyramidal, where the axial positions are occupied by the

NHC donor and a bridging bromide donor, while the three equatorial positions are occupied by the pyridyl donor and two bromide donors (one terminal and one bridging). The relatively narrow bite angle of the chelating NHC ligand (approximately 79°) acts to cause distortion about the copper centres. This distortion, towards a square pyramidal geometry, is most pronounced for the *trans* dimer, with a widening of the Br2-Cu1-N3 angle to 144° and a narrowing of the Br1-Cu1-N3 angle to 103°. While many of the bond lengths and angles of the two dimers (*cis* and *trans*) are broadly similar, there are a few quite noticeable differences between the two. For example, the C-Cu bond length of the *trans* dimer is 1.98 Å, while that of the *cis* dimer is somewhat shorter, at 1.93 Å. The Cu-$Br_{(equatorial)}$ bond length (2.67 Å) of the *trans* dimer is also 0.11 Å longer than the corresponding bond of the *cis* dimer (2.56 Å). The reason for these fairly substantial differences in bond lengths is not immediately obvious, though the impact of hydrogen bonding between the bromides (both bridging and terminal) and co-crystallised dichloromethane H atoms may have a significant effect.

Ligand precursor **L22** is the *para*-methylated analogue of **L19**, and as with **L19**, its synthesis and complexation to Ag^{I} to form complex **C22A** was described in Chapter 4. Again, reaction of one equivalent of **C22A** with $CuBr_2$ in anhydrous dichloromethane gave the desired Cu^{II} complex as a dark green solid in very good yield following work-up. Elemental analysis indicated the formation of a pure Cu^{II}-NHC complex (**C22D**). Connectivity was confirmed by the growth of single crystals suitable for X-ray diffraction analysis, which could be obtained *via* the vapour diffusion of diethyl ether in to a concentrated solution of the product in dichloromethane. Complex **C22D** was found to crystallise in the monoclinic crystal system, and the structural solution was performed in the space group $P2_1/n$ (Figure 5.5).

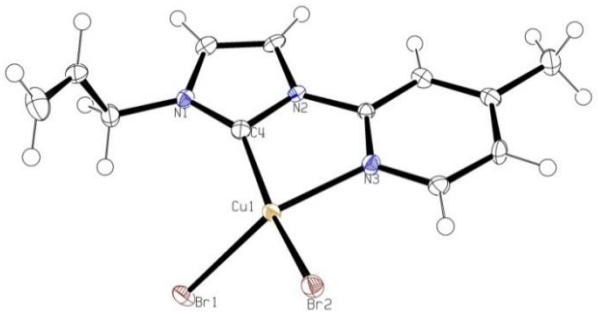

Figure 5.5 Molecular structure of **C22D**. Ellipsoids are drawn at the 50% probability level

Table 5.2 Selected bond distances (Å) and angles (deg) for **C22D**

C(4)-Cu(1)	1.973(3)	C(4)-Cu(1)-N(3)	80.7(1)
N(3)-Cu(1)	2.063(3)	C(4)-Cu(1)-Br(1)	97.3(1)
Cu(1)-Br(1) / Br(2)	2.3879(5) / 2.3668(5)	C(4)-Cu(1)-Br(2)	159.4(1)

In sharp contrast to complex **C19G**, complex **C22D** crystallised as a monomer rather than a (μ-$Br)_2$-bridged dimer. Seemingly, the addition of a methyl group in the *para* position of the pyridyl ring has had a significant effect on the solid state structure of the molecule. This presumably either occurs due to a slight enhancement in the σ-donor strength of the pyridyl ligand on the addition of a *para*-methyl group, rendering the metal centre electronically satisfied with a coordination number of 4. Alternatively, the monomeric nature of **C22D** may simply be a crystal packing effect.

The geometry about the 4-coordinate Cu^{II} centre is somewhat unusual in that it is neither truly square planar nor tetrahedral. The geometry can be described as 'tetragonally distorted' tetrahedral, and arises due to loss of degeneracy of the t_2 orbitals. The loss of degeneracy leads to an overall flattening of the coordination sphere of the Cu^{II} centre, rather than distortions in the metal-ligand bond lengths, resulting in a geometry approaching the square planar limit.[18a] The tetrahedral (or square planar) character of a given 4-cooridnate complex can, however, be quantified using the four-coordinate geometry index (τ_4) introduced by Houser *et al*..[18b] In the case of complex **C22D**, a value of 0.39 for τ_4 is obtained, which suggests an intermediate metal coordination geometry, though which is slightly closer to square planar than tetrahedral in nature.

Aside from the C-Cu bond length, the N-Cu and Cu-Br bond lengths of **C22D** are all somewhat shorter than those observed in complex **C19G**. For instance, the N-Cu bond length of **C22D** is 2.06 Å, which is approximately 0.07 Å shorter than the N-Cu bond lengths seen in complex **C19G**. This pronounced shortening of bond lengths in **C22D** (versus **C19G**) is likely to be a manifestation of the decreased coordination number of the metal centre, and thus increased electrostatic interaction between the positively charged metal centre and its ligands.

Ligand precursor **L23** is the *para*-methoxylated analogue of **L19** and again, its synthesis and complexation to Ag^I to form complex **C23A** was described in Chapter 4. Reaction of the Ag^I-NHC complex **C23A** with $CuBr_2$ under identical reaction conditions to those used for the synthesis of **C19G** and **C22D** yielded a green-yellow crystalline solid following work-up (complex **C23C**). Analysis of the complex by elemental analysis and single crystal X-ray diffraction illustrated its purity and connectivity. The single crystals of complex **C23C** suitable for X-ray diffraction analysis were obtained on standing of a dilute solution of the product in a mixture of dichloromethane/diethyl ether (1:4). The fact that these crystals were obtained from hydrous, aerobic solvent suggests that this complex is somewhat more stable under ambient conditions than complexes **C19G** and **C22D**, for which crystals could only be obtained from anhydrous/anaerobic solvent. Complex **C23C** was found to crystallise in the monoclinic crystal system, and a structural solution could be performed in the space group $P2_1/c$ (Figure 5.6).

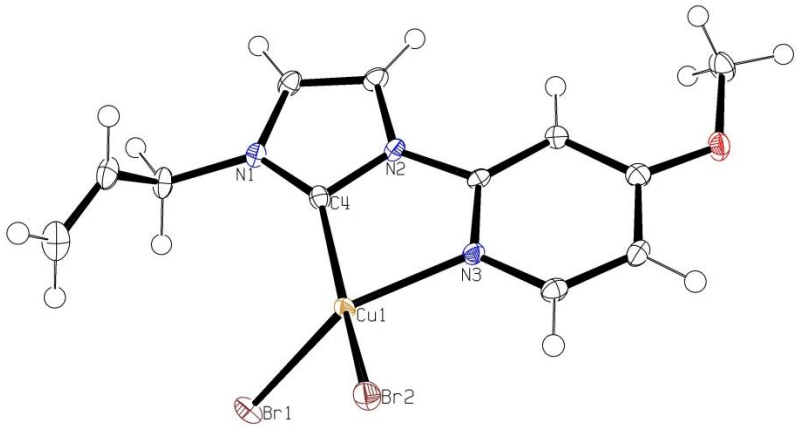

Figure 5.6 Molecular structure of **C23C**. Ellipsoids are drawn at the 50% probability level

Table 5.3 Selected bond distances (Å) and angles (deg) for **C23C**

C(4)-Cu(1)	1.966(2)	C(4)-Cu(1)-N(3)	80.96(8)
N(3)-Cu(1)	2.037(2)	C(4)-Cu(1)-Br(1)	100.39(7)
Cu(1)-Br(1)	2.3770(4)	C(4)-Cu(1)-Br(2)	152.12(7)
Cu(1)-Br(2)	2.3747(4)		

Similarly to complex **C22D**, **C23C** crystallised as a 4-coordinate monomer with a tetragonally distorted tetrahedral geometry. The metal-ligand bond lengths observed are generally in excellent agreement with those of **C22D**, reflecting the same coordination number and geometry about the metal centre. The N-Cu bond length in complex **C23C** (2.04 Å) is very slightly shortened with respect to complex **C22D** (2.06 Å), perhaps reflecting an increase in the σ-donor strength of the pyridyl nitrogen atom on addition of a *para*-methoxy substituent.

The ligands derived from ligand precursors **L19**, **L22** and **L23** (Figure 5.7) appear highly effective in stabilising both Cu^{I} and Cu^{II} centres, as illustrated by the work described in Chapters 3, 4 and this chapter. These ligands have allowed the facile synthesis, isolation and characterisation of rare examples of both 4- and 5-coordinate Cu^{II}-NHC complexes which remarkably, do not bear an anionic tether or acetate ligand.

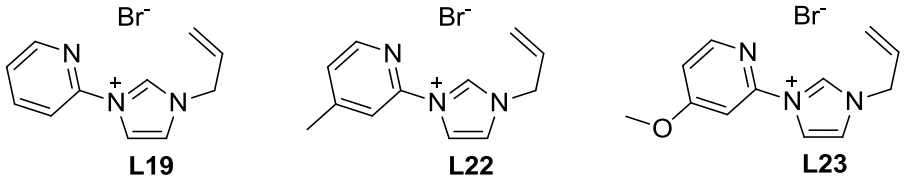

Figure 5.7 Ligand precursors **L19**, **L22** and **L23**

5.2.2 Crystallisation of [Cu(NHC)X_2.adduct]-Type Complexes

Due to the 4-coordinate tetragonally distorted tetrahedral coordination environment of complexes **C22D** and **C23C**, it was envisaged that these two complexes would be coordinatively unsaturated. Thus, crystallisation of **C22D** and **C23C** in the presence of a coordinating ligand would presumably lead to either a 5- or 6-coordinate [Cu(NHC)X_2.adduct]-type complex. The same would also be true for the (μ-Br)$_2$-bridged dimeric complex **C19G**, though coordination of another ligand would require cleavage of the (μ-Br)$_2$-bridge first.

Dissolution of complex **C19G** in pyridine and then precipitation by the immediate addition of pentane gave a turquoise-coloured crystalline solid, indicating a change in the coordination environment of the Cu^{II} centre from a (μ-Br)$_2$-bridged dimeric 5-coordinate complex (which is dark green in the solid-state). Crystallisation of this solid (**C19H**) on standing of a dilute dichloromethane/diethyl ether (1:4) solution gave a number of green polyhedral crystals which were suitable for X-ray diffraction analysis. Complex **C19H**, a [Cu(NHC)X_2.pyridine]-type complex was found to crystallise in the trigonal crystal system, with a structural solution being performed in the space group $P3_121$ (Figure 5.8).

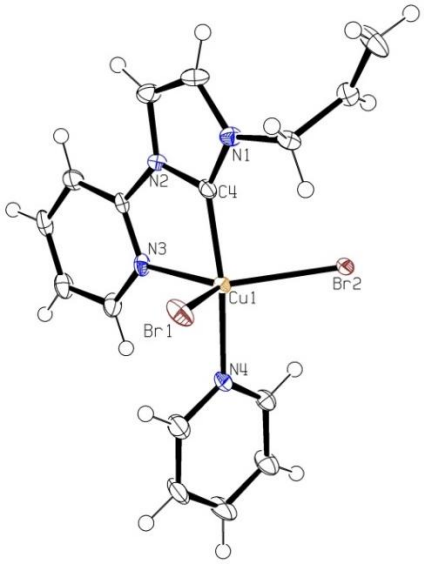

Figure 5.8 Molecular structure of **C19H**. Ellipsoids are drawn at the 50% probability level

Table 5.4 Selected bond distances (Å) and angles (deg) for **C19H**

C(4)-Cu(1)	1.951(3)	C(4)-Cu(1)-N(4)	169.1(1)
N(3)-Cu(1)	2.169(3)	C(4)-Cu(1)-N(3)	78.8(1)
N(4)-Cu(1)	2.036(3)	N(3)-Cu(1)-Br(1)	112.45(9)
Cu(1)-Br(1)	2.5154(8)	N(3)-Cu(1)-Br(2)	128.30(9)
Cu(1)-Br(2)	2.5268(6)	Br(1)-Cu(1)-Br(2)	118.27(2)

On addition of pyridine, the cleavage of the $(\mu\text{-Br})_2$-bridge occurs producing a 5-coordinate trigonal bipyramidal Cu^{II} complex. The bridging bromide in the axial position has been replaced by a pyridine donor. The NHC donor remains in the other axial position, with the equatorial coordination positions being occupied by the two bromides and pyridyl donor. The trigonal bipyramidal geometry of **C19H** is somewhat less distorted than that of the two independent Cu^{II} centres of **C19G**, which is exhibited by the bond angles between the equatorial ligands approaching 120°. Packing in the extended crystalline lattice is mainly dominated by $Br\text{---}H^{\delta+}$ interactions and π-π stacking.

Analogously, crystallisation of **C22D** and **C23C** in the presence of pyridine led to the formation of [Cu(NHC)X_2.pyridine]-type complexes (**C22E** and **C23D**), both of which contain an identical coordination environment to that of **C19H**. Complexes **C22E** and **C23D** were found to crystallise in the monoclinic (**C22E**) and trigonal (**C23D**) crystal systems, with the structural solutions being performed in the space groups $P2_1/c$ and $R\bar{3}$ respectively (Figure 5.9).

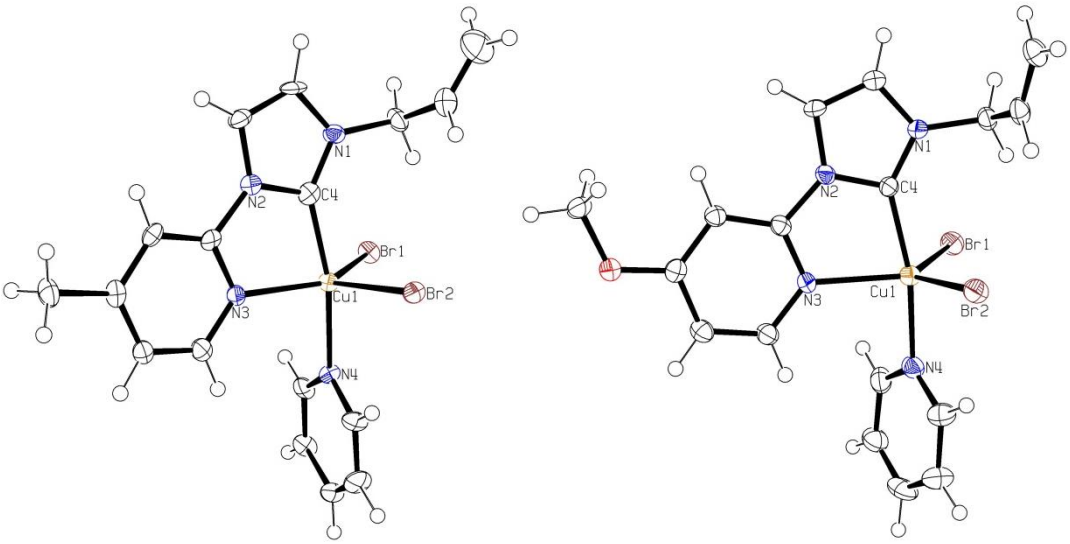

Figure 5.9 Molecular structures of **C22E** (left) and **C23D** (right). Ellipsoids are drawn at the 50% probability level. Co-crystallised pyridine solvent has been omitted for clarity

Table 5.5 Selected bond distances (Å) and angles (deg) for **C22E** and **C23D**

	C22E	**C23D**
C(4)-Cu(1)	1.962(5)	1.961(6)
N(3)-Cu(1)	2.148(3)	2.207(4)
N(4)-Cu(1)	2.031(3)	2.023(6)
Cu(1)-Br(1)	2.4783(7)	2.4876(8)
Cu(1)-Br(2)	2.5844(6)	2.5434(8)
C(4)-Cu(1)-N(4)	168.7(2)	168.6(2)
N(3)-Cu(1)-Br(1)	138.6(1)	124.4(1)
N(3)-Cu(1)-Br(2)	104.64(9)	108.8(1)
Br(1)-Cu(1)-Br(2)	116.34(2)	126.12(3)

As might be anticipated, the bond metrics of **C22E** and **C23D** are rather similar to each other, and indeed, highly comparable to **C19H**. Somewhat surprisingly however, the N3-Cu1 bond length of **C22E** (2.15 Å) is significantly shorter than that of **C23D** (2.21 Å), despite the presence of a strongly electron-donating methoxy-substituent on the pyridyl donor of **C23D**. Examination of the extended crystal lattice of **C23D** revealed a fascinating structure, with large solvent accessible channels running along the crystallographic c-axis (Figure 5.10). The channels were found to be approximately 13 Å in diameter, giving a remarkable solvent accessible void volume of 36.5% of the total unit cell volume. The channels were found to be occupied by pyridine solvent molecules, of which, one per asymmetric unit could be satisfactorily refined to convergence. More diffuse electron density had to be removed from the structure using the SQUEEZE routine in PLATON.

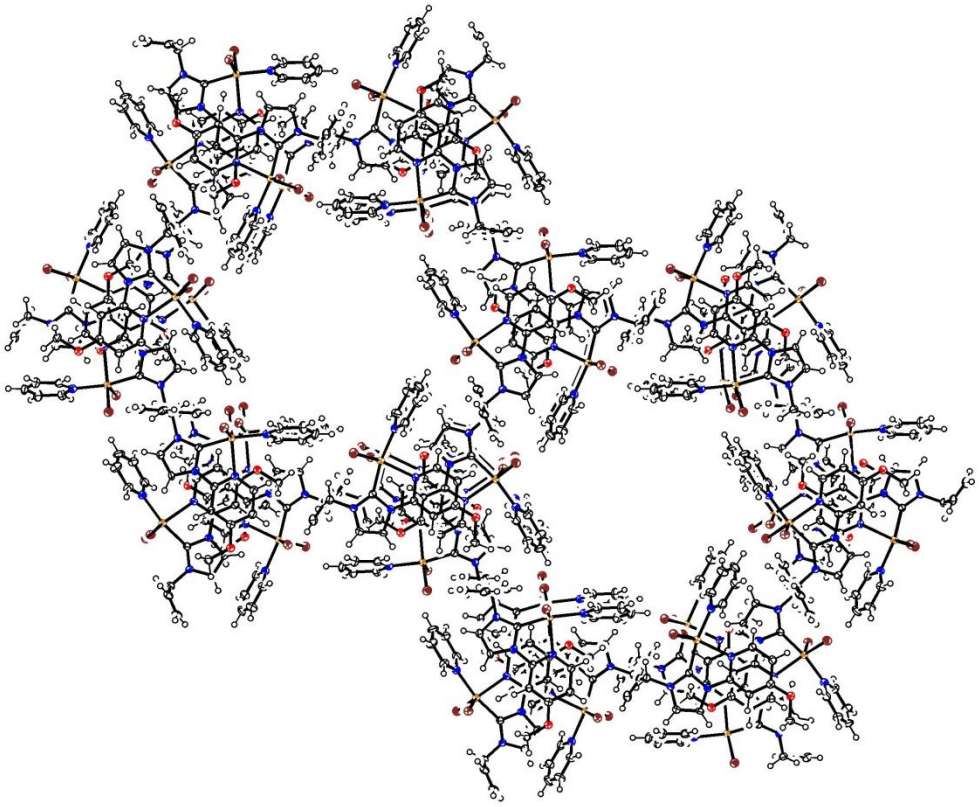

Figure 5.10 Large solvent accessible channels running along the crystallographic c-axis of **C23D**. Ellipsoids are drawn at the 50% probability level. Pyridine solvent molecules contained within the channels have been omitted for clarity

Crystallisation of **C19G** and **C23C** in the presence of another coordinating solvent, namely, dimethyl sulfoxide (DMSO), again gave two 5-coordinate trigonal bipyramidal structures (**C19I** and **C23E**), with occupation of one of the axial coordination sites by a DMSO molecule. In both cases, the DMSO molecule coordinates to the Cu^{II} centre through its oxygen atom (Figure 5.11).

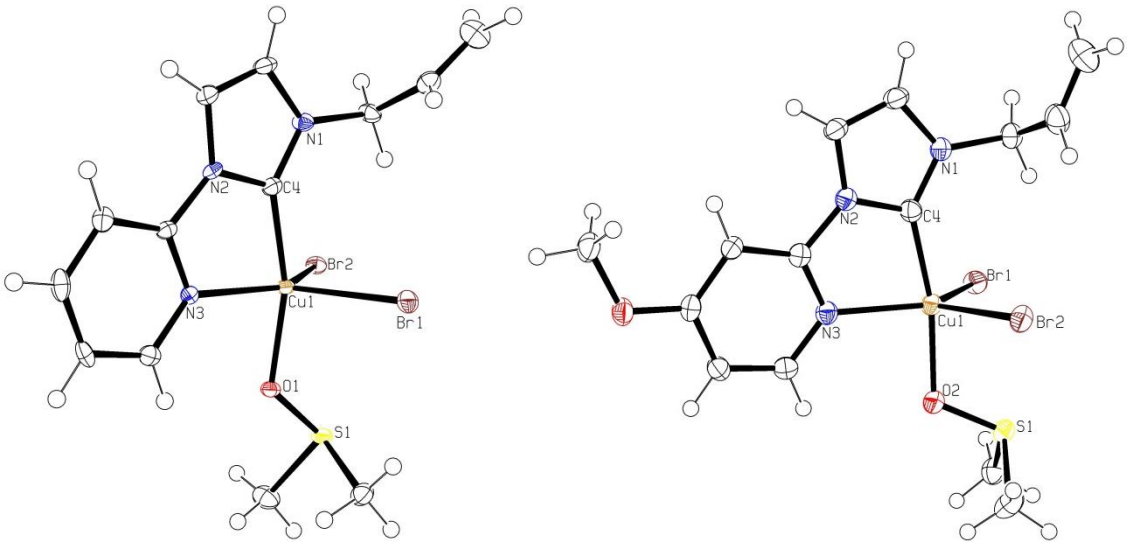

Figure 5.11 Molecular structures of **C19I** (left) and **C23E** (right). Ellipsoids are drawn at the 50% probability level. Co-crystallised diethyl ether solvent has been omitted for clarity

By crystallising several [Cu(NHC)X_2.adduct]-type complexes of **C19G**, **C22D** and **C23C**, it has been demonstrated that these complexes are indeed coordinatively unsaturated, and that their coordination sphere can be completed by the simple addition of one monodentate ligand, forming a 5-coordinate trigonal bipyramidal complex. With this in mind, the synthesis of [Cu$(NHC)_2$X]X'-type complexes was attempted, which would presumably resemble those adventitiously crystallised and described in Chapter 4.

5.2.3 Synthesis of [Cu$(NHC)_2$X]X'-Type Complexes

In analogy to the synthesis of the [Cu(NHC)X_2]-type complexes described earlier, the synthesis of [Cu$(NHC)_2$X]X'-type complexes was attempted using the transmetallation from a Ag^I-NHC route. In order to prevent the formation of $Ag_nBr_{n+1}^-$ anions and to introduce an extra coordination site on the Cu^{II} centre, one equivalent of $AgPF_6$ was used per equivalent of $CuBr_2$. The silver ion would act as a halide scavenger, with the AgBr formed precipitating immediately from solution due to its high lattice enthalpy. A general synthesis of [Cu$(NHC)_2$X]X'-type complexes is shown below (Scheme 5.2).

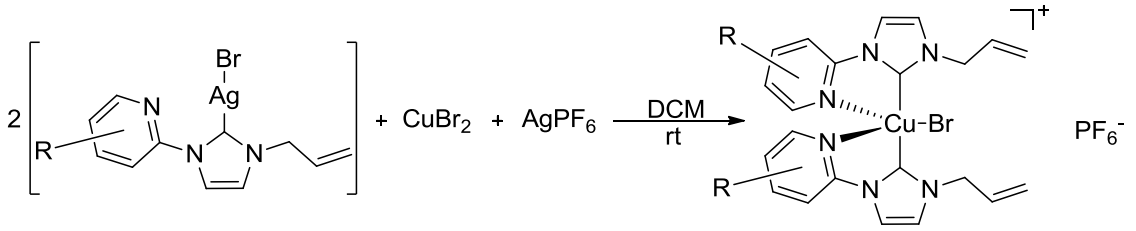

Scheme 5.2 Synthesis of [Cu$(NHC)_2$X]X'-type complexes

Thus, reaction of two equivalents of Ag^I-NHC complex **C19B** or **C22A** with one equivalent of $CuBr_2$ and one equivalent of $AgPF_6$ in anhydrous dichloromethane at room temperature led to the formation of blue solutions containing pale yellow precipitate (AgBr). After filtration to remove the silver halide precipitate, removal of the solvent and then recrystallisation from acetonitrile/diethyl ether gave the desired Cu^{II}-NHC products (**C19J** and **C22F**) as blue crystalline solids in good yield. The complexes could be characterised by high-resolution mass spectrometry and elemental analysis, both of which indicated the formulation of the products as being [Cu$(NHC)_2$Br]PF_6. Single crystals of both suitable for X-ray diffraction analysis were obtained by the vapour diffusion of diethyl ether in to a concentrated solution of the products in acetonitrile. *Bis*-NHC complexes **C19J** and **C22F** were found to crystallise in the triclinic crystal system, with the structural solutions of both being performed in the space group $P\bar{1}$ (Figure 5.12). Interestingly, the crystals of both complexes were obtained from wet, aerobic solvents; thus indicating the enhanced stability of these complexes versus the [Cu(NHC)X_2]-type complexes described earlier.

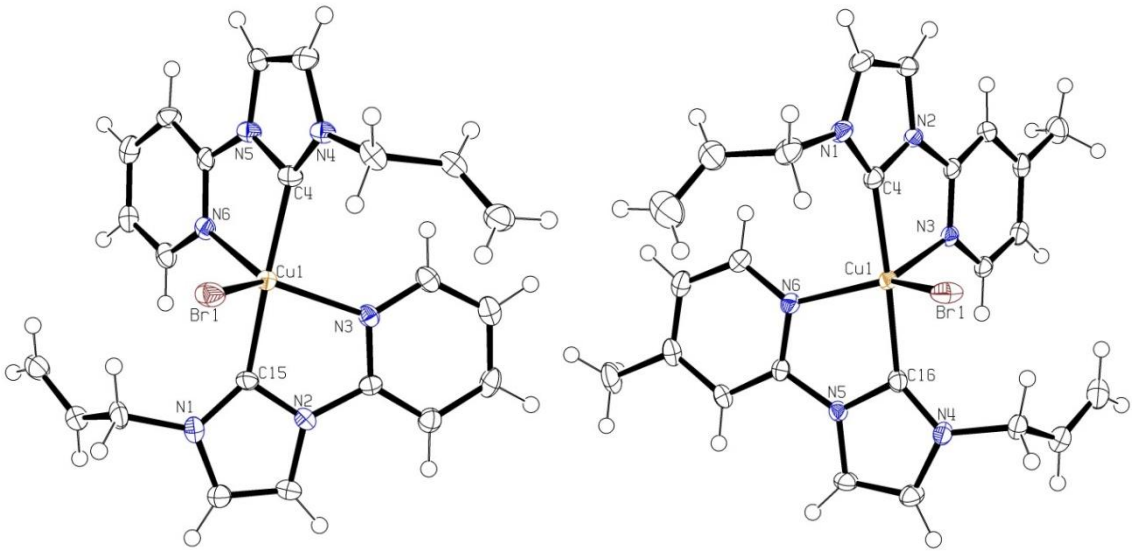

Figure 5.12 Molecular structures of **C19J** (left) and **C22F** (right). Ellipsoids are drawn at the 50% probability level. PF_6^- anions have been omitted for clarity

Table 5.6 Selected bond distances (Å) and angles (deg) for **C19J** and **C22F**

	C19J	**C22F**
C(4)-Cu(1)	2.014(8)	1.990(3)
C(15)/C(16)-Cu(1)	1.970(9)	1.984(3)
N(3)-Cu(1)	2.172(7)	2.164(2)
N(6)-Cu(1)	2.189(7)	2.139(2)
Cu(1)-Br(1)	2.503(1)	2.5140(4)
C(4)-Cu(1)-C(15)/C(16)	177.3(3)	177.2(1)
N(3)-Cu(1)-Br(1)	128.2(2)	116.69(5)
N(6)-Cu(1)-Br(1)	118.4(2)	135.54(6)
N(3)-Cu(1)-N(6)	113.5(3)	107.77(8)

As anticipated, the crystal structures reveal geometrically identical 5-coordinate trigonal bipyramidal complexes with the two NHC donors occupying the axial positions. The C-Cu bond lengths fall between 1.97 and 2.01 Å, which is at the upper end of the small number reported in the literature thus far (1.91 to 2.01 Å).[13a-c, 14-15, 15c] Indeed, the C-Cu bond lengths of complexes **C19J** and **C22F** are slightly longer than those of the analogous 5-coordinate pyridine and DMSO-adduct complexes **C19H**, **C19I** and **C22E** (1.95, 1.96 and 1.95 Å). This perhaps suggests that the strong σ-donor NHCs increase the electron density in the d_{z^2} orbital of the Cu^{II} centre (versus pyridine or DMSO), which in turn increases the repulsion between the electron density in the d_{z^2} orbital and the carbenic carbon σ-electrons, leading to a lengthening of the C-Cu bond lengths.

The wealth of different Cu^{II}-NHC complexes described within this chapter and Chapter 4 illustrates the pronounced ability of the pyridyl-tethered ligand set to stabilise both Cu^{I} and Cu^{II} centres. The 5-coordinate Cu^{II}-NHC complexes displayed an extremely strong preference for occupation of the axial coordination sites by the NHC donors (and thus, occupation of an equatorial site by the tethered-pyridyl donor). The reason for this preference may be that interaction of the strong σ-donating NHCs with a partially filled d-orbital (d_{z^2} orbital) is energetically preferred over interaction with the other filled d-orbitals. Alternatively, it has been demonstrated that equatorial π-bonding is significantly stronger than axial π-bonding. Therefore, ligands such as pyridines, which are capable of π-interactions with metal centres, are more likely to adopt an equatorial position than an axial position. In particular, a π-acceptor ligand such as the pyridyl (tethered to the NHC) prefers an eq⊥ orientation.[19] The interaction of a filled d-orbital on the Cu^{II} centre and the LUMO of the pyridyl donor is illustrated in Figure 5.13.

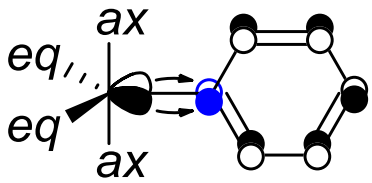

Figure 5.13 π-Acceptor interaction of a filled d-orbital (only half shown) on the Cu^{II} centre and the LUMO of the pyridyl donor (nitrogen shown in blue)[19]

5.3 Oxidative Decomposition of NHC Ligands

5.3.1 Haloimidazolium Salts

The synthesis of Cu^{II}-NHC complexes from ligand systems not bearing ancillary donors has been attempted by several different groups. It is typically observed that interaction of either a free carbene or a Ag^{I}-NHC complex (a latent free carbene) with ≥ 2 equivalents of Cu^{II}

halogenide leads to the formation of haloimidazolium (2-haloimidazolium) salts.[14b, 20] For instance, Nechaev reported that reaction of one equivalent of a Ag^{I}-NHC complex with two equivalents of $CuBr_2$ led to the formation of the corresponding haloimidazolium salt in quantitative yield (Scheme 5.3). Conversely, when 1 equivalent of a Cu^{II} halogenide interacts with either a free carbene or Ag^{I}-NHC complex, the presence of a product mixture containing a Cu^{I}-NHC species has been noted.[14b, 21] Reaction of an NHC with a Cu^{II} salt to give a haloimidazolium salt and/or a Cu^{I}-NHC complex is a redox process. During the reaction, the NHC undergoes a formal 1 electron oxidation process to give a haloimidazolium, at the same time, the Cu^{II} centre is reduced down to Cu^{I}.

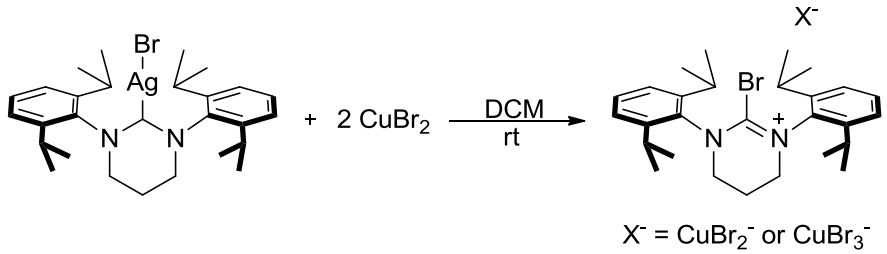

Scheme 5.3 Example of the formation of a haloimidazolium salt by reaction of a Ag^{I}-NHC complex with two equivalents of $CuBr_2$[18]

As a starting point for the investigation of the decomposition of these pyridyl-tethered NHC ligand systems, it was sensible to examine the decomposition of a comparable ligand, though which does not contain a pyridyl donor, in the presence of Cu^{II} salts. For this reason, the commonly-used NHC ligand precursor IMes.Cl (1,3-*bis*(2,4,6-trimethylphenyl)imidazolium chloride) (**L3**) was chosen. Before reaction with $CuBr_2$, it was necessary to form the Ag^{I}-NHC complex derived from **L3**. Thus, reaction of **L3** with 0.65 equivalents of Ag_2O at reflux in dichloromethane led to the formation of the desired Ag^{I}-NHC complex (**C3B**), which was isolated as a white crystalline solid. Characterisation data was in firm agreement with that already published in the literature.[22] Reaction of Ag^{I}-NHC complex (**C3B**) with $CuBr_2$ gave different products, depending on the equivalents of $CuBr_2$ used. For instance, reaction with 1 equivalent of $CuBr_2$ led to the formation of a 1:1 mixture of products thought to be a haloimidazolium salt (IMesBr.CuX_2) and Cu^{I}-NHC complex (IMes-Cu-X). The presence of a 1:1 mixture of two different products was indicated by NMR spectroscopy, with the identity of these compounds being confirmed using high-resolution mass spectrometry and unit cell parameters of crystals of the two different products. The halogen components of the two products were presumed to be a mixture of chloride and bromide. Conversely, reaction of Ag^{I}-NHC complex (**C3B**) with 2 equivalents of $CuBr_2$ cleanly led to the exclusive formation of haloimidazolium salt, which was isolated as a white crystalline solid (**C3C**). Full characterisation of **C3C** *via* NMR spectroscopy, high-resolution mass spectrometry and elemental analysis indicated the formulation of the haloimidazolium salt as (IMesBr.Cu_2X_3). A

scheme illustrating the reaction of the Ag^{I}-NHC complex with the two different equivalents of $CuBr_2$ is given below (Scheme 5.4).

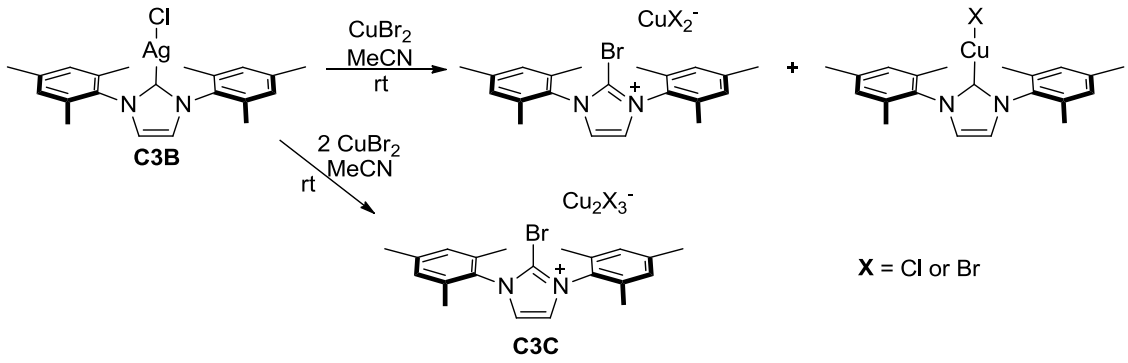

Scheme 5.4 Reactions of Ag^{I}-NHC complex (**C3B**) with $CuBr_2$

Single crystals of **C3C** suitable for X-ray diffraction analysis could be obtained *via* the vapour diffusion of diethyl ether in to a concentrated solution of the product in acetonitrile. Complex **C3C** was found to crystallise in the triclinic crystal system, with the structural solution being performed in the space group $P\bar{1}$ (Figure 5.14).

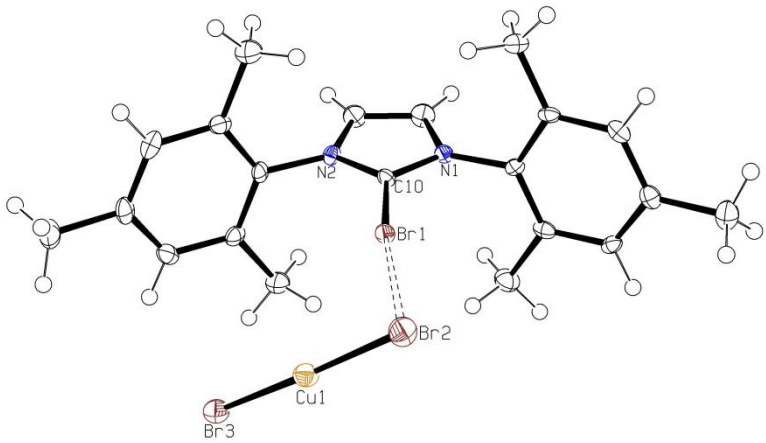

Figure 5.14 Molecular structure of **C3C**. Ellipsoids are drawn at the 50% probability level. Possible halogen bond shown by dashes

Table 5.7 Selected bond distances (Å) and angles (deg) for **C3C**

C(10)-Br(1)	1.844(3)	C(10)-Br(1)---Br(2)	172.56
Br(1)---Br(2)	3.289	Br(2)-Cu(1)-Br(3)	176.60(3)
Cu(1)-Br(2)	2.2116(8)		
Cu(1)-Br(3)	2.2073(8)		

In contrast to the elemental analysis data which indicated a $Cu_2Br_3^-$ anion, complex **C3C** crystallised as a haloimidazolium salt with a CuX_2^- anion. The two halides contained within the

copper dihalide anion are shown as bromides in Figure 5.14 (Br2 and Br3), though in reality were found to be a mixture of bromide and chloride with SOFs of 86% (Br) and 14% (Cl) for the halide labelled Br2 and 66% (Br) and 34% (Cl) for the halide labelled Br3. The presence of chloride in the product is not surprising since the Ag^{I}-NHC starting material contains only chloride. Predictably, the CuX_2^- anion crystallised with a near-linear geometry about the Cu^{I} centre.

Interestingly however, there appears to be a halogen bond between Br1 and the halide labelled Br2 (Figure 5.14), with a distance between the two of 3.29 Å, which is a distance well within the sum of the Van der Waals covalent radii. Halogen bonding relies on the ability of halogens (particularly the heavier halogens) to act as electrophiles under certain circumstances, leading to a **Y**-**X**---**D** interaction, where **Y** is a carbon, nitrogen or halogen, **X** is the electrophilic halogen (halogen bond donor) and **D** is an electron donor/Lewis base (halogen bond acceptor). Halogen bonds are able to arise as a result of anisotropicity in the electron density around the halogen bond donor halogen, resulting in a positive electrostatic potential surface located along the axis of the **Y**-**X** bond. This positive electrostatic potential surface is called the 'σ-hole'. At the same time, a belt of negative electrostatic potential is found around the equator of the halogen bond donor halogen (perpendicular to the **Y**-**X** axis). As a result of the location of the σ-hole, there is a strong preference of halogen bonded systems to attain a bond angle of approximately 180° with respect to the halogen bond donor halogen (**X**).[23] This is evident in the crystal structure of complex **C3C**, where the C10-Br1---Br2 bond angle is 173°. In this case, Br1 is the halogen bond donor and the halide labelled Br2 is the Lewis basic halogen bond acceptor. The presence of similar halogen bonds in the solid-state structures and solution phases of other haloimidazolium salts has led to their utilisation in anion recognition and supramolecular assembly.[24]

The formation of haloimidazolium salts, similar to those described above, was observed during initial attempts at synthesising complex **C23C**, a $[Cu(NHC)X_2]$-type complex. It became apparent that the presence of excess $CuBr_2$ in the reaction mixture was detrimental to both the yield and purity of the final product, as evidenced by the oily nature of the final products. Furthermore, crystallisation of the product of these reactions failed to lead to any crystals of the desired Cu^{II}-NHC product. Instead, the two different molecules which crystallised offered clues as to the effect of excess $CuBr_2$ in the reaction mixture in this case (Figure 5.15).

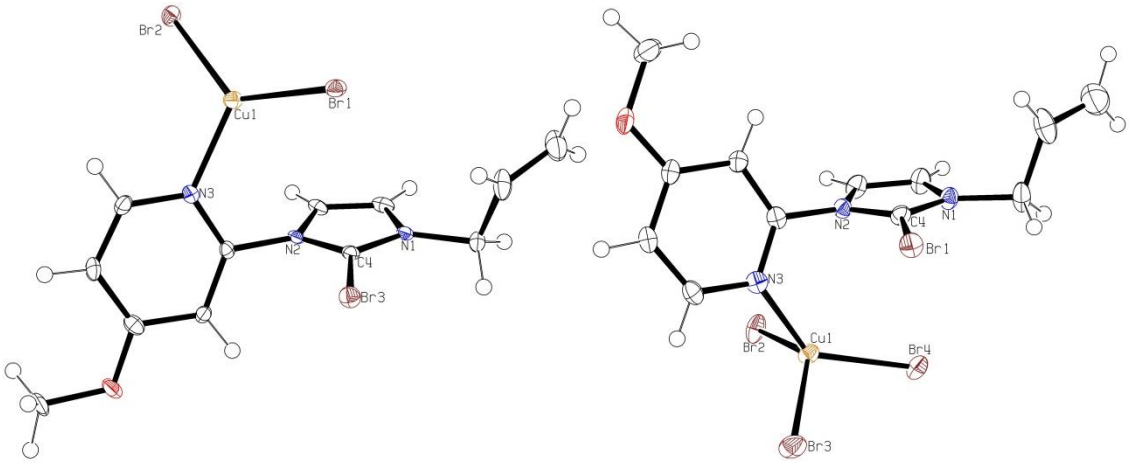

Figure 5.15 Molecular structures of complexes **C23F** (left) and **C23G** (right). Ellipsoids are drawn at the 50% probability level

Complexes **C23F** and **C23G** are both haloimidazolium salts, with either a Cu^{I}-containing $CuBr_2^-$ anion (**C23F**) or a Cu^{II}-containing $CuBr_3^-$ anion (**C23G**). Oxidation of the copper halide anion presumably occurs, producing **C23G** from **C23F** during crystallisation under ambient conditions. Analogously to complex **C3C**, complexes **C23F** and **C23G** both display evidence of halogen bonding, with Br---Br separations of 3.18 Å (Br3---Br2) in complex **C23F** and 3.44 Å (Br1---Br3) in complex **C23G**.

In light of this observation, the rational synthesis of a haloimidazolium salt was attempted using one of the pyridyl-tethered NHC ligand precursors described previously (**L19**). It has already been shown that reaction of one equivalent of $CuBr_2$ with one equivalent of the Ag^{I}-NHC complex (**C19B**) derived from **L19**, led to the clean formation of a Cu^{II}-NHC complex (**C19G**). Contrariwise, reaction of two equivalents of $CuBr_2$ with the Ag^{I}-NHC complex led to the formation of haloimidazolium salt (**C19K**) in high yield following work-up (Scheme 5.5). The haloimidazolium salt **C19K** was subject to full characterisation, with the high-resolution mass spectrum of **C19K** showing the dominant ion to be a $[imBr]^+$ fragment.

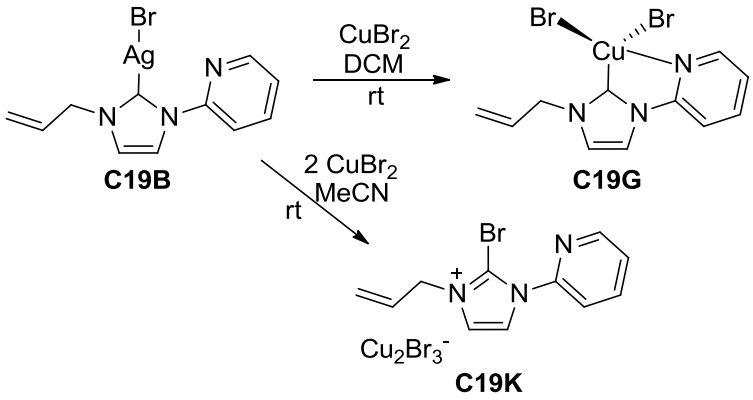

Scheme 5.5 Reactions of Ag^{I}-NHC complex (**C19B**) with $CuBr_2$

In order to try and gain a deeper mechanistic understanding of this reactivity and the formation of haloimidazolium salts, density functional theory (DFT) calculations were performed using ligand precursor **L19** as the model system. The results of the computations are illustrated below, in Scheme 5.6.

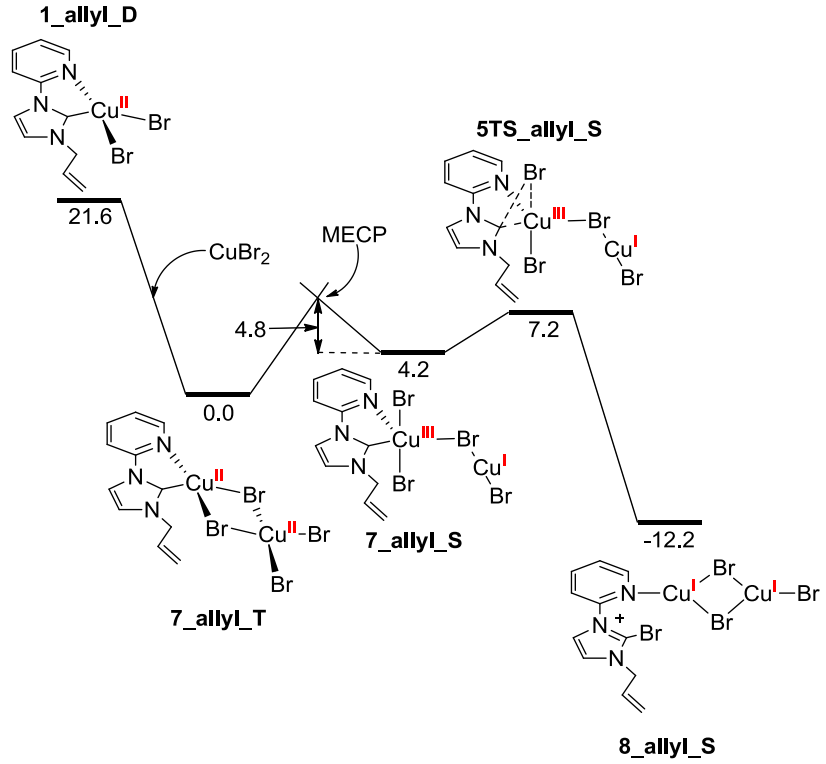

Scheme 5.6 Proposed mechanistic pathway for haloimidazolium (**C19K**) formation (relative free energies in kcal mol^{-1}) (MECP = minimum energy crossing point)

During the reaction of 2 equivalents of $CuBr_2$ with 1 equivalent of Ag^{I}-NHC complex (**C19B**), transmetallation occurs immediately on addition of solvent, as is evident in the immediate appearance of a large quantity of off-white precipitate (AgBr). This forms the Cu^{II}-NHC complex (**1_allyl_D**), which was separately synthesised and characterised earlier (**C19G**), and shown to be stable in the absence of excess $CuBr_2$. However, in the presence of a further equivalent of $CuBr_2$, a $(\mu\text{-Br})_2$-bridged dinuclear complex (**7_allyl_T**) is formed irreversibly. The formation of this binuclear complex is calculated to have a significant thermodynamic driving force (ΔG = -21.6 kcal mol^{-1}). The binuclear complex then undergoes a disproportionation process, with a relatively low thermodynamic barrier (ΔG = 9.0 kcal mol^{-1}), to give a binuclear Cu^{III}-Cu^{I} complex (**7_allyl_S**), where the pyridyl-tethered NHC ligand is coordinated to the Cu^{III} centre. The geometry about the Cu^{III} centre is calculated to be square pyramidal, with the pyridyl donor in the apical position. The binuclear Cu^{III}-Cu^{I} complex (**7_allyl_S**) then undergoes a facile reductive elimination process, which is calculated to have a very low activation barrier ($\Delta G^{\ddagger}$ = 3.0 kcal mol^{-1}). The product (**8_allyl_S**) of the reaction is the haloimidazolium salt (**C19K**), which was described earlier. Overall, the reaction of a Cu^{II}-NHC

complex with one equivalent of $CuBr_2$ to form a haloimidazolium salt with a Cu^{I}-containing anion is calculated to be spontaneous and exergonic under the reaction conditions used, with an overall ΔG of -33.8 kcal mol^{-1}.

Stack and co-workers reported a similar mechanism to that described above during the reaction of a Cu^{I}-NHC complex with Selectfluor, a strong oxidising agent/source of 'F^{+}'. This reaction produced a 2-chloroimidazolium salt quantitatively, which could be isolated and characterised. The mechanism of the reaction of Selectfluor with a Cu^{I}-NHC complex to form a 2-chloroimidazolium salt was found to invoke a $C_{carbene}$-X reductive elimination process from a Cu^{III}-NHC complex.[25] This is in firm agreement with the mechanism described above for the formation of haloimidazolium salt **C19K**.

The use of transition metal-NHC complexes in catalysis is becoming more and more widespread, partly due to the supposed stability of $C_{carbene}$-M bonds, which are meant to remain intact during a catalytic cycle. Given the pervasiveness of halide-containing transition metal-NHC complexes as catalysts in these organic transformations, the occurrence of $C_{carbene}$-X reductive elimination processes, as demonstrated here, may represent a major catalyst deactivation pathway, particularly among the late transition metals. This would be particularly important if the resultant metal centre is then incompetent in further oxidative addition processes, perhaps due to precipitation from solution (*e.g.* formation of Pd metal during cross-coupling processes).

Thus, the thorough mechanistic understanding of the decomposition of Cu-NHC complexes gained in this chapter so far perhaps provides clues as to the decompositorial fate of other Cu-NHC complexes used in catalysis. Furthermore, it may aid in the design of ligand systems that are more resistant to reductive elimination from higher oxidation state late transition metals.

5.3.2 Ligand Precursor L25: A Unique Example

At a cursory glance, it would be assumed that the coordination chemistry of ligand precursors **L19** and **L25** would be very similar; particularly as the NHC ring itself and pyridyl donor are identical. The only difference between the two is that **L19** contains an allyl *N*-substituent whereas **L25** contains a mesityl *N*-substituent. In terms of their electronic contributions to the NHC donor, there is little difference between the two. It is only when we consider the steric properties of the two that there is obviously a significant difference. However, as will be demonstrated during this section, the behaviour of these two ligands towards Cu^{II} centres is somewhat different.

The synthesis and characterisation of the Ag^{I}-NHC complex (**C25A**) derived from ligand precursor **L25** was described in Chapter 4. In stark contrast to the reactions to form Cu^{II}-NHC complexes **C19G**, **C22D** and **C23C**, which produced yellow-green solutions with copious off-

white precipitate (AgBr), reaction of one equivalent of $CuBr_2$ with **C25A** at room temperature, instead produced a dark yellow/brown solution, with AgBr precipitate. After filtration to remove the precipitated silver halide, and reduction of the solvent *in vacuo*, addition of excess diethyl ether induced the precipitation of a golden-yellow powder, which was initially assumed to be the desired Cu^{II}-NHC complex (Scheme 5.7). However, analysis by NMR spectroscopy was possible, indicating that the product formed was diamagnetic and thus presumably not a Cu^{II}-NHC complex (Figure 5.16).

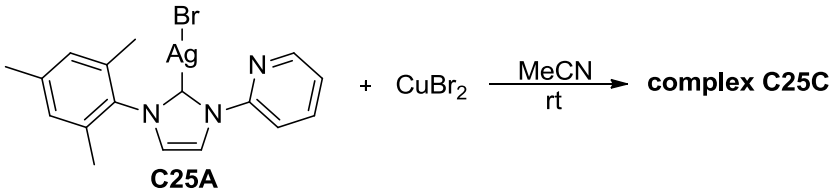

Scheme 5.7 Reaction to form complex **C25C**

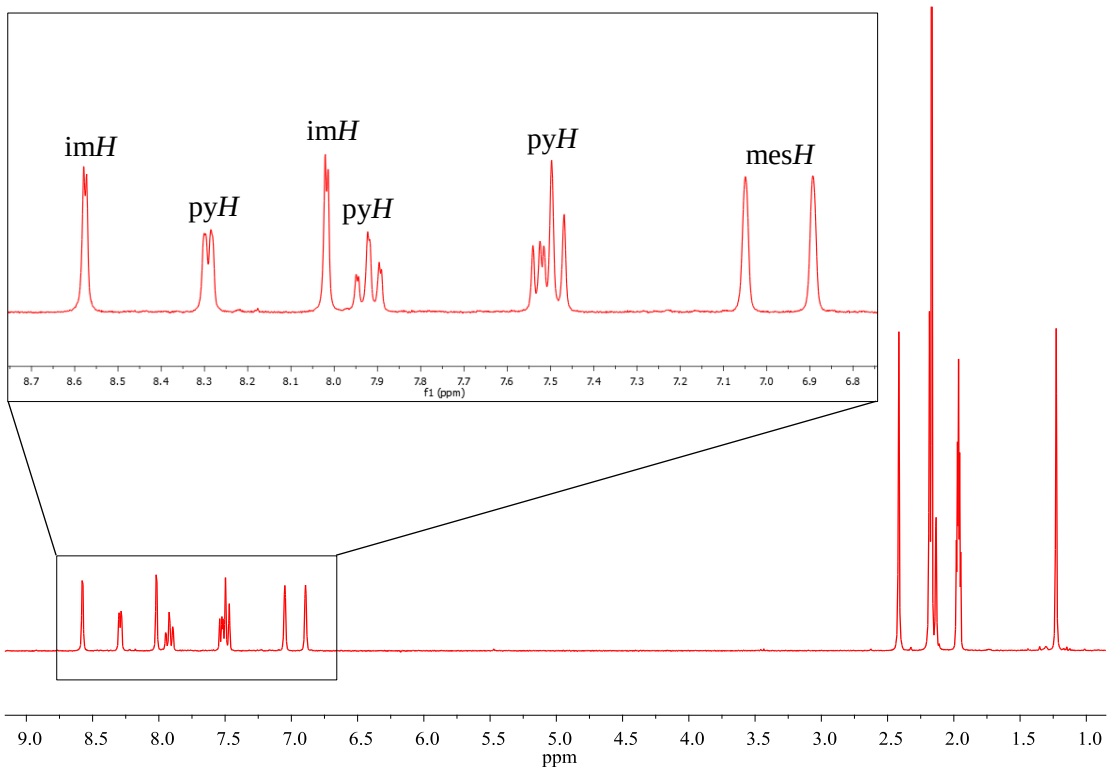

Figure 5.16 ^{1}H NMR spectrum of **C25C** (300 MHz, CD_3CN)

Figure 5.16 illustrates the ^{1}H NMR spectrum of **C25C**, where the aromatic region of the spectrum has been enlarged for clarity. Inspection of the spectrum reveals that there are the expected number of chemically inequivalent NHC backbone and pyridyl protons. Tellingly however, the aromatic mesityl protons, which are normally observed as one singlet resonance, are observed in two different environments (singlet peaks at 6.87 and 7.03 ppm). Also, the mesityl methyl protons, which are normally observed as two singlet peaks with a 1:2 ratio, are

instead observed as three singlet resonances (at 2.39, 2.16 and 1.20 ppm) with a ratio of 1:1:1. The particularly large upfield shift (1.20 ppm) of one of the mesityl methyl proton environments suggests that these protons are highly shielded, perhaps by interaction of these protons with the ring current on another neighbouring aromatic system. Furthermore, the splitting of all of the mesityl proton environments (both aromatic and methyl), suggests restricted rotation about certain bonds within the structure.

Strong evidence about the exact nature of **C25C** was provided by high-resolution mass spectrometry, where the dominant molecular ion corresponded to a $[2(\text{imidazolium}) - 2H]^{2+}$ fragment. The exact nature of complex **C25C** was finally confirmed using a combination of both elemental analysis and single crystal X-ray diffraction, with the crystals for X-ray diffraction analysis being obtained from the vapour diffusion of diethyl ether in to a concentrated solution of the product in acetonitrile. Complex **C25C** was found to crystallise in the triclinic crystal system, with the structural solution being performed in the space group $P\bar{1}$ (Figure 5.17).

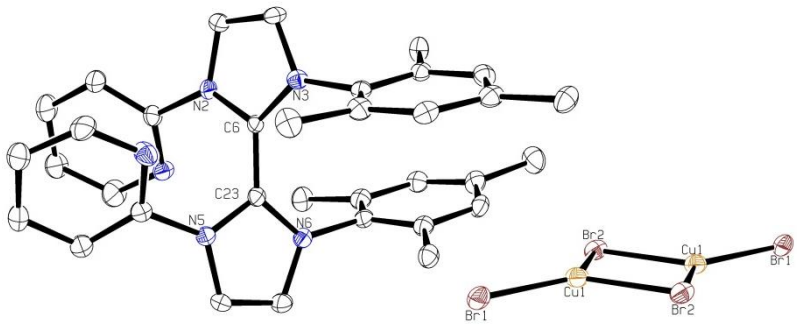

Figure 5.17 Molecular structure of **C25C**. Ellipsoids are drawn at the 30% probability level. H atoms have been omitted for clarity

Table 5.8 Selected bond distances (Å), angles and torsion angles (deg) for **C25C**

C(6)-C(23)	1.454(8)	Br(1)-Cu(1)-Br(2)	126.74(6)
N(2)-C(6) / N(3)-C(6)	1.343(8) / 1.353(8)	Br(1)-Cu(1)-Br(2')	128.19(6)
N(5)-C(23) / N(6)-C(23)	1.346(9) / 1.362(8)	Br(2)-Cu(1)-Br(2')	104.73(5)
Cu(1)-Br(1)	2.336(2)	N(2)-C(6)-C(23)-N(5)	54(1)
Cu(1)-Br(2)	2.427(1)	N(3)-C(6)-C(23)-N(6)	70.6(9)
Cu(1)-Br(2')	2.441(2)		

Surprisingly, the golden-yellow product of the reaction (>80% isolated yield) between **C25A** and one equivalent of $CuBr_2$ was found to be a C-C coupled *bis*-imidazolium salt with a Cu^{I}-containing $Cu_2Br_4^{2-}$ anion. The structure is confirmed as a *bis*-imidazolium salt, rather than as its 2 electron-reduced enetetraamine counterpart by the presence of a counteranion, the relatively long C-C bond length (C6-C23) observed in **C25C** (1.45 Å) and the lack of coplanarity between the two 5-membered heterocyclic rings (Figure 5.18).

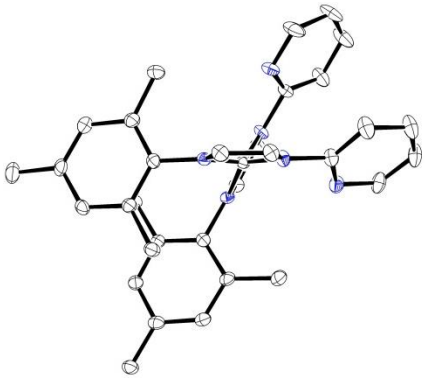

Figure 5.18 View along the C-C (C6-C23) bond axis of **C25C**. Ellipsoids are drawn at the 30% probability level. $Cu_2Br_4^{2-}$ anion and H atoms have been omitted for clarity

Under identical reaction conditions then (room temperature, < 24 hours), the two similar Ag^{I}-NHC complexes (**C19B** and **C25A**) demonstrated remarkably divergent reactivity with one equivalent of $CuBr_2$ (Scheme 5.8).

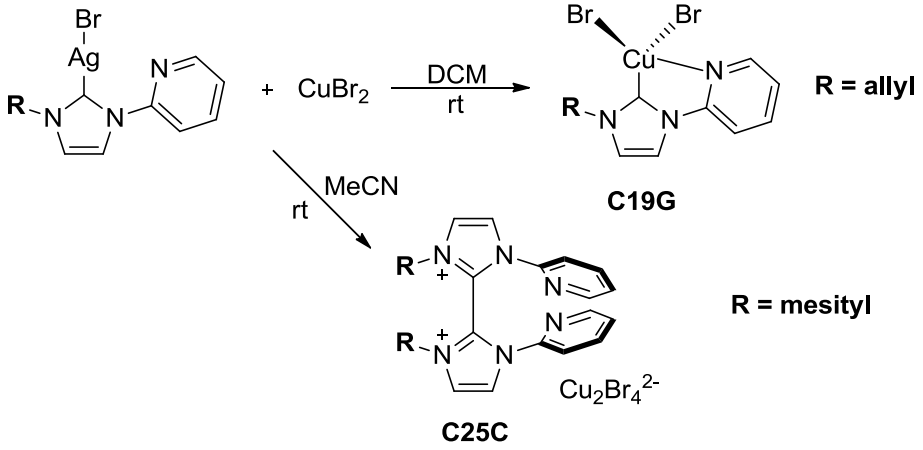

Scheme 5.8 Formation of either **C19G** or **C25C** by reaction of a Ag^{I}-NHC complex with $CuBr_2$

When **R** is allyl, the corresponding Cu^{II}-NHC complex (**C19G**) is isolated as the only product. However, when **R** is mesityl, the C-C coupled *bis*-imidazolium salt (**C25C**) is isolated as the sole product from the reaction, in very good yield. The latter reaction represents a C-C bond-forming reaction occurring under exceptionally mild conditions. This reactivity is particularly unusual, especially when considering that the majority of the $C_{carbene}$-C bond-forming reactions described so far in the literature have involved either $C_{carbene}$-C reductive elimination reactions

from group 10-NHC complexes,[26] or migratory insertion reactions.[27] These, and related NHC decomposition processes, were discussed in a recent book.[28] To our knowledge however, the decompositorial C-C coupling of two NHC ligands to form a *bis*-imidazolium salt is unprecedented.

In order to further exemplify this seemingly novel C-C coupling chemistry within the coordination sphere of copper, a structurally similar ligand precursor (to **L25**) containing a *para*-methylpyridine *N*-substituent was synthesised. The synthetic procedure followed was similar to that used for the synthesis of **L25**, *i.e*. a dry melt. The *para*-methylpyridine-substituted ligand precursor (**L26**) was obtained in somewhat poorer yield (44%) than ligand precursor **L25** (91%), which was explained by the concomitant formation of an intractable black oily solid, along with the product (**L26**). Ligand precursor **L26** was subject to full characterisation, including by elemental analysis and single crystal X-ray diffraction analysis. The single crystals were obtained *via* the vapour diffusion of diethyl ether in to a concentrated solution of the product in acetonitrile. **L26** was found to crystallise in the monoclinic crystal system, with the structural solution being performed in the space group *C*2/c (Figure 5.19).

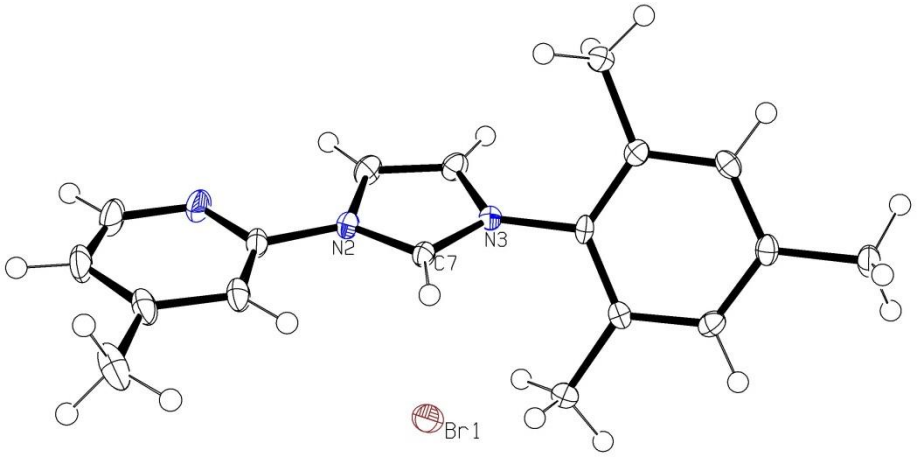

Figure 5.19 Molecular structure of **L26**. Ellipsoids are drawn at the 50% probability level

Reaction of **L26** with Ag_2O at reflux in dichloromethane led to the loss of the C2 proton of the imidazolium salt, as indicated by ^{1}H NMR spectroscopy, indicating that complexation to a Ag^I centre had been successful. Further analysis by high-resolution MS illustrated a $[Ag(NHC)_2]^+$ fragment as the dominant ion. Analysis by proton-decoupled ^{13}C NMR spectroscopy did not illustrate a resonance corresponding to the carbenic carbon atom, which is presumably due to the fluxional behaviour of the complex in solution. Single crystals of the Ag^I-NHC complex (**C26A**) could be obtained *via* the vapour diffusion of pentane in to a concentrated chloroform solution (Figure 5.20).

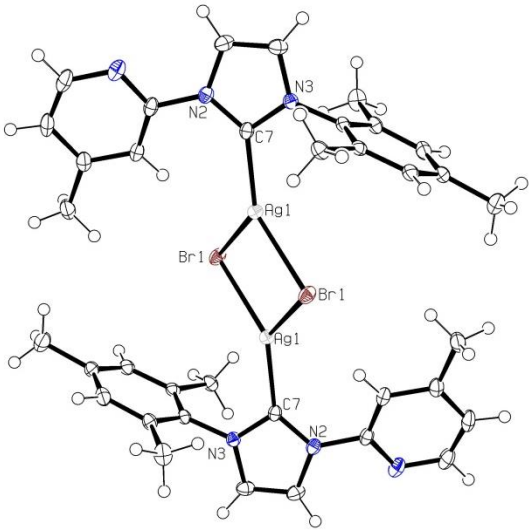

Figure 5.20 Molecular structure of **C26A**. Ellipsoids are drawn at the 50% probability level

Complex **C26A** crystallised as a $(\mu\text{-Br})_2$-bridged dimer, which is slightly surprising when mindful of the considerable steric bulk of the mesityl and pyridyl *N*-substituents. Moreover, there appears to be a notably short interaction between one of the pyridyl H atoms (labelled H5) and the silver and bromine atoms (labelled Ag1 and Br1) of the $(\mu\text{-Br})_2$-bridged core, which is highlighted in Figure 5.21. This is suggested to be a significant attractive interaction on the basis that the pyridyl ring appears to be inclined to facilitate this interaction (torsion angle of approximately 21° between the NHC and pyridyl rings). If no attractive interaction were present, the pyridyl ring would be expected to incline away from the $(\mu\text{-Br})_2$-bridged core (to give a torsion angle of approximately 90° between the NHC and pyridyl rings) in order to minimise its steric impact on the large silver and bromine atoms, just as the mesityl aromatic rings appear to do.

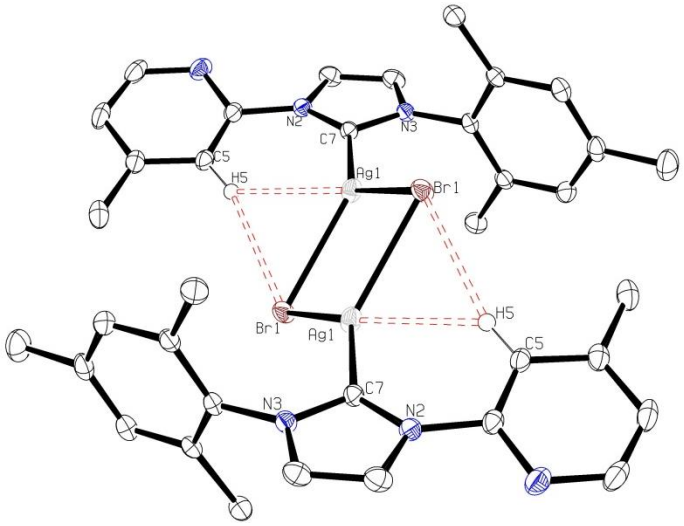

Figure 5.21 Molecular structure of **C26A** illustrating H---Ag/Br interaction (red dashed lines). Ellipsoids are drawn at the 50% probability level. Most H atoms have been omitted for clarity

Since the hydrogen atoms of **C26A** were placed in calculated positions and refined using a riding model, a quantitatively accurate discussion of H---Ag/Br contact distances is not possible. However, assuming that the geometrically constrained pyridyl C-H bond length (labelled C5-H5) of 0.95 Å is a reasonably accurate reflection of reality, the H atom approaches the silver and bromine atoms at distances of 2.65 and 2.97 Å respectively, both of which fall well within the sum of the Van der Waals radii. The H---Ag interaction is particularly short, and is a full 0.27 Å shorter than the sum of the Van der Waals radii (2.92 Å).[29] While it might be tempting to assign this as an agostic-type interaction, Desiraju *et al*. warned against this approach. Instead, owing to the contact angles (C5-H5---Ag1 and C5-H5---Br1) being greater than 100°, the assignment of the H---Ag/Br interactions as a bifurcated hydrogen bond between two hydrogen bond acceptors (Ag and Br) is somewhat more accurate.[30] Indeed, Braga *et al*. termed such an interaction as an 'intermolecular multicentre hetero-acceptor (IMH) hydrogen bond'. IMH interactions were explained to require the interaction of a suitable hydrogen bond donor with an electron-rich metal centre bound to an electronegative main group atom.[31] In the case of compound **C26A**, the hydrogen atom labelled H5 (bound to the electron-poor pyridyl ring) acts as the hydrogen bond donor, the Ag^{I} centre acts as the electron-rich metal centre and the bromine atom acts as the electronegative main group atom.

Analogously to the formation of the C-C coupled product **C25C**, reaction of one equivalent of the Ag^{I}-NHC complex **C26A** with $CuBr_2$ in anhydrous acetonitrile led to the formation of a yellow powder (**C26B**) following work-up. Analysis of this yellow powder by NMR spectroscopy was again possible, indicating the presence of a diamagnetic material (Figure 5.22).

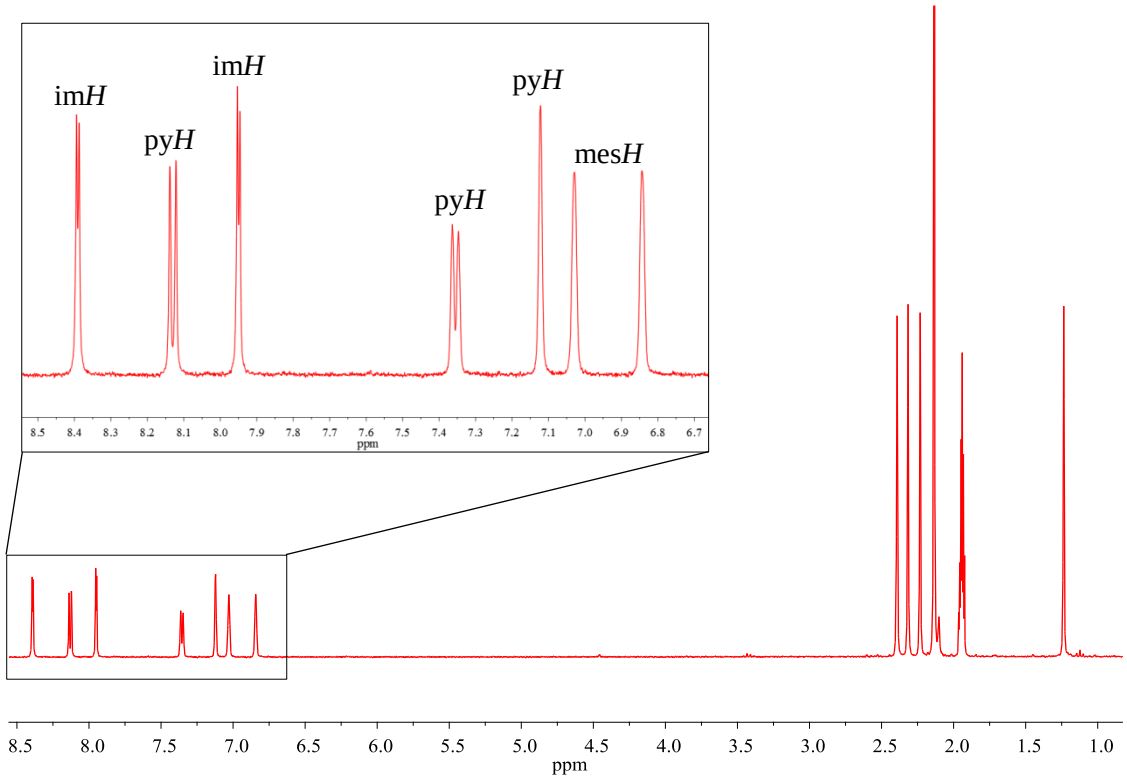

Figure 5.22 ^{1}H NMR spectrum of **C26B** (300 MHz, CD_3CN)

The NMR spectrum of **C26B** has been provided above, with the aromatic region enlarged for the sake of discussion. Similarly to compound **C25C**, the mesityl aromatic protons are non-equivalent, and are observed as singlet resonances at 6.84 and 7.03 ppm. The reason for this, which is clear on examination of the molecular structure of **C25C**, is restricted rotation about the *bis*-imidazolium C-C bond (labelled C7-C25 in Figure 5.23). Yellow needles suitable for X-ray diffraction analysis could be obtained *via* the vapour diffusion of diethyl ether in to a concentrated solution of **C26B** in acetonitrile. The crystals were found to belong to the triclinic crystal system, with the structural solution being performed in the space group $P\bar{1}$ (Figure 5.23). Compound **C26B** was found to be structurally analogous to **C25C**, containing a single bond between the two imidazolium C2 carbon atoms (labelled C7-C25).

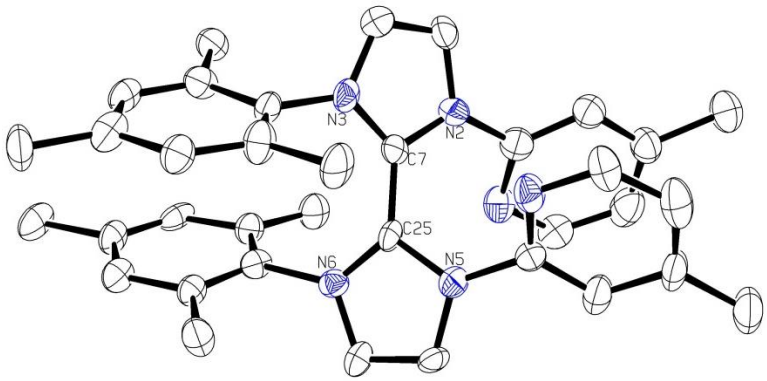

Figure 5.23 Molecular structure of **C26B**. Ellipsoids are drawn at the 50% probability level. H atoms and $Cu_2Br_4^{2-}$ anion have been omitted for clarity

Table 5.9 Selected bond distances (Å) and torsion angles (deg) for **C26B**

C(7)-C(25)	1.47(1)	N(2)-C(7)-C(25)-N(5)	45(1)
N(2)-C(7) / N(3)-C(7)	1.34(1) / 1.34(1)	N(3)-C(7)-C(25)-N(6)	61(1)
N(5)-C(25) / N(6)-C(25)	1.37(1) / 1.34(1)		

The mesityl methyl protons of **C26B** are observed in three unique chemical environments with a ratio of 1:1:1. One of these proton resonances is shifted significantly upfield (1.24 ppm) due to interaction with the aromatic ring current region of the neighbouring mesityl aromatic system, which is depicted graphically in Figure 5.24.

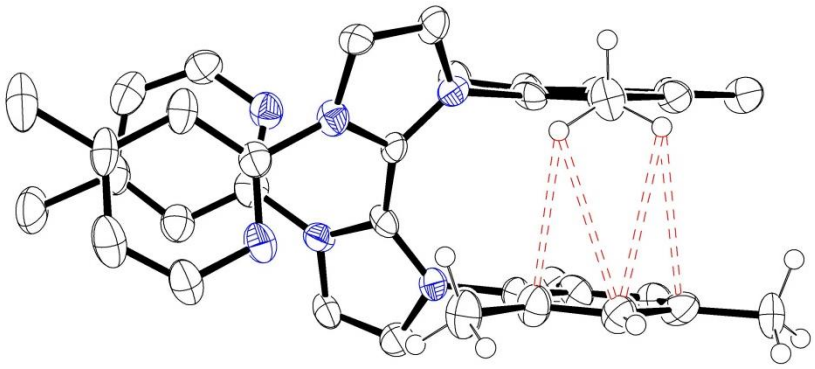

Figure 5.24 Molecular structure of **C26B** illustrating π-H interaction (red dashed lines). Ellipsoids are drawn at the 50% probability level. Most H atoms and $Cu_2Br_4^{2-}$ anion have been omitted for clarity

Thus, this reactivity appears to be more general than just a 'one-off', and may be operative as a catalyst decomposition pathway in certain Cu-NHC-catalysed reactions. To gain a deeper mechanistic understanding of this rather unique C-C coupling chemistry, DFT calculations were again performed. For the sake of clarity, the overall mechanism has been split in to two, and each part shall be discussed in turn (Schemes 5.9a and 5.9b).

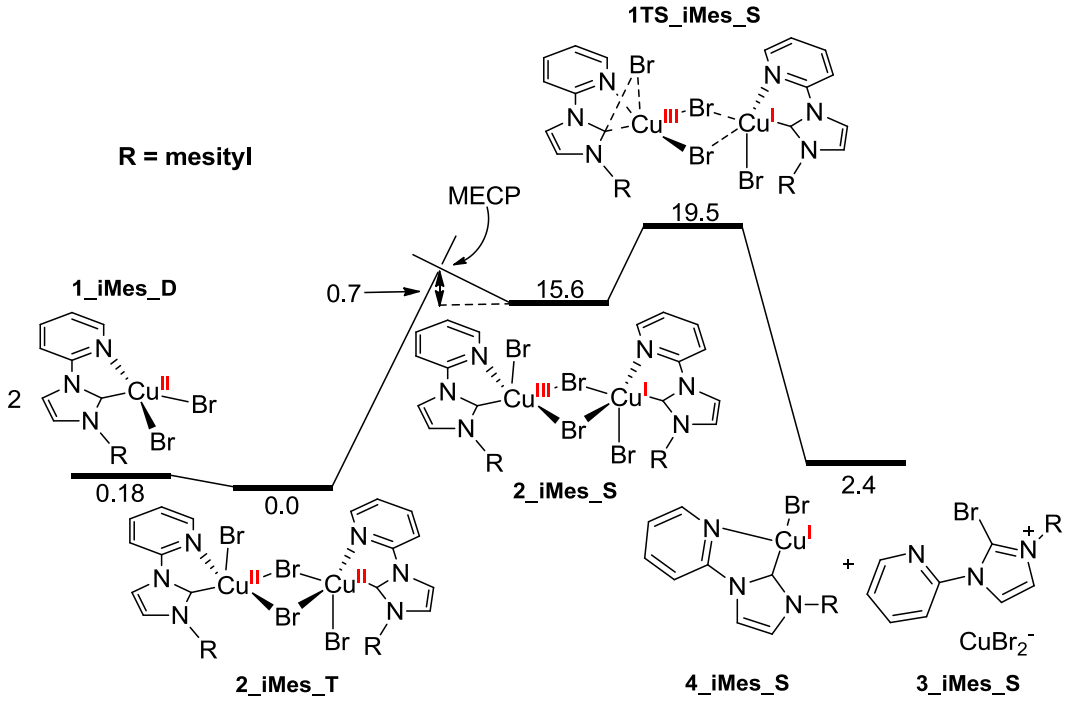

Scheme 5.9a Proposed mechanistic pathway (part 1) for *bis*-imidazolium formation (relative free energies in kcal mol^{-1}) (MECP = minimum energy crossing point)

Initially (not shown above), a transmetallation reaction occurs forming a Cu^{II}-NHC complex (**1_iMes_D**), as is evident in the immediate appearance of a large quantity of an off-white precipitate (AgBr). This complex then dimerises forming a $(\mu\text{-Br})_2$-bridged dimer, which would presumably be structurally similar to those in the solid-state structure of **C19G**. The dimerisation process is likely to be reversible due to the negligible energetic difference between the monomer (**1_iMes_D**) and $(\mu\text{-Br})_2$-bridged dimer (**2_iMes_T**). However, the $(\mu\text{-Br})_2$-bridged dimer is able to undergo a disproportionation process, with a reasonably low barrier (ΔG = 16.3 kcal mol^{-1}), forming a mixed valent binuclear $(\mu\text{-Br})_2$-bridged Cu^{I}-Cu^{III} complex (**2_iMes_S**). The Cu^{III} centre then undergoes a facile reductive elimination reaction ($\Delta G^{\ddagger}$ = 3.9 kcal mol^{-1}) of a haloimidazolium salt (**3_iMes_S**) and at the same time, one molecule of a Cu^{I}-NHC complex (**4_iMes_S**) is formed. This Cu^{I}-NHC complex is likely to have the same structure as complex **C25B**, which was described in Chapter 4. Overall, this first part of the mechanism is slightly endergonic (ΔG = 2.4 kcal mol^{-1}) and thus a non-spontaneous process. The second part of the mechanism (Scheme 5.9b) is, however, an exergonic process, which therefore acts to thermodynamically 'pull' the first part of the reaction to completion.

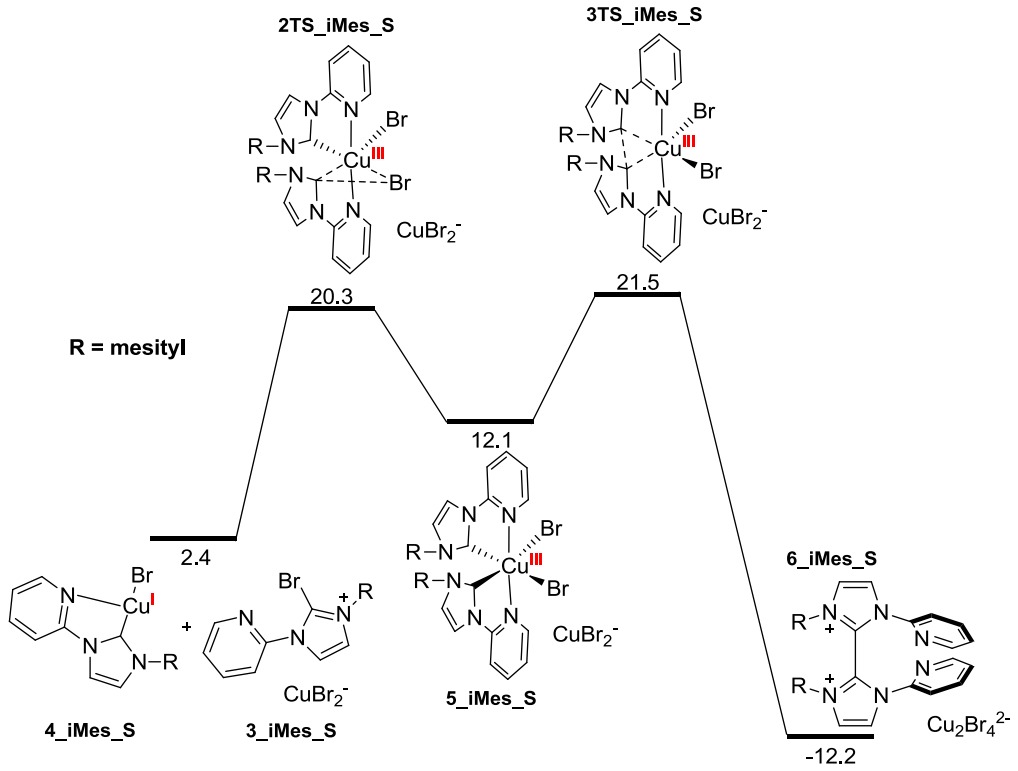

Scheme 5.9b Proposed mechanistic pathway (part 2) for *bis*-imidazolium formation (relative free energies in kcal mol^{-1})

As illustrated in Scheme 5.9b, the Cu^{I}-NHC complex (**4_iMes_S**) then oxidatively adds the haloimidazolium salt (**3_iMes_S**), forming an octahedral Cu^{III}-NHC complex (**5_iMes_S**), where the NHC donors have a *cis* arrangement with respect to each other and the two pyridyl donors have a *trans* arrangement. The Cu^{III}-NHC complex (**5_iMes_S**) is calculated to be highly stabilised by the presence of strong π-π stacking interactions between the electron-rich mesityl aromatic substituents and electron-poor pyridyl aromatic substituents (Figure 5.25).

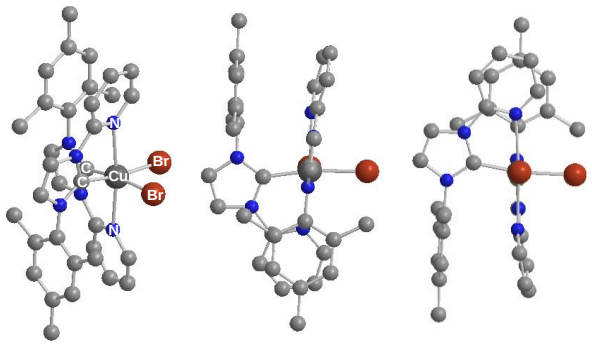

Figure 5.25 Calculated stabilising π-π stacking interaction in the postulated Cu^{III}-NHC complex (**5_iMes_S**)

The final step of the reaction mechanism is reductive elimination of the two *cis* NHC donors of the Cu^{III}-NHC complex (**5_iMes_S**), which occurs with a relatively low activation barrier ($\Delta G^{\ddagger}$

= 9.4 kcal mol^{-1}), forming the *bis*-imidazolium salt (complex **C25C**). This final step of the reaction is exergonic, which renders the overall mechanism exergonic under the reaction conditions employed (ΔG = -12.2 kcal mol^{-1}).

The complete mechanism comprises a surprisingly complex disproportionation-reductive elimination-oxidative addition-reductive elimination (DROR) pathway, which to the best of our knowledge, is unprecedented. It is especially unusual when considering the fact that NHC ligands are generally considered to be redox innocent ligands, yet in this reaction, one of the NHC ligands undergoes a successive 1 electron oxidation-reduction-oxidation process.

To provide some evidence in support of this reaction pathway, the synthesis and subsequent reaction of postulated intermediate(s) in this reaction mechanism was attempted. The most obvious target intermediates were the Cu^{I}-NHC complex (**4_iMes_S**) and haloimidazolium salt (**3_iMes_S**), both of which are highlighted in Scheme 5.10. The reaction of these molecules under identical conditions to those used in the reaction of Ag^{I}-NHC complex **C25A** with one equivalent of $CuBr_2$, should yield the *bis*-imidazolium salt (complex **C25C**).

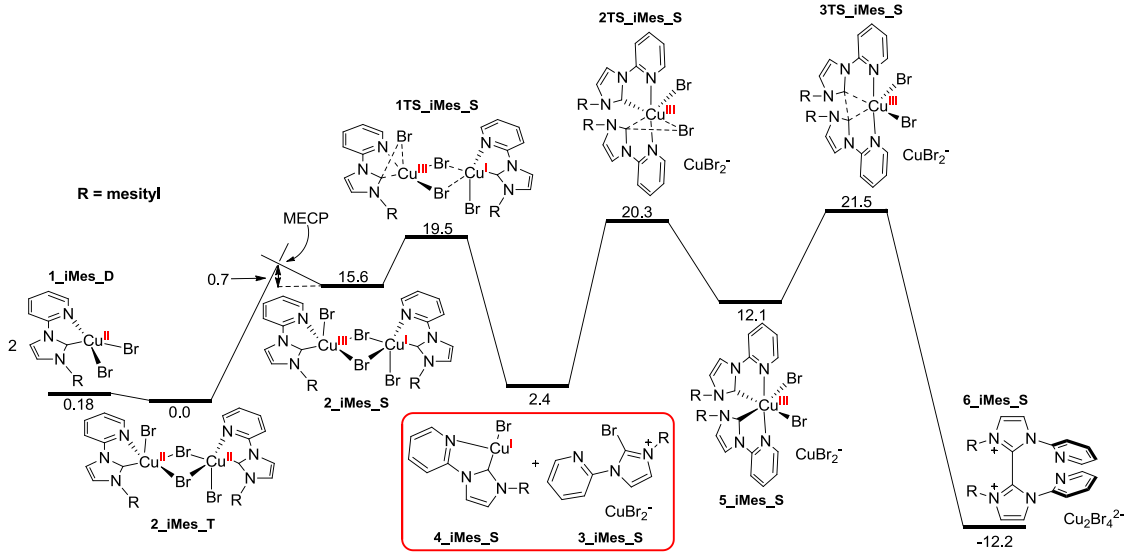

Scheme 5.10 Proposed mechanistic pathway for *bis*-imidazolium formation (relative free energies in kcal mol^{-1}) (MECP = minimum energy crossing point)

The synthesis and characterisation of Cu^{I}-NHC complex (**4_iMes_S**) was described in Chapter 4 (complex **C25B**), where its activity in an Ullmann-type coupling reaction was examined. The synthesis of the haloimidazolium salt (**3_iMes_S**) had not however been attempted previously. Using a modified literature procedure first reported by Metrangolo and Resnati *et al.*,[32] reaction of the imidazolium salt **L25** with a slight excess of the brominating agent *N*-bromosuccinimide (NBS) led to the clean formation of the corresponding haloimidazolium salt, **L27**, which was isolated in 72% yield as a white crystalline solid following work-up. Analysis of the compound by ^{1}H NMR spectroscopy indicated the expected loss of the imidazolium C2 proton.

Furthermore, elemental analysis confirmed the empirical formula and purity of haloimidazolium salt, **L27**. Single crystals of **L27** suitable for X-ray diffraction analysis could be obtained *via* the vapour diffusion of diethyl ether in to a concentrated solution of the product in acetonitrile. **L27** was found to crystallise in the triclinic crystal system, with the structural solution being performed in the space group $P\bar{1}$ (Figure 5.26).

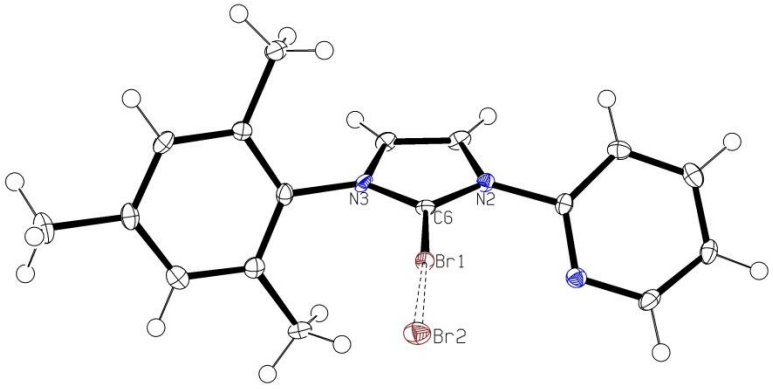

Figure 5.26 Molecular structure of **L27**. Ellipsoids are drawn at the 50% probability level. Possible halogen bond shown by dashes

The solid-state structure of **L27** reveals the expected structure, where substitution of the imidazolium C2 proton with a bromine atom has been successfully achieved. Of note in this structure is the presence of a strong halogen bond, with a separation of 3.16 Å between the two independent halogen atoms.

Reaction of haloimidazolium salt **L27** (**3_iMes_S**) with Cu^{I}-NHC complex **C25B** (**4_iMes_S**) in the presence of one equivalent of CuBr (used to form the $CuBr_2^-$ anion, to replicate **3_iMes_S** in the proposed mechanism) in anhydrous acetonitrile at room temperature again produced a dark yellow/brown solution, from which the *bis*-imidazolium salt (complex **C25C**) could be isolated as the only product in 83% yield (Scheme 5.11).

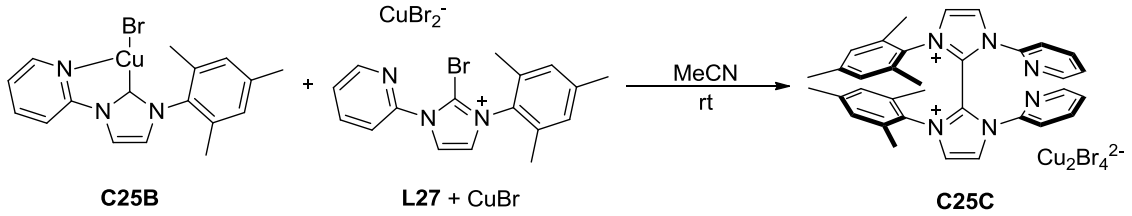

Scheme 5.11 Formation of complex **C25C** from the reaction of a haloimidazolium with a Cu^{I}-NHC complex

The fact that the *bis*-imidazolium salt (complex **C25C**) was the only isolable product from the reaction of haloimidazolium salt **L27** (**3_iMes_S**) with Cu^{I}-NHC complex **C25B** (**4_iMes_S**) in the presence of one equivalent of CuBr is fairly compelling evidence that this apparently novel DROR mechanism is in operation with this substrate. Furthermore, the occurrence of this

reactivity under extremely mild conditions warrants the consideration of this type of reaction pathway as a very plausible catalyst deactivation mechanism.

Possible NHC decomposition reaction mechanisms other than the DROR mechanism were also investigated computationally. These included both a radical-based process and a concerted nucleophilic attack by an NHC on a haloimidazolium salt. However, both of these alternative reaction mechanisms were found to be energetically unfeasible under the extremely mild reaction conditions used. For instance, a possible concerted-type reaction mechanism was found to have a very high activation barrier ($\Delta G^{\ddagger}$ = 40.8 kcal mol^{-1}) under the reaction conditions used (Scheme 5.12). It is postulated that the strength of the π-π stacking interaction between the electron-rich mesityl and electron-poor pyridyl rings is one of the main contributing factors as to why the formation of the *bis*-imidazolium salt occurs *via* the DROR mechanism rather than any other mechanism. The coordination of the pyridyl donors to the high oxidation state Cu^{III}-NHC complex also appears to have a significant stabilising role.

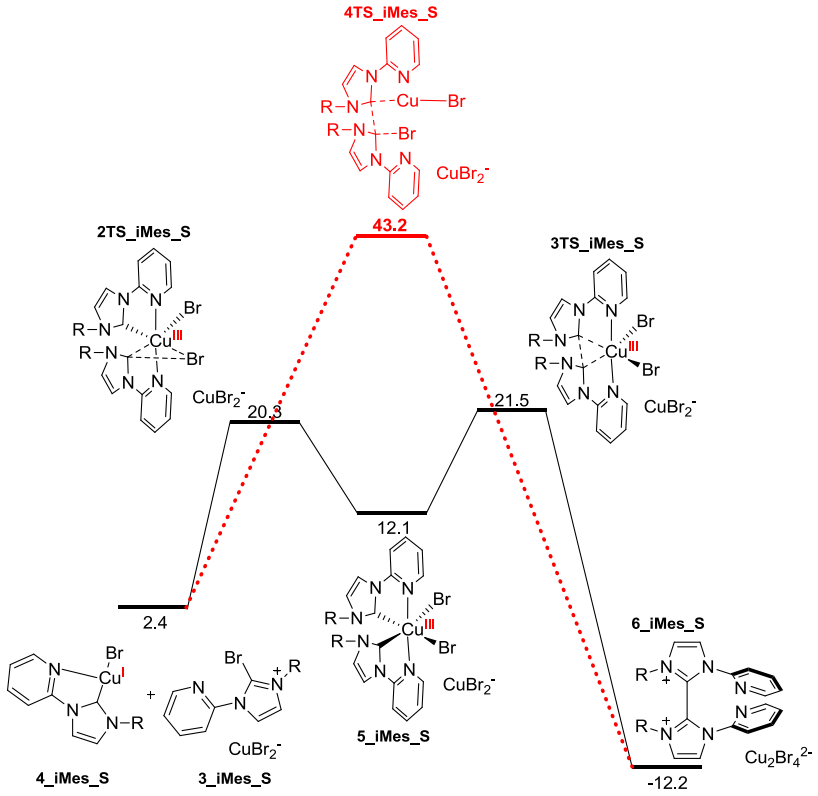

Scheme 5.12 Proposed mechanistic pathway (part 2) including possible concerted-type pathway (shown in red) for *bis*-imidazolium formation (relative free energies in kcal mol^{-1})

Given the apparent energetic feasibility of the DROR mechanism, it is perhaps surprising then that the Cu^{II}-NHC complexes **C19G**, **C22D** and **C23C** appeared to be stable under the reaction conditions used for their synthesis. In theory, these allyl-containing Cu^{II}-NHC complexes, once formed, should be susceptible to the same type of decomposition reactivity as the mesityl-containing Cu-NHC complex. Particularly as the pyridyl donors of the allyl-containing Cu^{II}-

NHC complexes would be as capable of stabilising the high oxidation state Cu^{III}-NHC complex as the mesityl-containing Cu^{II}-NHC complex. In order to investigate this apparent disparity in reactivity between the allyl- and mesityl-containing Cu^{II}-NHC complexes, DFT calculations were performed on the possible decomposition of the allyl-containing complex **C19G** (Scheme 5.13).

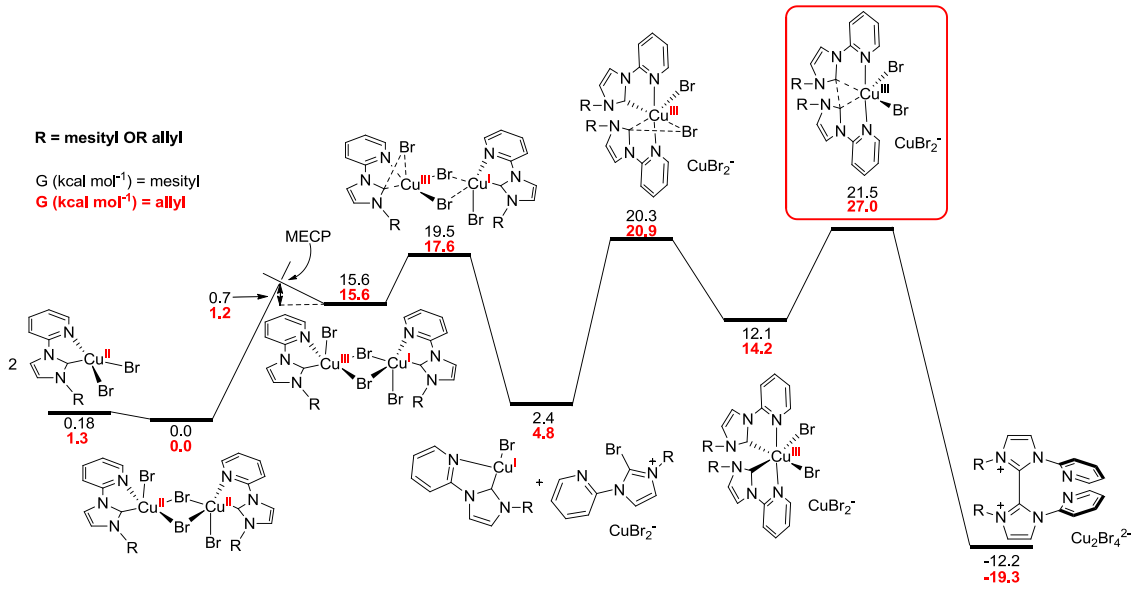

Scheme 5.13 Proposed mechanistic pathway for *bis*-imidazolium formation from allyl- (red) or mesityl-containing (black) Cu^{II}-NHC complexes (relative free energies in kcal mol^{-1}) (MECP = minimum energy crossing point)

Scheme 5.13 provides the relative free energies (in kcal mol^{-1}) of the starting materials, intermediates, transition states and final products in the postulated mechanism of *bis*-imidazolium formation, for both the allyl- and mesityl-containing examples. While most of the values are rather similar, a large difference between the calculated Gibbs free energy values occurs for the transition state of the reductive elimination of the *bis*-imidazolium from the Cu^{III}-NHC complex (indicated by the red box in Scheme 5.13). In this case, the transition state for the reductive elimination of the *bis*-imidazolium from an allyl-containing Cu^{III}-NHC complex is calculated to be 5.5 kcal mol^{-1} more endergonic than reductive elimination from a mesityl-containing Cu^{III}-NHC complex. Furthermore, the activation energy for the reductive elimination of a haloimidazolium salt ($\Delta G^{\ddagger}$ = 6.7 kcal mol^{-1}) from an allyl-containing Cu^{III}-NHC complex is significantly lower than the activation energy for the reductive elimination of a *bis*-imidazolium salt ($\Delta G^{\ddagger}$ = 12.8 kcal mol^{-1}). This is presumably due to the absence of strong, stabilising π-π interactions between electron-rich and electron-poor aromatic systems. Thus, even if an allyl-containing Cu^{III}-NHC complex were formed during the reaction, *via* the oxidative addition of a haloimidazolium salt to a Cu^{I}-NHC complex, the reverse reaction (reductive elimination of a haloimidazolium salt) to re-form the haloimidazolium salt and Cu^{I}-NHC complex is somewhat

more energetically favourable than the reductive elimination of a *bis*-imidazolium salt. Conversely, reductive elimination of a haloimidazolium salt ($\Delta G^{\ddagger}$ = 8.2 kcal mol^{-1}) from a mesityl-containing Cu^{III}-NHC complex is only fractionally more favourable than reductive elimination of a *bis*-imidazolium salt ($\Delta G^{\ddagger}$ = 9.4 kcal mol^{-1}) from the same complex. These energetic differences help illustrate why the *bis*-imidazolium salt is the only isolable product when there is a mesityl *N*-substituent, while the Cu^{II}-NHC complex is the only isolable product when there is an allyl *N*-substituent.

Therefore, it is clear that subtle differences in ligand design can have remarkable effects on the ultimate fate of the ligand and metal centre during a complexation reaction, and thus presumably, during a catalytic cycle. Indeed, the irreversible loss of the mesityl-tethered NHC ligand (derived from ligand precursor **L25**) *via* this facile $C_{carbene}$-$C_{carbene}$ coupling reaction may provide an explanation as to why this ligand performs no better than CuI alone during the Ullmann-type coupling reactions described in Chapter 4.

It has been observed that the proposed intermediates (a haloimidazolium salt and a Cu^{I}-NHC complex) of the DROR mechanism can react to form a C-C coupled *bis*-imidazolium salt (Scheme 5.11) and that the formation of a *bis*-imidazolium salt from an allyl-substituted Cu^{II}-NHC complex is not observed under the reaction conditions used. On this basis, we sought to synthesise a *bis*-imidazolium salt containing two different *N*-substituents (including one allyl *N*-substituent) *via* reaction of differently-substituted haloimidazolium salts and Cu^{I}-NHC complexes (Figure 5.27 and Scheme 5.14).

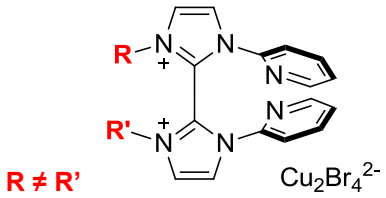

Figure 5.27 Target hetero-*bis*-imidazolium salt

To synthesise the target compound, mesityl-containing haloimidazolium salt **L27** was reacted with allyl-containing Cu^{I}-NHC complex **C19C** in the presence of one equivalent of CuBr (used to form the $CuBr_2^-$ anion) in anhydrous acetonitrile at room temperature (Scheme 5.14).

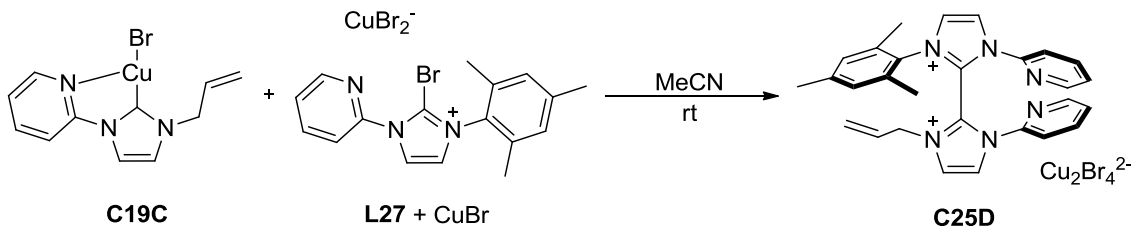

Scheme 5.14 Attempted formation of complex **C25D** from the reaction of a haloimidazolium with a Cu^{I}-NHC complex

Following work-up, a brown oily solid was obtained, which was analysed by NMR spectroscopy and high-resolution MS. The ^{1}H NMR spectrum of the oily solid revealed a mixture of two different products, though the major product appeared to be the desired hetero-*bis*-imidazolium salt (**C25D**). An NMR spectrum of the reaction mixture is provided below (Figure 5.28). The easily identifiable resonances corresponding to the minor product are indicated by asterisks, while those of the major product (**C25D**) are unmarked.

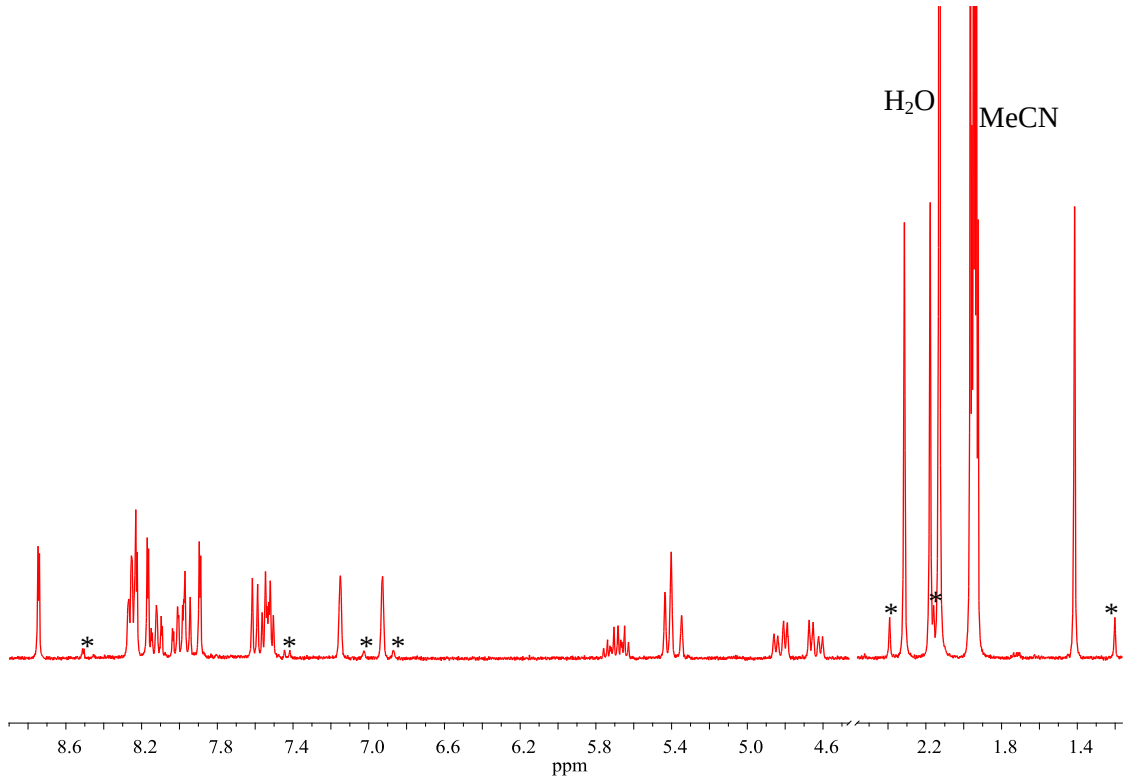

Figure 5.28 ^{1}H NMR spectrum of the product mixture formed by the reaction of **C19C** and **L27** in the presence of CuBr (* depicts the minor product – **C25C**) (300 MHz, CD_3CN)

Of note in the NMR spectrum above, is the splitting of the mesityl aromatic resonances belonging to the major product in to two singlet peaks at 6.93 and 7.15 ppm respectively, which is in accord with the NMR data obtained for the other two C-C coupled *bis*-imidazolium salts (**C25C** and **C26B**) synthesised thus far. This is compelling evidence that the major product of this reaction must be a *bis*-imidazolium salt. Furthermore, since the major product contains resonances which appear to belong to an allyl functional group and others which belong to a mesityl functional group, the major product can be safely assigned as the desired hetero-*bis*-imidazolium salt (**C25D**). Interestingly, the allyl methylene protons, which are normally observed as a doublet, have become diastereotopic, occurring as two doublet of doublet resonances centred at 4.64 and 4.82 ppm. This presumably occurs due to restricted rotation of the allyl group caused by the close proximity of a sterically demanding aromatic group (mesityl or pyridyl) in the structure of the hetero-*bis*-imidazolium salt (**C25D**).

The minor product observed in the reaction mixture can be identified as the homo-*bis*-imidazolium compound (**C25C)** by overlaying the spectrum obtained from this reaction with the spectrum of a sample of pure, fully characterised **C25C**. The overlain spectra are illustrated below in Figure 5.29. The ratio of the two products was measured to be approximately 20:1 (**C25D**:**C25C**) by ^{1}H NMR spectroscopy.

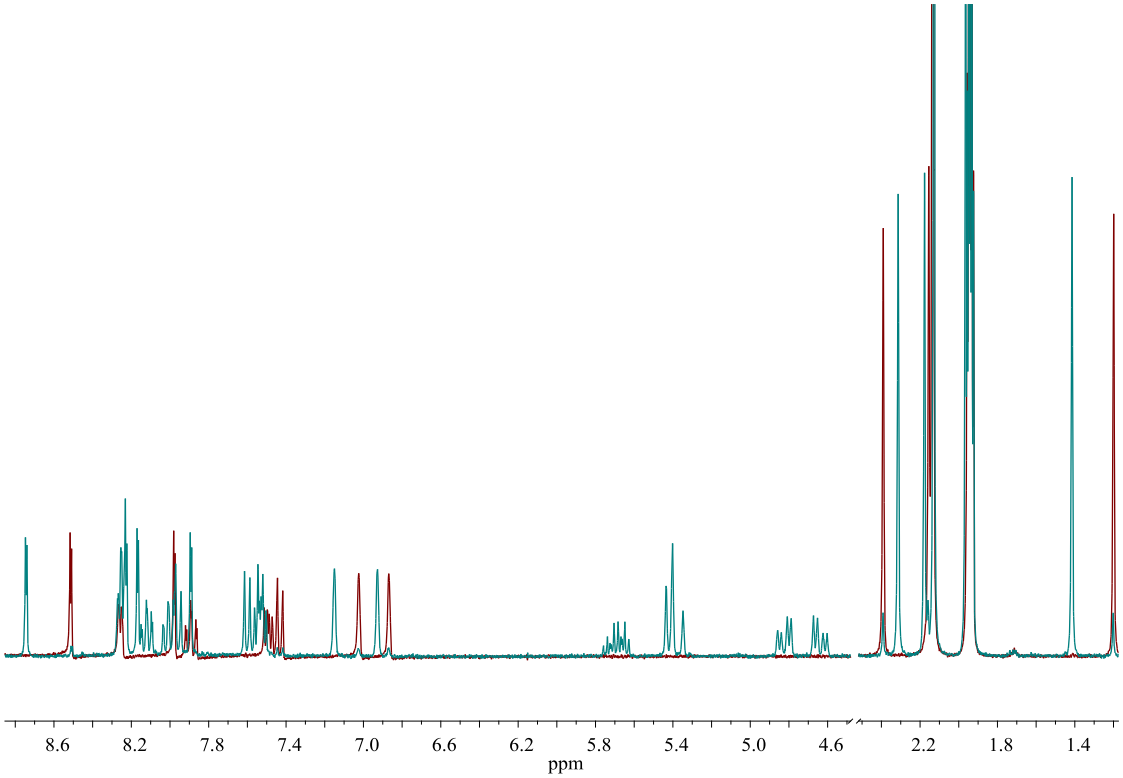

Figure 5.29 Overlay of the ^{1}H NMR spectra of the product mixture containing **C25D** and **C25C** (turquoise) and pure **C25C** (dark red) (300 MHz, CD_3CN)

The characterisation of the product mixture by elemental analysis and X-ray diffraction analysis was precluded by the oily nature of the product mixture. However, a high-resolution mass spectrum of the product mixture confirmed the presence of both the hetero-*bis*-imidazolium salt (**C25D**) and the homo-*bis*-imidazolium salt (**C25C**). The structural assignment of the cations observed in the mass spectrum is provided on the spectrum itself (Figure 5.30).

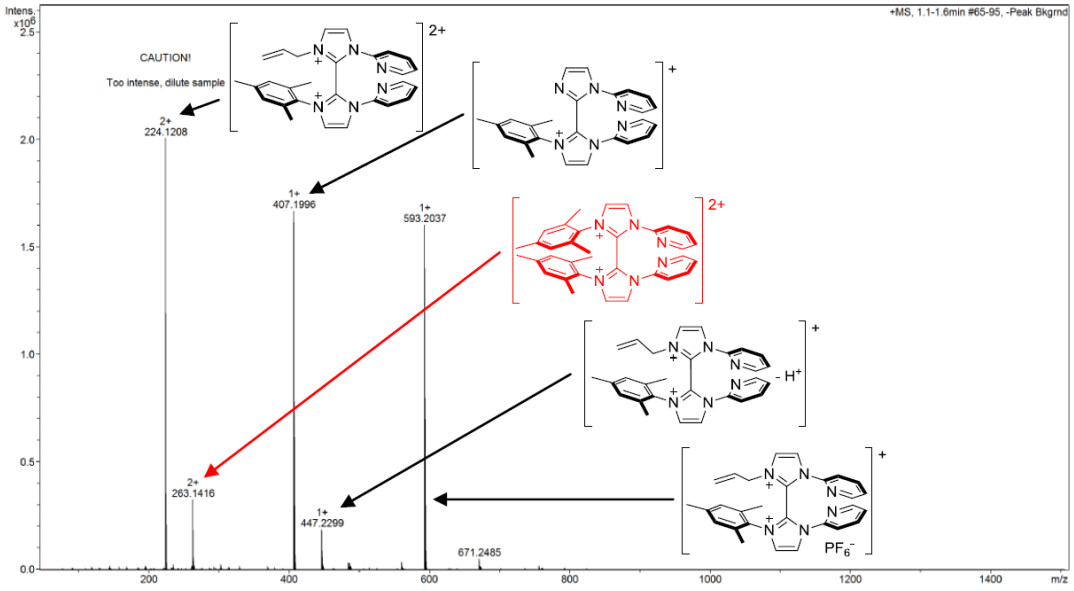

Figure 5.30 High-resolution mass spectrum of the product mixture (containing **C25C** and **C25D**)

The reaction of Cu^{I}-NHC complex **C19C** with haloimidazolium salt **L27** in the presence of one equivalent of CuBr to form a homo-*bis*-imidazolium salt (**C25C**) along with the desired hetero-*bis*-imidazolium salt (**C25D**) was somewhat unexpected (Scheme 5.15). It was anticipated that the hetero-*bis*-imidazolium salt (**C25D**) would be the only product of the reaction.

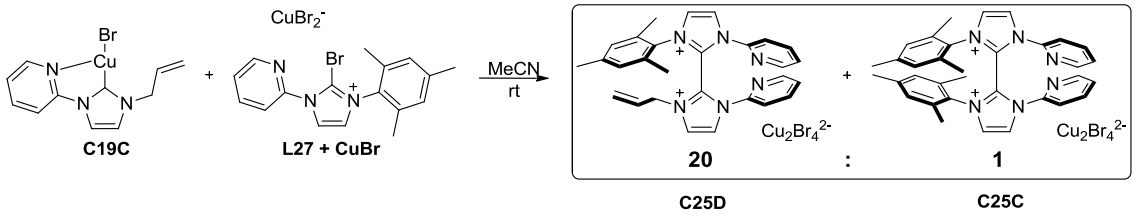

Scheme 5.15 Reaction of Cu^{I}-NHC complex **C19C** with haloimidazolium salt **L27** to form homo-*bis*-imidazolium salt (**C25C**) and hetero-*bis*-imidazolium salt (**C25D**)

It is suggested that the occurrence of homo-*bis*-imidazolium salt (**C25C**) in the reaction mixture, albeit in relatively modest amounts, further corroborates the proposed DROR mechanism described earlier. For instance, if the reaction of a Cu^{I}-NHC complex with haloimidazolium salt was to proceed *via* a concerted-type mechanism, proceeding from the starting materials *via* a transition state to the product, the formation of the homo-*bis*-imidazolium salt (**C25C**) would be impossible. However, the DROR mechanism can provide an explanation as to the appearance of the homo-*bis*-imidazolium salt (**C25C**) in the reaction mixture (Schemes 5.16 and 5.18).

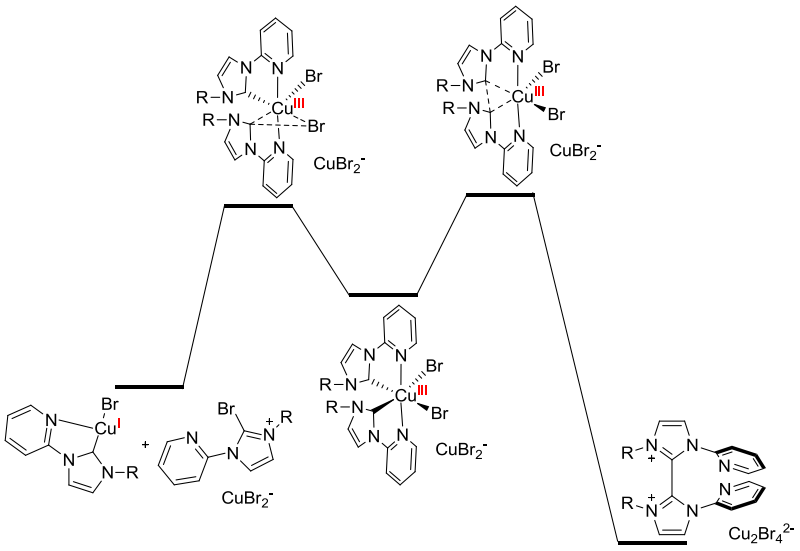

Scheme 5.16 Proposed mechanistic pathway (part 2) for *bis*-imidazolium formation

The DROR mechanism evokes the oxidative addition of a haloimidazolium salt (*e.g.* **L27**) to a Cu^{I}-NHC complex (*e.g.* **C19C**) to form a Cu^{III} *bis*-NHC complex intermediate. This intermediate can then follow one of three distinct reductive elimination pathways, one of which includes the reductive elimination of the hetero-*bis*-imidazolium salt (**C25D**) (Scheme 5.18). This is highly likely to be a terminal step in the reaction mechanism, since the oxidative addition of a *bis*-imidazolium salt to a low oxidation state metal centre is extremely unusual, to our knowledge having only been reported once in the literature, by Baker and co-workers.[33] In this example, the oxidative addition of the C-C bond of a bridged cyclophane-derived *bis*-imidazolium to Pd^{0} to form a Pd^{II} *bis*-NHC complex was reported, though the reaction was only successful under forcing conditions and where a highly reactive (with respect to oxidative addition) $[Pd(PPh_3)_2Br]^-$ species could be generated *in situ* (Scheme 5.17). Furthermore, unbridged *bis*-imidazolium salts (*i.e.* *bis*-imidazolium salts similar to **C25C** and **C25D**) were found to be completely unreactive with respect to oxidative addition to a Pd^{0} centre.

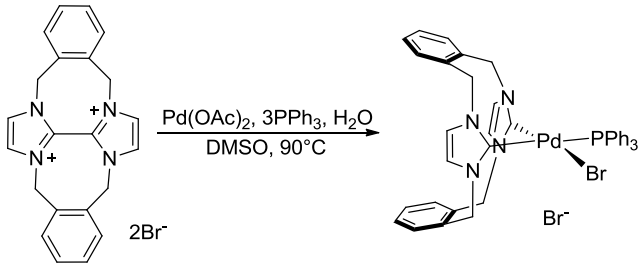

Scheme 5.17 Synthesis of a Pd^{II}-*bis*NHC complex *via* oxidative addition of the C-C bond of a bridged cyclophane-derived *bis*-imidazolium to Pd^{0} [33]

As explained above, the intermediate Cu^{III} *bis*-NHC complex (Scheme 5.18 – 'Intermediate 1') can undergo any of three distinct reductive elimination pathways, one of which comprised the irreversible reductive elimination of the hetero-*bis*-imidazolium salt (**C25D**). A second possible

pathway (from 'Intermediate 1') is reductive elimination to re-form the starting haloimidazolium salt (**L27**) and Cu^{I}-NHC complex (**C19C**). The third possible pathway is reductive elimination to form a different haloimidazolium salt (**C19K**) and Cu^{I}-NHC complex (**C25B**) (Scheme 5.18 – blue box). In this scenario, the haloimidazolium salt contains an allyl *N*-substituent and is likely to be structurally analogous to the haloimidazolium salt **C19K** described earlier. The Cu^{I}-NHC complex contains a mesityl *N*-substituent and is likely to be identical to the complex described in Chapter 4 (**C25B**). The two pairs of reactants (**C19C** & **L27** (green box) and **C19K** & **C25B** (blue box)) can then react together to re-form the Cu^{III} *bis*-NHC complex ('Intermediate 1'). Alternatively, **C25B** can oxidatively add the haloimidazolium salt **L27** (red box), as was demonstrated unambiguously earlier (Scheme 5.11). This reaction generates a different Cu^{III} *bis*-NHC complex ('Intermediate 2'), from which, reductive elimination can either re-form **C25B** and **L27**, or alternatively, irreversibly form homo-*bis*-imidazolium salt (**C25C**). Thus, the formation of the homo-*bis*-imidazolium salt (**C25C**) can be accounted for if the reaction proceeds *via* the DROR mechanism. It might be expected that allyl-substituted haloimidazolium salt **C19K** and allyl-substituted Cu^{I}-NHC complex **C19C** could react in a similar manner to form a different Cu^{III} *bis*-NHC complex, from which reductive elimination could produce an allyl-containing homo-*bis*-imidazolium salt. However, as described in Scheme 5.13 and its associated discussion, the reductive elimination of an allyl-containing homo-*bis*-imidazolium salt from a Cu^{III} *bis*-NHC complex is energetically unfavourable under the reaction conditions employed.

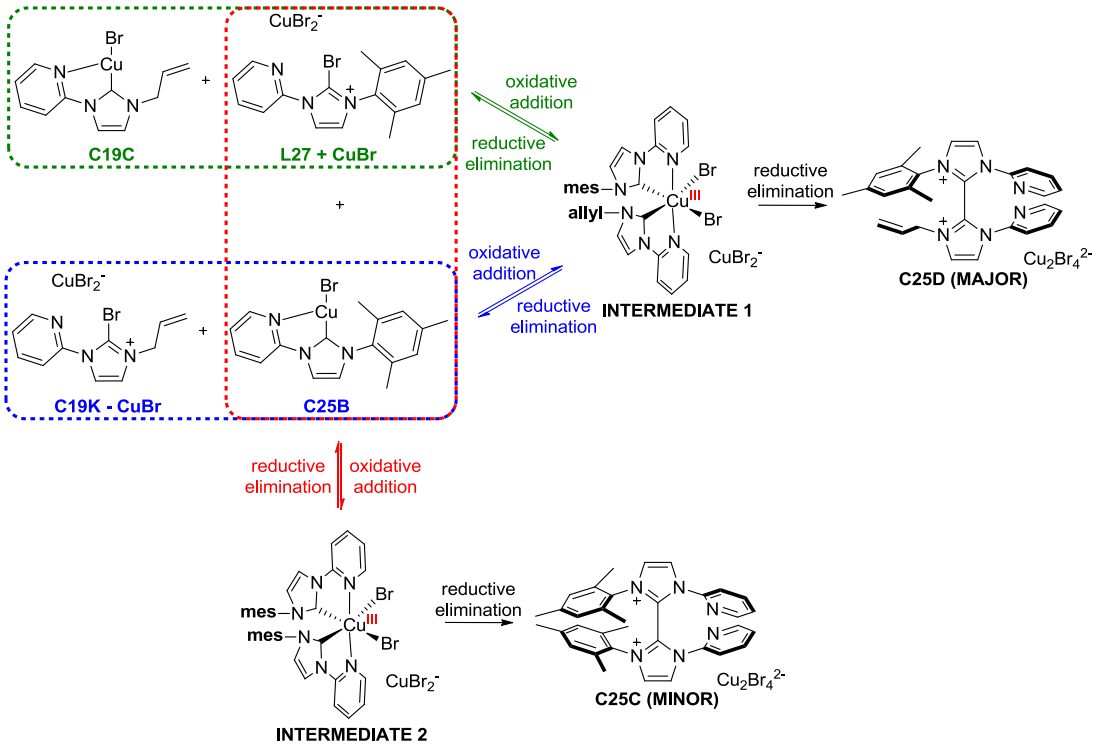

Scheme 5.18 Proposed reaction pathways accounting for the formation of homo-*bis*-imidazolium (**C25C**) and hetero-*bis*-imidazolium (**C25D**)

Finally, for the sake of comparison, the reaction of Ag^{I}-NHC complex **C25A** with two equivalents of $CuBr_2$ was performed, under identical conditions used for the synthesis of the C-C coupled product **C25C**. After work-up, again a yellow crystalline solid was produced which could be fully analysed. Comparison of the ^{1}H NMR spectrum of the haloimidazolium salt, **L27**, with that of the product of this reaction (**C25E**) illustrated that they were very similar, suggesting that **C25E** is a haloimidazolium salt. This was further confirmed by high-resolution MS, where the dominant ion corresponded to an $[imBr]^{+}$ fragment. The solid-state structure was finally established using both elemental analysis and single crystal X-ray diffraction analysis. The crystals suitable for X-ray diffraction analysis could be obtained *via* the vapour diffusion of diethyl ether in to a concentrated solution of **C25E** in acetonitrile. The product crystallised in the triclinic crystal system, with the structural solution being performed in the space group $P\bar{1}$ (Figure 5.31).

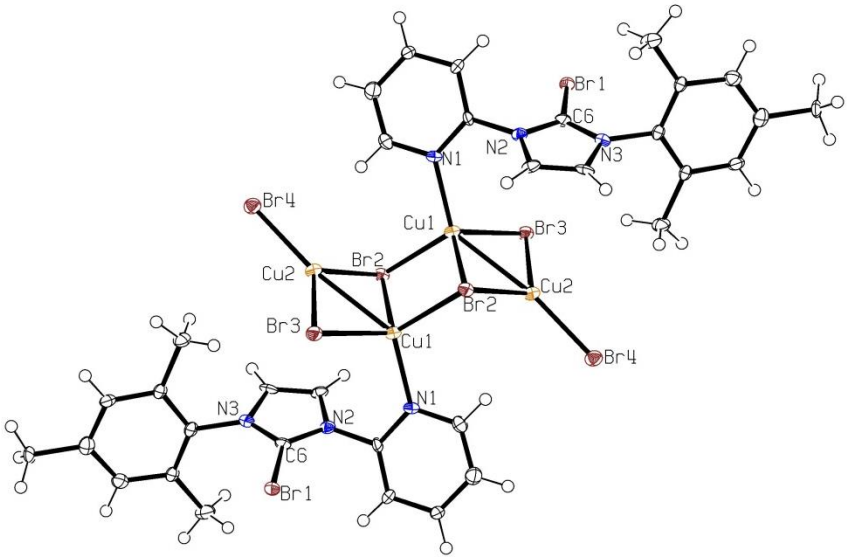

Figure 5.31 Molecular structure of **C25E**. Ellipsoids are drawn at the 50% probability level. The $Cu_4Br_6^{2-}$-bridged dimer is shown

As illustrated in Figure 5.31, **C25E** is shown to be a haloimidazolium salt, which crystallised as a $Cu_4Br_6^{2-}$-bridged dimer, with coordination to one of the copper centres by a pyridyl *N*-donor. A halogen bonded 1D polymer propagates throughout the extended crystalline lattice, with halogen bonding interactions between the Br1 and Br4 atoms of neighbouring $Cu_4Br_6^{2-}$-bridged dimeric units.

The formation of haloimidazolium salt **C25E** by reaction of Ag^{I}-NHC complex **C25A** with two equivalents of $CuBr_2$ was investigated computationally (Scheme 5.19). It was anticipated that the mechanism would be largely similar to that postulated for the formation of **C19K** (Scheme 5.6), and indeed, this was found to be the case. Reaction of $CuBr_2$ with the Cu^{II}-NHC complex (**1_iMes_D**) occurs rapidly and irreversibly (ΔG = -20.8 kcal mol^{-1}) to form a $(\mu\text{-Br})_2$-bridged

dinuclear complex (**7_iMes_T**). This then undergoes a facile disproportionation and reductive elimination reaction to produce the haloimidazolium salt **C25E** (**8_iMes_S**).

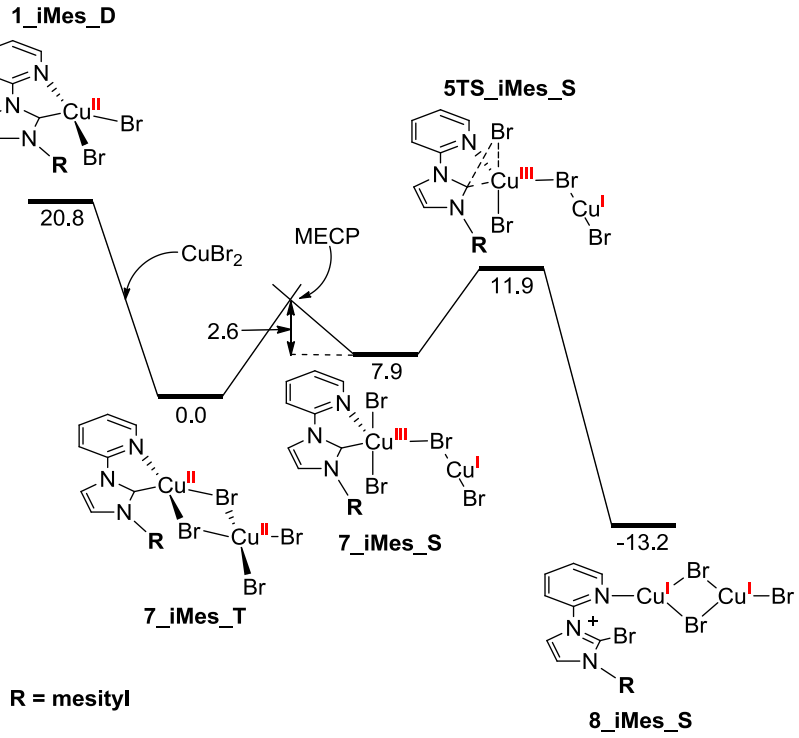

Scheme 5.19 Proposed mechanistic pathway for haloimidazolium (**C25E**) formation (relative free energies in kcal mol^{-1}) (MECP = minimum energy crossing point)

5.4 Conclusions

Using the pyridyl-tethered ligand set, a range of Cu^{II} *mono*- and *bis*-NHC complexes were rationally synthesised and characterised, where the Cu^{II} centres possessed either 'tetragonally distorted' tetrahedral or trigonal bipyramidal geometries. The 5-coordinate Cu^{II}-NHC complexes were found to display a strong preference for occupation of the axial position by the NHC donor. The relative stability of these complexes, with respect to oxidative decomposition, is somewhat unusual and can be attributed to the stabilising effect of the ancillary pyridyl donor and formation of a 5-membered chelate ring.

Furthermore, the oxidative decomposition of some of the Cu^{II}-NHC complexes under certain circumstances was examined. When the *N*-substituents were mesityl and pyridyl or *para*-methylpyridyl, reaction of the corresponding Ag^{I}-NHC complex with 1 equivalent of $CuBr_2$ surprisingly led to the formation of an oxidatively-coupled *bis*-imidazolium salt. The mechanism of this reaction was investigated computationally, and was found to consist of a surprisingly complex 'DROR' pathway. Further evidence for this proposed mechanism was provided by the reaction of two of the postulated reaction intermediates to form the same *bis*-imidazolium salt. It was also found that reaction of a $[Cu(NHC)Br_2]$-type complex with $CuBr_2$

invariably led to formation of the corresponding 2-haloimidazolium with a Cu^{I}-containing counteranion. The mechanism of this reaction was found to consist of initial formation of a $(\mu\text{-}Br)_2$-bridged dinuclear complex, followed by a disproportionation reaction and then finally reductive elimination of the haloimidazolium salt from an intermediate Cu^{III}-NHC complex (Scheme 5.20).

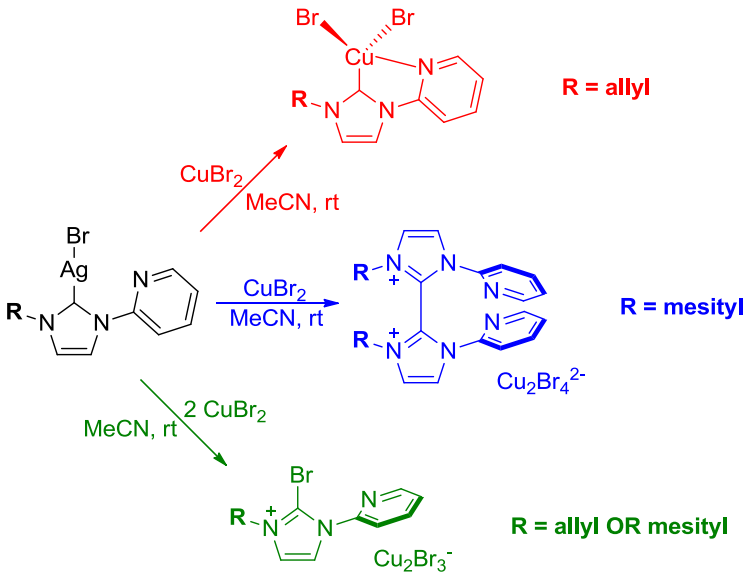

Scheme 5.20 Oxidative decomposition of NHC ligands

5.5 Future Work

As a continuation of the work described in this chapter, the eventual fate of the pyridyl- and picolyl-tethered ligands during the Ullmann coupling (described in Chapter 4) should be examined. This is in light of the observations, described in this chapter, of the non-innocence of NHC ligands under certain reaction conditions and particularly, the observation that an extremely facile reductive elimination reaction of a *bis*-imidazolium salt can occur. It could be envisaged, for example, that a similar reductive elimination of an aryl-NHC during the Ullmann coupling reaction could occur, which would represent a major catalyst deactivation pathway (Scheme 5.21).

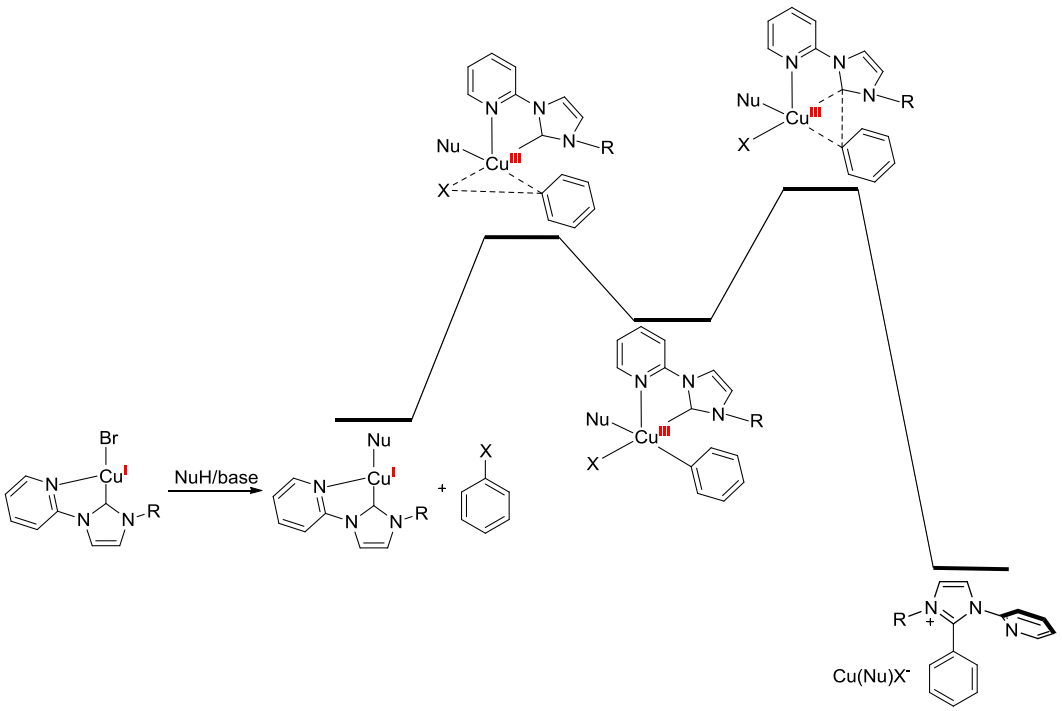

Scheme 5.21 Possible mechanism of NHC decomposition during an Ullmann-type coupling reaction

An investigation of this sought may help to guide further ligand development, with the aim of producing ligand systems which are resistant to this type of decomposition pathway.

5.6 References

[1] H. Hope, M. M. Olmstead, P. P. Power, J. Sandell, X. Xu, *Journal of the American Chemical Society* **1985**, *107*, 4337-4338.

[2] M. Stollenz, C. Große, F. Meyer, *Chemical Communications* **2008**, 1744-1746.

[3] A. G. Jarvis, A. C. Whitwood, I. J. S. Fairlamb, *Dalton Transactions* **2011**, *40*, 3695-3702.

[4] H. V. R. Dias, J. A. Flores, J. Wu, P. Kroll, *Journal of the American Chemical Society* **2009**, *131*, 11249-11255.

[5] X. Kou, H. V. R. Dias, *Dalton Transactions* **2009**, 7529-7536.

[6] S. J. Hibble, S. M. Cheyne, A. C. Hannon, S. G. Eversfield, *Inorganic Chemistry* **2002**, *41*, 4990-4992.

[7] J. Barluenga, L. A. López, O. Löber, M. Tomás, S. García-Granda, C. Alvarez-Rúa, J. Borge, *Angewandte Chemie International Edition* **2001**, *40*, 3392-3394.

[8] F. I. Rodríguez, J. J. Esch, A. E. Hall, B. M. Binder, G. E. Schaller, A. B. Bleecker, *Science* **1999**, *283*, 996-998.

[9] F. Ullmann, J. Bielecki, *Berichte der deutschen chemischen Gesellschaft* **1901**, *34*, 2174-2185.

[10] P. K. Fraser, S. Woodward, *Tetrahedron Letters* **2001**, *42*, 2747-2749.

[11] G. Zarca, I. Ortiz, A. Urtiaga, *Journal of Membrane Science* **2013**, *438*, 38-45.

[12] X. Hu, I. Castro-Rodriguez, K. Meyer, *Journal of the American Chemical Society* **2003**, *125*, 12237-12245.

[13] a) P. L. Arnold, M. Rodden, K. M. Davis, A. C. Scarisbrick, A. J. Blake, C. Wilson, *Chemical Communications* **2004**, *0*, 1612-1613; b) A. O. Larsen, W. Leu, C. N. Oberhuber, J. E. Campbell, A. H. Hoveyda, *Journal of the American Chemical Society* **2004**, *126*, 11130-11131; c) J. J. Van Veldhuizen, J. E. Campbell, R. E. Giudici, A. H. Hoveyda, *Journal of the American Chemical Society* **2005**, *127*, 6877-6882; d) B. Liu, Y. Zhang, D. Xu, W. Chen, *Chemical Communications* **2011**, *47*, 2883-2885.

[14] a) J. Yun, D. Kim, H. Yun, *Chemical Communications* **2005**, *0*, 5181-5183; b) E. L. Kolychev, V. V. Shuntikov, V. N. Khrustalev, A. A. Bush, M. S. Nechaev, *Dalton Transactions* **2011**, *40*, 3074-3076.

[15] a) C. Y. Legault, C. Kendall, A. B. Charette, *Chemical Communications* **2005**, *0*, 3826-3828; b) S. Simonovic, A. C. Whitwood, W. Clegg, R. W. Harrington, M. B. Hursthouse, L. Male, R. E. Douthwaite, *European Journal of Inorganic Chemistry* **2009**, *2009*, 1786-1795; c) B. Liu, B. Liu, Y. Zhou, W. Chen, *Organometallics* **2010**, *29*, 1457-1464; d) J. M. Smith, J. R. Long, *Inorganic Chemistry* **2010**, *49*, 11223-11230.

[16] J. Haider, K. Kunz, U. Scholz, *Advanced Synthesis & Catalysis* **2004**, *346*, 717-722.

[17] a) Q.-X. Liu, M.-C. Shi, Z.-Q. Wang, S.-W. Liu, S.-S. Ge, Y. Zang, X.-G. Wang, J.-H. Guo, *Polyhedron* **2010**, *29*, 2121-2126; b) Q.-X. Liu, J. Yu, X.-J. Zhao, S.-W. Liu, X.-Q. Yang, K.-Y. Li, X.-G. Wang, *CrystEngComm* **2011**, *13*, 4086-4096.

[18] a) M. A. Halcrow, *Chemical Society Reviews* **2013**, *42*, 1784-1795; b) L. Yang, D. R. Powell, R. P. Houser, *Dalton Transactions* **2007**, 955-964.

[19] A. R. Rossi, R. Hoffmann, *Inorganic Chemistry* **1975**, *14*, 365-374.

[20] D. Hirsch-Weil, D. R. Snead, S. Inagaki, H. Seo, K. A. Abboud, S. Hong, *Chemical Communications* **2009**, 2475-2477.

[21] A. Grandbois, M.-È. Mayer, M. Bédard, S. K. Collins, T. Michel, *Chemistry – A European Journal* **2009**, *15*, 9655-9659.

[22] T. Ramnial, C. D. Abernethy, M. D. Spicer, I. D. McKenzie, I. D. Gay, J. A. C. Clyburne, *Inorganic Chemistry* **2003**, *42*, 1391-1393.

[23] P. Metrangolo, F. Meyer, T. Pilati, G. Resnati, G. Terraneo, *Angewandte Chemie International Edition* **2008**, *47*, 6114-6127.

[24] a) C. J. Serpell, N. L. Kilah, P. J. Costa, V. Félix, P. D. Beer, *Angewandte Chemie International Edition* **2010**, *49*, 5322-5326; b) A. Caballero, N. G. White, P. D. Beer, *Angewandte Chemie International Edition* **2011**, *50*, 1845-1848; c) N. L. Kilah, M. D.

Wise, C. J. Serpell, A. L. Thompson, N. G. White, K. E. Christensen, P. D. Beer, *Journal of the American Chemical Society* **2010**, *132*, 11893-11895.

[25] B.-L. Lin, P. Kang, T. D. P. Stack, *Organometallics* **2010**, *29*, 3683-3685.

[26] a) D. S. McGuinness, M. J. Green, K. J. Cavell, B. W. Skelton, A. H. White, *Journal of Organometallic Chemistry* **1998**, *565*, 165-178; b) D. S. McGuinness, K. J. Cavell, B. W. Skelton, A. H. White, *Organometallics* **1999**, *18*, 1596-1605; c) D. S. McGuinness, K. J. Cavell, *Organometallics* **2000**, *19*, 4918-4920; d) A. M. Magill, D. S. McGuinness, K. J. Cavell, G. J. P. Britovsek, V. C. Gibson, A. J. P. White, D. J. Williams, A. H. White, B. W. Skelton, *Journal of Organometallic Chemistry* **2001**, *617-618*, 546-560; e) D. S. McGuinness, N. Saendig, B. F. Yates, K. J. Cavell, *Journal of the American Chemical Society* **2001**, *123*, 4029-4040; f) D. J. Nielsen, A. M. Magill, B. F. Yates, K. J. Cavell, B. W. Skelton, A. H. White, *Chemical Communications* **2002**, 2500-2501; g) W. J. Marshall, V. V. Grushin, *Organometallics* **2003**, *22*, 1591-1593; h) S. Caddick, F. G. N. Cloke, P. B. Hitchcock, J. Leonard, A. K. d. K. Lewis, D. McKerrecher, L. R. Titcomb, *Organometallics* **2002**, *21*, 4318-4319; i) A. T. Normand, A. Stasch, L.-L. Ooi, K. J. Cavell, *Organometallics* **2008**, *27*, 6507-6520; j) A. T. Normand, M. S. Nechaev, K. J. Cavell, *Chemistry – A European Journal* **2009**, *15*, 7063-7073.

[27] a) A. A. Danopoulos, N. Tsoureas, J. C. Green, M. B. Hursthouse, *Chemical Communications* **2003**, 756-757; b) E. Becker, V. Stingl, G. Dazinger, M. Puchberger, K. Mereiter, K. Kirchner, *Journal of the American Chemical Society* **2006**, *128*, 6572-6573; c) E. Becker, V. Stingl, G. Dazinger, K. Mereiter, K. Kirchner, *Organometallics* **2007**, *26*, 1531-1535.

[28] J. M. Praetorius, C. M. Crudden, in *N-Heterocyclic Carbenes: From Laboratory Curiosities to Efficient Synthetic Tools*, The Royal Society of Chemistry, **2011**, pp. 77-118.

[29] A. Bondi, *The Journal of Physical Chemistry* **1964**, *68*, 441-451.

[30] T. S. Thakur, G. R. Desiraju, *Chemical Communications* **2006**, 552-554.

[31] D. Braga, F. Grepioni, E. Tedesco, K. Biradha, G. R. Desiraju, *Organometallics* **1997**, *16*, 1846-1856.

[32] M. Cametti, K. Raatikainen, P. Metrangolo, T. Pilati, G. Terraneo, G. Resnati, *Organic & Biomolecular Chemistry* **2012**, *10*, 1329-1333.

[33] M. V. Baker, D. H. Brown, V. J. Hesler, B. W. Skelton, A. H. White, *Organometallics* **2006**, *26*, 250-252.

Chapter 6
Experimental

6.1 Methods and Instrumentation

6.1.1 Reagents and Manipulations

All reagents were used as supplied or prepared as outlined, without need for further purification, unless otherwise stated. 4-Methoxypyridine-*N*-oxide hydrate was dehydrated by heating at 50°C under vacuum (approximately 1 hour). Compounds previously reported in the literature were prepared according to literature procedure, with appropriate literature citation, and fully characterised using NMR spectroscopy and mass spectrometry unless otherwise stated. Manipulations were performed using standard Schlenk line and glovebox techniques. Argon and N_2 were passed through a twin-column drying apparatus containing molecular sieves (4Å) and phosphorus pentoxide. Anhydrous solvents were passed over activated alumina to remove water, copper catalyst to remove oxygen and molecular sieves to remove any remaining water *via* the Dow-Grubbs solvent system. Anhydrous deuterated chloroform and acetonitrile were dried over CaH_2, cannula filtered or distilled and then degassed using freeze-pump-thaw cycles prior to use.

6.1.2 NMR Spectroscopy

^{1}H and $^{13}C\{^{1}H\}$ NMR spectra were recorded on either a Bruker DPX300 spectrometer (operating frequency 300.1 MHz for ^{1}H and 75.48 MHz for $^{13}C\{^{1}H\}$), a Bruker Avance500 spectrometer or a Bruker DRX500 spectrometer (both with an operating frequency of 500.13 MHz for ^{1}H and 125.80 MHz for $^{13}C\{^{1}H\}$). All spectra were recorded at 298 K (unless otherwise stated) in deuterated solvent. Chemical shift values are quoted in parts per million (ppm, δ) and coupling constants, *J*, are quoted in Hertz (Hz). Assignment of ^{1}H NMR spectra was aided by the use of 2D $^{1}H^{1}H$ COSY experiments and the assignment of $^{13}C\{^{1}H\}$ NMR spectra was aided by $^{13}C\{^{1}H\}$ dept 135 experiments.

6.1.3 Mass Spectrometry

High-resolution mass spectra were collected by Ms. Tanya Marinko-Covell on a Bruker Daltonics or Bruker MaXis mass spectrometer instrument operating in the positive ion electrospray mode. Samples were injected directly from feed solutions and acquired over the *m/z* range 50 – 4000. All spectra were recorded using an acetonitrile / water mix as the eluent and a sodium formate solution as a calibrant.

6.1.4 Microanalyses

Microanalyses were performed by either Mr. Ian Blakeley or Ms. Tanya Marinko-Covell using a Carlo Erba Elemental Analyser MOD 1106 spectrometer in the University of Leeds, School of Chemistry.

6.1.5 X-Ray Crystallography

X-ray diffraction data were collected on either a Bruker Nonius X8 diffractometer fitted with an Apex II detector with Mo-K_α radiation (λ = 0.71073 Å) or an Agilent SuperNova diffractometer fitted with an Atlas CCD detector with Mo-K_α radiation (λ = 0.71073 Å) or Cu-K_α radiation (λ = 1.54184 Å). Crystals were mounted under Fomblin on Mitegen or nylon loops. Crystals were held at either 150, 120 or 100 K using an Oxford Cryosystems low temperature device during unit cell determination and data collection. Data sets were corrected for absorption effects using a multiscan method, and the structures were solved either by direct methods using SHELXS-97 or charge flipping (Superflip) interfaced through the program Olex2. Refinement was by full-matrix least squares on F2 using ShelXL-97, interfaced through either the program X-Seed or Olex2. All hydrogen atoms were included at geometrically estimated positions using a riding model unless otherwise stated. Graphics of the crystal structures outlined in this report were generated using Ortep-3.

6.1.6 DFT Calculations

All DFT calculations were performed by Dr Alireza Ariafard (University of Tasmania, Australia).

Gaussian 09[1] was used to fully optimize all the structures reported in this thesis at the M06 level of density functional theory (DFT)[2] in dichloromethane using the CPCM solvation model.[3] The effective-core potential of Hay and Wadt with a double-ξ valence basis set (LANL2DZ)[4] was chosen to describe Cu. The 6-31G(d) basis set was used for other atoms.[5] Polarization functions were also added for Cu (ξ_f = 3.525).[6] This basis set combination will be referred to as BS1. Frequency calculations were carried out at the same level of theory as those for the structural optimisation. Transition structures were located using the Berny algorithm. Intrinsic reaction coordinate (IRC)[7] calculations were used to confirm the connectivity between transition structures and minima. To further refine the energies obtained from the M06/BS1 calculations, we carried out single-point energy calculations for all of the structures with a larger basis set (BS2) in dichloromethane using the CPCM solvation model at M06 level. To estimate the corresponding Gibbs energies, ΔG, the entropy corrections were calculated at the M06/BS1 level, adjusted by the method proposed by Okuno[8] and finally added to the single-point energies. BS2 utilizes the 6-311+G(2d,p) basis set on all atoms. We have used the

potential and Gibbs free energies obtained from the M06/BS2//M06/BS1 calculations in dichloromethane throughout this thesis.

Minimum energy crossing points (MECPs) between the triplet and singlet states have been located using the code of Harvey *et al*. at the M06/BS1 level theory in dichloromethane.[9] **N_R_X** and **NTS_R_X** in the figures are the nomenclatures used for the species on the energy profiles, where X = **S** stands for singlet, **D** for doublet and **T** for triplet spin states. **N** represents the minimum structures, **NTS** corresponds to the transition structures, and **R** stands for the organic substituent on one of the N atoms of the NHC ligand.

6.1.7 General Carousel Reaction Procedure

3,5-Dimethylphenol (0.15 g, 1.2 mmol), 4-iodoanisole (0.23 g, 1.0 mmol), '*catalyst*' (0.10 mmol) and Cs_2CO_3 (0.65 g, 2.0 mmol) were added to a carousel tube mounted on a Radley's Carousel 12 Plus parallel reactor, and dried *in vacuo*. To these was added anhydrous acetonitrile (5 ml) *via* syringe. The resulting mixture was heated with vigorous stirring at 90°C for 24 hours. After this time, the mixture was cooled and a 100 μl aliquot was withdrawn from the reaction mixture using a microsyringe, and added to 2 ml of a 10 mM stock solution of *p*-cymene (internal standard) in dichloromethane. The solution containing reaction mixture and internal standard was filtered through celite and subsequently analysed by GC.

6.1.8 Gas Chromatography

Analysis of the carousel reaction mixtures was performed on a Bruker 430-GC Gas Chromatograph fitted with a Bruker BR-5ms column. Oxygen-free nitrogen was used as the inert carrier gas. Detection of the volatile compounds was performed with a flame ionisation detector (FID) and synthetic air and hydrogen gas (generated by a Parker Domnick Hunter 20H-MD Hydrogen Generator). A 'ramped' temperature regime was followed during each run, whereby the temperature of the column was held at 50°C between 0-1 minutes, and then ramped at 20°C/min between 1-14 minutes reaching a temperature of 310°C, and then finally the temperature was held constant at 310°C between 14-19 minutes. The % yield of the product was determined by taking an average of three GC runs.

6.2 Experimental Details

6.2.1 Preparation of P1[10]

2,6-Diisopropylaniline (40 g, 0.23 mol) was dissolved in methanol (100 ml). The mixture was stirred for 5 minutes to ensure thorough dissolution. Glyoxal (40 % in water) (13 ml, 0.11 mol) was syringed in to the reaction mixture followed by the addition of a few drops of formic acid. The mixture was stirred for 20 hours. A thick, yellow precipitate formed very quickly after

addition of the glyoxal and formic acid. The precipitate was filtered and washed with methanol, yielding a yellow crystalline solid. Yield: 27 g, 73 mmol, 64%.

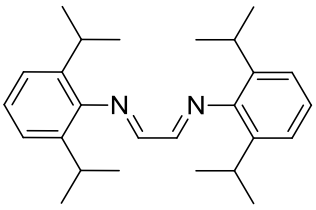

^{1}H NMR (300 MHz, $CDCl_3$) δ 8.09 (s, 2H, N=CH-CH=N), 7.22 – 7.11 (m, 6H, ArH), 2.94 (sept, J = 6.9 Hz, 4H, C**H**$(CH_3)_2$), 1.20 (d, J = 6.9 Hz, 24H, CH(C**H**$_3)_2$). ^{13}C{^{1}H} NMR (75 MHz, $CDCl_3$) δ 163.3, 148.2, 136.9, 125.3, 123.3, 28.2, 23.5. HRMS (ESI^+): *m/z* 377.2969 $[M + H]^+$ calculated $[M + H]^+$ 377.2957. Analysis Calculated for $C_{26}H_{36}N_2$: C, 82.93; H, 9.64; N, 7.44. Found: C, 82.90; H, 9.65; N, 7.35.

Consistent with data previously reported.[10]

6.2.2 Preparation of P2[11]

2,6-Dimethylaniline (3.4 g, 28 mmol), glyoxal (40% in water) (1.6 ml, 14 mmol) and ethanol (25 ml) were added to a 100 ml round-bottomed flask. Following the addition of a few drops of formic acid, the mixture was stirred at room temperature for 4 hours. A yellow precipitate formed almost immediately. The precipitate was filtered, washed with ice-cold water and finally dried *in vacuo*, producing the product as a yellow micro-crystalline solid. Yield: 1.7 g, 6.4 mmol, 46%.

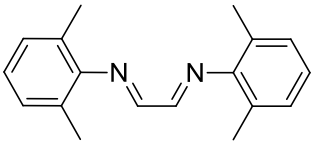

^{1}H NMR (500 MHz, $CDCl_3$) δ 8.03 (s, 2H, N=CH-CH=N), 7.04 – 6.88 (m, 6H, ArH), 2.10 (s, 12H, CH_3). ^{13}C{^{1}H} NMR (126 MHz, $CDCl_3$) δ 163.6, 150.0, 128.4, 126.5, 124.9, 18.4. HRMS (ESI^+): *m/z* 265.1708 $[M + H]^+$ calculated $[M + H]^+$ 265.1699.

Consistent with data previously reported.[11]

6.2.3 Preparation of P3[10]

2,4,6-Trimethylaniline (5.6 g, 41 mmol), glyoxal (40% in water) (2.4 ml, 21 mmol) and ethanol (40 ml) were added to a 250 ml round-bottomed flask. Following the addition of a few drops of formic acid, the mixture was stirred at room temperature for 24 hours. A yellow precipitate formed almost immediately. The precipitate was filtered, washed with ice-cold ethanol and finally dried *in vacuo*, producing the product as a yellow crystalline solid. Yield: 3.6 g, 12 mmol, 60%.

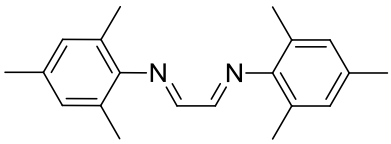

^{1}H NMR (500 MHz, $CDCl_3$) δ 8.12 (s, 2H, N=CH-CH=N), 6.93 (s, 4H, ArH), 2.31 (s, 6H, p-CH_3), 2.18 (s, 12H, o-CH_3). ^{13}C{^{1}H} NMR (126 MHz, $CDCl_3$) δ 163.6, 147.6, 134.4, 129.1, 126.7, 20.9, 18.3. HRMS (EI^+): *m/z* 291.1864 $[M + H]^+$ calculated $[M + H]^+$ 291.1861. Analysis Calculated for $C_{20}H_{24}N_2$: C, 82.15; H, 8.27; N, 9.58. Found: C, 81.20; H, 8.20; N, 9.45.

Consistent with data previously reported.[10]

6.2.4 Preparation of P13[12]

1,3-*Bis*(bromomethyl)benzene (5.0 g, 19 mmol) and imidazole (26 g, 0.38 mol) were added to an oven-dried Schlenk flask and dried *in vacuo*. Anhydrous methanol (75 ml) was added to the mixture and the solution was heated at reflux for 48 hours. After this time, the methanol was removed *in vacuo* to give a pale brown/orange oil. Water (75 ml) was added to the oil and the aqueous layer was extracted with chloroform (3 x 75 ml). The chloroform fractions were collected and combined and then washed with water. Finally, the chloroform fraction was dried with $CaCl_2$, filtered and the solvent removed *in vacuo* to yield a yellow oil. Trituration of the oil with diethyl ether led to the crystallisation of the product as a white solid. Yield: 2.4 g, 10 mmol, 53%.

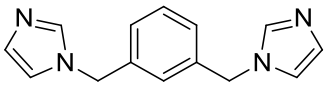

^{1}H NMR (300 MHz, $CDCl_3$) δ 7.52 (s, 2H, NCHN), 7.33 (t, J = 7.7 Hz, 1H, ArH), 7.09 (s, 2H, imH), 7.09 (d, J = 7.7 Hz, 2H, ArH), 6.91 (s, 1H, ArH), 6.87 (s, 2H, imH), 5.09 (s, 4H, CH_2). ^{13}C{^{1}H} NMR (75 MHz, $CDCl_3$) δ 137.6, 137.4, 130.2, 129.9, 127.2, 126.0, 119.4, 50.6. HRMS (ESI^+): *m/z* 239.1292 $[M + H]^+$ calculated $[M + H]^+$ 239.1291.

Consistent with data previously reported.[12]

6.2.5 Preparation of P17[13]

Acetic acid (99%) (10 ml), aqueous formaldehyde (37-41%) (3.0 ml, 40 mmol) and aqueous glyoxal (40%) (4.6 ml, 40 mmol) were added to a two-necked round-bottomed flask and heated to 70°C. A solution of acetic acid (99%) (10 ml), ammonium acetate in water (3.1 g in 2 ml, 40 mmol) and mesitylamine (5.6 ml, 40 mmol) was added dropwise over a period of 1 hour. The solution was heated at 70°C for 6 hours and then at room temperature for a further 16 hours. The mixture was then cooled to room temperature and was slowly added to a saturated aqueous solution of $NaHCO_3$ (40 g). The crude product precipitated as a black solid which was collected by filtration and recrystallised repeatedly from acetone / water to give the pure product as a light brown solid. Yield: 2.5 g, 14 mmol, 34%.

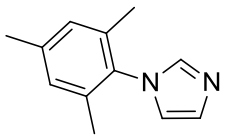

^{1}H NMR (500 MHz, $CDCl_3$) δ 7.44 (s, 1H, NCHN), 7.23 (s, 1H, imH), 6.97 (s, 2H, ArH), 6.89 (s, 1H, imH), 2.34 (s, 3H, p-CH_3), 1.99 (s, 6H, o-CH_3). ^{13}C{^{1}H} NMR (75 MHz, $CDCl_3$) δ 139.0, 137.6, 135.5, 133.5, 129.6, 129.1, 120.2, 21.1, 17.4. HRMS (ESI^+): *m/z* 187.1236 $[M + H]^+$ calculated $[M + H]^+$ 187.1230.

Consistent with data previously reported.[13]

6.2.6 Preparation of P18[14]

Acetic acid (99%) (10 ml), aqueous formaldehyde (37-41%) (3.0 ml, 40 mmol) and aqueous glyoxal (40%) (4.6 ml, 40 mmol) were added to a two-necked round-bottomed flask and heated to 70°C. A solution of acetic acid (99%) (10 ml), ammonium acetate in water (3.1 g in 2 ml, 40 mmol) and o-anisidine (4.5 ml, 40 mmol) was added dropwise over a period of 1 hour. The solution was heated at 70°C overnight. The mixture was then cooled to room temperature and was slowly added to a saturated aqueous solution of $NaHCO_3$ (40 g). The crude product oiled-out as an orange oil, which was collected by decanting-off the solvent and washing repeatedly with water. The product was extracted in to diethyl ether and the solvent removed *in vacuo* to yield the pure product as a yellow oil, which slowly crystallises on standing. Yield: 2.7 g, 16 mmol, 39%.

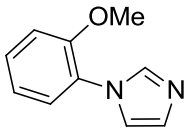

^{1}H NMR (500 MHz, $CDCl_3$) δ 7.80 (s, 1H, NCHN), 7.41 – 7.35 (m, 1H, ArH), 7.32 – 7.28 (m, 1H, ArH), 7.22 (s, 1H, imH), 7.19 (s, 1H, imH), 7.10 – 7.03 (m, 2H, ArH), 3.87 (s, 3H, OCH_3). ^{13}C{^{1}H} NMR (75 MHz, $CDCl_3$) δ 152.7, 137.9, 129.0, 128.8, 126.6, 125.6, 121.1, 120.3, 112.4, 55.9. HRMS (ESI^+): *m/z* 175.0871 $[M + H]^+$ calculated $[M + H]^+$ 175.0866.

Consistent with data previously reported.[14]

6.2.7 Preparation of P19[15]

In a modification of a literature procedure,[16] a Schlenk flask was charged with imidazole (0.75 g, 11 mmol), K_2CO_3 (2.1 g, 15 mmol), CuI (0.14 g, 0.8 mmol) and DL-proline (0.17 g, 1.6 mmol), which were dried and degassed *in vacuo*. To these, 2-bromopyridine (1.6 g, 10 mmol) and anhydrous dimethylsulfoxide (6 ml) were added by syringe and the suspension was heated at 90°C for 12 hours. The mixture was then allowed to cool to room temperature. The reaction mixture was partitioned between water (200 ml) and dichloromethane (200 ml) and the organic layer collected. The aqueous layer was extracted with dichloromethane (3 x 200 ml) and the organic layers combined. The combined organic layer was washed with water (4 x 200 ml), dried over Na_2SO_4 and the dichloromethane removed *in vacuo* to give the crude product as a pale yellow oil. The crude product was purified by flash column chromatography (silica gel), eluting with ethyl acetate / petroleum ether (1:1) → ethyl acetate / petroleum ether / methanol (4.5:4.5:1). The pure product was obtained as a colourless oil. Yield: 1.0 g, 7.1 mmol, 71%.

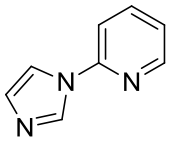

^{1}H NMR (500 MHz, $CDCl_3$) δ 8.50 (dd, J = 4.8, 1.5 Hz, 1H, pyH), 8.40 (s, 1H, NCHN), 7.84 (td, J = 8.2, 1.5 Hz, 1H, pyH), 7.66 (s, 1H, imH), 7.38 (d, J = 8.2 Hz, 1H, pyH), 7.27 – 7.24 (m, 1H, pyH), 7.22 (s, 1H, imH). ^{13}C{^{1}H} NMR (126 MHz, $CDCl_3$) δ 149.2, 149.1, 139.0, 135.0, 130.4, 122.1, 116.2, 112.4. HRMS (ESI^+): *m/z* 146.0719 $[M + H]^+$ calculated $[M + H]^+$ 146.0713.

Consistent with data previously reported.[15]

6.2.8 Preparation of P20[16]

A small ampoule was charged with 2,6-dibromopyridine (1.2 g, 5.0 mmol), imidazole (0.75 g, 11 mmol), K_2CO_3 (2.1 g, 15 mmol), CuI (0.14 g, 0.80 mmol) and DL-proline (0.17 g, 1.6 mmol). These were dried and degassed *in vacuo*. To this mixture, anhydrous dimethylsulfoxide (6 ml) was added by syringe and the mixture was heated with stirring at 90°C for 18 hours. The reaction mixture was then allowed to cool to room temperature. The cooled reaction mixture was partitioned between water (100 ml) and dichloromethane (100 ml) and the organic layer was collected. The aqueous layer was extracted with dichloromethane (3 x 100 ml) and the organic layers were combined. The combined organic layers were washed with water (4 x 200 ml) and dried over Na_2SO_4. Finally, the solvent was removed *in vacuo* to yield a white solid, which was recrystallised from dichloromethane / hexane to give the pure product as a white solid. Yield: 0.62 g, 2.9 mmol, 59%.

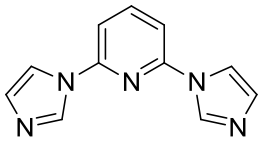

^{1}H NMR (300 MHz, $CDCl_3$) δ 8.37 (s, 2H, NCHN), 7.96 (t, J = 8.0 Hz, 1H, pyH), 7.66 (s, 2H, imH), 7.28 (d, J = 8.0 Hz, 2H, pyH), 7.22 (s, 2H, imH). ^{13}C{^{1}H} NMR (75 MHz, $CDCl_3$) δ 148.5, 142.2, 135.1, 131.3, 116.3, 109.8. HRMS (ESI^+): *m/z* 212.0928 $[M + H]^+$ calculated $[M + H]^+$ 212.0931.

Consistent with data previously reported.[16]

6.2.9 Preparation of P21[17]

2-Bromo-5-nitropyridine (2.0 g, 9.8 mmol) and sodium imidazolide (0.99 g, 11 mmol) were added to a Schlenk flask and dried *in vacuo*. To these was added anhydrous dimethylformamide (40 ml), and the resultant suspension was stirred for 1.5 hours at room temperature. After this time, water (150 ml) was added to quench the reaction, and the resultant solid was collected by filtration, washed repeatedly with water and dried in air. Yield: 1.9 g, 9.8 mmol, quantitative.

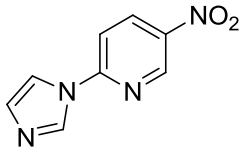

^{1}H NMR (300 MHz, $CDCl_3$) δ 9.34 (d, J = 2.5 Hz, 1H, pyH), 8.64 (dd, J = 9.0, 2.5 Hz, 1H, pyH), 8.50 (s, 1H, NCHN), 7.72 (s, 1H, imH), 7.52 (d, J = 9.0 Hz, 1H, pyH), 7.27 (s, 1H, imH). ^{13}C{^{1}H} NMR (75 MHz, $CDCl_3$) δ 152.4, 145.9, 142.4, 135.8, 134.9, 132.0, 116.5, 111.8. HRMS (ESI^+): *m/z* 191.0569 $[M + H]^+$ calculated $[M + H]^+$ 191.0564.

Consistent with data previously reported.[17]

6.2.10 Preparation of P22[18]

In a modification of a literature procedure,[16] imidazole (1.0 g, 15 mmol), K_2CO_3 (2.7 g, 14 mmol), DL-proline (0.24 g, 2.1 mmol) and CuI (0.20 g, 1.0 mmol) were added to an ampoule

and dried/degassed *in vacuo*. To these was added 2-bromo-4-methylpyridine (1.5 ml, 13 mmol) and anhydrous DMSO (8 ml). The mixture was heated at 100°C with vigorous stirring for 5 hours. After this time, the mixture was partitioned between DCM (100 ml) and H_2O (100 ml). The H_2O layer was extracted with DCM (3 x 100 ml) and the combined organic layers washed with H_2O (100 ml) and saturated aqueous EDTA (2 x 100 ml). The combined organics were then dried over $CaCl_2$ and the solvent removed *in vacuo*, giving the product as a yellow oil. Yield: 1.7 g, 10 mmol, 80%.

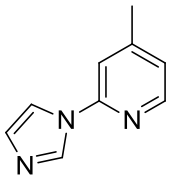

^{1}H NMR (300 MHz, $CDCl_3$) δ 8.31 (s, 1H, NCHN), 8.30 (d, J = 5.1 Hz, 1H, pyH), 7.62 (s, 1H, imH), 7.17 (s, 1H, imH), 7.14 (s, 1H, pyH), 7.03 (d, J = 5.1 Hz, 1H, pyH), 2.41 (s, 3H, CH_3). ^{13}C{^{1}H} NMR (75 MHz, $CDCl_3$) δ 150.7, 149.4, 148.8, 135.2, 130.7, 123.2, 116.2, 113.1, 21.3. HRMS (ESI^+): *m/z* 160.0870 $[M + H]^+$ calculated $[M + H]^+$ 160.0869.

Consistent with data previously reported.[18]

6.2.11 Preparation of P23

In a modification of a literature procedure,[19] a small round-bottomed flask was charged with anhydrous 4-methoxypyridine-*N*-oxide (0.94 g, 7.5 mmol) and 1,1'-sulfonyldiimidazole (2.2 g, 11 mmol). To these was added anhydrous toluene (20 ml). The resultant mixture was stirred at 100°C for 2 hours during which time, a dark oil formed. The dark oil was collected by decanting-off the solution, and taken up in to a 2M NaOH solution (50 ml). This solution was extracted with dichloromethane (3 x 100 ml) and the combined organic layers were washed with water (2 x 100 ml), dried over $CaCl_2$ and the solvent removed *in vacuo* to give the product as a pale orange oil. Yield: 0.80 g, 4.6 mmol, 61%.

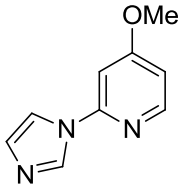

^{1}H NMR (300 MHz, $CDCl_3$) δ 8.27 (s, 1H, imH), 8.24 (d, J = 5.8 Hz, 1H, pyH), 7.55 (s, 1H, imH), 7.13 (s, 1H, imH), 6.78 (d, J = 2.2 Hz, 1H, pyH), 6.72 (dd, J = 5.8, 2.2 Hz, 1H, pyH), 3.86 (s, 3H, OCH_3). ^{13}C{^{1}H} NMR (75 MHz, $CDCl_3$) δ 167.9, 150.3, 135.1, 130.6, 116.3, 108.3, 98.8, 55.7. HRMS (ESI^+): *m/z* 176.0821 $[M + H]^+$ calculated $[M + H]^+$ 176.0818.

6.2.12 Preparation of L1[10]

Precursor **P1** (27 g, 73 mmol) was dissolved in ethyl acetate (200 ml). In a separate flask, paraformaldehyde (2.2 g, 73 mmol) was added to HCl in dioxane (4 M) (27 ml, 0.11 mol) and stirred for 20 minutes to complete dissolution. The paraformaldehyde was added dropwise (cannula transfer) to the diazabutadiene solution which had been cooled to 0°C, over 30 minutes. The mixture was gradually allowed to warm to room temperature and stirred overnight. The resulting brown mixture was filtered and washed repeatedly with ethyl acetate until the filtrate ran clear. The

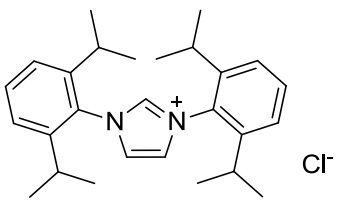

off-white solid was dissolved in dichloromethane, calcium chloride was added to absorb any moisture and the mixture filtered again. The dichloromethane was removed *in vacuo* to yield a pale yellow solid, which turned purple on standing under nitrogen. The purple solid was redissolved in dichloromethane (it was necessary to add a couple of drops of water to allow dissolution to occur). Diethyl ether was added to precipitate the pure product as a slightly off-white, crystalline solid. Yield: 19 g, 44 mmol, 61%.

^{1}H NMR (300 MHz, CD_2Cl_2) δ 11.32 (s, 1H, NCHN), 7.79 (s, 2H, imH), 7.60 (t, J = 7.8 Hz, 2H, ArH), 7.37 (d, J = 7.8 Hz, 4H, ArH), 2.41 (sept, 4H, C**H**$(CH_3)_2$), 1.26 (d, J = 7.4 Hz, 12H, CH(C**H**$_3)_2$), 1.24 (d, J = 7.7 Hz, 12H, CH(C**H**$_3)_2$). ^{13}C{^{1}H} NMR (75 MHz, CD_2Cl_2) δ 145.7, 141.4, 132.5, 130.7, 126.1, 125.2, 29.7, 25.0, 23.9. HRMS (ESI$^+$): *m/z* 389.2952 [M - Cl]$^+$ calculated [M - Cl]$^+$ 389.2951. Analysis Calculated for $C_{27}H_{37}ClN_2$: C, 76.29; H, 8.77; N, 6.59. Found: C, 75.10; H, 8.75; N, 6.35.

Consistent with data previously reported.[10]

6.2.13 Preparation of L2[20]

In a modification of a literature procedure,[21] precursor **P2** (1.0 g, 3.8 mmol) was dissolved in toluene (20 ml). To this, paraformaldehyde (0.11 g, 3.8 mmol) was added and the mixture was heated at 100°C until most of the paraformaldehyde had dissolved (circa 20 minutes). The oil bath was removed from under the reaction vessel and once the mixture had cooled slightly, HCl in dioxane (4 M) (0.95 ml) was syringed in to the reaction mixture. On addition of the HCl in dioxane, the yellow solution immediately turned red and then a dark brown precipitate formed. The mixture was stirred at 70°C for 5 hours during which time the solution turned black. After 5 hours, the oil bath was removed and the mixture was stirred at room temperature for a further 17 hours. A thick black solid formed on the surface of the round-bottomed flask. The mixture was filtered under inert conditions leaving a tar-like solid coating the reaction flask. The solid was washed with anhydrous tetrahydrofuran, filtered and dried *in vacuo*, producing a dark brown sludge, which was dried *in vacuo*. The solid was vigorously stirred in tetrahydrofuran (50 ml) overnight, filtered and again dried *in vacuo*, producing the imidazolium chloride as a dark purple, hygroscopic solid. Yield: 0.63 g, 2.0 mmol 53%.

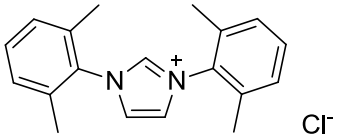

^{1}H NMR (300 MHz, $CDCl_3$) δ 10.93 (s, 1H, NCHN), 7.73 (s, 2H, imH), 7.34 – 7.29 (m, 2H, ArH), 7.17 (d, J = 7.5 Hz, 4H, ArH), 2.20 (s, 12H, CH_3). ^{13}C{^{1}H} NMR (75 MHz, $CDCl_3$) δ 139.9, 134.9, 133.5, 131.4, 129.6, 125.0, 18.2. HRMS (ESI$^+$): *m/z* 277.1693 [M - Cl]$^+$ calculated [M - Cl]$^+$ 277.1699.

Consistent with data previously reported.[20]

6.2.14 Preparation of L3[10]

In a modification of a literature procedure,[21] precursor **P3** (1.7 g, 5.7 mmol) was dissolved in toluene (30 ml). To this, paraformaldehyde (0.17 g, 5.7 mmol) was added and the mixture was heated at 100°C until most of the paraformaldehyde dissolved (circa 20 minutes). The oil bath was removed from under the reaction vessel and once the mixture had cooled slightly, HCl in dioxane (4 M) (1.4 ml) was slowly added to the reaction mixture. On addition of the HCl in dioxane, the yellow solution immediately turned red and then a dark brown precipitate formed. The mixture was stirred at 50°C for 15 hours during which time the solution turned black. The mixture was stirred at room temperature for a further 30 hours. The mixture was filtered under inert conditions leaving a dark brown solid. The solid was washed repeatedly with anhydrous tetrahydrofuran, gradually becoming lighter in colour. Washing was continued until the washing phase was colourless. The light brown solid was dissolved in a saturated aqueous solution of $NaHCO_3$ and washed with ethyl acetate (3 x 50 ml). The aqueous layer was extracted with dichloromethane (3 x 100 ml) and dried over $CaCl_2$. The dichloromethane was removed *in vacuo* to yield an off-white solid. The product was recrystallised by dissolving it in the minimum amount of dichloromethane and adding diethyl ether to precipitate the product, producing a white solid. Yield: 0.20 g, 0.60 mmol 10%.

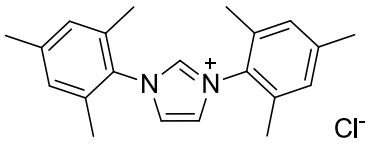

^{1}H NMR (500 MHz, CD_2Cl_2) δ 11.06 (s, 1H, NCHN), 7.67(s, 2H, imH), 7.06 (s, 4H, ArH), 2.36 (s, 6H, p-CH_3), 2.16 (s, 12H, o-CH_3). ^{13}C{^{1}H} NMR (75 MHz, CD_2Cl_2) δ 142.0, 140.8, 135.1, 131.6, 130.5, 125.2, 21.7, 18.2. HRMS (ESI^+): *m/z* 305.2014 $[M - Cl]^+$ calculated $[M - Cl]^+$ 305.2012. Analysis Calculated for $C_{21}H_{25}ClN_2$: C, 73.99; H, 7.39; N, 8.22. Found: C, 73.50; H, 7.60; N, 8.15.

Consistent with data previously reported.[10]

6.2.15 Preparation of L4[22]

To an aqueous solution of **L1** (3.0 g, 7.1 mmol), NH_4PF_6 (5.8 g, 35 mmol) in water was slowly added and allowed to stir for 30 minutes. A white precipitate formed almost immediately. The precipitate was filtered, washed repeatedly with water and dried in an oven affording the product as a white solid. Yield: 3.6 g, 6.7 mmol, 95%.

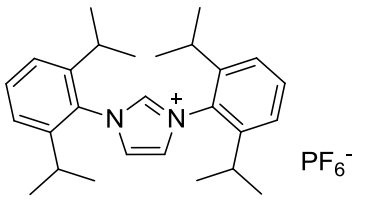

^{1}H NMR (500 MHz, $(CD_3)_2CO$) δ 9.84 (s, 1H, NCHN), 8.47 (s, 2H, imH), 7.74 (t, J = 7.8 Hz, 2H, ArH), 7.58 (d, J = 7.8 Hz, 4H, ArH), 2.67 – 2.58 (m, 4H, C**H**$(CH_3)_2$), 1.34 (d, J = 6.8 Hz, 12H, CH(C**H**$_3)_2$), 1.28 (d, J = 6.9 Hz, 12H, CH(C**H**$_3)_2$). ^{13}C{^{1}H} NMR (75 MHz, $(CD_3)_2CO$) δ

146.2, 139.5, 133.1, 131.1, 127.4, 125.7, 24.6, 23.8. Analysis Calculated for $C_{27}H_{37}F_6N_2P$: C, 60.67; H, 6.98; N, 5.24. Found: C, 60.75; H, 6.95; N, 5.15.

Consistent with data previously reported.[22]

6.2.16 Preparation of L5

To an aqueous solution of crude **L2** (0.50 g, 1.6 mmol), NH_4PF_6 (1.3 g, 8.0 mmol) in water was slowly added and allowed to stir for 30 minutes. A white precipitate formed almost immediately. The precipitate was filtered, washed repeatedly with water and dried affording the product as a slightly off-white solid. Yield: 0.28 g, 0.70 mmol, 42%.

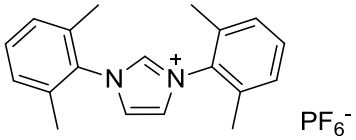

^{1}H NMR (300 MHz, $(CD_3)_2CO$) δ 9.56 (s, 1H, NCHN), 8.27 (s, 2H, imH), 7.59 – 7.47 (m, 2H, ArH), 7.41 (d, J = 7.5 Hz, 4H, ArH), 2.29 (s, 12H, CH_3). $^{13}C\{^1H\}$ NMR (75 MHz, $(CD_3)_2CO$) δ 139.1, 135.9, 134.5, 132.1, 130.0, 126.0, 17.5. Analysis Calculated for $C_{19}H_{21}F_6N_2P$: C, 54.03; H, 5.01; N, 6.63. Found: C, 54.05; H, 5.00; N, 6.60.

6.2.17 Preparation of L6[23]

To an aqueous solution of **L3** (2.0 g, 5.9 mmol), NH_4PF_6 (4.8 g, 29 mmol) in water was slowly added and allowed to stir for 30 minutes. A white precipitate formed almost immediately. The precipitate was filtered, washed repeatedly with water and dried affording a white solid. Yield: 2.3 g, 5.1 mmol, 87%.

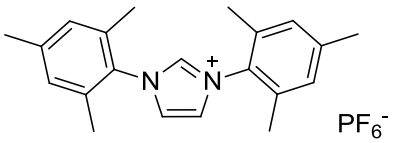

^{1}H NMR (500 MHz, $CDCl_3$) δ 8.55 (s, 1H, NCHN), 7.52 (s, 2H, imH), 7.02 (s, 4H, ArH), 2.34 (s, 6H, p-CH_3), 2.08 (s, 12H, o-CH_3). $^{13}C\{^1H\}$ NMR (126 MHz, $CDCl_3$) δ 141.7, 136.6, 134.1, 130.4, 130.1, 125.4, 21.3, 17.2. Analysis Calculated for $C_{21}H_{25}F_6N_2P$: C, 56.00; H, 5.59; N, 6.22. Found: C, 55.80; H, 5.60; N, 6.10.

Consistent with data previously reported.[23]

6.2.18 Preparation of L8[24]

Benzyl bromide (2.0 ml, 17 mmol) was dissolved in anhydrous tetrahydrofuran (40 ml) under inert conditions. To this, *N*-methylimidazole (1.5 ml, 19 mmol) was slowly added and the mixture was stirred at room temperature for 3 days. A colourless suspension/clear oil formed very quickly following combination of the reactants. After 3 days, the mixture was allowed to settle and the solvent carefully decanted-off. The clear oil was washed repeatedly with acetone and dried *in vacuo* to give the product as a clear oil. Yield: 3.0 g, 12 mmol, 70%.

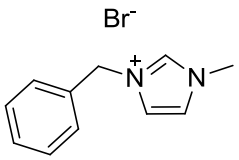

^{1}H NMR (300 MHz, $(CD_3)_2SO$) δ 9.34 (s, 1H, NCHN), 7.84 (s, 1H, imH), 7.75 (s, 1H, imH), 7.50 – 7.32 (m, 5H, ArH), 5.46 (s, 2H, CH_2), 3.87 (s, 3H, CH_3). $^{13}C\{^{1}H\}$ NMR (75 MHz, $(CD_3)_2SO$) δ 136.6, 134.9, 128.9, 128.7, 128.3, 124.0, 122.3, 51.7, 35.9. HRMS (ESI^+): *m/z* 173.1079 $[M - Br]^+$ calculated $[M - Br]^+$ 173.1073. Analysis Calculated for $C_{11}H_{13}N_2Br.H_2O$: C, 48.72; H, 5.58; N, 10.33. Found: C, 48.05; H, 5.20; N, 10.20.

Consistent with data previously reported.[24]

6.2.19 Preparation of L9[25]

To an aqueous solution of **L8** (1.3 g, 4.9 mmol), NH_4PF_6 (4.0 g, 25 mmol) in water was slowly added and allowed to stir for 30 minutes. A white precipitate formed almost immediately. The precipitate was filtered, washed repeatedly with water, dried and then recrystallised from acetone / diethyl ether affording **L9** as a white crystalline solid. Yield: 1.5 g, 4.6 mmol, 94%.

Single crystals suitable for X-ray diffraction analysis were grown by the vapour diffusion of pentane in to a concentrated solution of the ligand in dichloromethane, producing colourless plate crystals.

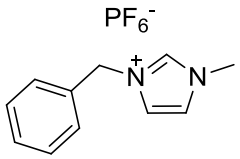

^{1}H NMR (300 MHz, $(CD_3)_2CO$) δ 9.11 (s, 1H, NCHN), 7.77 (s, 1H, imH), 7.74 (s, 1H, imH), 7.54 – 7.39 (m, 5H, ArH), 5.59 (s, 2H, CH_2), 4.08 (s, 3H, CH_3). $^{13}C\{^{1}H\}$ NMR (75 MHz, $(CD_3)_2CO$) δ 137.6, 135.2, 130.1, 130.0, 129.5, 125.2, 123.5, 53.8, 36.8. Analysis Calculated for $C_{11}H_{13}F_6N_2P$: C, 41.52; H, 4.12; N, 8.80. Found: C, 41.05; H, 4.05; N, 8.65.

Consistent with data previously reported.[25]

6.2.20 Preparation of L11[26]

Benzimidazole (1.4 g, 12 mmol) and K_2CO_3 (2.4 g, 18 mmol) were added to a Schlenk flask. Anhydrous acetonitrile (60 ml) was added to the mixture and the suspension was stirred at room temperature for 20 minutes. Benzyl bromide (2.8 ml, 23 mmol) was added and the suspension stirred for a further 2 days. The suspension was transferred to a round-bottomed flask and the solvent removed *in vacuo*. Water (150 ml) was added to the resulting solid and the suspension stirred for 1 hour and then filtered. The off-white solid was then washed successively with acetone and diethyl ether to yield the product as a white solid. Yield: 4.0 g, 11 mmol, 90%.

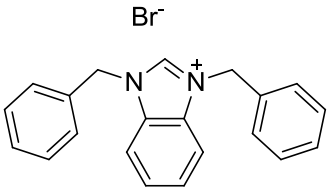

^{1}H NMR (500 MHz, $(CD_3)_2SO$) δ 10.22 (s, 1H, NCHN), 8.05 – 7.89 (m, 2H, ArH), 7.65 – 7.58 (m, 2H, ArH), 7.54 (d, J = 7.1 Hz, 4H, ArH), 7.45 – 7.33 (m, 6H, ArH), 5.83 (s, 4H, CH_2). $^{13}C\{^{1}H\}$ NMR (75 MHz, $(CD_3)_2SO$) δ 142.6, 133.8, 131.0, 128.9, 128.7, 128.3, 126.7, 114.0,

50.0. HRMS (ESI^+): *m/z* 299.1535 $[M - Br]^+$ calculated $[M - Br]^+$ 299.1543. Analysis Calculated for $C_{21}H_{19}BrN_2.⅔H_2O$: C, 64.46; H, 5.24; N, 7.16. Found: C, 64.15; H, 5.35; N, 7.10.

Consistent with data previously reported.[26]

6.2.21 Preparation of L12

To a methanolic solution of **L11** (2.0 g, 5.3 mmol), NH_4PF_6 (4.3 g, 26 mmol) in methanol was slowly added and allowed to stir for 30 minutes. A white precipitate formed almost immediately. The precipitate was filtered, washed repeatedly with methanol and dried. Yield: 2.3 g, 5.1 mmol, 97%.

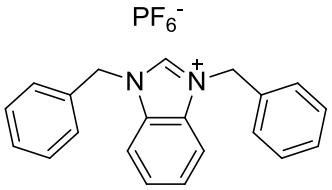

^1H NMR (500 MHz, $(CD_3)_2CO$) δ 9.83 (s, 1H, NCHN), 8.08 – 7.93 (m, 2H, ArH), 7.78 – 7.65 (m, 2H, ArH), 7.60 – 7.57 (m, 4H, ArH), 7.48 – 7.39 (m, 6H, ArH), 5.94 (s, 4H, CH_2). $^{13}C\{^1H\}$ NMR (75 MHz, $(CD_3)_2CO$) δ 143.1, 134.3, 132.8, 130.1, 130.0, 129.4, 128.1, 115.0, 51.9. Analysis Calculated for $C_{21}H_{19}F_6N_2P$: C, 56.76; H, 4.31; N, 6.30. Found: C, 56.90; H, 4.30; N, 6.30.

6.2.22 Preparation of L13A[12]

1,3-(Bisbromomethyl)benzene (2.5 g, 9.4 mmol) was dissolved in anhydrous acetone (100 ml). A solution of precursor **P13** (2.3 g, 9.4 mmol) in acetone (100 ml) was added slowly over 4 hours at room temperature. The mixture was then stirred for 18 hours, during which time a white precipitate formed, which was collected by filtration and washed repeatedly with acetone and diethyl ether to give the pure product as a white, microcrystalline solid. Yield: 2.7 g, 5.4 mmol, 57%.

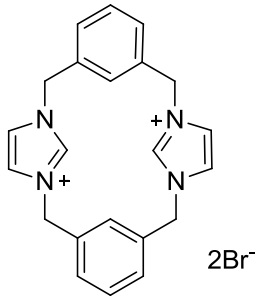

^1H NMR (300 MHz, $(CD_3)_2SO$) δ 9.50 (s, 2H, NCHN), 7.86 (s, 4H, imH), 7.60 (d, J = 7.4 Hz, 4H, ArH), 7.54 – 7.45 (m, 2H, ArH), 7.17 (s, 2H, ArH), 5.46 (s, 8H, CH_2). $^{13}C\{^1H\}$ NMR (126 MHz, $(CD_3)_2SO$) δ 136.3, 136.0, 129.4, 129.1, 126.0, 123.1, 51.7. HRMS (ESI^+): *m/z* 421.1041 $[M - Br]^+$ calculated $[M - Br]^+$ 421.1022. Analysis Calculated for $C_{22}H_{22}Br_2N_4.(CH_3)_2SO$: C, 49.67; H, 4.86; N, 9.65. Found: C, 49.45; H, 4.80; N, 9.85.

Consistent with data previously reported.[12]

6.2.23 Preparation of L13B

To a methanolic solution of **L13A** (1.2 g, 2.4 mmol), NH_4PF_6 (3.9 g, 24 mmol) in methanol was slowly added and allowed to stir for 30 minutes. A white precipitate formed almost immediately. The precipitate was filtered, washed repeatedly with methanol and dried. Yield: 1.3 g, 2.0 mmol, 84%.

^{1}H NMR (500 MHz, $(CD_3)_2SO$) δ 9.22 (s, 2H, imH), 7.81 (d, J = 1.4 Hz, 4H, imH), 7.58 (d, J = 6.4 Hz, 4H, ArH), 7.56 – 7.50 (m, 2H, ArH), 6.94 (s, 2H, ArH), 5.43 (s, 8H, CH_2). ^{13}C{^{1}H} NMR (126 MHz, $(CD_3)_2SO$) δ 136.2, 136.1, 129.5, 129.1, 125.5, 123.2, 51.8. Analysis Calculated for $C_{22}H_{22}F_{12}N_4P_2$: C, 41.79; H, 3.51; N, 8.86. Found: C, 42.15; H, 3.65; N, 9.00.

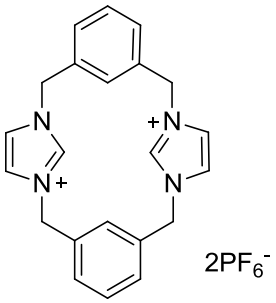

6.2.24 Preparation of L14[27]

In a modification of a literature procedure,[28] allyl bromide (8.0 ml, 94 mmol) was added to a stirring suspension of benzimidazole (4.7 g, 40 mmol) and $NaHCO_3$ (10 g) in acetonitrile (100 ml). The mixture was stirred at ambient temperature for 7 days. After this time, the mixture was filtered and the solvent removed *in vacuo* to yield a pale yellow crystalline solid. The product was purified by dissolving in a minimum amount of hot acetonitrile, and then placing in a freezer at -30°C. The product crystallised as large off-white crystals. Yield: 4.4 g, 16 mmol, 39%.

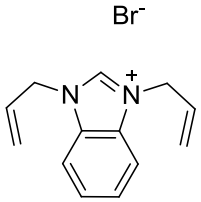

^{1}H NMR (500 MHz, $CDCl_3$) δ 11.41 (s, 1H, NCHN), 7.85 – 7.66 (m, 2H, ArH), 7.67 – 7.53 (m, 2H, ArH), 6.12 (ddt, J = 16.7, 10.3, 6.1 Hz, 2H, C**H**=CH_2), 5.50 (d, J = 16.7 Hz, 2H, CH=CH**H**$_{(trans)}$), 5.46 (d, J = 10.3 Hz, 2H, CH=CH**H**$_{(cis)}$), 5.32 (d, J = 6.1 Hz, 4H, NCH_2). ^{13}C{^{1}H} NMR (126 MHz, $CDCl_3$) δ 143.0, 131.5, 129.6, 127.3, 122.1, 113.8, 50.3. HRMS (ESI^+): *m/z* 199.1222 $[M - Br]^+$ calculated $[M - Br]^+$ 199.1230. Analysis Calculated for $C_{13}H_{15}BrN_2$: C, 55.93; H, 5.42; N, 10.03. Found: C, 55.70; H, 5.40; N, 10.10.

Consistent with data previously reported.[27]

6.2.25 Preparation of L15[28]

A round-bottomed flask was charged with *N*-methylimidazole (2.4 ml, 30 mmol). Allyl bromide (8.0 ml, 92 mmol) was added dropwise with stirring. The mixture quickly thickened and darkened forming a brown / orange oil, which was stirred for a further 24 hours. Volatiles were removed from the oil *in vacuo*. Yield: 6.1 g, 30 mmol, quantitative.

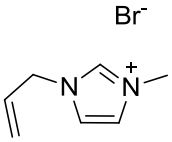

^{1}H NMR (500 MHz, $(CD_3)_2SO$) δ 9.24 (s, 1H, NCHN), 7.77 (s, 1H, imH), 7.75 (s, 1H, imH), 6.04 (ddt, J = 17.0, 10.2, 5.9 Hz, 1H, C**H**=CH_2), 5.35 (ddd, J = 10.2, 2.5, 1.3 Hz, 1H, CH=CH**H**$_{(cis)}$), 5.30 (ddd, J = 17.0, 2.5, 1.3 Hz, 1H, CH=CH**H**$_{(trans)}$), 4.88 (d, J = 5.9 Hz, 2H, NCH_2), 3.88 (s, 3H, NCH_3). ^{13}C{^{1}H} NMR (75 MHz, $(CD_3)_2SO$) δ 136.6, 131.8, 123.7, 122.3, 120.1, 50.7, 35.8. HRMS (ESI^+): *m/z* 123.0921 $[M - Br]^+$ calculated $[M - Br]^+$ 123.0917. Analysis Calculated for $C_7H_{11}BrN_2$: C, 41.40; H, 5.46; N, 13.79; Br, 39.35. Found: C, 41.10; H, 5.45; N, 13.60; Br, 39.30.

Consistent with data previously reported.[28]

6.2.26 Preparation of L16[28]

A large Schlenk flask fitted with a condenser was charged with imidazole (2.7 g, 40 mmol), $NaHCO_3$ (10 g), allyl bromide (14 ml, 0.16 mol) and acetonitrile (150 ml). The suspension was heated for 4 days at reflux. After his time, the suspension was filtered and the volatiles removed *in vacuo* to give a golden-yellow oil. Yield: 5.4 g, 23 mmol, 59%.

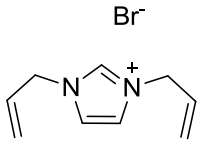

^{1}H NMR (300 MHz, $(CD_3)_2SO$) δ 9.25 (s, 1H, NCHN), 7.78 (d, J = 1.6 Hz, 2H, imH), 6.06 (ddt, J = 16.7, 10.3, 6.0 Hz, 2H, C**H**=CH_2), 5.37 (ddd, J = 10.3, 2.5, 1.3 Hz, 2H, CH=CH**H$_{(cis)}$**), 5.30 (ddd, J = 16.7, 2.5, 1.3 Hz, 2H, CH=CH**H$_{(trans)}$**), 4.88 (d, J = 6.0 Hz, 4H, NCH_2). ^{13}C{^{1}H} NMR (75 MHz, $(CD_3)_2SO$) δ 136.2, 131.7, 122.7, 120.2, 50.9. HRMS (ESI^+): *m/z* 150.1144 $[M + H - Br]^+$ calculated $[M + H - Br]^+$ 150.1151. Analysis Calculated for $C_9H_{13}N_2Br.¼H_2O$: C, 46.27; H, 5.82; N, 11.99. Found: C, 46.40; H, 5.70; N, 11.65.

Consistent with data previously reported.[28]

6.2.27 Preparation of L17

To a stirring solution of precursor **P17** (0.38 g, 2.0 mmol) in acetonitrile (30 ml) was added allyl bromide (0.4 ml, 4.1 mmol). The solution was stirred at ambient temperature for 4 days. After this time, the volatiles were removed *in vacuo* producing an off-white solid. The solid was washed with diethyl ether to yield the product as a white solid. Yield: 0.59 g, 1.9 mmol, 95%.

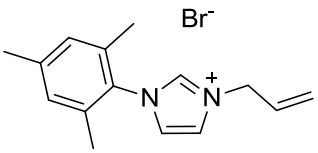

Single crystals suitable for X-ray analysis were grown by the vapour diffusion of diethyl ether in to a concentrated acetonitrile solution of the product.

^{1}H NMR (500 MHz, $CDCl_3$) δ 10.43 (s, 1H, NCHN), 7.74 (t, J = 1.6 Hz, 1H, imH), 7.19 (t, J = 1.6 Hz, 1H, imH), 6.98 (s, 2H, ArH), 6.12 (ddt, J = 16.8, 10.2, 6.3 Hz, 1H, C**H**=CH_2), 5.51 (d, J = 16.8 Hz, 1H, CH=CH**H$_{(trans)}$**), 5.46 (d, J = 10.2 Hz, 1H, CH=CH**H$_{(cis)}$**), 5.42 (d, J = 6.3 Hz, 2H, NCH_2), 2.33 (s, 3H, p-CH_3), 2.07 (s, 6H, o-CH_3). ^{13}C{^{1}H} NMR (126 MHz, $CDCl_3$) δ 141.5, 138.3, 134.3, 130.8, 130.6, 130.0, 123.3, 122.8, 122.4, 52.5, 21.2, 17.8. HRMS (ESI^+): *m/z* 227.1547 $[M - Br]^+$ calculated $[M - Br]^+$ 227.1543. Analysis Calculated for $C_{15}H_{19}N_2Br.¼H_2O$: C, 57.79; H, 6.31; N, 8.99. Found: C, 58.15; H, 6.25; N, 9.00.

6.2.28 Preparation of L18

Precursor **P18** (0.72 g, 4.1 mmol) was dissolved in acetonitrile (50 ml). To this solution, allyl bromide (0.72 ml, 8.3 mmol) was added and the mixture was stirred at ambient temperature for 5 days. After this time, the volatiles were removed *in vacuo* and the resulting material was

washed repeatedly with diethyl ether to yield the product as an orange oil, which slowly crystallises on standing under a dry atmosphere at ambient temperature. Yield: 1.1 g, 3.7 mmol, 89%.

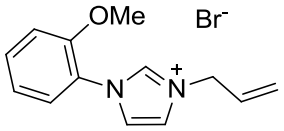

^{1}H NMR (500 MHz, $CDCl_3$) δ 10.55 (s, 1H, NCHN), 7.64 (dd, J = 7.8, 1.5 Hz, 1H, ArH), 7.53 (t, J = 1.7 Hz, 1H, imH), 7.51 (t, J = 1.7 Hz, 1H, imH), 7.51 – 7.46 (m, 1H, ArH), 7.13 – 7.08 (m, 2H, ArH), 6.11 (ddt, J = 16.8, 10.1, 6.5 Hz, 1H, C**H**=CH_2), 5.55 (dd, J = 16.8, 0.7 Hz, 1H, CH=CH**H**$_{(trans)}$), 5.47 (dd, J = 10.1, 0.7 Hz, 1H, CH=CH**H**$_{(cis)}$), 5.35 (d, J = 6.5 Hz, 2H, NCH_2), 3.93 (s, 3H, OCH_3). ^{13}C{^{1}H} NMR (75 MHz, $CDCl_3$) δ 152.0, 137.2, 131.9, 130.2, 125.8, 123.3, 123.2, 122.7, 121.9, 121.6, 112.7, 56.4, 52.3. HRMS (ESI^+): *m/z* 215.1177 $[M - Br]^+$ calculated $[M - Br]^+$ 215.1179. Analysis Calculated for $C_{13}H_{15}BrN_2O.½H_2O$: C, 51.33; H, 5.30; N, 9.21. Found: C, 51.30; H, 5.10; N, 9.05.

6.2.29 Preparation of L19

Precursor **P19** (0.25 g, 1.7 mmol) was dissolved in a stirring solution of diisopropyl ether (100 ml). Allyl bromide (3.0 ml, 34 mmol) was added to this solution and the mixture was heated at reflux for 4 days. After this time, the resulting off-white solid was collected by filtration, washed repeatedly with diethyl ether and dried *in vacuo* to give the crude product as a white solid. The product was recrystallised from chloroform / diethyl ether to give the product as a white crystalline solid. Yield: 0.43 g, 1.6 mmol, 94%.

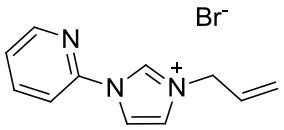

Single crystals suitable for X-ray diffraction analysis were grown by layering diethyl ether over a concentrated solution of the product in chloroform.

^{1}H NMR (300 MHz, $CDCl_3$) δ 11.76 (s, 1H, NCHN), 8.57 – 8.47 (m, 2H, pyH), 8.32 (t, J = 1.7 Hz, 1H, imH), 8.08 – 7.99 (m, 1H, pyH), 7.50 (t, J = 1.7 Hz, 1H, imH), 7.48 – 7.42 (m, 1H, pyH), 6.12 (ddt, J = 16.8, 10.1, 6.5 Hz, 1H, C**H**=CH_2), 5.59 (d, J = 16.8 Hz, 1H, CH=CH**H**$_{(trans)}$), 5.51 (dd, J = 10.1, 0.6 Hz, 1H, CH=CH**H**$_{(cis)}$), 5.24 (d, J = 6.5 Hz, 2H, NCH_2). ^{13}C{^{1}H} NMR (75 MHz, $CDCl_3$) δ 149.1, 146.1, 140.8, 136.0, 129.7, 125.3, 123.5, 122.0, 119.1, 115.2, 52.8. HRMS (ESI^+): *m/z* 186.1030 $[M - Br]^+$ calculated $[M - Br]^+$ 186.1026. Analysis Calculated for $C_{11}H_{12}BrN_3.¼H_2O$: C, 48.82; H, 4.66; N, 15.53. Found: C, 49.00; H, 4.35; N, 15.35.

6.2.30 Preparation of L20

Precursor **P20** (0.27 g, 1.3 mmol) was dissolved in acetonitrile (100 ml). To this, allyl bromide (0.24 ml, 2.7 mmol) was added and the mixture was stirred at ambient temperature for 6 days and then at 50°C for 3 days. After this time, the volatiles were removed *in vacuo* and the resulting off-white solid was recrystallised from acetonitrile / diethyl ether to give the product as an off-white solid. Yield: 0.33 g, 0.73 mmol, 57%.

Single crystals suitable for X-ray diffraction analysis were grown by the vapour diffusion of diethyl ether in to a concentrated solution of the product in acetonitrile.

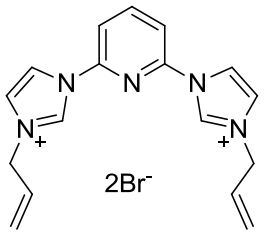

^{1}H NMR (300 MHz, $(CD_3)_2SO$) δ 10.65 (s, 2H, NCHN), 8.86 (t, J = 1.9 Hz, 2H, imH), 8.61 (t, J = 8.1 Hz, 1H, pyH), 8.28 (d, J = 8.1 Hz, 2H, pyH), 8.10 (t, J = 1.9 Hz, 2H, imH), 6.25 – 6.09 (m, 2H, C**H**=CH_2), 5.58 – 5.32 (m, 4H, CH=C**H$_2$**), 5.04 (d, J = 5.9 Hz, 4H, NCH_2). ^{13}C{^{1}H} NMR (75 MHz, $(CD_3)_2SO$) δ 145.3, 144.8, 136.0, 131.1, 123.8, 120.9, 119.6, 114.3, 51.6. HRMS (ESI^+): *m/z* 372.0828 $[M - Br]^+$ calculated $[M - Br]^+$ 372.0818. Analysis Calculated for $C_{17}H_{19}Br_2N_5.2H_2O$: C, 41.74; H, 4.74; N, 14.32. Found: C, 41.90; H, 4.30; N, 14.00.

6.2.31 Preparation of L21

Precursor **P21** (0.42 g, 2.2 mmol), allyl bromide (1.0 ml, 11 mmol) and acetonitrile (100 ml) were added to a round-bottomed flask. The mixture was heated at reflux for 20 hours with stirring. After this time, the solution was allowed to cool to ambient temperature and the solvent was reduced in volume (to approximately 20 ml). Slow addition of diethyl ether (60 ml) led to the precipitation of a crystalline off-white solid, which was collected by vacuum filtration, washed repeatedly with diethyl ether and dried *in vacuo*. Yield: 0.69 g, 2.2 mmol, quantitative.

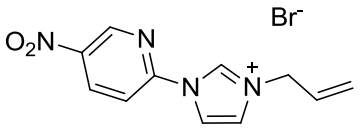

Single crystals suitable for X-ray diffraction analysis were grown by the vapour diffusion of diethyl ether in to a concentrated solution of the product in acetonitrile.

^{1}H NMR (300 MHz, $CDCl_3$) δ 12.22 (s, 1H, NCHN), 9.34 (d, J = 2.5 Hz, 1H, pyH), 9.12 (d, J = 9.0 Hz, 1H, pyH), 8.84 (dd, J = 9.0, 2.5 Hz, 1H, pyH), 8.42 (t, J = 1.8 Hz, 1H, imH), 7.51 (t, J = 1.8 Hz, 1H, imH), 6.15 (ddt, J = 16.7, 10.3, 6.6 Hz, 1H, C**H**=CH_2), 5.64 (d, J = 16.7 Hz, 1H, CH=CH**H$_{(trans)}$**), 5.58 (d, J = 10.3 Hz, 1H, CH=CH**H$_{(cis)}$**), 5.22 (d, J = 6.6 Hz, 2H, NCH_2). ^{13}C{^{1}H} NMR (75 MHz, $CDCl_3$) δ 149.2, 145.1, 144.6, 137.0, 136.3, 129.3, 124.1, 123.0, 119.6, 116.2, 53.1. HRMS (ESI^+): *m/z* 231.0882 $[M - Br]^+$ calculated $[M - Br]^+$ 231.0877. Analysis Calculated for $C_{11}H_{11}BrN_4O_2.½H_2O$: C, 41.27; H, 3.78; N, 17.50. Found: C, 41.40; H, 3.60; N, 17.45.

6.2.32 Preparation of L22

Precursor **P22** (0.80 g, 5.0 mmol), allyl bromide (2.0 ml, 23 mmol), and acetonitrile (50 ml) were placed in a small round-bottomed flask and heated to reflux for 16 hours. After this time, the mixture was cooled to room temperature and the volume of solvent reduced *in vacuo* (to approximately 15 ml). Slow addition of diethyl ether (35 ml) to the

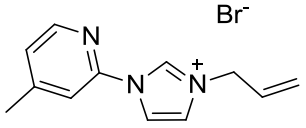

stirring acetonitrile solution led to the precipitation of the product as an off-white crystalline solid, which was collected by vacuum filtration, washed repeatedly with diethyl ether, and dried *in vacuo*. Yield: 1.3 g, 4.5 mmol, 89%.

Single crystals suitable for X-ray diffraction analysis were grown by the vapour diffusion of pentane in to a concentrated solution of the product in chloroform.

^{1}H NMR (300 MHz, $CDCl_3$): δ 11.34 (s, 1H, NCHN), 8.42-8.21 (m, 3H, pyH and imH), 7.67 (s, 1H, imH), 7.20 (d, J = 4.9 Hz, 1H, pyH), 6.09 (ddt, J = 16.9, 10.1, 6.5 Hz, 1H, C**H**═CH_2), 5.56 (d, J = 16.9 Hz, 1H, CH═CH**H**$_{(trans)}$), 5.44 (d, J = 10.1 Hz, 1H, CH═**C**H**H**$_{(cis)}$), 5.21 (d, J = 6.5 Hz, 2H, NCH_2), 2.48 (s, 3H, CH_3). ^{13}C{^{1}H} NMR (75 MHz, $CDCl_3$): δ 152.9, 148.6, 146.1, 135.2, 129.8, 126.2, 123.2, 122.5, 119.2, 115.5, 52.6, 21.3. HRMS (ESI^+): *m/z* 200.1180 [M – Br]$^+$ calculated [M – Br]$^+$ 200.1182. Analysis Calculated for $C_{12}H_{14}BrN_3.½H_2O$: C, 49.84; H, 5.23; N, 14.53. Found: C, 49.60; H, 5.10; N, 14.35. Mp: 158.6–160.4 °C.

6.2.33 Preparation of L23

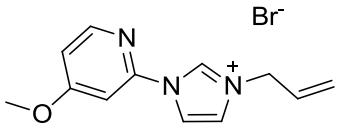

Precursor **P23** (0.28 g, 1.6 mmol), allyl bromide (2 ml, 23 mmol) and acetonitrile (50 ml) were added to a round-bottomed flask. The resulting solution was stirred at room temperature for 4 days. After this time, the solvent was reduced in volume (to 25 ml) *in vacuo*, and diethyl ether added (50 ml) to induce the precipitation of the product as an off-white crystalline solid. The solid was collected by filtration, washed repeatedly with diethyl ether, and dried *in vacuo*. Yield: 0.43 g, 1.5 mmol, 91%.

^{1}H NMR (300 MHz, $CDCl_3$) δ 11.72 (s, 1H, NCHN), 8.32 (s, 1H, imH), 8.21 (d, J = 5.8 Hz, 1H, pyH), 8.13 (d, J = 2.0 Hz, 1H, pyH), 7.49 (s, 1H, imH), 7.26 (pyH resonance obscured by $CHCl_3$ signal), 6.90 (dd, J = 5.8, 2.1 Hz, 1H, pyH), 6.11 (ddt, J = 16.8, 10.1, 6.5 Hz, 1H, C**H**=CH_2), 5.57 (d, J = 16.8 Hz, 1H, CH=CH**H**$_{(trans)}$), 5.49 (d, J = 10.1 Hz, 1H, CH=CH**H**$_{(cis)}$), 5.15 (d, J = 6.5 Hz, 2H, NCH_2), 4.10 (s, 3H, OCH_3). ^{13}C{^{1}H} NMR (75 MHz, $CDCl_3$) δ 169.2, 149.3, 147.9, 136.1, 129.7, 123.4, 121.8, 119.4, 113.8, 100.0, 58.0, 52.8. HRMS (ESI^+): *m/z* 216.1134 [M – Br]$^+$ calculated [M – Br]$^+$ 216.1131. Analysis Calculated for $C_{12}H_{14}BrN_3O.⅔H_2O$: C, 46.77; H, 5.02; N, 13.64. Found: C, 46.60; H, 4.80; N, 13.30.

6.2.34 Preparation of L24

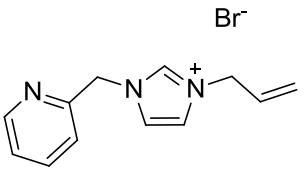

2-Bromomethylpyridine.HBr (0.51 g, 2.0 mmol), *N*-allylimidazole (0.23 g, 2.1 mmol), K_2CO_3 (1.4 g, 10 mmol) and acetonitrile (50 ml) were placed in a round-bottomed flask and stirred vigorously at room temperature for 24 hours. After this time, the mixture was

filtered and the solvent removed *in vacuo* to give a pale orange oil. Dissolution in acetonitrile (20 ml) followed by reprecipitation with diethyl ether (50 ml) (twice) gave the pure product as a pale yellow oil. Yield: 0.56 g, 2.0 mmol, quantitative.

^{1}H NMR (300 MHz, $CDCl_3$): δ 10.60 (s, 1H, NCHN), 8.52 (d, J= 4.7 Hz, 1H, pyH), 7.82 (d, J = 7.7 Hz, 1H, pyH), 7.74 (td, J = 7.7, 1.7 Hz, 1H, pyH), 7.66 (s, 1H, imH), 7.33-7.26 (m, 2H, pyH and imH), 6.01 (ddt, J = 16.6, 10.0, 6.5 Hz, 1H, C**H**═CH_2), 5.78 (s, 2H, NC**H**$_2$-pyridyl), 5.53-5.41 (m, 2H, CH═C**H$_2$**), 4.95 (d, J = 6.5 Hz, 2H, NCH_2). ^{13}C{^{1}H} NMR (75 MHz, $CDCl_3$): δ 152.5, 150.0, 137.9, 137.6, 129.6, 124.3, 124.2, 123.1, 121.3, 110.1, 54.2, 52.4. HRMS (ESI$^+$): *m/z* 200.1181 $[M - Br]^+$ calculated $[M - Br]^+$ 200.1182. Analysis Calculated for $C_{12}H_{14}BrN_3.H_2O$: C, 48.34; H, 5.41; N, 14.09. Found: C, 48.70; H, 5.10; N, 14.90.

6.2.35 Preparation of L25[29]

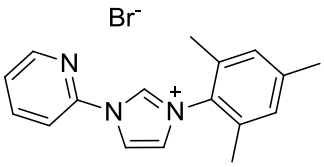

To a small round-bottomed flask was added precursor **P17** (1.1 g, 5.8 mmol) and 2-bromopyridine (0.58 ml, 6.0 mmol). The flask was submerged as fully as possible in silicone oil, sealed and the mixture was heated at 160°C with stirring for 10 hours. After this time, the solid formed was collected and washed with diethyl ether. Recrystallisation from chloroform / diethyl ether gave the pure product as an off-white microcrystalline solid. Yield: 1.8 g, 5.3 mmol, 91%.

Single crystals suitable for X-ray diffraction analysis were grown by the vapour diffusion of diethyl ether in to a concentrated solution of the product in acetonitrile.

^{1}H NMR (300 MHz, $CDCl_3$) δ 11.45 (s, 1H, imH), 9.25 (d, J = 8.2 Hz, 1H, pyH), 8.91 (t, J = 1.8 Hz, 1H, imH), 8.53 (dd, J = 4.9, 1.1 Hz, 1H, pyH), 8.11 (td, J = 8.2, 1.8 Hz, 1H, pyH), 7.49 (dd, J = 7.4, 4.9 Hz, 1H, pyH), 7.33 (t, J = 1.8 Hz, 1H, imH), 7.05 (s, 2H, mesH), 2.35 (s, 3H, p-CH_3), 2.19 (s, 6H, o-CH_3). ^{13}C{^{1}H} NMR (75 MHz, $CDCl_3$) δ 148.8, 146.1, 141.8, 141.1, 136.4, 134.2, 130.7, 130.2, 125.7, 123.9, 120.2, 116.7, 21.3, 18.0. HRMS (ESI$^+$): *m/z* 264.1496 [M - Br]$^+$ calculated [M - Br]$^+$ 264.1495. Analysis Calculated for $C_{17}H_{18}BrN_3$: C, 59.31; H, 5.27; N, 12.21. Found: C, 59.45; H, 5.25; N, 12.35.

Consistent with data previously reported.[29]

6.2.36 Preparation of L26

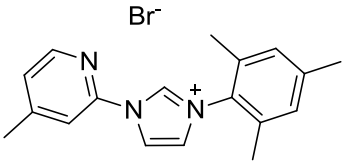

In a modification of a literature procedure,[29] to a small round-bottomed flask was added precursor **P17** (0.20 g, 1.1 mmol) and 2-bromo-4-methylpyridine (0.14 ml, 1.3 mmol). The flask was sealed, fully submerged in silicone oil and the mixture was heated at 160°C with stirring for 24 hours. After this time, the mixture was

triturated with ethyl acetate (25 ml). Repeated recrystallization from acetonitrile / diethyl ether gave the product as a light brown solid. Yield: 0.17 g, 0.48 mmol, 44 %.

Single crystals suitable for X-ray diffraction analysis were grown by the vapour diffusion of diethyl ether in to a concentrated solution of the product in acetonitrile.

^{1}H NMR (300 MHz, $CDCl_3$) δ 11.38 (s, 1H, NCHN), 9.16 (s, 1H, pyH), 8.84 (s, 1H, imH), 8.36 (d, *J* = 5.0 Hz, 1H, pyH), 7.33 – 7.27 (m, 2H, pyH & imH), 7.06 (s, 2H, mesH), 2.61 (s, 3H, $pyCH_3$), 2.36 (s, 3H, p-CH_3), 2.19 (s, 6H, o-CH_3). ^{13}C{^{1}H} NMR (75 MHz, $CDCl_3$) δ 153.8, 148.3, 146.1, 141.8, 136.4, 134.2, 130.7, 130.2, 126.7, 123.8, 120.2, 117.1, 21.3, 21.3, 18.0. HRMS (ESI^+): *m/z* 278.1660 $[M - Br]^+$ calculated $[M - Br]^+$ 278.1652. Analysis Calculated for $C_{18}H_{20}BrN_3$: C, 60.34; H, 5.63; N, 11.73. Found: C, 60.50; H, 5.60; N, 11.80.

6.2.37 Preparation of L27

In a modification of a literature procedure,[30] ligand precursor **L25** (0.12 g, 0.35 mmol) and *N*-bromosuccinimide (0.071 g, 0.40 mmol) were added to a small ampoule and dried/degassed *in vacuo*. To these was added anhydrous acetonitrile (10 ml) *via* a cannula. The resultant pale yellow solution was stirred at room temperature for 3 days. After this time, the solution was concentrated to approximately 4 ml. Slow addition of an excess of ethyl acetate (50 ml) induced the precipitation of the product as a white crystalline solid, which was collected, washed with ethyl acetate (50 ml), and dried *in vacuo*. Yield: 0.11 g, 0.25 mmol, 73%.

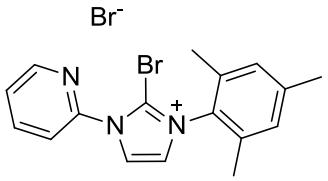

Single crystals suitable for X-ray diffraction analysis were obtained *via* the vapour diffusion of diethyl ether in to a concentrated solution of the product in acetonitrile.

^{1}H NMR (300 MHz, CD_3CN) δ 8.73 (dd, J = 4.9, 1.0 Hz, 1H, pyH), 8.25 – 8.14 (m, 2H, pyH & imH), 7.95 (d, J = 8.1 Hz, 1H), 7.81 (d, J = 2.3 Hz, 1H, imH), 7.72 (dd, J = 7.5, 4.9 Hz, 1H, pyH), 7.20 (s, 2H, mesH), 2.40 (s, 3H, p-CH_3), 2.09 (s, 6H, o-CH_3). ^{13}C{^{1}H} NMR (75 MHz, CD_3CN) δ 150.9, 148.3, 143.2, 141.2, 136.1, 131.7, 130.8, 127.6, 126.5, 126.4, 124.8, 121.2, 21.2, 17.8. HRMS (ESI^+): *m/z* 342.0600 $[M - Br]^+$ calculated $[M - Br]^+$ 342.0600. Analysis Calculated for $C_{17}H_{17}Br_2N_3$: C, 48.25; H, 4.05; N, 9.93. Found: C, 48.20; H, 4.00; N, 9.90.

6.2.38 Preparation of C1

Ligand precursor **L1** (0.43 g, 1.0 mmol) was added to an oven-dried 3-necked round-bottomed flask and dried/degassed *in vacuo* for 1 hour. To this, anhydrous acetonitrile (15 ml) was cannula transferred, dissolving the imidazolium salt. The electrodes were inserted in to the round-bottomed flask and the solution was degassed (by bubbling with argon for >1 hour). The electrodes were then placed in the reaction mixture and the mixture was

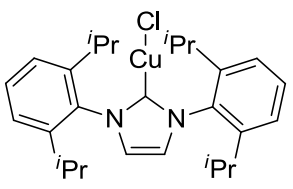

electrolysed at 60 mA for 90 mins (3Q). The mixture was filtered and the acetonitrile removed *in vacuo*. The residue was washed with diethyl ether to yield the product as an off-white solid. Yield: 0.30 g, 0.62 mmol, 62%.

^{1}H NMR (300 MHz, $(CD_3)_2CO$) δ 7.70 (s, 2H, imH), 7.55 (t, *J* = 7.7 Hz, 2H, ArH), 7.41 (d, *J* = 7.7 Hz, 4H, ArH), 2.67 (m, 4H, C**H**$(CH_3)_2$), 1.31 (d, *J* = 6.9 Hz, 12H, CH(C**H**$_3)_2$), 1.25 (d, *J* = 6.9 Hz, 12H, CH(C**H**$_3)_2$). ^{13}C{^{1}H} NMR (75 MHz, $(CD_3)_2CO$) δ 180.9, 146.6, 135.8, 131.2, 124.9, 29.5, 25.0, 24.0. HRMS (ESI$^+$): *m/z* 509.1734 $[M + Na]^+$ calculated $[M + Na]^+$ 509.1755. Analysis Calculated for $C_{27}H_{36}ClCuN_2$: C, 66.51; H, 7.44; N, 5.75; Cl, 7.27. Found: C, 66.30; H, 7.45; N, 5.70; Cl, 6.95.

Consistent with data previously reported.[31]

6.2.39 Preparation of C2

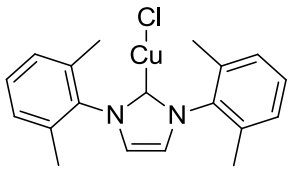

Ligand precursor **L2** (0.30 g, 0.97 mmol) was added to a three-necked round-bottomed flask. Anhydrous acetonitrile (10 ml) was added and the copper electrodes (1 x 3 cm^2) were inserted in to the reaction mixture. The solution was degassed (by bubbling with argon for >1 hour). The potential across the electrodes was adjusted so that a current of 50 mA was maintained throughout the reaction. The mixture was electrolysed for 120 minutes (4Q), filtered and the solvent removed *in vacuo*. The resulting solid was washed with water, filtered and recrystallised from chloroform / diethyl ether, producing **C2** as a white solid. Yield: 0.16 g, 0.43 mmol, 44%.

^{1}H NMR (500 MHz, $CDCl_3$) δ 7.31 (t, *J* = 7.3 Hz, 2H, ArH), 7.20 (d, *J* = 7.3 Hz, 4H, ArH), 7.10 (s, 2H, imH), 2.16 (s, 12H, CH_3). ^{13}C{^{1}H} NMR (126 MHz, $CDCl_3$) δ 179.0, 137.63, 135.09, 129.84, 129.03, 122.32, 17.99. HRMS (ESI$^+$): *m/z* 380.1172 $[M – Cl + MeCN]^+$ calculated $[M – Cl + MeCN]^+$ 380.1183. Analysis Calculated for $C_{19}H_{20}ClCuN_2.½H_2O$: C, 59.37; H, 5.51; N, 7.29. Found: C, 59.55; H, 5.30; N, 7.15.

Consistent with data previously reported.[32]

6.2.40 Preparation of C3A

An oven-dried, three-necked, round-bottomed flask was charged with ligand precursor **L3** (0.34 g, 1.0 mmol). This was thoroughly dried/degassed *in vacuo*. Anhydrous acetonitrile (15 ml) was cannula transferred in to the flask dissolving the imidazolium salt. The solution was degassed (by bubbling with argon for >1 hour). The two copper electrodes were inserted in to the reaction flask and purged with argon (for >30 minutes) and then inserted in to the reaction mixture. A potential was applied such that a current of 50 mA flowed through the solution. The solution was electrolysed for 2Q. Following

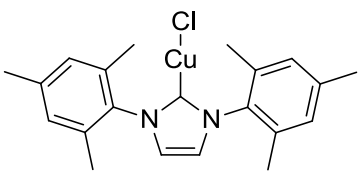

electrolysis, the mixture was filtered through celite and the solvent removed from the filtrate *in vacuo* to yield a pale yellow solid. The solid was washed with water, diethyl ether and recrystallised from dichloromethane / diethyl ether to yield the product as a white crystalline solid. Yield: 0.24 g, 0.59 mmol, 59%.

^{1}H NMR (500 MHz, $CDCl_3$) δ 7.05 (s, 2H, imH), 7.00 (s, 4H, ArH), 2.34 (s, 6H, CH_3), 2.10 (s, 12H, CH_3). $^{13}C\{^{1}H\}$ NMR (126 MHz, $CDCl_3$) δ 179.3, 139.7, 135.2, 134.7, 129.6, 122.4, 21.2, 17.9. HRMS (ESI^+): *m/z* 408.1502 $[M - Cl + MeCN]^+$ calculated $[M - Cl + MeCN]^+$ 408.1502. Analysis Calculated for $C_{21}H_{24}ClCuN_2$: C, 62.52; H, 6.00; N, 6.94; Cl, 8.79. Found: C, 62.45; H, 6.00; N, 6.80; Cl, 8.90.

Consistent with data previously reported.[32]

6.2.41 Preparation of C3B[33]

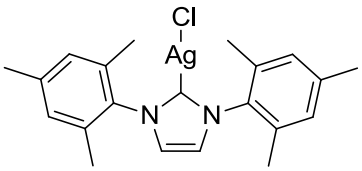

A Schlenk flask was charged with imidazolium chloride (0.35 g, 1.0 mmol), Ag_2O (0.14 g, 0.62 mmol) and activated 4Å molecular sieves. These were dried and degassed *in vacuo*. To these was added anhydrous dichloromethane (40 ml). The resultant dark suspension was heated at reflux (45°C) in the absence of light for 16 hours. After this time, the mixture was cooled and filtered, and the dichloromethane reduced *in vacuo* (to approximately 10 ml). Addition of pentane (40 ml) led to the precipitation of the product as a white crystalline solid. Yield: 0.37 g, 0.82 mmol, 79%.

^{1}H NMR (500 MHz, $CDCl_3$) δ 7.13 (d, *J* = 1.8 Hz, 2H, imH), 6.99 (s, 4H, ArH), 2.35 (s, 6H, p-CH_3), 2.07 (s, 12H, o-CH_3). $^{13}C\{^{1}H\}$ NMR (126 MHz, $CDCl_3$) δ ($C_{carbene}$ not observed), 139.8, 135.3, 134.6, 129.6, 122.8, 21.1, 17.7.

Consistent with data previously reported.[33]

6.2.42 Preparation of C3C

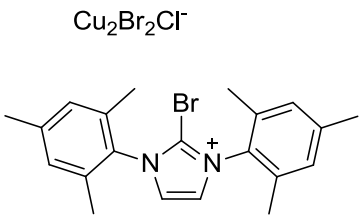

Complex **C3B** (0.11 g, 0.24 mmol) and $CuBr_2$ (0.11 g, 0.48 mmol) were added to a small Schlenk flask and dried/degassed *in vacuo*. To these was added anhydrous acetonitrile (25 ml). The resultant suspension was stirred at room temperature in the absence of light for 5 hours. After this time, the mixture was filtered to remove the precipitated silver halide, and the solution was concentrated in vacuo (to approximately 10 ml). Slow addition of diethyl ether (90 ml) led to the precipitation of the pure product as a white crystalline solid, which was collected by filtration and dried. Yield: 0.12 g, 0.17 mmol, 70%.

Single crystals suitable for X-ray diffraction analysis were obtained *via* the vapour diffusion of diethyl ether in to a concentrated solution of the product in acetonitrile.

^{1}H NMR (300 MHz, CD_3CN) δ 7.93 (s, 2H, imH), 7.22 (s, 4H, mesH), 2.40 (s, 6H, p-CH_3), 2.08 (s, 12H, o-CH_3). $^{13}C\{^{1}H\}$ NMR (75 MHz, CD_3CN) δ 143.3, 135.7, 131.3, 130.8, 127.8, 125.4, 21.2, 17.7. HRMS (ESI^+): *m/z* 383.1118 $[M - Cu_2X_3]^+$ calculated $[M - Cu_2X_3]^+$ 383.1117. Analysis Calculated for $C_{21}H_{24}Br_3ClCu_2N_2$: C, 35.69; H, 3.42; N, 3.96. Found: C, 36.00; H, 3.40; N, 3.90.

Note: The counter-anion was found to contain a mixture of chloride and bromide, with the elemental analysis suggesting a formula of $[Cu_2Br_2Cl]^-$. The yield is calculated with respect to this formula.

6.2.43 Preparation of C4

An oven-dried, three-necked, round-bottomed flask was charged with **L4** (0.53 g, 1.0 mmol). This was thoroughly dried/degassed *in vacuo*. Anhydrous acetonitrile (15 ml) was cannula transferred in to the flask dissolving the imidazolium salt. The solution was degassed (by bubbling with argon for >1 hour). The two copper electrodes were inserted in to the reaction flask and purged with argon (for > 30 minutes) and then inserted in to the reaction mixture. A potential was applied such that a current of 50 mA flowed through the solution. The solution was electrolysed for 10Q. Following electrolysis, the mixture was filtered and the solvent removed *in vacuo* to give an off-white solid. Repeated recrystallisation from acetone / pentane gave the product as a white crystalline solid. Yield: 0.21 g, 0.21 mmol, 43%.

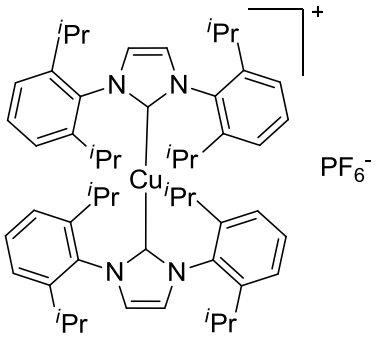

^{1}H NMR (300 MHz, $(CD_3)_2CO$) δ 7.55 (s, 4H, imH), 7.54 (t, *J* = 7.8 Hz, 4H, ArH), 7.25 (d, J = 7.8 Hz, 8H, ArH), 2.41 (hept, *J* = 6.9 Hz, 8H, C**H**$(CH_3)_2$), 1.04 (d, *J* = 6.9 Hz, 24H, CH(C**H**$_3)_2$), 0.94 (d, *J* = 6.9 Hz, 24H, CH(C**H**$_3)_2$). $^{13}C\{^{1}H\}$ NMR (75 MHz, $(CD_3)_2CO$) δ 178.3, 146.0, 135.9, 131.5, 126.7, 125.4, 29.5, 24.8, 24.5. HRMS (ESI^+): *m/z* 839.5071 $[M - PF_6]^+$ calculated $[M - PF_6]^+$ 839.5048. Analysis Calculated for $C_{54}H_{72}CuF_6N_4P$: C, 65.80; H, 7.36; N, 5.68. Found: C, 65.55; H, 7.35; N, 5.55.

Consistent with data previously reported.[34]

6.2.44 Preparation of C5

An oven dried round-bottomed flask was charged with **L5** (0.42 g, 1.0 mmol) and dried/degassed *in vacuo*. Acetonitrile (15 ml) was syringed in to the reaction vessel and N_2 was bubbled through the mixture to remove any dissolved O_2. The electrodes were inserted in to the reaction flask and purged with nitrogen. The electrodes were then inserted in to the reaction

flask and the solution was electrolysed (at 40 mA) for 200 minutes. The dark solution was filtered and the solvent removed *in vacuo* producing a pale green solid. The solid was dissolved in acetone and filtered through celite to remove the insoluble green particulates. Finally, the solvent was removed *in vacuo* producing the product as an off-white solid. Yield: 0.14 g, 0.18 mmol, 37%.

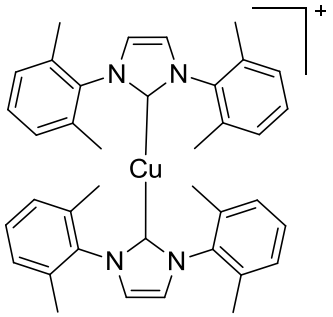

Single crystals suitable for X-ray analysis were grown by the vapour diffusion of diethyl ether in to a concentrated acetone solution of the product.

^{1}H NMR (500 MHz, $(CD_3)_2CO$) δ 7.52 (s, 4H, imH), 7.42 (t, *J* = 7.5 Hz, 4H, ArH), 7.26 (d, *J* = 7.5 Hz, 8H, ArH), 1.78 (s, 24H, CH_3). $^{13}C\{^{1}H\}$ NMR (75 MHz, $(CD_3)_2CO$) δ 178.1, 138.3, 135.9, 130.7, 129.6, 124.0, 17.5. HRMS (ESI^+): *m/z* 615.2558 $[M - PF_6]^+$ calculated $[M - PF_6]^+$ 615.2543. Analysis Calculated for $C_{38}H_{40}CuF_6N_4P.½H_2O$: C, 59.25; H, 5.37; N, 7.27. Found: C, 59.15; H, 5.25; N, 7.35.

6.2.45 Preparation of C6

An oven-dried, three-necked, round-bottomed flask was charged with **L6** (0.45 g, 1.0 mmol). This was thoroughly dried/degassed *in vacuo*. Anhydrous acetonitrile (15 ml) was cannula transferred in to the flask dissolving the imidazolium salt. The solution was degassed (by bubbling with argon for >1 hour). The two copper electrodes were inserted in to the reaction flask and purged with argon (for > 30 minutes) and then inserted in to the reaction mixture. A potential was applied such that a current of 100 mA flowed through the solution. The solution was electrolysed for 14Q. Following electrolysis, the mixture was filtered through celite and the solvent volume reduced *in vacuo* (to approximately 5 ml). Water (50 ml) was added to precipitate the product, which was collected by filtration. The crude product was recrystallised from chloroform/diethyl ether producing the pure product as a white crystalline solid. Yield: 0.30 g, 0.37 mmol, 73%.

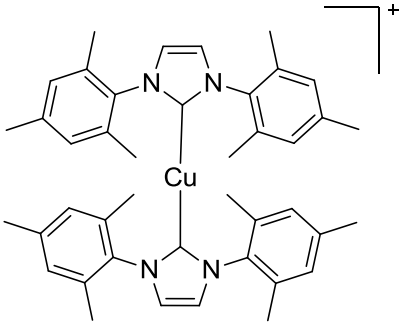

^{1}H NMR (500 MHz, $CDCl_3$) δ 7.01 (s, 4H, imH), 6.89 (s, 8H, ArH), 2.42 (s, 12H, p-CH_3), 1.67 (s, 24H, o-CH_3). $^{13}C\{^{1}H\}$ NMR (75 MHz, $CDCl_3$) δ 177.6, 139.6, 134.7, 134.6, 129.3, 122.9, 21.3, 17.1. HRMS (ESI^+): *m/z* 671.3180 $[M - PF_6]^+$ calculated $[M - PF_6]^+$ 671.3170. Analysis Calculated for $C_{42}H_{48}CuF_6N_4P$: C, 61.72; H, 5.92; N, 6.85. Found: C, 61.55; H, 5.95; N, 6.70.

Consistent with data previously reported.[34]

6.2.46 Preparation of C7

An oven-dried, three-necked, round-bottomed flask was charged with **L7** (0.29 g, 2.0 mmol). This was thoroughly dried/degassed *in vacuo*. Anhydrous acetonitrile (15 ml) was cannula transferred in to the flask dissolving the imidazolium salt. The solution was degassed (by bubbling with argon for >1 hour). The two copper electrodes were inserted in to the reaction flask and purged with argon (for > 30 minutes) and then inserted in to the reaction mixture. A potential was applied such that a current of 50 mA flowed through the solution. The solution was electrolysed for 2Q. Following electrolysis, the mixture was filtered under an inert atmosphere and the solvent removed from the filtrate *in vacuo* to yield an orange oil, which was taken in to a glovebox.

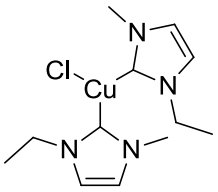

Note: A yield and elemental analysis could not be obtained due to the oily nature of the product and its pronounced air/moisture sensitivity.

^{1}H NMR (300 MHz, $CDCl_3$) δ 6.92 (d, *J* = 1.4 Hz, 1H, imH), 6.89 (d, *J* = 1.4 Hz, 1H, imH), 4.10 (q, *J* = 7.3 Hz, 2H, C**H**$_2$CH$_3$), 3.76 (s, 3H, CH_3), 1.40 (t, *J* = 7.3 Hz, 3H, CH_2C**H**$_3$). ^{13}C{^{1}H} NMR (126 MHz, $CDCl_3$) δ 176.0, 121.9, 120.2, 46.4, 38.3, 17.1. HRMS (ESI$^+$): *m/z* 283.0991 $[Cu(NHC)_2]^+$ calculated $[Cu(NHC)_2]^+$ 283.0978.

6.2.47 Preparation of C8

An oven-dried, three-necked, round-bottomed flask was charged with **L8** (0.25 g, 1.0 mmol). This was thoroughly dried/degassed *in vacuo*. Anhydrous acetonitrile (15 ml) was cannula transferred in to the flask dissolving the imidazolium salt. The solution was degassed (by bubbling with argon for >1 hour). The two copper electrodes were inserted in to the reaction flask and purged with argon (for > 30 minutes) and then inserted in to the reaction mixture. A potential was applied such that a current of 50 mA flowed through the solution. The solution was electrolysed for 2Q. Following electrolysis, the mixture was filtered under an inert atmosphere and the solvent removed from the filtrate *in vacuo* to yield a pale yellow oil. The yellow oil was washed three times with tetrahydrofuran, each time decanting-off and keeping the tetrahydrofuran solution from the oil. The tetrahydrofuran was removed *in vacuo* to yield colourless crystals. Yield: 0.21 g, 0.67 mmol, 67%.

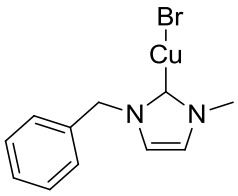

Single crystals suitable for X-ray diffraction analysis were grown by slow evaporation of a concentrated solution of the product in tetrahydrofuran.

^{1}H NMR (500 MHz, $CDCl_3$) δ 7.25 – 7.18 (m, 5H, ArH), 6.87 (d, *J* = 1.7 Hz, 1H, imH), 6.82 (d, *J* = 1.7 Hz, 1H, imH), 5.22 (s, 2H, CH_2), 3.73 (s, 3H, CH_3). ^{13}C{^{1}H} NMR (126 MHz, $CDCl_3$) δ 178.7, 135.8, 129.6, 129.2, 128.1, 122.2, 120.7, 55.3, 38.4. HRMS (ESI$^+$): *m/z* 317.0834 [M –

Br + 2MeCN]$^+$ calculated [M – Br + 2MeCN]$^+$ 317.0822. Analysis Calculated for $C_{11}H_{12}BrCuN_2$: C, 41.85; H, 3.83; N, 8.87. Found: C, 41.55; H, 3.95; N; 9.15.

6.2.48 Preparation of C9

An oven-dried, three-necked, round-bottomed flask was charged with **L9** (0.32g, 1.0 mmol). This was thoroughly dried/degassed *in vacuo*. Anhydrous acetonitrile (15 ml) was cannula transferred in to the flask dissolving the imidazolium salt. The solution was degassed (by bubbling with argon for >1 hour). The two copper electrodes were inserted in to the reaction flask and purged with argon (for > 30 minutes) and then inserted in to the reaction mixture. A potential was applied such that a current of 50 mA flowed through the solution. The solution was electrolysed for 5Q. Following electrolysis, the mixture was filtered to produce a brown/black oily solid. In a glovebox, dichloromethane was added to the solid and the suspension was filtered. The dichloromethane was allowed to evaporate, yielding colourless crystals of the complex. Yield: 0.16 g, 0.29 mmol, 58%.

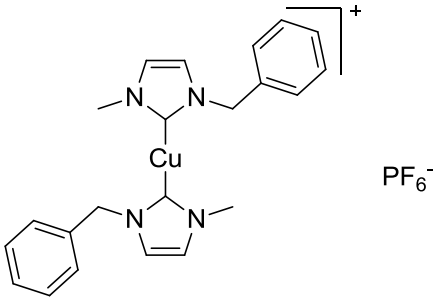

^{1}H NMR (300 MHz, CD_3CN) δ 7.40 – 7.22 (m, 5H, ArH), 7.11 (d, *J* = 1.8 Hz, 1H, imH), 7.09 (d, *J* = 1.8 Hz, 1H, imH), 5.25 (s, 2H, CH_2), 3.74 (s, 3H, CH_3). ^{13}C{^{1}H} NMR (75 MHz, CD_3CN) δ 179.1, 138.3, 129.8, 129.0, 128.6, 123.3, 122.2, 54.9, 38.5. HRMS (ESI$^+$): *m/z* 407.1291 [M – PF_6]$^+$ calculated [M – PF_6]$^+$ 407.1291.

6.2.49 Preparation of C10

An oven-dried, three-necked, round-bottomed flask was charged with **L10** (0.33 g, 1.0 mmol). This was thoroughly dried/degassed *in vacuo*. Anhydrous acetonitrile (15 ml) was cannula transferred in to the flask dissolving the imidazolium salt. The solution was degassed (by bubbling with argon for >1 hour). The two copper electrodes were inserted in to the reaction flask and purged with argon (for > 30 minutes) and then inserted in to the reaction mixture. A potential was applied such that a current of 50 mA flowed through the solution. The solution was electrolysed for 2Q. Following electrolysis, the mixture was filtered under an inert atmosphere and the solvent removed from the filtrate *in vacuo* to yield a pale brown oil.

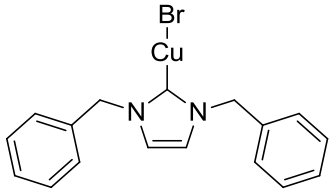

Note: A yield and elemental analysis could not be obtained due to the oily nature of the product and its pronounced air/moisture sensitivity.

Single crystals suitable for X-ray diffraction analysis were grown by vapour diffusion of diethyl ether in to a concentrated solution of the product in tetrahydrofuran.

^{1}H NMR (500 MHz, $CDCl_3$) δ 7.30 – 7.17 (m, 10H, ArH), 6.77 (s, 2H, imH), 5.23 (s, 4H, CH_2). $^{13}C\{^{1}H\}$ NMR (75 MHz, $CDCl_3$) δ 177.9, 135.8, 129.1, 128.6, 128.1, 121.0, 55.2. HRMS (ESI^+): *m/z* 559.1898 $[Cu(NHC)_2]^+$ calculated $[Cu(NHC)_2]^+$ 559.1917.

6.2.50 Preparation of C11

An oven-dried, three-necked, round-bottomed flask was charged with **L11** (0.38 g, 1.0 mmol). This was thoroughly dried/degassed *in vacuo*. Anhydrous acetonitrile (15 ml) was cannula transferred in to the flask dissolving the imidazolium salt. The solution was degassed (by bubbling with argon for >1 hour). The two copper electrodes were inserted in to the reaction flask and purged with argon (for > 30 minutes) and then inserted in to the reaction mixture. A potential was applied such that a current of 50 mA flowed through the solution. The solution was electrolysed for 1.5Q. Following electrolysis, the mixture was filtered and the solvent removed from the filtrate *in vacuo* to yield a pale yellow solid. This was recrystallised twice from dichloromethane / diethyl ether to yield the product as a white crystalline solid. Yield: 0.30 g, 0.68 mmol, 68%.

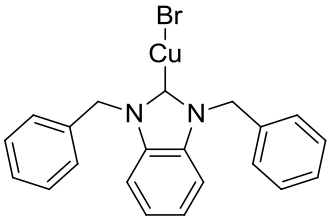

Single crystals suitable for X-ray analysis were grown by vapour diffusion of pentane in to a concentrated dichloromethane solution of the product.

^{1}H NMR (300 MHz, CD_2Cl_2) δ 7.48 – 7.19 (m, 14H, ArH/imH), 5.69 (s, 4H, CH_2). $^{13}C\{^{1}H\}$ NMR (75 MHz, CD_2Cl_2) δ ($C_{carbene}$ not observed), 135.9, 129.6, 129.0, 128.0, 124.7, 112.5, 53.4. HRMS (ESI^+): *m/z* 361.0771 $[M - Br]^+$ calculated $[M - Br]^+$ 361.0761. Analysis Calculated for $C_{21}H_{18}BrCuN_2.CH_2Cl_2$: C, 50.16; H, 3.83; N, 5.32. Found: C, 50.65; H, 3.90; N, 5.30.

6.2.51 Preparation of C12

An oven-dried, three-necked, round-bottomed flask was charged with **L12** (0.44 g, 1.0 mmol). This was thoroughly dried/degassed *in vacuo*. Anhydrous acetonitrile (15 ml) was cannula transferred in to the flask dissolving the imidazolium salt. The solution was degassed (by bubbling with argon for >1 hour). The two copper electrodes were inserted in to the reaction flask and purged with argon (for > 30 minutes) and then inserted in to the reaction mixture. A potential was applied such that a current of 50 mA flowed through the solution. The solution was electrolysed for 11Q. Following electrolysis, the mixture was filtered under an inert atmosphere and the solvent removed from the filtrate *in vacuo* to yield a brown solid. This was washed with a little anhydrous tetrahydrofuran (5 ml), dried, dissolved in anhydrous dichloromethane and filtered. Finally, the

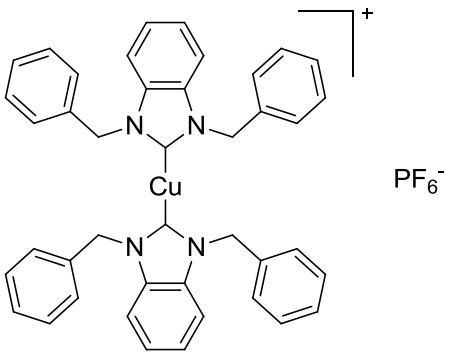

dichloromethane was removed *in vacuo* to give the product as a white crystalline solid. Yield: 0.26 g, 0.32 mmol, 65%.

Single crystals suitable for X-ray diffraction analysis were grown by the vapour diffusion of pentane in to a concentrated solution of the product in dichloromethane.

^{1}H NMR (300 MHz, $(CD_3)_2CO$) δ 7.68 (dd, J = 6.1, 3.1 Hz, 4H, ArH), 7.42 (dd, J = 6.1, 3.1 Hz, 4H, ArH), 7.39 – 7.23 (m, 20H, ArH), 5.71 (s, 8H, CH_2). $^{13}C\{^{1}H\}$ NMR (75 MHz, $(CD_3)_2CO$) δ 176.5, 137.1, 134.9, 130.0, 129.2, 128.5, 125.3, 113.1, 52.9. HRMS (ESI^+): *m/z* 659.2227 $[M - PF_6]^+$ calculated $[M - PF_6]^+$ 659.2230. Analysis Calculated for $C_{42}H_{36}CuF_6N_4P.H_2O$: C, 61.27; H, 4.65; N, 6.81. Found: C, 61.55; H, 4.55; N, 6.80.

6.2.52 Preparation of C13

An oven-dried, three-necked, round-bottomed flask was charged with **L13B** (0.63 g, 1.0 mmol). This was thoroughly dried/degassed *in vacuo*. Anhydrous acetonitrile (15 ml) was cannula transferred in to the flask dissolving the imidazolium salt. The solution was degassed (by bubbling with argon for >1 hour). The two copper electrodes were inserted in to the reaction flask and purged with argon (for > 30 minutes) and then inserted in to the reaction mixture. A potential was applied such that a current of approximately 10 mA flowed through the solution. The solution was electrolysed for 5.5Q. Following electrolysis, the mixture was filtered through celite and the solvent removed from the filtrate *in vacuo*. Recrystallisation from acetonitrile/water followed by washing with methanol and diethyl ether gave the pure product as a white crystalline solid. Yield: 0.39 g, 0.36 mmol, 71%.

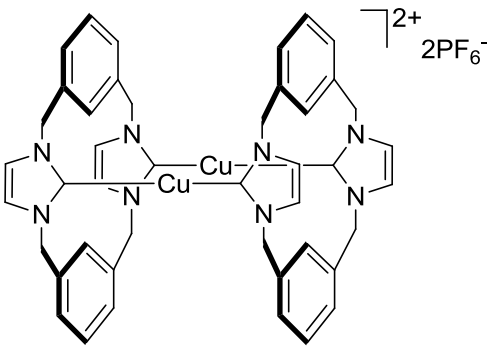

Single crystals suitable for X-ray diffraction analysis were grown by vapour diffusion of diethyl ether in to a concentrated solution of the product in acetonitrile.

^{1}H NMR (501 MHz, $(CD_3)_2SO$) δ 7.26 (t, J = 7.6 Hz, 4H, ArH), 7.20 (s, 8H, imH), 7.15 (d, J = 7.6 Hz, 8H, ArH), 5.69 (s, 4H, ArH), 5.16 (s, 16H, CH_2). $^{13}C\{^{1}H\}$ NMR (75 MHz, $(CD_3)_2SO$) δ 177.5, 138.0, 128.5, 126.0, 122.7, 119.8, 52.7. ^{1}H NMR (500 MHz, CD_3CN) δ 7.26 (t, J = 7.6 Hz, 4H, ArH), 7.14 (d, J = 7.6 Hz, 8H, ArH), 6.93 (s, 8H, imH), 5.73 (s, 4H, ArH), 5.18 (d, J = 16.5 Hz, 8H, CH_2), 5.09 (d, J = 16.5 Hz, 8H, CH_2).$^{13}C\{^{1}H\}$ NMR (126 MHz, CD_3CN) δ 178.6, 138.9, 129.9, 127.5, 123.6, 121.2, 54.5. HRMS (ESI^+): *m/z* 403.0997 $[M - 2PF_6]^{2+}$ calculated $[M - 2PF_6]^{2+}$ 403.0978. Analysis Calculated for $C_{44}H_{40}Cu_2F_{12}N_8P_2$: C, 48.14; H, 3.67; N, 10.21. Found: C, 48.15; H, 3.60; N, 10.20.

6.2.53 Preparation of C14

A Schlenk flask was charged with **L14** (0.42 g, 1.5 mmol), Cu_2O (0.43 g, 3.0 mmol) and 4Å molecular sieves. These were dried and degassed thoroughly *in vacuo*. Anhydrous dichloromethane (30 ml) was added *via* cannula and the mixture was stirred at reflux for 24 hours. After this time, the mixture was allowed to cool and was filtered under inert conditions. The solvent was removed from the filtrate *in vacuo* to give the product as a white solid. Yield: 0.30 g, 0.88 mmol, 59%.

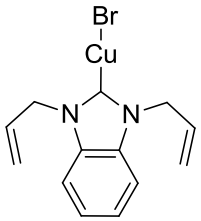

Single crystals suitable for X-ray diffraction analysis were grown by the slow evaporation of a concentrated solution of the product in chloroform.

^{1}H NMR (500 MHz, $CDCl_3$) δ 7.46 – 7.42 (m, 2H, ArH), 7.41 – 7.36 (m, 2H, ArH), 6.04 (ddt, J = 17.0, 10.3, 5.7 Hz, 2H, C**H**=CH_2), 5.36 (dd, J = 10.3, 0.8 Hz, 2H, CH=CH**H$_{(cis)}$**), 5.29 (dd, J = 17.0, 0.8 Hz, 2H, CH=CH**H$_{(trans)}$**), 5.06 (d, J = 5.7 Hz, 4H, NCH_2). ^{13}C{^{1}H} NMR (126 MHz, $CDCl_3$) δ 186.1, 133.8, 131.9, 124.1, 119.5, 111.82, 51.5. HRMS (ESI$^+$): *m/z* 261.0440 [M – Br]$^+$ calculated [M – Br]$^+$ 261.0448. Analysis Calculated for $C_{13}H_{14}BrCuN_2$: C, 45.69; H, 4.13; N, 8.20. Found: C, 45.40; H, 4.30; N, 7.90.

6.2.54 Attempted Synthesis of C15

In a glovebox, a small round-bottomed flask was charged with **L15** (1.0 g, 4.9 mmol), CuBr (0.72 g, 5.0 mmol) and ^{t}BuOK (0.72 g, 6.4 mmol). To this was added anhydrous tetrahydrofuran (35 ml). The resultant brown suspension was stirred at room temperature for 3 days. After this time, the mixture was filtered and the solvent removed from the filtrate *in vacuo* to yield a brown oil.

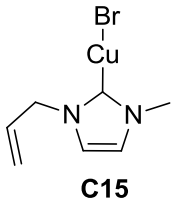

C15

Analysis of the brown oil by ^{1}H and ^{13}C{^{1}H} NMR spectroscopy (in $CDCl_3$) revealed the presence of the desired product (**C15**) along with two allyl rearrangement products (**C15AR1** and **C15AR2**). This is exemplified by the presence of three low field resonances at 177.7ppm, 177.8ppm and 178.7ppm in the ^{13}C{^{1}H} NMR spectrum, attributable to the three different Cu^I-NHC complexes. Furthermore, slow evaporation of a solution of the product(s) in tetrahydrofuran led to the formation of a number of clear needles, which were suitable for X-ray diffraction analysis. The structure shows the allyl rearrangement product, **C15AR1**.

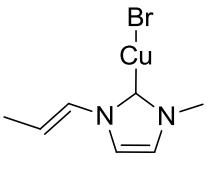

C15AR1

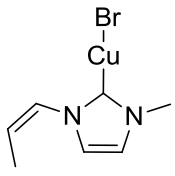

C15AR2

6.2.55 Preparation of C15

A Schlenk flask was charged with **L15** (0.60 g, 3.0 mmol), Cu_2O (0.85 g, 5.9 mmol) and 4Å molecular sieves. These were dried and degassed thoroughly *in vacuo*. Anhydrous

dichloromethane (40 ml) was added *via* cannula and the mixture was stirred at reflux for 80 hours. After this time, the mixture was allowed to cool and was filtered under inert conditions. The solvent was removed from the filtrate *in vacuo* to give the product as a white solid. Yield: 0.39 g, 1.5 mmol, 50%.

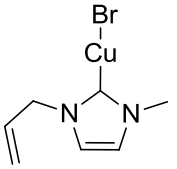

Single crystals suitable for X-ray diffraction analysis were grown by the slow evaporation of a concentrated solution of the product in dichloromethane.

^{1}H NMR (300 MHz, $CDCl_3$) δ 6.91 (s, 1H, imH), 6.91 (s, 1H, imH), 5.94 (ddt, *J* = 16.3, 10.2, 6.0 Hz, 1H, C**H**=CH_2), 5.36 – 5.20 (m, 2H, CH=C**H$_2$**), 4.72 (d, *J* = 6.0 Hz, 2H, NCH_2), 3.83 (s, 3H, CH_3). ^{13}C{^{1}H} NMR (75 MHz, $CDCl_3$) δ 178.1, 132.6, 122.0, 120.7, 119.8, 53.8, 38.4. HRMS (ESI^+): *m/z* 185.0145 $[M - Br]^+$ calculated $[M - Br]^+$ 185.0135. Analysis Calculated for $C_7H_{10}BrCuN_2$: C, 31.65; H, 3.79; N, 10.55. Found: C, 31.30; H, 3.80; N, 10.10.

6.2.56 Preparation of C16

A Schlenk flask was charged with **L16** (0.54 g, 2.4 mmol), Cu_2O (0.67 g, 4.7 mmol) and 4Å molecular sieves. These were dried and degassed thoroughly *in vacuo*. Anhydrous dichloromethane (35 ml) was added *via* cannula and the mixture was stirred at reflux for 24 hours. After this time, the mixture was allowed to cool and was filtered under inert conditions. The solvent was removed from the filtrate *in vacuo* to give the product as a pale yellow oil. Yield: 0.35 g, 1.2 mmol, 51%.

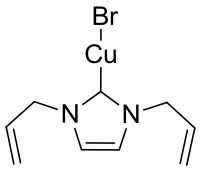

^{1}H NMR (300 MHz, $CDCl_3$) δ 6.93 (s, 2H, imH), 5.95 (ddt, *J* = 16.6, 10.2, 6.0 Hz, 2H, C**H**=CH_2), 5.31 (dd, *J* = 10.2, 0.9 Hz, 2H, CH=CH**H$_{(cis)}$**), 5.26 (dd, *J* = 16.6, 0.9 Hz, 2H, HC=CH**H$_{(trans)}$**), 4.73 (d, *J* = 6.0, 4H, NCH_2). ^{13}C{^{1}H} NMR (75 MHz, $CDCl_3$) δ 177.8, 132.6, 120.8, 120.0, 54.0. HRMS (ESI^+): *m/z* 211.0280 $[M - Br]^+$ calculated $[M - Br]^+$ 211.0291. Analysis Calculated for $C_9H_{12}BrCuN_2$: C, 37.35; H, 4.20; N, 9.70. Found: C, 37.06; H, 4.15; N, 9.61.

6.2.57 Preparation of C17

A Schlenk flask was charged with **L17** (0.32 g, 1.0 mmol), Cu_2O (0.30 g, 2.1 mmol) and 4Å molecular sieves. These were dried and degassed thoroughly *in vacuo*. Anhydrous dichloromethane (20 ml) was added *via* cannula and the mixture was stirred at reflux for 60 hours. After this time, the mixture was allowed to cool and was filtered under inert conditions. The solvent was removed from the filtrate *in vacuo* to give the product as a clear oil, which slowly crystallised on standing. Yield: 0.24 g, 0.64 mmol, 62%.

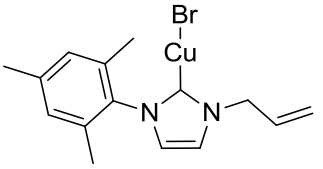

Single crystals suitable for X-ray diffraction analysis were grown by the vapour diffusion of pentane in to a concentrated solution of the product in dichloromethane.

^{1}H NMR (300 MHz, $CDCl_3$) δ 7.10 (d, *J* = 1.7 Hz, 1H, imH), 6.95 (s, 2H, ArH), 6.87 (d, *J* = 1.7 Hz, 1H, imH), 6.03 (ddt, *J* = 15.8, 10.2, 5.8 Hz, 1H, C**H**=CH_2), 5.35 (dd, *J* = 10.2, 0.7 Hz, 1H, CH=CH**H**$_{(cis)}$), 5.26 (d, *J* = 15.8 Hz, 1H, CH=CH**H**$_{(trans)}$), 4.85 (d, *J* = 5.8 Hz, 2H, NCH_2), 2.31 (s, 3H, p-CH_3), 2.00 (s, 6H, o-CH_3). ^{13}C{^{1}H} NMR (75 MHz, $CDCl_3$) δ 179.0, 139.5, 135.2, 134.7, 132.7, 129.5, 122.5, 120.7, 119.7, 53.9, 21.2, 17.9. HRMS (ESI^+): *m/z* 330.1024 [M – Br + MeCN]$^+$ calculated [M – Br + MeCN]$^+$ 330.1026. Analysis Calculated for $C_{15}H_{18}BrCuN_2.⅔CH_2Cl_2$: C, 44.13; H, 4.57; N, 6.57. Found: C, 44.60; H, 5.00; N, 6.10.

6.2.58 Preparation of C18

A Schlenk flask was charged with **L18** (0.58 g, 2.0 mmol), Cu_2O (0.57 g, 4.0 mmol) and 4Å molecular sieves. These were dried and degassed thoroughly *in vacuo*. Anhydrous dichloromethane (30 ml) was added *via* cannula and the mixture was stirred at reflux for 74 hours. After this time, the mixture was allowed to cool and was filtered under inert conditions. The solvent was removed from the filtrate *in vacuo* to give the product as a yellow oil, which slowly crystallised on standing. Yield: 0.41 g, 1.2 mmol, 58%.

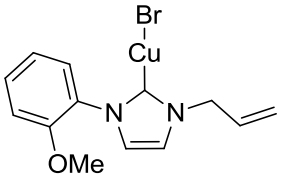

Single crystals suitable for X-ray diffraction analysis were grown by the slow evaporation of a concentrated solution of the product in dichloromethane.

^{1}H NMR (300 MHz, $CDCl_3$) δ 7.51 (dd, *J* = 8.0, 1.3 Hz, 1H, ArH), 7.41 (td, *J* = 8.0, 1.3 Hz, 1H, ArH), 7.18 (d, *J* = 1.7 Hz, 1H, imH), 7.06 (t, *J* = 8.0 Hz, 2H, ArH), 7.01 (d, *J* = 1.7 Hz, 1H, imH), 6.04 (ddt, *J* = 16.5, 10.3, 6.0 Hz, 1H, C**H**=CH_2), 5.42 – 5.30 (m, 2H, CH=C**H$_2$**), 4.85 (d, *J* = 6.0 Hz, 2H, NCH_2), 3.85 (s, 3H, OC*H*$_3$). ^{13}C{^{1}H} NMR (75 MHz, $CDCl_3$) δ 178.6, 153.1, 132.5, 130.4, 128.4, 127.5, 123.4, 121.2, 120.0, 119.8, 112.5, 56.0, 54.2. HRMS (ESI^+): *m/z* 277.0360 [M – Br]$^+$ calculated [M – Br]$^+$ 277.0397. Analysis Calculated for $C_{13}H_{14}BrCuN_2O$: C, 43.65; H, 3.94; N, 7.83. Found: C, 44.00; H, 4.40; N, 7.35.

6.2.59 Preparation of C19A

A small ampoule was charged with **L19** (0.10 g, 0.38 mmol), CuBr (0.055 g, 0.38 mmol) and Cs_2CO_3 (0.62 g). These were dried and degassed thoroughly *in vacuo*. To these, anhydrous acetonitrile (15 ml) was added and the mixture was heated at 50°C for 16 hours. After this time, the mixture was filtered and the solvent removed *in vacuo* to give the product as a yellow solid. Yield: 0.085 g, 0.17 mmol, 88%.

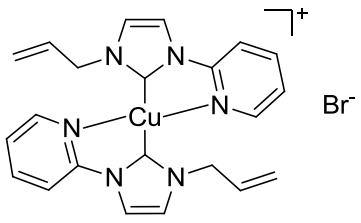

^{1}H NMR (300 MHz, CD_3CN) δ 8.19 (d, J = 4.6 Hz, 2H, pyH), 7.99 – 7.84 (m, 6H, pyH / imH), 7.35 – 7.25 (m, 4H, pyH / imH), 6.03 (dq, J = 10.9, 5.7 Hz, 2H, C**H**=CH_2), 5.23 – 5.10 (m, 4H, CH=C**H$_2$**), 4.77 (d, J = 5.7 Hz, 4H, NCH_2). ^{13}C{^{1}H} NMR (126 MHz, CD_3CN) δ 183.7, 151.8,

149.3, 140.8, 134.5, 124.0, 123.3, 118.8, 117.9, 114.3, 55.0, 54.9. HRMS (ESI^+): *m/z* 433.1261 $[M - Br]^+$ calculated $[M - Br]^+$ 433.1196. Analysis Calculated for $C_{22}H_{22}BrCuN_6$: C, 51.42; H, 4.31; N, 16.35. Found: C, 51.15; H, 4.25; N, 16.55.

6.2.60 Preparation of C19B

Ligand precursor **L19** (0.34 g, 1.3 mmol) and Ag_2O (0.19 g, 0.83 mmol) were added to a Schlenk flask along with 4Å molecular sieves. To these was added anhydrous dichloromethane (30 ml) and the dark suspension was stirred overnight in the absence of light. After this time, the dark suspension was filtered and the solvent removed *in vacuo* to yield the crude product as a white oily solid. Recrystallisation from a minimum amount of acetone/pentane gave the pure product as a white crystalline solid. Yield: 0.39 g, 1.0 mmol, 81%.

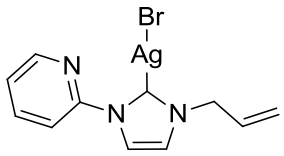

Single crystals suitable for X-ray diffraction analysis were grown by the vapour diffusion of diethyl ether in to a concentrated solution of the product in chloroform.

^1H NMR (300 MHz, $CDCl_3$) δ 8.50 (dd, J = 4.9, 1.4 Hz, 1H, pyH), 8.13 (d, J = 7.9 Hz, 1H, pyH), 7.88 (dd, J = 7.9, 1.4 Hz, 1H, pyH), 7.85 (d, J = 1.9 Hz, 1H, imH), 7.36 (ddd, J = 7.6, 4.9, 0.8 Hz, 1H, pyH), 7.16 (d, J = 1.9 Hz, 1H, imH), 6.01 (ddt, J = 16.3, 10.3, 6.0 Hz, 1H, C**H**=CH_2), 5.39 – 5.27 (m, 2H, CH=C**H$_2$**), 4.89 (d, J = 6.0, 2H, NCH_2). $^{13}C\{^1H\}$ NMR (75 MHz, $CDCl_3$) δ 181.6, 151.0, 149.1, 139.5, 132.4, 123.9, 121.7, 120.4, 120.3, 115.6, 55.4. HRMS (ESI^+): *m/z* 477.0953 $[Ag(NHC)_2]^+$ calculated $[Ag(NHC)_2]^+$ 477.0951. Analysis Calculated for $C_{11}H_{11}AgBrN_3$.⅓MeCN: C, 36.24; H, 3.13; N, 12.07. Found: C, 36.50; H, 3.00; N, 11.50.

6.2.61 Preparation of C19C

In a glovebox, **C19B** (0.32 g, 0.85 mmol) was dissolved in dichloromethane (35 ml). With stirring, solid CuBr was added (0.13 g, 0.93 mmol). Immediately, the solution began to turn yellow with the concomitant formation of a pale yellow precipitate (AgBr). The suspension was stirred for 2 hours and then filtered to remove the insoluble AgBr / CuBr. The solid was washed with dichloromethane until the filtrate ran clear. The solvent was removed from the filtrate *in vacuo* to yield the product as a yellow crystalline powder. Yield: 0.20 g, 0.62 mmol, 73%.

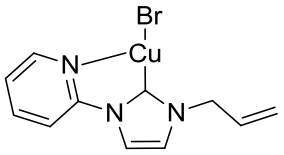

Single crystals suitable for X-ray diffraction analysis were grown on standing of a dilute solution of the product in dichloromethane / pentane (1:2).

^1H NMR (300 MHz, $CDCl_3$) δ 8.55 (br s, 1H), 8.08 (br s, 1H), 7.91 (t, *J* = 7.7 Hz, 1H), 7.80 (br s, 1H), 7.37 (br s, 1H), 7.10 (br s, 1H), 6.12 – 5.94 (m, 1H, C**H**=CH_2), 5.39 (d, *J* = 10.0 Hz, 1H,

CH=CH**H**$_{(cis)}$), 5.36 (d, *J* = 17.0 Hz, 1H, CH=CH**H**$_{(trans)}$), 4.88 (br s, 2H, NCH_2) HRMS (ESI^+): *m/z* 289.0517 $[M - Br + MeCN]^+$ calculated $[M - Br + MeCN]^+$ 289.0509. Analysis Calculated for $C_{11}H_{11}BrCuN_3$: C, 40.20; H, 3.37; N, 12.78. Found: C, 39.90; H, 3.30; N, 12.50.

Note: Unequivocal assignment of the aromatic resonances to either pyridyl or backbone NHC protons is hampered due to spectrum broadening. A $^{13}C\{^1H\}$ spectrum was also not obtained due to broadening.

6.2.62 Preparation of C19G

Silver complex **C19B** (0.21 g, 0.57 mmol) and $CuBr_2$ (0.13 g, 0.57 mmol) were added to a small Schlenk flask and dried/degassed *in vacuo*. To these was added anhydrous dichloromethane (35 ml), and the resultant suspension was stirred at room temperature in the absence of light for 24 hours. After this time, the dark green suspension was filtered to remove the precipitated AgBr and the dichloromethane removed *in vacuo* to give the product as a green oily solid. Trituration with tetrahydrofuran gave the pure product as a dark green solid. Yield: 0.13 g, 0.32 mmol, 57%.

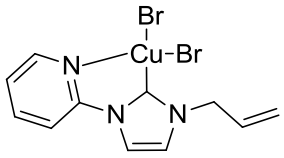

Very dark green single crystals suitable for X-ray diffraction analysis were grown *via* the vapour diffusion of diethyl ether in to a concentrated solution of the complex in dichloromethane.

Analysis Calculated for $C_{11}H_{11}Br_2CuN_3.\frac{1}{3}C_4H_8O$: C, 34.24; H, 3.18; N, 9.71. Found: C, 34.60; H, 3.20; N, 9.40.

6.2.63 Preparation of C19J

Silver complex **C19B** (0.11 g, 0.28 mmol), $CuBr_2$ (0.032 g, 0.14 mmol) and $AgPF_6$ (0.036 g, 0.14 mmol) were added to a small Schlenk flask and dried/degassed *in vacuo*. To these was added anhydrous dichloromethane (30 ml), and the resultant suspension was stirred at room temperature in the absence of light for 16 hours. After this time, the blue suspension was filtered to remove the precipitated AgBr and the dichloromethane removed *in vacuo* to give the crude product as a blue solid. Recrystallisation from acetonitrile/diethyl ether gave the pure product as a blue crystalline solid. Yield: 0.059g, 90 μmol, 63%.

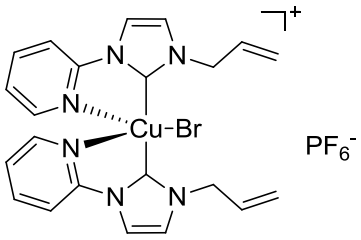

Single crystals suitable for X-ray diffraction analysis could be grown *via* the vapour diffusion of diethyl ether in to a concentrated solution of the product in acetone.

HRMS (ESI$^+$): *m/z* 216.5596 $[M - Br - PF_6]^{2+}$ calculated $[M - Br - PF_6]^{2+}$ 216.5595. Analysis Calculated for $C_{22}H_{22}BrCuF_6N_6P$: C, 40.10; H, 3.37; N, 12.76. Found: C, 40.30; H, 3.30; N, 12.70.

6.2.64 Preparation of C19K

Silver complex **C19B** (0.16 g, 0.43 mmol) and $CuBr_2$ (0.20 g, 0.86 mmol) were added to a Schlenk flask and dried/degassed *in vacuo*. To these was added anhydrous acetonitrile (17 ml) *via* a cannula. The resultant suspension was stirred in the absence of light at room temperature for 1.5 hours. After this time, the precipitated AgBr was removed *via* filtration and the solution was concentrated to approximately 5 ml. Slow addition of an excess of diethyl ether (50 ml) induced the precipitation of the product as a dark oil, which produced a dark foam on drying *in vacuo*. Yield: 0.22 g, 0.35 mmol, 82%.

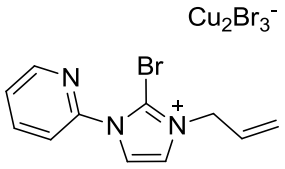

^{1}H NMR (300 MHz, CD_3CN) δ 8.73 (d, *J* = 3.7 Hz, 1H, pyH), 8.15 (td, *J* = 8.1, 1.5 Hz, 1H, pyH), 7.92 (d, *J* = 2.2 Hz, 1H, imH), 7.77 (d, *J* = 8.1 Hz, 1H, pyH), 7.75 – 7.68 (m, 2H, pyH & imH), 6.05 (ddt, *J* = 16.5, 10.4, 6.0 Hz, 1H, C**H**=CH_2), 5.55 – 5.42 (m, 2H, CH=C**H$_2$**), 4.89 (d, *J* = 6.0 Hz, 2H, NCH_2). ^{13}C{^{1}H} NMR (126 MHz, CD_3CN) δ 150.7, 148.1, 141.2, 130.2, 127.8, 125.6, 125.5, 122.6, 122.4, 121.7, 54.0. HRMS (ESI$^+$): *m/z* 264.0136 $[M - Cu_2Br_3]^+$ calculated for $[M - Cu_2Br_3]^+$ 264.0131. Analysis Calculated for $C_{11}H_{11}Br_4Cu_2N_3$.AgBr: C, 16.12; H, 1.35; N, 5.13. Found: C, 16.20; H, 1.30; N, 5.00.

*Note: Repeated elemental analyses of samples of compound **C19K** were found to give the C, H and N content as slightly lower than expected. Spectroscopic analysis does not indicate the presence of organic impurities. On this basis, we postulate that the low C, H and N content derives from the presence of AgBr, which is left over from the transmetallation process.*

6.2.65 Preparation of C20A

An ampoule was charged with **L20** (0.15 g, 0.33 mmol), CuBr (0.10 g, 0.66 mmol) and Cs_2CO_3 (1.1 g, 3.3 mmol). These were dried and degassed thoroughly *in vacuo*. Anhydrous acetonitrile (15 ml) was added and the suspension was heated at 50°C for 1.5 hours. After this time, the mixture was allowed to cool to ambient temperature, filtered and the solvent removed *in vacuo* to give the crude product as a yellow solid. The product was recrystallised from acetonitrile / diethyl ether. Yield: 0.10 g, 0.10 mmol, 60%.

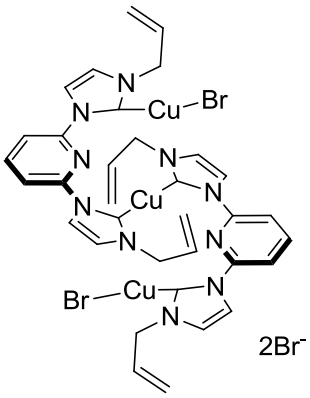

Single crystals of **C20A** suitable for X-ray diffraction analysis were grown by cooling a saturated solution of the product from 333 K to ambient temperature in anhydrous acetonitrile ($[Cu_3Br_2L_2]$Br.MeCN). Single crystals of **C20B**, the decomposition product of **C20A**, suitable

for X-ray diffraction analysis were grown by the slow evaporation of a concentrated solution of **C20A** in hydrous acetonitrile ($[Cu_2L_2]_2Br.2H_2O$).

^{1}H NMR (500 MHz, CD_3CN, 333.6K) δ 8.28 (t, J = 8.0 Hz, 2H, pyH), 7.81 (d, J = 2.0 Hz, 4H, imH), 7.73 (d, J = 8.0 Hz, 4H, pyH), 7.23 (d, J = 2.0 Hz, 4H, imH), 5.72 – 5.61 (m, 4H, C**H**=CH_2), 5.02 (d, J = 10.3 Hz, 4H, CH=CH**H$_{(cis)}$**), 4.93 (d, J = 16.5 Hz, 4H, CH=CH**H$_{(trans)}$**), 4.40 (d, J = 4.5 Hz, 8H, NCH_2). ^{13}C{^{1}H} NMR (126 MHz, CD_3CN, 333.6 K) δ 181.9, 150.6, 145.1, 134.0, 124.5, 120.0, 119.9, 114.7, 55.4. HRMS (ESI^+): *m/z* 354.0787 $[Cu_2(NHC)_2]^{2+}$ calculated $[Cu_2(NHC)_2]^{2+}$ 354.0774. Analysis Calculated for $C_{34}H_{34}Br_3Cu_3N_{10}$: C, 40.31; H, 3.38; N, 13.83. Found: C, 41.60; H, 3.45; N, 13.85.

6.2.66 Preparation of C21A

To freshly activated 4Å molecular sieves was added **L21** (0.16 g, 0.51 mmol) and Ag_2O (0.070 g, 0.30 mmol). To these was added anhydrous dichloromethane (50 ml) and the resultant dark suspension was stirred at room temperature in the absence of light for 18 hours. After this time the mixture was filtered and the solid washed repeatedly with hot acetonitrile. The combined organics were reduced in volume *in vacuo* to 30 ml. Slow addition of diethyl ether induced the precipitation of the product as off-white needles, which were collected and dried. Yield: 0.14 g, 0.34 mmol, 68%.

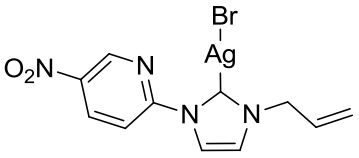

^{1}H NMR (300 MHz, DMSO-d_6) δ 9.17 (d, J = 2.7 Hz, 1H, pyH), 8.85 (dd, J = 9.0, 2.7 Hz, 1H, pyH), 8.39 – 8.26 (m, 2H, pyH and imH), 7.79 (d, J = 1.9 Hz, 1H, pyH), 6.12 (ddt, J = 17.1, 10.5, 5.6 Hz, 1H, C**H**=CH_2), 5.30 (dd, J = 10.5, 0.9 Hz, 1H, CH=CH**H$_{(cis)}$**), 5.23 (dd, J = 17.1, 0.9 Hz, 1H, CH=CH**H$_{(trans)}$**), 4.94 (d, J = 5.6 Hz, 2H, NCH_2). ^{13}C{^{1}H} NMR (75 MHz, DMSO-d_6) δ 182.3, 153.5, 144.5, 143.7, 135.6, 133.7, 124.1, 120.6, 118.8, 115.6, 54.45. HRMS (ESI^+): *m/z* 567.0622 $[Ag(NHC)_2]^+$ calculated $[Ag(NHC)_2]^+$ 567.0653. Analysis Calculated for $C_{11}H_{10}AgBrN_4O_2$: C, 31.61; H, 2.41; N, 13.40. Found: C, 31.80; H, 2.20; N, 13.20.

6.2.67 Preparation of C21B

Silver complex **C21A** (0.082 g, 0.20 mmol) and CuBr (0.056 g, 0.39 mmol) were added to a Schlenk flask in a glovebox. To these was added anhydrous dichloromethane (25 ml). The resulting suspension was stirred at ambient temperature in the absence of light for 3.5 hours. After this time, the suspension was filtered to remove AgBr / CuBr and the pale orange filtrate collected. Anhydrous pentane (40 ml) was added to the stirring filtrate and a crystalline red solid formed, which was collected by filtration and dried *in vacuo*. Yield: 0.046 g, 0.12 mmol, 63%.

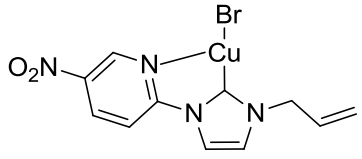

Single crystals suitable for X-ray diffraction analysis were grown by the slow evaporation of a concentrated acetonitrile solution of the product.

^{1}H NMR (300 MHz, $CDCl_3$) δ 9.38 (br s, 1H, pyH), 8.72 (dd, *J* = 8.8, 2.6 Hz, 1H, pyH), 8.59 (br d, *J* = 8.8 Hz, 1H, pyH), 7.97 (br s, 1H, imH), 7.16 (br s, 1H, imH), 6.05 (ddt, *J* = 16.3, 10.2, 6.1 Hz, 1H, C**H**=CH_2), 5.50 – 5.38 (m, 2H, CH=C**H$_2$**), 4.92 (d, *J* = 6.1 Hz, 2H, NCH_2). ^{13}C{^{1}H} NMR (126 MHz, $CDCl_3$) δ (some of the ^{13}C resonances are not observed due to broadening) 145.2, 135.1, 131.5, 121.4, 119.8, 114.4, 55.4. HRMS (ESI^+): *m/z* 334.0371 $[M - Br + MeCN]^+$ calculated $[M - Br + MeCN]^+$ 334.0360. Analysis Calculated for $C_{11}H_{10}BrCuN_4O_2$: C, 35.36; H, 2.70; N, 14.99. Found: C, 35.45; H, 2.65; N, 14.75.

6.2.68 Preparation of C22A

To freshly activated 4Å molecular sieves was added **L22** (0.40 g, 1.4 mmol) and Ag_2O (0.22 g, 0.9 mmol). To these was added anhydrous dichloromethane (30 ml) and the mixture was stirred at room temperature in the absence of light for 2.5 hours. After this time, the mixture was filtered and the solvent removed *in vacuo* to give the crude product. Recrystallisation from chloroform / pentane gave the pure product as a white solid. Yield: 0.43 g, 1.1 mmol, 78%.

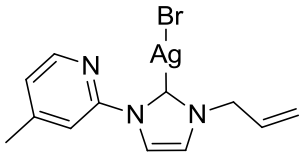

Single crystals suitable for X-ray diffraction analysis were grown by the vapour diffusion of pentane in to a concentrated solution of the product in chloroform.

^{1}H NMR (300 MHz, $CDCl_3$) δ 8.38 (d, J = 5.0 Hz, 1H, pyH), 7.89 (s, 1H, pyH), 7.81 (d, J = 1.9 Hz, 1H, imH), 7.19 (d, J = 5.0 Hz, 1H, pyH), 7.14 (d, J = 1.9 Hz, 1H, imH), 6.01 (ddt, J = 16.3, 10.4, 6.0 Hz, 1H, C**H**=CH_2), 5.41 – 5.28 (m, 2H, CH=C**H$_2$**), 4.86 (d, J = 6.0 Hz, 2H, NCH_2), 2.48 (s, 3H, CH_3). ^{13}C{^{1}H} NMR (75 MHz, $CDCl_3$) δ 181.1, 151.5, 151.1, 148.8, 132.3, 125.1, 121.5, 120.5, 120.4, 116.2, 55.4, 21.5. HRMS (ESI^+): *m/z* 505.1267 $[Ag(NHC)_2]^+$ calculated $[Ag(NHC)_2]^+$ 505.1264. Analysis Calculated for $C_{12}H_{13}AgBrN_3$: C, 37.24; H, 3.39; N, 10.86. Found: C, 37.55; H, 3.30; N, 10.70.

6.2.69 Preparation of C22B

Silver complex **C22A** (0.39 g, 1.0 mmol) and CuBr (0.22 g, 1.5 mmol) were added to a small ampoule. To these was added anhydrous dichloromethane (35 ml) and the resultant yellow suspension was stirred at room temperature in the absence of light for 3 days. After this time, the yellow suspension was filtered to remove AgBr and unreacted CuBr and the solvent removed *in vacuo* to give the product as a yellow solid. Yield: 0.31 g, 0.91 mmol, 91%.

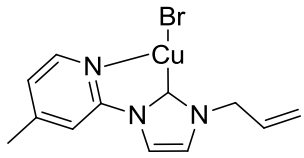

Single crystals suitable for X-ray diffraction analysis were grown on standing of a solution of the product in a mixture of chloroform/hexane (1:2).

^{1}H NMR (300 MHz, $CDCl_3$) δ 7.81 (br s), 7.08 (br s), 5.98 (br s), 5.32 (br s), 4.77 (br s), 2.31 (br s). HRMS (ESI^+): *m/z* 303.0665 $[M - Br + MeCN]^+$ calculated $[M - Br + MeCN]^+$ 303.0665. Analysis Calculated for $C_{12}H_{13}BrCuN_3$: C, 42.06; H, 3.82; N, 12.26. Found: C, 42.00; H, 3.80; N, 12.10.

Note: Unequivocal assignment of the resonances is hampered due to spectrum broadening. A $^{13}C\{^1H\}$ spectrum was also not obtained due to broadening.

6.2.70 Preparation of C22D

Silver complex **C22A** (0.10 g, 0.26 mmol) and $CuBr_2$ (0.058 g, 0.26 mmol) were added to a small Schlenk flask. To these was added anhydrous dichloromethane (25 ml), and the resultant suspension was stirred at room temperature in the absence of light for 18 hours. After this time, the dark green suspension was filtered to remove the precipitated AgBr and the dichloromethane removed *in vacuo* to give the product as a green solid. Yield: 0.091 g, 0.22 mmol, 83%.

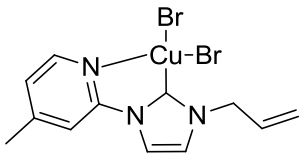

Black single crystals suitable for X-ray diffraction analysis were grown *via* the vapour diffusion of diethyl ether in to a concentrated solution of the complex in dichloromethane.

Analysis Calculated for $C_{12}H_{13}Br_2CuN_3$: C, 34.11; H, 3.10; N, 9.94. Found: C, 34.00; H, 3.10; N, 9.60.

6.2.71 Preparation of C22F

Silver complex **C22A** (0.051 g, 0.13 mmol), $CuBr_2$ (0.015 g, 0.07 mmol) and $AgPF_6$ (0.017 g, 0.07 mmol) were added to a small Schlenk flask. To these was added anhydrous dichloromethane (15 ml), and the resultant suspension was stirred at room temperature in the absence of light for 4 hours. After this time, the blue suspension was filtered to remove the precipitated AgBr and the dichloromethane removed *in vacuo* to give the crude product as a blue solid. Recrystallisation from acetonitrile/diethyl ether gave the pure product as a blue crystalline solid. Yield: 0.035g, 51 μmol, 77%.

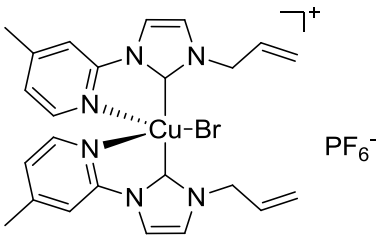

Single crystals suitable for X-ray diffraction analysis could be grown *via* the vapour diffusion of diethyl ether in to a concentrated solution of the product in acetonitrile.

HRMS (ESI$^+$): *m/z* 230.5750 $[M - Br - PF_6]^{2+}$ calculated $[M - Br - PF_6]^{2+}$ 230.5752. Analysis Calculated for $C_{24}H_{26}BrCuF_6N_6P$: C, 41.96; H, 3.82; N, 12.23. Found: C, 42.10; H, 3.80; N, 12.00.

6.2.72 Preparation of C23A

Ligand precursor **L23** (0.16 g, 0.54 mmol) and Ag_2O (0.081 g, 0.35 mmol) were added to a Schlenk flask along with freshly-activated 4 Å molecular sieves. To these was added anhydrous dichloromethane (25 ml) and the mixture was stirred in the absence of light at room temperature for 2.5 hours. After this time, the mixture was filtered through celite and the solvent removed *in vacuo* to yield the crude product as an off-white, oily solid. Recrystallisation from acetone/pentane gave the pure product as a white solid. Yield: 0.17 g, 0.43 mmol, 80%.

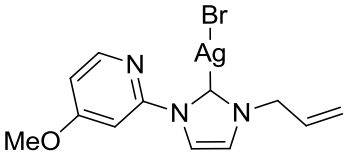

^{1}H NMR (300 MHz, $CDCl_3$) δ 8.30 (d, J = 5.8 Hz, 1H, pyH), 7.87 (d, J = 1.9 Hz, 1H, imH), 7.67 (d, J = 2.2 Hz, 1H, pyH), 7.13 (d, J = 1.9 Hz, 1H, imH), 6.89 (dd, J = 5.8, 2.2 Hz, 1H, pyH), 6.01 (ddt, J = 16.3, 10.2, 6.0 Hz, 1H, C**H**=CH_2), 5.40 (d, J = 10.2 Hz, 1H, CH=CH**H$_{(cis)}$**), 5.34 (d, J = 17.0 Hz, 1H, CH=CH**H$_{(trans)}$**), 4.85 (d, J = 6.0 Hz, 2H, NCH_2), 4.00 (s, 3H, OCH_3). ^{13}C NMR (75 MHz, $CDCl_3$) δ ($C_{carbene}$ not observed), 168.2, 152.6, 149.8, 132.3, 121.4, 120.7, 120.5, 111.8, 100.5, 56.5, 55.4. HRMS (ESI$^+$): *m/z* 537.1167 $[Ag(NHC)_2]^+$ calculated $[Ag(NHC)_2]^+$ 537.1163. Analysis Calculated for $C_{12}H_{13}AgBrN_3O$: C, 35.76; H, 3.25; N, 10.43. Found: C, 35.85; H, 3.15; N, 10.10.

6.2.73 Preparation of C23B

Silver complex **C23A** (0.15 g, 0.37 mmol) and CuBr (0.059 g, 0.41 mmol) were added to a small Schlenk flask in a glovebox. To these was added anhydrous dichloromethane (25 ml). The suspension formed was stirred at room temperature in the absence of light for 16 hours. After this time, the suspension was filtered to remove AgBr/CuBr and the yellow filtrate collected. The solvent was removed *in vacuo* to give the product as a yellow crystalline solid. Yield: 0.11 g, 0.31 mmol, 84%.

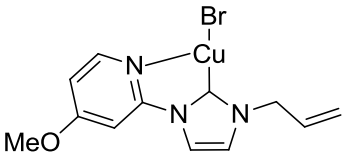

^{1}H NMR (300 MHz, $CDCl_3$) δ 8.31 (br s, 1H), 7.82 (br s, 1H), 7.78 (br s, 1H), 7.07 (br s, 1H), 6.88 (br s, 1H), 6.14 – 5.94 (m, 1H, C**H**=CH_2), 5.45 – 5.32 (m, 2H, CH=C**H$_2$**), 4.86 (br s, 2H, NCH_2), 4.02 (s, 3H, OCH_3). HRMS (ESI$^+$): *m/z* 319.0615 $[M - Br + MeCN]^+$ calculated $[M - Br + MeCN]^+$ 319.0615. Analysis Calculated for $C_{12}H_{13}BrCuN_3O$: C, 40.18; H, 3.65; N, 11.71. Found: C, 40.25; H, 3.65; N, 11.60.

Note: Unequivocal assignment of the aromatic resonances to either pyridyl or backbone NHC protons is hampered due to spectrum broadening. A $^{13}C\{^1H\}$ spectrum was also not obtained due to broadening.

6.2.74 Preparation of C23C

Silver complex **C23A** (0.022 g, 55 μmol) and $CuBr_2$ (0.012 g, 55 μmol) were added to a small Schlenk flask. To these was added anhydrous dichloromethane (15 ml), and the resultant suspension was stirred at room temperature in the absence of light for 18 hours. After this time, the dark yellow suspension was filtered to remove the precipitated AgBr and the dichloromethane removed *in vacuo*. Recrystallisation of the crude product from dichloromethane/diethyl ether gave the pure product as a green-yellow crystalline solid. Yield: 0.021 g, 47 μmol, 86%.

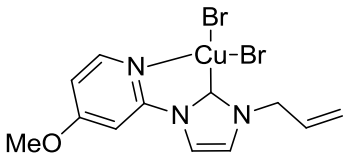

Single crystals suitable for X-ray diffraction analysis could be obtained on standing of a solution of the product in acetonitrile/diethyl ether (1:4).

Analysis Calculated for $C_{12}H_{13}Br_2CuN_3O.½CH_2Cl_2$: C, 31.21; H, 2.93; N, 8.73. Found: C, 31.40; H, 2.70; N, 8.50.

6.2.75 Preparation of C24A

To freshly activated 4Å molecular sieves was added **L24** (0.15 g, 0.54 mmol) and Ag_2O (0.21 g, 0.91 mmol). To these was added anhydrous dichloromethane (40 ml) and the resultant dark suspension was stirred at room temperature in the absence of light for 16 hours. After this time the mixture was filtered and the organics removed *in vacuo* to yield the product as a white oily solid. Yield: 0.16 g, 0.41 mmol, 76%.

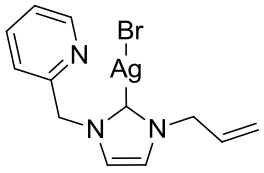

^{1}H NMR (300 MHz, $CDCl_3$) δ 8.57 (d, J = 4.2 Hz, 1H, pyH), 7.70 (td, J = 7.8, 1.7 Hz, 1H, pyH), 7.34 (d, J = 7.8 Hz, 1H, pyH), 7.30 – 7.22 (m, 1H, pyH), 7.20 (d, J = 1.7 Hz, 1H, imH), 6.99 (d, J = 1.7 Hz, 1H, imH), 5.95 (ddt, J = 16.6, 10.3, 5.9 Hz, 1H, C**H**=CH_2), 5.39 (s, 2H, py-CH_2), 5.32 (dd, J = 10.3, 0.8 Hz, 1H, CH=CH$\mathbf{H_{(cis)}}$), 5.24 (dd, J = 16.6, 0.8 Hz, 1H, CH=CH$\mathbf{H_{(trans)}}$), 4.73 (d, J = 5.9 Hz, 2H, NCH_2). $^{13}C\{^1H\}$ NMR (75 MHz, $CDCl_3$) δ 181.7, 155.2, 149.8, 137.4, 132.8, 123.4, 122.7, 122.1, 121.4, 119.6, 57.1, 54.4. HRMS (ESI^+): *m/z* 505.1263 $[Ag(NHC)_2]^+$ calculated $[Ag(NHC)_2]^+$ 505.1264.

6.2.76 Preparation of C24B

Silver complex **C24A** (0.43 g, 1.1 mmol) and CuBr (0.29 g, 2.0 mmol) were added to a small Schlenk flask. To these was added anhydrous dichloromethane (30 ml). The suspension formed was stirred at room temperature in the absence of light for 24 hours. After this time, the

suspension was filtered to remove AgBr/CuBr and the yellow filtrate collected. The solvent was removed *in vacuo* to give the product as a pale yellow crystalline solid. Yield: 0.22 g, 0.64 mmol, 33%.

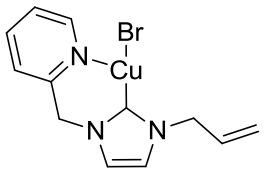

^{1}H NMR (300 MHz, $CDCl_3$) δ 8.76 (br s, 1H), 7.74 (t, *J* = 7.3 Hz, 1H, pyH), 7.42 (d, *J* = 7.3 Hz, 1H, pyH), 7.30 (br s, 1H), 7.05 (br s, 1H), 6.91 (br s, 1H), 6.01 – 5.83 (m, 1H, C**H**=CH_2), 5.55 (s, 2H, py-CH_2), 5.28 – 5.12 (m, 2H, CH=C**H$_2$**), 4.67 (d, *J* = 5.2 Hz, 2H, NCH_2). HRMS (ESI^+): *m/z* 262.0397 $[M - Br]^+$ calculated $[M - Br]^+$ 262.0400. Analysis Calculated for $C_{12}H_{13}BrCuN_3$: C, 42.06; H, 3.82; N, 12.26. Found: C, 41.80; H, 3.75; N, 11.80.

Note: Unequivocal assignment of the aromatic resonances to either pyridyl or backbone NHC protons is hampered due to spectrum broadening. A $^{13}C\{^1H\}$ spectrum was also not obtained due to broadening.

6.2.77 Preparation of C25A[35]

To freshly activated 4Å molecular sieves was added **L25** (0.21 g, 0.61 mmol) and Ag_2O (0.093 g, 0.45 mmol). To these was added anhydrous dichloromethane (30 ml) and the resultant dark suspension was stirred at reflux in the absence of light for 16 hours. After this time the mixture was filtered and the organics removed *in vacuo* to give an oily white solid. Recrystallisation from acetone/pentane gave the product as a white solid. Yield: 0.19 g, 0.42 mmol, 69%.

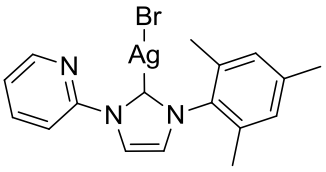

^{1}H NMR (300 MHz, $CDCl_3$) δ 8.54 (d, J = 4.6 Hz, 1H, pyH), 8.28 (d, J = 8.2 Hz, 1H, pyH), 8.10 (d, J = 1.7 Hz, 1H, imH), 7.92 (td, J = 8.2, 1.7 Hz, 1H, pyH), 7.40 (dd, J = 8.2, 4.6 Hz, 1H, pyH), 7.09 (d, J = 1.7 Hz, 1H, imH), 6.97 (s, 2H, mesH), 2.34 (s, 3H, p-CH_3), 2.04 (s, 6H, o-CH_3). $^{13}C\{^1H\}$ NMR (75 MHz, $CDCl_3$) δ ($C_{carbene}$ not observed), 150.8, 149.0, 139.8, 139.6, 135.7, 134.7, 129.7, 124.0, 123.3, 120.3, 115.7, 21.2, 18.0. HRMS (ESI^+): *m/z* 633.1912 $[Ag(NHC)_2]^+$ calculated $[Ag(NHC)_2]^+$ 633.1890. Analysis Calculated for $C_{17}H_{17}AgBrN_3$: C, 45.26; H, 3.80; N, 9.31. Found: C, 45.80; H, 3.80; N, 9.15.

Consistent with data previously reported.[35]

6.2.78 Preparation of C25B

Silver complex **C25A** (0.33 g, 0.73 mmol) was dissolved in anhydrous dichloromethane (25 ml). To this was added solid CuBr (0.11 g, 0.80 mmol). The yellow suspension formed was stirred at room temperature in the absence of light for 16 hours. After this time, the suspension was filtered and the volatiles removed *in vacuo* to give the crude product as a yellow solid. Recrystallisation from tetrahydrofuran / pentane gave the pure product as a yellow crystalline solid. Yield: 0.26 g, 0.65 mmol, 89%.

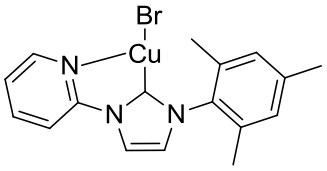

Single crystals suitable for X-ray diffraction analysis were grown by the vapour diffusion of pentane in to a concentrated solution of the product in chloroform.

^{1}H NMR (501 MHz, $CDCl_3$) δ 8.55 (br s, 1H), 8.35 (br s, 1H), 8.08 (br s, 1H), 7.94 (s, 1H), 7.42 (br s, 1H), 7.07 (br s, 1H), 6.97 (s, 2H, mesH), 2.33 (s, 3H, p-CH_3), 2.07 (s, 6H, o-CH_3). HRMS (ESI^+): *m/z* 367.0977 $[M - Br + MeCN]^+$ calculated $[M - Br + MeCN]^+$ 367.0978. Analysis Calculated for $C_{17}H_{17}BrCuN_3$: C, 50.19; H, 4.21; N, 10.33. Found: C, 50.15; H, 4.20; N, 10.30.

Note: Unequivocal assignment of the aromatic resonances to either pyridyl or backbone NHC protons is hampered due to spectrum broadening. A $^{13}C\{^1H\}$ spectrum was also not obtained due to broadening.

6.2.79 Preparation of C25C

Method A: Silver complex **C25A** (0.050 g, 0.11 mmol) and $CuBr_2$ (0.025 g, 0.11 mmol) were added to a small ampoule and dried/degassed *in vacuo*. To these was added anhydrous acetonitrile (20 ml) *via* a cannula. The resultant suspension was stirred in the absence of light at room temperature for 16 hours. After this time, the precipitated AgBr was removed *via* filtration and the solution was concentrated to approximately 5 ml. Slow addition of an excess of diethyl ether (50 ml) induced the precipitation of the product as a yellow microcrystalline solid, which was collected, washed with diethyl ether (20 ml), and dried *in vacuo*. Yield: 0.044 g, 45 μmol, 82%.

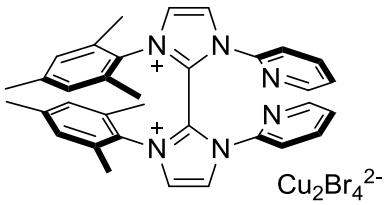

Method B: Ligand precursor **L27** (0.016 g, 38 μmol) and CuBr (0.0054 g, 38 μmol) were added to a small ampoule and dried/degassed *in vacuo*. To these was added anhydrous acetonitrile (4 ml). With stirring, an anhydrous acetonitrile (4 ml) solution of **C25B** (0.015 g, 38 μmol) was immediately added and the resultant solution was stirred at room temperature for 18 hours. After this time, the slow addition of an excess of diethyl ether (25 ml) induced the precipitation of the product as a yellow solid, which was collected, washed with diethyl ether (25 ml), and dried *in vacuo*. Yield: 0.031 g, 31 μmol, 83%.

Single crystals suitable for X-ray diffraction analysis were obtained *via* the vapour diffusion of diethyl ether in to a concentrated solution of the product in acetonitrile.

^{1}H NMR (300 MHz, CD_3CN) δ 8.55 (d, *J* = 2.0 Hz, 2H, imH), 8.27 (dd, *J* = 4.6, 0.9 Hz, 2H, pyH), 7.99 (d, *J* = 2.0 Hz, 2H, imH), 7.90 (td, *J* = 8.1, 1.6 Hz, 2H, pyH), 7.54 – 7.43 (m, 4H, pyH), 7.03 (s, 2H, mesH), 6.87 (s, 2H, mesH), 2.39 (s, 6H, p-CH_3), 2.16 (s, 6H, o-CH_3), 1.20 (s, 6H, o-CH_3). $^{13}C\{^1H\}$ NMR (75 MHz, CD_3CN) δ 150.6, 146.8, 144.1, 142.5, 137.8, 136.2, 131.5, 131.4, 131.2, 130.4, 127.9, 126.6, 21.1, 19.3, 17.6. HRMS (ESI^+): *m/z* 263.1424 $[M - Cu_2Br_4]^{2+}$ calculated $[M - Cu_2Br_4]^{2+}$ 263.1417. Analysis Calculated for $C_{34}H_{34}Br_4Cu_2N_6$: C, 41.95; H, 3.52; N, 8.63. Found: C, 41.80; H, 3.50; N, 8.50.

6.2.80 Preparation of C25D

Ligand precursor **L27** (0.031 g, 74 μmol) and CuBr (0.011 g, 74 μmol) were added to a small ampoule and dried/degassed *in vacuo*. To these was added anhydrous acetonitrile (5 ml). With stirring, an anhydrous acetonitrile (5 ml) solution of **C19C** (0.024 g, 74 μmol) was immediately added and the resultant solution was stirred at room temperature for 48 hours. After this time, the slow addition of an excess of diethyl ether (35 ml) induced the precipitation of the product as a brown oily solid, which was collected, washed with diethyl ether (35 ml), and dried *in vacuo*. Yield: 0.046 g.

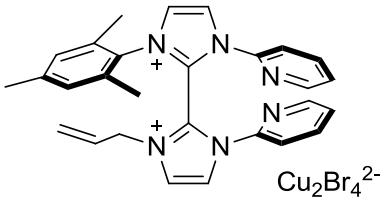

*Note: Analysis by ^{1}H NMR indicated that the product was a mixture containing the hetero-coupled (**C25D**) and homo-coupled (**C25C**) products in an approximate 20:1 (hetero:homo) ratio. The ^{1}H and $^{13}C\{^{1}H\}$ resonances and mass spectrum data are reported for the hetero-coupled product (**C25D**).*

^{1}H NMR (300 MHz, CD_3CN) δ 8.74 (d, *J* = 2.2 Hz, 1H, imH), 8.29 – 8.21 (m, 3H, pyH & imH), 8.17 (d, *J* = 2.2 Hz, 1H, imH), 8.16 – 8.08 (m, 1H, pyH), 8.05 – 7.93 (m, 2H, pyH), 7.89 (d, *J* = 2.2 Hz, 1H, imH), 7.60 (d, *J* = 8.3 Hz, 1H, pyH), 7.58 – 7.49 (m, 2H, pyH), 7.15 (s, 1H, mesH), 6.93 (s, 1H, mesH), 5.77 – 5.61 (m, 1H, C**H**=CH_2), 5.47 – 5.33 (m, 2H, CH=C**H**$_2$), 4.82 (dd, *J* = 15.1, 5.9 Hz, 1H, NCH_2), 4.64 (dd, *J* = 15.1, 6.2 Hz, 1H, NCH_2), 2.31 (s, 3H, p-CH_3), 2.18 (s, 3H, o-CH_3), 1.41 (s, 3H, o-CH_3). $^{13}C\{^{1}H\}$ NMR (75 MHz, CD_3CN) δ 150.6, 150.5, 147.5, 147.0, 143.7, 142.5, 142.4, 135.7, 135.5, 131.6, 131.4, 130.6, 129.4, 128.9, 127.8, 127.7, 127.4, 126.7, 126.4, 126.1, 125.9, 124.5, 118.0, 117.6, 53.6, 41.4, 21.1, 18.3, 17.3. HRMS (ESI^+): *m/z* 224.1184 $[M - Cu_2Br_4]^{2+}$ calculated $[M - Cu_2Br_4]^{2+}$ 224.1182.

6.2.81 Preparation of C25E

Silver complex **C25A** (0.11 g, 0.24 mmol) and $CuBr_2$ (0.11 g, 0.49 mmol) were added to a small Schlenk flask and dried/degassed *in vacuo*. To these was added anhydrous acetonitrile (25 ml) *via* a cannula. The resultant suspension was stirred in the absence of light at room temperature for 18 hours. After this time, the precipitated AgBr was removed *via* filtration and the solution was concentrated to approximately 8 ml. Slow addition of an excess of diethyl ether (50 ml) induced the precipitation of the product as a yellow crystalline solid, which was collected, washed with diethyl ether (50 ml), and dried *in vacuo*. Yield: 0.12 g, 0.17 mmol, 71%.

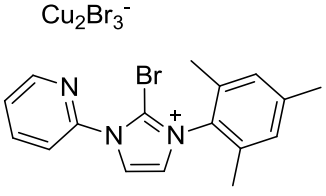

Single crystals suitable for X-ray diffraction analysis were obtained *via* the vapour diffusion of diethyl ether in to a concentrated solution of the product in acetonitrile.

^{1}H NMR (300 MHz, CD_3CN) δ 8.75 (d, *J* = 4.4 Hz, 1H, pyH), 8.26 – 8.15 (m, 2H, pyH & imH), 7.95 (d, *J* = 8.1 Hz, 1H, pyH), 7.83 (d, *J* = 2.3 Hz, 1H, imH), 7.73 (dd, *J* = 7.6, 4.4 Hz, 1H, pyH), 7.21 (s, 2H, mesH), 2.40 (s, 3H, p-CH_3), 2.09 (s, 6H, o-CH_3). ^{13}C{^{1}H} NMR (75 MHz, CD_3CN) δ 150.8, 148.1, 143.3, 141.3, 136.0, 131.5, 130.8, 127.7, 126.8, 126.7, 123.4, 121.2, 21.2, 17.8. HRMS (ESI$^+$): *m/z* 342.0600 $[M - Cu_2Br_3]^+$ calculated $[M - Cu_2Br_3]^+$ 342.0600. Analysis Calculated for $C_{17}H_{17}Br_2N_3.H_2O$: C, 28.04; H, 2.63; N, 5.77. Found: C, 27.60; H, 2.30; N, 5.60.

6.2.82 Preparation of C26A

A small Schlenk flask was charged with activated 4 Å molecular sieves, **L26** (0.12 g, 0.33 mmol) and Ag_2O (0.050 g, 0.22 mmol), which were further dried/degassed *in vacuo*. To these was added anhydrous dichloromethane (25 ml) *via* cannula. The resultant dark mixture was stirred at reflux (45°C) in the absence of light for 18 hours. After this time, the mixture was cooled and filtered and the solvent removed *in vacuo* to give a white oily solid. Trituration with a small quantity of acetone (3 ml), followed by addition of pentane (30 ml) gave the pure product as a white solid. Yield: 0.12 g, 0.26 mmol, 78%.

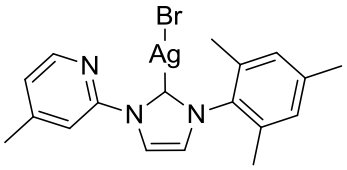

Single crystals suitable for X-ray diffraction analysis could be obtained *via* the vapour diffusion of pentane in to a concentrated solution of the product in chloroform.

^{1}H NMR (300 MHz, $CDCl_3$) δ 8.41 (d, *J* = 5.1 Hz, 1H, pyH), 8.09 (s, 1H, pyH), 8.04 (d, *J* = 1.9 Hz, 1H, imH), 7.22 (d, *J* = 5.1 Hz, 1H, pyH), 7.08 (d, *J* = 1.9 Hz, 1H, imH), 6.99 (s, 2H, mesH), 2.49 (s, 3H, pyCH_3), 2.35 (s, 3H, p-CH_3), 2.04 (s, 6H, o-CH_3). ^{13}C{^{1}H} NMR (75 MHz, $CDCl_3$) δ ($C_{carbene}$ not observed), 151.5, 151.0, 148.8, 140.0, 135.7, 134.7, 129.8, 125.2, 123.2, 120.3, 116.4, 21.5, 21.2, 18.0. HRMS (ESI$^+$): *m/z* 661.2203 $[Ag(NHC)_2]^+$ calculated $[Ag(NHC)_2]^+$ 661.2203. Analysis Calculated for $C_{18}H_{19}AgBrN_3$: C, 46.48; H, 4.12; N, 9.03. Found: C, 46.30; H, 4.00; N, 8.90.

6.2.83 Preparation of C26B

Silver complex **C26A** (0.097 g, 0.21 mmol) and $CuBr_2$ (0.047 g, 0.21 mmol) were added to a small ampoule and dried/degassed *in vacuo*. To these was added anhydrous acetonitrile (20 ml) *via* a cannula. The resultant suspension was stirred in the absence of light at room temperature for 16 hours. After this time, the precipitated AgBr was removed *via* filtration and the solution was

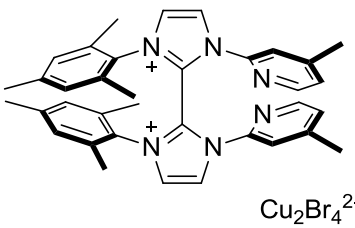

$Cu_2Br_4^{2-}$

concentrated to approximately 5 ml. Slow addition of an excess of diethyl ether (50 ml) induced the precipitation of the product as a yellow microcrystalline solid, which was collected, washed with diethyl ether (20 ml), and dried *in vacuo*. Yield: 0.078 g, 78 μmol, 75%.

Single crystals suitable for X-ray diffraction analysis were obtained *via* the vapour diffusion of diethyl ether in to a concentrated solution of the product in acetonitrile.

^{1}H NMR (300 MHz, CD_3CN) δ 8.39 (d, *J* = 2.1 Hz, 2H, imH), 8.13 (d, *J* = 5.0 Hz, 2H, pyH), 7.95 (d, *J* = 2.1 Hz, 2H, imH), 7.36 (d, *J* = 5.0 Hz, 2H, pyH), 7.12 (s, 2H, pyH), 7.03 (s, 2H, mesH), 6.84 (s, 2H, mesH), 2.39 (s, 6H, p-CH_3), 2.32 (s, 6H, pyCH_3), 2.23 (s, 6H, o-CH_3), 1.24 (s, 6H, o-CH_3). ^{13}C{^{1}H} NMR (126 MHz, CD_3CN) δ 154.8, 149.9, 146.8, 144.0, 137.7, 136.2, 131.5, 131.4, 131.2, 130.4, 128.2, 126.7, 126.5, 118.9, 21.1, 21.1, 19.0, 17.6. HRMS (ESI^{+}): *m/z* 277.1577 $[M - Cu_2Br_4]^{2+}$ calculated $[M - Cu_2Br_4]^{2+}$ 277.1573. Analysis Calculated for $C_{36}H_{38}Br_4Cu_2N_6$.½AgBr: C, 39.48; H, 3.50; N, 7.67. Found: C, 39.20; H, 3.50; N, 7.50.

*Note: Repeated elemental analyses of samples of compound **C26B** were found to consistently give the C, H and N content as slightly lower than expected. Spectroscopic analysis does not indicate the presence of organic impurities. On this basis, we postulate that the low C, H and N content derives from the presence of AgBr, which is left over from the transmetallation process.*

6.3 References

[1] M. J. Frisch, G. W. Trucks, H. B. Schlegel, G. E. Scuseria, M. A. Robb, J. R. Cheeseman, G. Scalmani, V. Barone, B. Mennucci, G. A. Petersson, H. Nakatsuji, M. Caricato, X. Li, H. P. Hratchian, A. F. Izmaylov, J. Bloino, G. Zheng, J. L. Sonnenberg, M. Hada, M. Ehara, K. Toyota, R. Fukuda, J. Hasegawa, M. Ishida, T. Nakajima, Y. Honda, O. Kitao, H. Nakai, T. Vreven, Jr, J. E. Peralta, F. Ogliaro, M. Bearpark, J. J. Heyd, E. Brothers, K. N. Kudin, V. N. Staroverov, R. Kobayashi, J. Normand, K. Raghavachari, A. Rendell, J. C. Burant, S. S. Iyengar, J. Tomasi, M. Cossi, N. Rega, J. M. Millam, M. Klene, J. E. Knox, J. B. Cross, V. Bakken, C. Adamo, J. Jaramillo, R. Gomperts, R. E. Stratmann, O. Yazyev, A. J. Austin, R. Cammi, C. Pomelli, J. W. Ochterski, R. L. Martin, K. Morokuma, V. G. Zakrzewski, G. A. Voth, P. Salvador, J. J. Dannenberg, S. Dapprich, A. D. Daniels, Farkas, J. B. Foresman, J. V. Ortiz, J. Cioslowski, D. J. Fox, *Gaussian 09 Revision A.02*, Gaussian Inc. Wallingford CT 2009, **2009**.

[2] Y. Zhao, D. G. Truhlar, *Accounts of Chemical Research* **2008**, *41*, 157-167.

[3] a) A. D. Becke, *The Journal of Chemical Physics* **1993**, *98*, 5648-5652; b) B. Miehlich, A. Savin, H. Stoll, H. Preuss, *Chemical Physics Letters* **1989**, *157*, 200-206; c) C. Lee, W. Yang, R. G. Parr, *Physical Review B* **1988**, *37*, 785-789.

[4] a) P. J. Hay, W. R. Wadt, *The Journal of Chemical Physics* **1985**, *82*, 270-283; b) W. R. Wadt, P. J. Hay, *The Journal of Chemical Physics* **1985**, *82*, 284-298.

[5] P. C. Hariharan, J. A. Pople, *Theoretica Chimica Acta* **1973**, *28*, 213-222.

[6] A. W. Ehlers, M. Böhme, S. Dapprich, A. Gobbi, A. Höllwarth, V. Jonas, K. F. Köhler, R. Stegmann, A. Veldkamp, G. Frenking, *Chemical Physics Letters* **1993**, *208*, 111-114.

[7] a) K. Fukui, *The Journal of Physical Chemistry* **1970**, *74*, 4161-4163; b) K. Fukui, *Accounts of Chemical Research* **1981**, *14*, 363-368.

[8] Y. Okuno, *Chemistry – A European Journal* **1997**, *3*, 212-218.

[9] a) J. N. Harvey, M. Aschi, H. Schwarz, W. Koch, *Theoretical Chemistry Accounts* **1998**, *99*, 95-99; b) J. N. Harvey, M. Aschi, *Physical Chemistry Chemical Physics* **1999**, *1*, 5555-5563.

[10] X. Bantreil, S. P. Nolan, *Nature. Protocols* **2011**, *6*, 69-77.

[11] E. Merino, E. Poli, U. Diaz, D. Brunel, *Dalton Transactions* **2012**, *41*, 10913-10918.

[12] M. V. Baker, M. J. Bosnich, D. H. Brown, L. T. Byrne, V. J. Hesler, B. W. Skelton, A. H. White, C. C. Williams, *The Journal of Organic Chemistry* **2004**, *69*, 7640-7652.

[13] G. Occhipinti, V. R. Jensen, K. W. Törnroos, N. Å. Frøystein, H.-R. Bjørsvik, *Tetrahedron* **2009**, *65*, 7186-7194.

[14] S. Aspin, L. López-Suárez, P. Larini, A.-S. Goutierre, R. Jazzar, O. Baudoin, *Organic Letters* **2013**, *15*, 5056-5059.

[15] B. M. Choudary, C. Sridhar, M. L. Kantam, G. T. Venkanna, B. Sreedhar, *Journal of the American Chemical Society* **2005**, *127*, 9948-9949.

[16] H.-Y. Gong, B. M. Rambo, E. Karnas, V. M. Lynch, J. L. Sessler, *Nature Chemistry* **2010**, *2*, 406-409.

[17] M. J. McPhillie, R. Trowbridge, K. R. Mariner, A. J. O'Neill, A. P. Johnson, I. Chopra, C. W. G. Fishwick, *ACS Medicinal Chemistry Letters* **2011**, *2*, 729-734.

[18] A. Raba, M. R. Anneser, D. Jantke, M. Cokoja, W. A. Herrmann, F. E. Kühn, *Tetrahedron Letters* **2013**, *54*, 3384-3387.

[19] J. M. Keith, *The Journal of Organic Chemistry* **2007**, *73*, 327-330.

[20] L. Hintermann, *Beilstein Journal of Organic Chemistry* **2007**, *3*, 22.

[21] L. Jafarpour, E. D. Stevens, S. P. Nolan, *Journal of Organometallic Chemistry* **2000**, *606*, 49-54.

[22] S. Wei, X.-G. Wei, X. Su, J. You, Y. Ren, *Chemistry – A European Journal* **2011**, *17*, 5965-5971.

[23] D. M. Lindsay, D. McArthur, *Chemical Communications* **2010**, *46*, 2474-2476.

[24] E. E. Alberto, A. L. Braga, M. R. Detty, *Tetrahedron* **2012**, *68*, 10476-10481.

[25] S. V. Dzyuba, R. A. Bartsch, *ChemPhysChem* **2002**, *3*, 161-166.

[26] S. Patil, J. Claffey, A. Deally, M. Hogan, B. Gleeson, L. M. Menéndez Méndez, H. Müller-Bunz, F. Paradisi, M. Tacke, *European Journal of Inorganic Chemistry* **2010**, *2010*, 1020-1031.

[27] F. E. Hahn, C. Holtgrewe, T. Pape, M. Martin, E. Sola, L. A. Oro, *Organometallics* **2005**, *24*, 2203-2209.

[28] F. Ekkehardt Hahn, B. Heidrich, T. Pape, A. Hepp, M. Martin, E. Sola, L. A. Oro, *Inorganica Chimica Acta* **2006**, *359*, 4840-4846.

[29] S. Grundemann, M. Albrecht, A. Kovacevic, J. W. Faller, R. H. Crabtree, *Journal of the Chemical Society, Dalton Transactions* **2002**, 2163-2167.

[30] M. Cametti, K. Raatikainen, P. Metrangolo, T. Pilati, G. Terraneo, G. Resnati, *Organic & Biomolecular Chemistry* **2012**, *10*, 1329-1333.

[31] V. Jurkauskas, J. P. Sadighi, S. L. Buchwald, *Organic Letters* **2003**, *5*, 2417-2420.

[32] S. Okamoto, S. Tominaga, N. Saino, K. Kase, K. Shimoda, *Journal of Organometallic Chemistry* **2005**, *690*, 6001-6007.

[33] T. Ramnial, C. D. Abernethy, M. D. Spicer, I. D. McKenzie, I. D. Gay, J. A. C. Clyburne, *Inorganic Chemistry* **2003**, *42*, 1391-1393.

[34] S. Díez-González, E. D. Stevens, N. M. Scott, J. L. Petersen, S. P. Nolan, *Chemistry – A European Journal* **2008**, *14*, 158-168.

[35] V. Khlebnikov, A. Meduri, H. Mueller-Bunz, T. Montini, P. Fornasiero, E. Zangrando, B. Milani, M. Albrecht, *Organometallics* **2012**, *31*, 976-986.